Novel Pathways for the Coordination and Activation of the E_4 Tetrahedron (E_4 = P_4, AsP_3, As_4)

Dissertation

zur Erlangung des

DOKTORGRADES DER NATURWISSENSCHAFTEN

(Dr. rer. nat.)

der Naturwissenschaftlichen Fakultät IV – Chemie und Pharmazie

der Universität Regensburg

vorgelegt von

Diplom-Chemiker

Christoph Schwarzmaier

aus Altötting

Regensburg 2012

Diese Arbeit wurde angeleitet von Prof. Dr. Manfred Scheer.

Promotionsgesuch eingereicht am:	08.11.2012
Tag der mündlichen Prüfung:	30.11.2012

Vorsitzender:	Prof. Dr. Nikolaus Korber
Prüfungsausschuss:	Prof. Dr. Manfred Scheer
	Prof. Dr. Henri Brunner
	Prof. Dr. Bernhard Dick

Universität Regensburg

Eidesstattliche Erklärung

Ich erkläre hiermit an Eides statt, dass ich die vorliegende Arbeit ohne unzulässige Hilfe Dritter und ohne Benutzung anderer als der angegebenen Hilfsmittel angefertigt habe; die aus anderen Quellen direkt oder indirekt übernommenen Daten und Konzepte sind unter Angabe des Literaturzitats gekennzeichnet.

_____

Christoph Schwarzmaier

This thesis was elaborated within the period from November 2008 till November 2012 in the Institute of Inorganic Chemistry at the University of Regensburg, under the supervision of Prof. Dr. Manfred Scheer.

Parts of this work have already been published:

- C. Schwarzmaier, A. Noor, G. Glatz, M. Zabel, A. Y. Timoshkin, B. M. Cossairt, C. C. Cummins, R. Kempe, M. Scheer: Formation of *cyclo*-E_4^{2-} Units (E_4 = P_4, As_4, AsP_3) by a complex with Cr–Cr Quintuple Bond; *Angew. Chem.* **2011**, *123*, 7421–7424; *Angew. Chem. Int. Ed.* **2011**, *50*, 7283–7286.
- C. Schwarzmaier, M. Sierka, M. Scheer: Intact As_4 tetrahedra, side-on coordinated to metal cations; *Angew. Chem.*, published online DOI: 10.1002/ange.201208226; *Angew. Chem. Int. Ed.*, published online DOI: 10.1002/anie.201208226.

To my family

“Climb the mountain not to plant your flag, but to embrace the challenge, enjoy the air and behold the view. Climb it so you can see the world, not so the world can see you.”

David McCullough, Jr.

Table of Contents

1. Introduction

1.1 Phosphorus and Arsenic

The elements phosphorus and arsenic have been known for centuries and play a major role in our daily life. The annual production of phosphate rock adds up to about 150 million tons,[1] of which about 90 % is used as fertilizers. The remnant is reduced to elemental phosphorus (annual production 500000 tons[2]) that serves as key intermediate for the production of detergents and organophosphorus compounds. Arsenic, with an annual production of about 50000 tons[3] is mainly used in metal alloys, pesticides and the fabrication of 13-15 semiconductors for the electronics industry.

Elemental phosphorus was first discovered by the German alchemist Hennig Brand in 1669 during his search for the philosophers stone.[4] Today, three different allotropic modifications of the element are known: black, red and white phosphorus. At ambient conditions black phosphorus is thermodynamically the most stable allotrope, built up by undulated layers of condensed P_6 rings (see Scheme 1).[5] The nature of red phosphorus is still not fully understood. Roth *et al.* proposed the classification in types I, II, III, IV and V red phosphorus based on optical microscopy, X-ray powder diffraction and differential thermal analysis (DTA).[6]

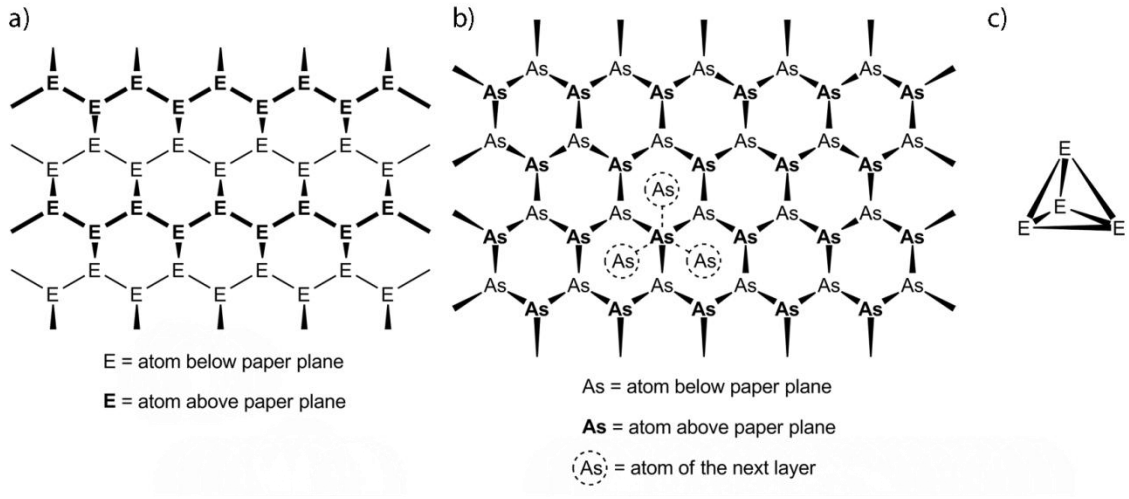

Scheme 1. Structures[7] of a) black phosphorus/arsenic b) grey arsenic c) white phosphorus and yellow arsenic. (E = P, As)

Commercial available red phosphorus mainly consists of an amorphous polymeric network of different building units (Type I). Annealing at elevated temperatures leads to four distinct

crystalline phases. The types II and III are still not characterized crystallographically.[8] Type IV of red phosphorus, commonly referred to as fibrous phosphorus, was structurally characterized by Ruck *et al.* recently[9] while the structure of type V, normally known as Hittorf's or violet phosphorus, has already been determined in 1966.[10] Both allotropes consist of tubes that are either linked parallel (type IV) or crosswise (type V). The tubes themselves are built up by alternating P_8 cuneane-like structures and P_9 cages that are linked together by P_2 units. Two new modifications of the element, that possess P_{12} cages as central building units, have been reported by Pfitzner and co workers.[11] White phosphorus, the molecular modification of the element, consists of discrete P_4 tetrahedra that have been investigated by X-ray structure analysis in the β-[12] and γ-phase.[13] It is a waxy material that is only slightly light- and temperature sensitive, and therefore convenient to use for industrial applications and academic research.

Arsenic, was first isolated by Albertus Magnus around 1250[7] and exists in three different allotropic modifications: grey, black and yellow arsenic. The thermodynamically most stable allotrope at room temperature is grey or metallic arsenic which crystallizes in the rhombohedral crystal system.[14] It is built up by undulated double layers, which consist of condensed As_6 rings. The layers are packed very closely so that every arsenic atom is coordinated in a distorted octahedral way by six other arsenic atoms (see Scheme 1). The structure therefore resembles a cubic packing, which is consistent with the matlloid character of arsenic. Black arsenic can be divided into an amorphous modification as well as a metastable orthorhombic one. The latter was first described in 1957[15] and further characterized recently by Nilges *et al.*[16] In both cases solid solutions of arsenic and phosphorus were investigated. Pure orthorhombic black arsenic is still not known. Finally, yellow arsenic consists of discrete As_4 tetrahedra and is isostructural with white phosphorus. It was first discovered and described as an allotrope of elemental arsenic by Bettendorf.[17] Until now, several amorphous and crystalline modifications of yellow arsenic are known[18] but not well investigated because solid yellow arsenic transforms into grey arsenic at elevated temperatures and upon exposure to light.[19] Hence, its chemistry and application in industry is not well developed and remains challenging.

With the synthesis of the first As_2 and *cyclo*-As_3 ligand complexes in the late 1960s, Dahl *et al.* introduced unsubstituted group 15 element-ligands into organometallic chemistry by using grey arsenic as the starting material.[20] The reactivity of white phosphorus towards transition metals has been extensively studied by Scherer et al. in the 1980s, [21] leading to numerous substituent-free polyphosphorus frameworks. In the same group, reactivity studies of yellow arsenic towards transition metal complexes were carried out that nicely show the similarities between the two homologues. In recent years the chemistry of the heavier main group elements has again moved into the focus of interest as their different electronic properties, compared to

their lighter congeners, promise new reaction pathways and properties.[22] It therefore seems valuable to further investigate the analogies and differences of white phosphorus and yellow arsenic by means of their reactivity towards transition metals as well as their coordination behavior.

1.2 Transition-metal-mediated degradation of white phosphorus and yellow arsenic

White phosphorus is the industrial key intermediate on the way to detergents and other organophosphorus compounds. These processes involve the use of hazardous reagents such as chlorine gas, Grignard reagents or alkali metals. Hence, the search for milder activation ways of the P_4 tetrahedron is of great interest. In the last decades the activation of white phosphorus with transition metal fragments and main group elements has become an active research area in chemistry, and P_n ligand complexes of almost every transition metal have been synthesized.[23] As yellow arsenic is unstable at ambient conditions, especially when exposed to light, its use for industrial processes is limited. Furthermore only few results regarding its reactivity towards transition metal fragments are known so far.

The activation of the E_4 tetrahedron (E = P, As) can either be induced by an electrophilic or nucleophilic interaction. This can take place with an unsaturated transition metal fragment which is often generated by thermolysis or photolysis of a precursor compound or with main group nucleophiles and electrophiles. This usually leads to the cleavage of one or more E–E bonds (Scheme 2). The resulting E_4, E_3, E_2 and E_1 ligands are either stabilized in the coordination sphere of the metal used, where they are kinetically stabilized by large substituents, or the E_n ligands can undergo reaggregation steps to yield larger E_n ligands with n > 4.

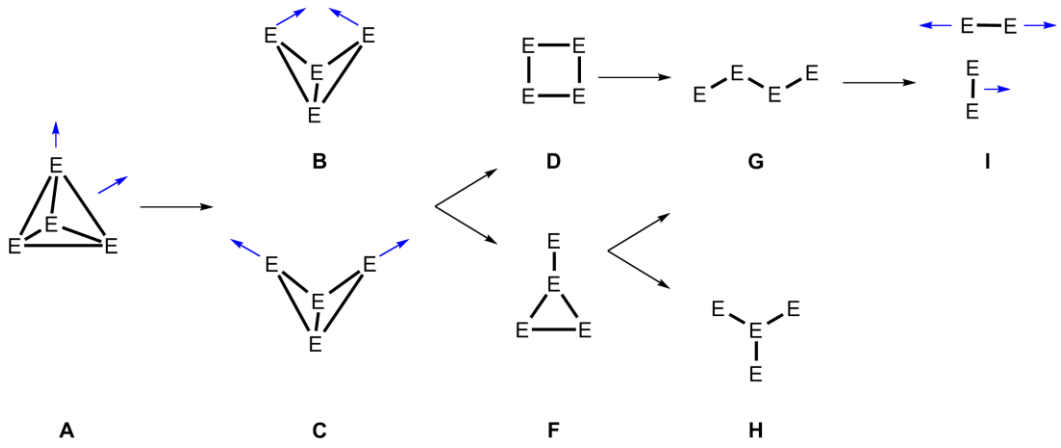

Scheme 2. Successive degradation of the E_4 tetrahedron (E = P, As). Blue arrows indicate the bonding/coordination mode.

E_n ligand complexes containing a type **A** moiety are characterized by coordination of the intact E_4 tetrahedron. In 1979 Sacconi *et al.* succeeded in the synthesis of $[(np_3)Ni(\eta^1\text{-}P_4)]$ (**1**)[24] (np_3 = Tris(2-diphenylphosphinoethyl)amine) as the first complex bearing an intact, vertex coordinating P_4 tetrahedron. In the following years, several other complexes were reported in which white phosphorus acts as monodentate ligand, including the neutral complex $[W(CO)_3(PCy_3)_2(\eta^1\text{-}P_4)]$ (**2**)[25] as well as the cationic complexes $[(triphos)Re(CO)_2(\eta^1\text{-}P_4)]^+[OTf]^-$ (**3**)[26] (triphos = 1,1,1-tris(diphenylphosphinomethyl)ethane) and $[Cp^RML_2(\eta^1\text{-}P_4)]^+[A]^-$ (Cp^R = Cp*, M = Fe, L = ½ dppe (**4a**)[27]; Cp^R = Cp*, M = Ru, L = ½ dppe (**4b**)[27]; Cp^R = Cp*, M = Ru, L = PEt_3 (**4c**)[27]; Cp^R = Cp, M = Ru, L = PPh_3 (**4d**)[28]; Cp^R = Cp, M = Os, L = PPh_3 (**4e**)[29]; [A] = Cl, OTf, BPh_4, PF_6). Besides the bonding via the lone pairs of white phosphorus, the tetrahedral unit can also use its filled σ-orbitals of the P–P bonds to coordinate to a metal fragment. This side-on coordination mode was first described by Krossing *et al.* in 2002 for the weakly coordinated complex $[Ag(\eta^2\text{-}P_4)_2]^+[pftb]^-$ (**5a**)[30] (pftb = $Al\{OC(CF_3)_3\}_4$) and in the following years for the analogous complexes $[Cu(\eta^2\text{-}P_4)_2]^+[pftb]^-$ (**5b**)[31] and $[Au(\eta^2\text{-}P_4)_2]^+[GaCl_4]^-$ (**5c**),[32] which are the first homoleptic P_4 containing complexes known so far. In the case of yellow arsenic, neither the coordination via the lone pairs nor the side-on coordination of the intact tetrahedron is known to date.

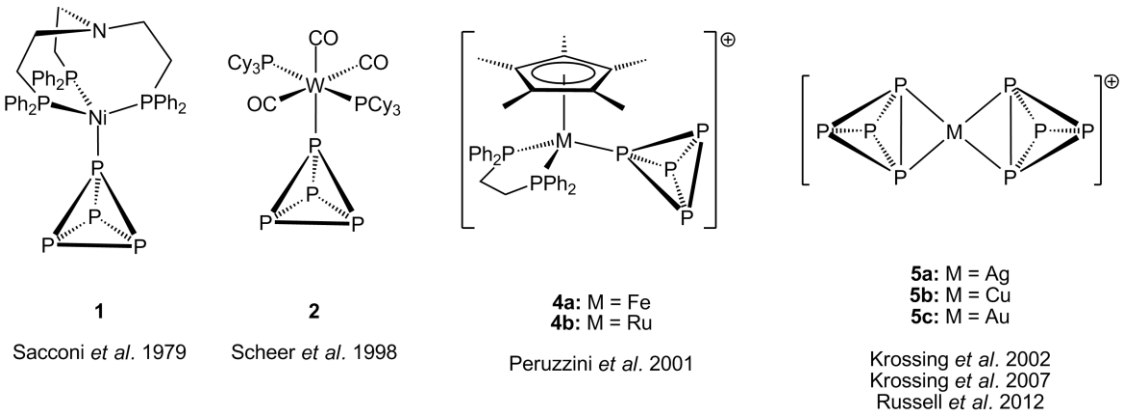

Figure 1. Selected examples of complexes with an intact P_4 tetrahedron as the ligand.

The simple side-on coordination of the tetrahedron elongates the coordinating P–P bond and may be seen as the first step of an oxidative addition reaction under the cleavage of an E–E bond and the formal reduction to an E_4^{2-} unit (type **B**). The first P_n ligand complexes $[L_2RhCl(\eta^{1:1}\text{-}P_4)]$[33] (L = PPh_3 (**6a**), P(*m*-tol)$_3$ (**6b**), P(*p*-tol)$_3$ (**6c**), $AsPh_3$ (**6d**)) reported by Ginsberg *et al.* were thought to be type **A** ligand complexes with an intact P_4 tetrahedron and a Rh(I) metal center. Theoretical calculations by Krossing *et al.* indicate Rh(III) as central atom and a P_4^{2-} ligand.[30] For As_4 a type **B** coordination mode could be realized by the thermolysis of $[\{Cp^*Co(\mu\text{-}CO)\}_2]$

with yellow arsenic.[34] Depending on reaction time, stochiometry and temperature the desired product [Cp*Co(CO)($\eta^{1:1}$-As_4)] (**7**) can be obtained in moderate yields.

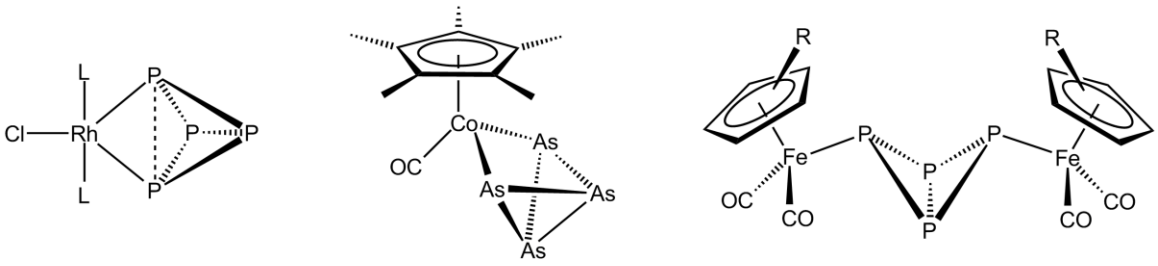

6a: L = PPh_3
6b: L = P(*m*-Tol)$_3$
6c: L = P(*p*-Tol)$_3$
6d: L = $AsPh_3$

Ginsberg *et al*. 1971

7

Scherer *et al*. 1992

9a: Cp^R = Cp''
9b: Cp^R = Cp'''

Scherer *et al*. 1996
Scherer *et al*. 1998

Figure 2. Selected examples of E_4 butterfly complexes.

The bridging coordination mode of a butterfly ligand (type **C**) could so far only be accessed with phosphorus. First results were obtained by Fluck *et al.* in 1985 who reported on the reaction of P_4 with *s*MesLi in the presence of *s*MesBr.[35] The resulting product [*s*Mes_2P_4] (**8**) is obtained in low yields but is one of the scarce examples of a direct C–P bond formation reaction with white phosphorus as the phosphorus source. In contrast to **8**, which derives from a nucleophilic attack of a carbanion, a radical mechanism for the selective cleavage of one bond of the P_4 tetrahedron is much more common. Scherer and co workers reported on the synthesis of the butterfly complexes [{$Cp^RFe(CO)_2$}$_2$(μ,$\eta^{1:1}$-P_4)] (Cp^R = Cp'' (**9a**)[36], Cp'''(**9b**)[37]) by photolysis (**9a**) and thermolysis (**9b**) of the corresponding iron dimer [{$Cp^RFe(CO)_2$}$_2$] (Cp^R = Cp'' (**10a**), Cp''' (**10b**)) together with white phosphorus. The dimeric iron precursor possesses a direct Fe–Fe bond that can be cleaved homolytically to release 17 valence electron (VE) iron(I) species that react with the P_4 tetrahedron as metal centered radicals under the cleavage of one P–P bond.[38]

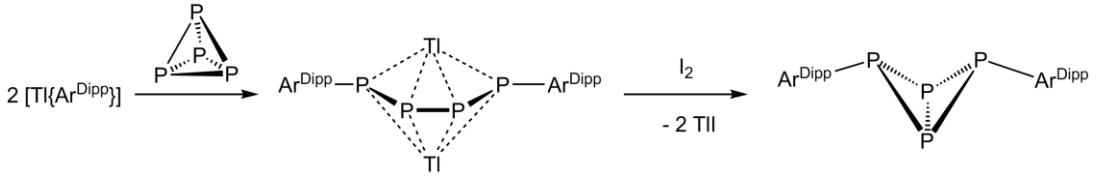

13 **12**

(1)

The same principle was expanded to main group elements by Lappert *et al*. The diphosphane [P{N($SiMe_3$)$_2$}{N^iPr_2}]$_2$ is known to dissociate reversibly in solution to give phosphinyl radicals. Subsequent reaction with white phosphorus yields P_4[P{N($SiMe_3$)$_2$}{N^iPr_2}]$_2$ (**11**) with a tetraphosphabicyclobutane unit as central motif.[39] Beside the direct formation of a butterfly

moiety, Power *et al.* reported on the formation of the diaryltetraphosphabicyclobutane $[(Ar^{Dipp})_2P_4]$ (**12**) (Ar^{Dipp} = C_6H_3-2,6-(C_6H_3-2,6-$^iPr_2$)$_2$) in a two-step reaction.[40] In a first step $[Tl(Ar^{Dipp})]$ reacts as a nucleophile with P_4 to yield $Tl_2[(Ar^{Dipp})_2P_4]$ (**13**) consisting of a diaryltetraphosphabutadienediid unit which is stabilized by two Tl(I) cations. In a second step, **13** is oxidized with I_2 to give **12** as isomerization product of the initially formed diaryltetraphosphabutadiene (equation 1).

The cleavage of a second bond of the E_4 tetrahedron leads either to a *cyclo*-E_4 ligand (type **D**) or a *cyclo*-E_3 unit with an additional exocyclic E atom (type **F**). *Cyclo*-E_4 ligands of type **D** are known for phosphorus as well as arsenic and can be accessed with early transition metal complexes. The first examples of *cyclo*-E_4 ligands (E = P, As) were given by Scherer *et al.* in 1989 by irradiation of $[Cp^*Nb(CO)_4]$ with white phosphorus or yellow arsenic, respectively. The obtained complexes $[Cp^*Nb(CO)_2(\eta^4\text{-}P_4)]$ (**14a**)[41] and $[Cp^*Nb(CO)_2(\eta^4\text{-}As_4)]$ (**14b**)[42] possess a *cyclo*-E_4 ligand that shows a kite-like distortion in both cases. For **14a** the nature of the cyclic ligand was investigated by variable-temperature NMR experiments that indiacte a formal P_4^{2-} ring that consists of an allyl-like P_3^- unit and a phosphido-like anion. Recently, Fryzuk *et al.* provided another example of a complex containing a *cyclo*-P_4 ligand.[43] By the reaction of $[Zr(P_2N_2)Cl_2]$ (P_2N_2 = $PhP(CH_2SiMe_2NSiMe_2CH_2)_2PPh$) with white phosphorus under reducing conditions the D_{2d} symmetric complex $[\{Zr(P_2N_2)\}_2(\mu,\eta^{4:4}\text{-}P_4)]$ (**15**) is formed. The P_4 unit in **15** is almost perfectly square planar and can be regarded as P_4^{4-} ligand.

Photolysis of the bridging butterfly complex **9a** leads to a successive loss of all four carbonyl ligands accompanied by a rearrangement of the tetraphosphabicyclobutane framework.[36] The final decarbonylation step gives rise to the type **G** complex $[\{Cp''Fe\}_2(\mu,\eta^{4:4}\text{-}P_4)]$ (**16a**). For complex **9b** a total loss of all carbonyl ligands was observed during thermolysis in boiling decalin yielding the two complexes $[\{Cp'''Fe\}_2(\mu,\eta^{4:4}\text{-}P_4)]$ (**16b**) and $[Cp'''Fe(\eta^5\text{-}P_5)]$.[37] The pseudo-triple-decker complexes **16** are characterized by a butadiene-like P_4^{2-} chain, bridging two iron fragments. NMR investigations indicate a distinct dynamic behavior in solution involving the intermediary formation of a *cyclo*-P_4^{2-} ligand.

A more direct way to a linear P_4 chain was presented by Bertrand and co workers who used the sterically demanding, menthyl-substituted *cyclic* (alkyl)-(amino)carbene (^{Menthyl}CAAC) (**17**) for the activation of white phosphorus (equation 2).[44] It could be shown earlier that CAACs resemble transition metals by means of a filled σ-type and a vacant π-type orbital, and can be used for the activation of small molecules such as hydrogen and ammonia.[45] The reaction of **17** with white phosphorus leads to $[(^{Menthyl}CAAC)_2P_4]$ (**18**) as a mixture of the *E*- and *Z*-isomer in good yields (equation 2). As the P_4 chain is protected by the bulky menthyl substituents no further

aggregation to larger P_n frameworks is observed, which is the case when N-heterocyclic carbenes (NHC) are used.[46]

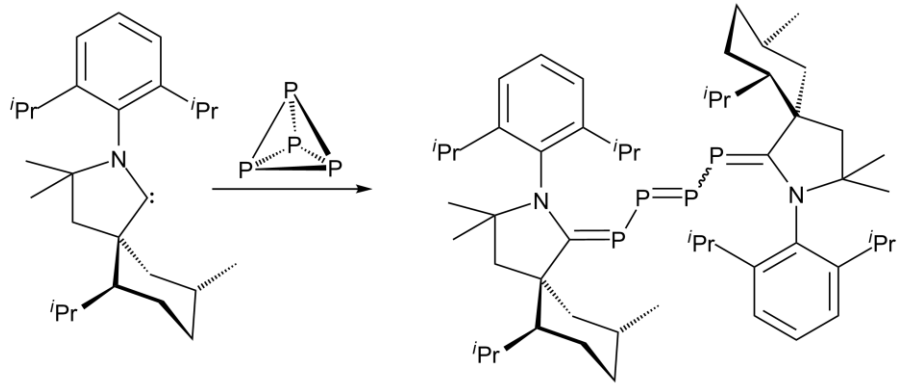

17 **18** (2)

When the cyclohexyl-substituted cyclic (alkyl)-(amino)carbene (^{cHex}CAAC) (**19**) is used for the reaction with P_4 two different products can be isolated (equation 3).[47] A formal 6 e^- reduction of white phosphorus leads to the tripodal *iso*-tetraphosphane derivative [(^{cHex}CAAC)$_3$P$_4$] (**20**) in which three bonds of the tetrahedron are cleaved (type **H**). Besides **20** the further fragmentized type **J** species [(^{cHex}CAAC)$_2$P$_2$] (**21**) could be structurally characterized which is reminiscent of a 2,3-diphosphabutadiene or the NHC stabilized bis(phosphinidene).[48] So far, no reactivity studies of stable carbenes with yellow arsenic have been reported.

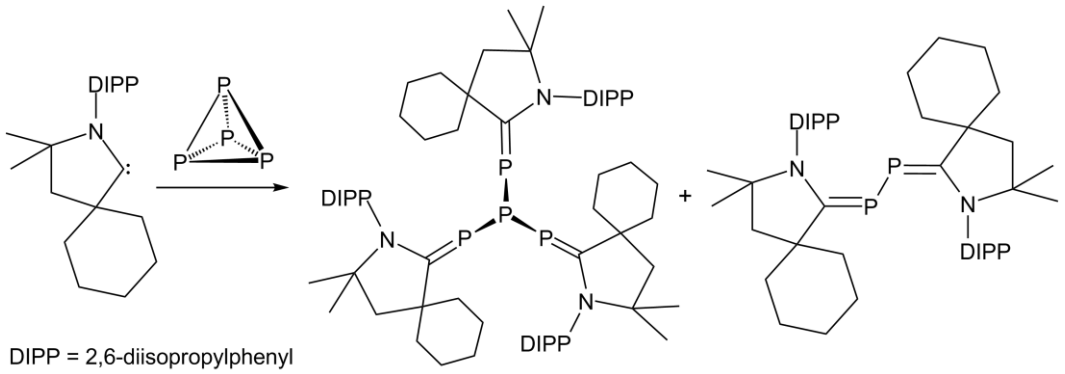

DIPP = 2,6-diisopropylphenyl

19 **20** **21** (3)

1.3 Mixed P_nAs_m ligand complexes

A plethora of different P_n and As_n ligand complexes have been synthesized but only a small number is known which exhibit mixed P_nAs_m ligands. These mixed E_n ligand complexes bear the potential to investigate the coordination behavior of phosphorus and arsenic at the same time. First results for this interesting class of compound were presented by Mays *et al.* who reacted the anionic complex $Li^+[\{CpMo(CO)_2\}_2(\mu\text{-}PH_2)]^-$ with ECl_3 (E = As, Sb) to yield the tetrahedrane complexes $[\{CpMo(CO)_2\}_2(\mu,\eta^{2:2}\text{-}PE)]$ (E = As (**22a**), Sb (**22b**)) in moderate yields.[49] Two years later Scheer *et al.* reported on the synthesis of $[\{CpCr(CO)_2\}(\eta^3\text{-}P_2E)]$ (E = As (**23a**), Sb (**23b**)) by the reaction of $[\{CpCr(CO)_2\}_2(\mu,\eta^{2:2}\text{-}P_2)]$ with ECl_3 (E = As, Sb).[50] The largest mixed P_nAs_m ligand complexes known so far can be obtained in the authors diploma thesis by the reaction of **9b** with yellow arsenic in boiling decalin with the loss of all carbonyl ligands.[51] Coloumn chromatographic workup yields the complexes $[\{Cp'''Fe\}_2(\mu,\eta^{4:4}P_nAs_{4-n})]$ (**24**) (n = 2 – 3) and $[Cp'''Fe(\eta^5\text{-}P_nAs_{5-n})]$ (**25**) (n = 1 – 4) (equation 4).

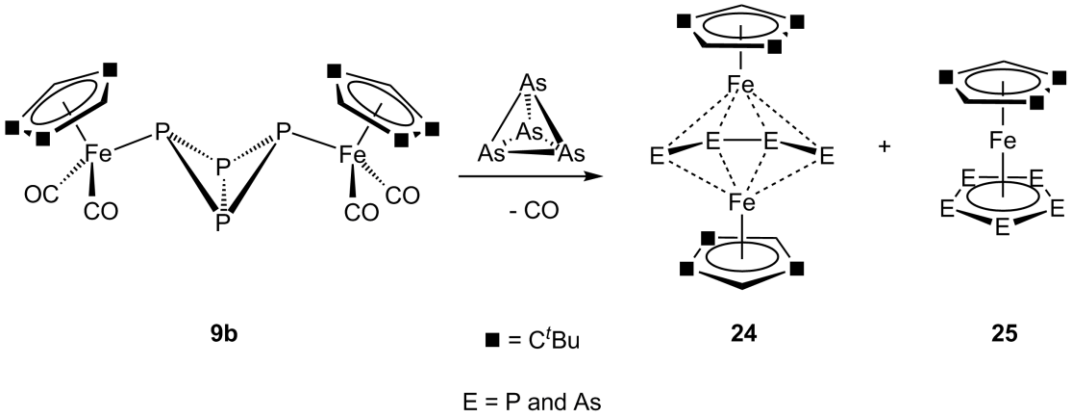

(4)

Recently, Cummins *et al.* reported the synthesis of the interpnictide AsP_3 which opens new ways in the synthesis of mixed P_nAs_m ligand complexes. AsP_3 is obtained from the reaction of the P_3^{3-} synthon $Na^+[\{ODipp\}_3Nb(\eta^3\text{-}P_3)]^-$ (Dipp = 2,6-diisopropylphenyl) with $AsCl_3$.[52] First results regarding its coordination behavior towards lewis acidic transition metal fragments were obtained by the reaction of AsP_3 with $[Cp^*Fe(dppe)]^+[BPh_4]^-$ or $[Mo(P^iPr_3)_2(CO)_3]$, respectively, to yield the type **A** complexes $[Cp^*Fe(dppe)(\eta^1\text{-}AsP_3)]^+[BPh_4]^-$ (**26**) and $[(P^iPr_3)_2(CO)_3Mo(\eta^1\text{-}AsP_3)]$ (**27**) (Figure 3).[53] In both cases, the metal center is only coordinated by a phosphorus vertex, pointing to a better σ-coordination ability of phosphorus compared to arsenic and therefore a distinct selectivity during the reaction.

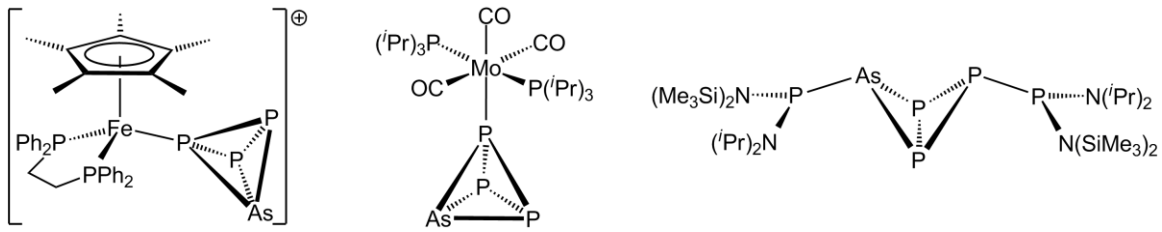

Figure 3. Selected examples of mixed P_nAs_m complexes synthesized from AsP_3.

Regioselectivity can also be observed for the cleavage of one bond of AsP_3. The reaction of $[P\{N(SiMe_3)_2\}\{N^iPr_2\}]_2$ with AsP_3 yields $AsP_3[P\{N(SiMe_3)_2\}\{N^iPr_2\}]_2$ (**28**) within a few minutes.[53] Crystal structure determination together with ^{31}P NMR investigations show a selective cleavage of an As–P bond leading to the depicted framework (Figure 3) of **28**. The regioselectivity can be explained by weaker As–P bonds compared to P–P bonds (the difference in energy is 6 kcal mol^{-1}).

1.4 The coordination chemistry of E_n ligand complexes

As E_n ligand complexes (E = P, As) possess sterically accessible lone pairs, as well as filled σ-orbitals of E–E bonds, they can act as electron-donor ligands towards Lewis acids. The first example of the coordination ability of a P_n ligand complex was given by Scherer *et al.* who coordinated $[\{CpMo(CO)_2\}_2(\mu,\eta^{2:2}\text{-}P_2)]$ (**29**) to the 16 valence electron (VE) species $[Cr(CO)_5]$ as well as the 14 VE fragment $[Re(CO)_3Br]$.[54]

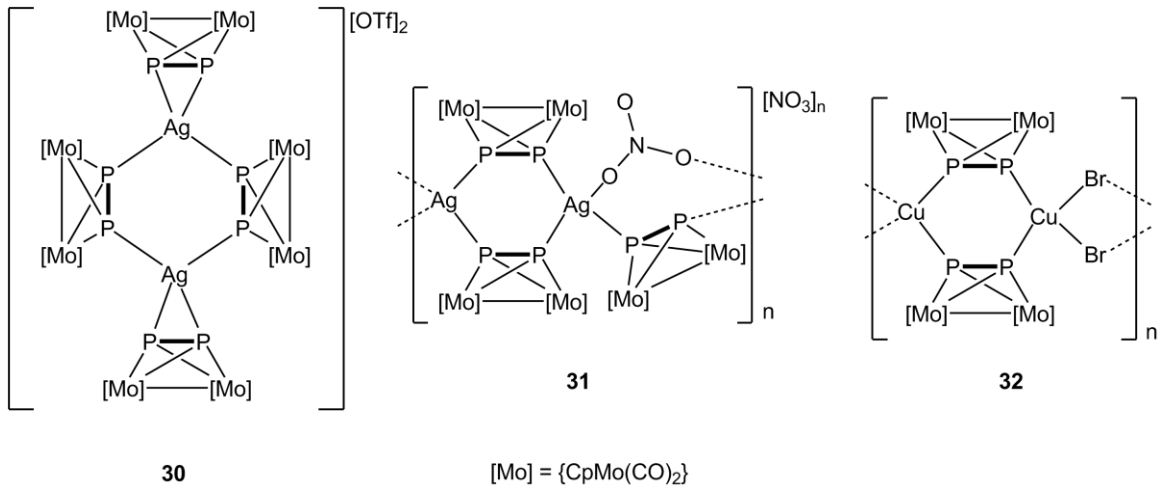

Figure 4. First oligomeric and polymeric coordination compounds based on **29**.

In our group, mainly coinage metal halides and monovalent cations of the groups 11 and 13 are used as Lewis acids, which give access to a broad variety of oligomeric, polymeric and spherical aggregates on the interface between coordination- and supramolecular chemistry.[55] First results were obtained by the reaction of **29** with Ag(OTf), $AgNO_3$ or CuBr leading to the discrete complex **30** as well as the charged and uncharged polymers **31** and **32**, respectively (Figure 4). Compound **30** consists of a central Ag_2P_4 six-membered ring in which the two silver cations are bridged terminally by two units of **29**. The coordination sphere of the cations is completed by two additional units of **29** in a side-on coordination mode. Due to the rather weak coordinating $[OTf]^-$ counterion compound **30** is slightly soluble and dissociates in solution. Using the stronger coordinating $[NO_3]^-$ counterion no discrete compound is obtained, but the charged 1D polymer **31** in which one half of the nitrate anions together with one unit of **29** link the Ag_2P_4 six-membered rings. In the case of **32** the resulting 1D polymer is formed by Cu_2P_4 six-membered rings that are linked by two bromine atoms to form linear strands.

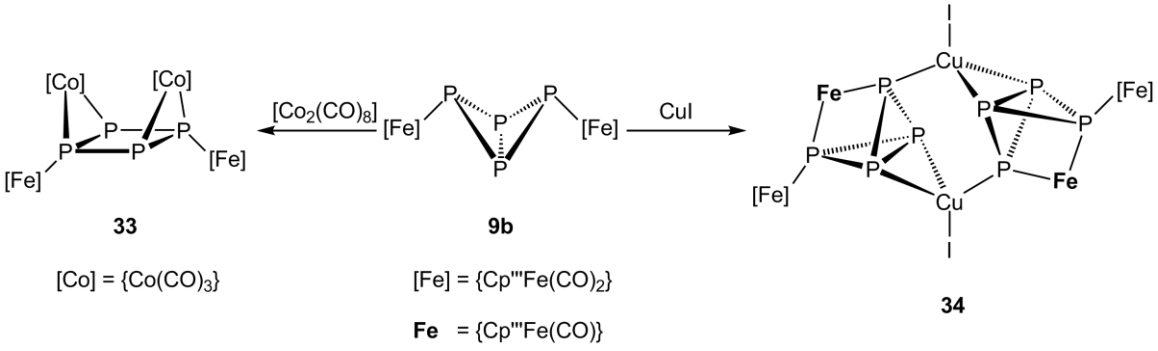

Scheme 3. First results concerning the coordination behavior of $[\{Cp'''Fe(CO)_2\}_2(\mu,\eta^{1:1}\text{-}P_4)]$ (**9b**).

First results regarding the coordination chemistry of $[\{Cp'''Fe(CO)_2\}_2(\mu,\eta^{1:1}\text{-}P_4)]$ (**9b**) were obtained recently in our group.[56] The reaction of **9b** with $[Co_2(CO)_8]$ leads to a P–P bond cleavage in the bicyclic butterfly framework to yield $[\{Cp'''Fe(CO)_2\}_2(\mu_4,\eta^{1:1:2:2}\text{-}P_4)\{Co(CO)_3\}_2]$ (**33**) with a *cyclo*-P_4 unit as central structural motif (Scheme 3). Reacting **9b** with three equivalents of CuI preserves the bicyclic P_4 framework but causes the loss of one iron-bound carbonyl ligand and subsequent rearrangement with one terminal $[Cp'''Fe(CO)_2]$ and one bridging [Cp'''Fe(CO)] fragment. Two CuI units are linked together by the rearranged butterfly complex to form the dimer $[\{Cp'''Fe(CO)_2\}\{Cp'''Fe(CO)\}(\mu_4,\eta^{1:1:2:2})\{CuI\}]_2$ (**34**). Coordination compounds with an unchanged butterfly framework of **9b** are not known so far.

The potential of E_n ligand complexes to form novel coordination compounds is exemplified by the coordination behavior of the *cyclo*-E_5 ligand complexes [Cp*Fe(η^5-P_5)] (**35a**)[57] and [Cp*Fe(η^5-As_5)] (**35b**)[58] towards copper(I)-halides. The reaction of **35a** with one equivalent of CuCl yields the 1D polymeric compound [{Cp*Fe(μ,$\eta^{1:1:5}$)}CuCl]$_n$ (**36**)[59] in which the *cyclo*-P_5 ligand shows a 1,2-coordination mode and bridges two copper atoms. The so-formed Cu_2P_4 six membered rings are linked together by two chlorine atoms. The basic framework of **36** therefore resembles that of **32**. Surprisingly, by using CuBr and CuI under the same reaction conditions the 2D polymeric coordination compounds [{Cp*Fe(μ,$\eta^{1:1:1:5}$)}CuX]$_n$ (X = Br (**37a**), I (**37b**)) are formed. The polymers **37** feature a 1,2,4-substitution pattern of the *cyclo*-P_5 ring which generates two-dimensional layers. However, in both cases the coordination compounds are formed due to σ-type interactions of the pentaphosphaferrocene with the Lewis acidic copper(I)-halides.

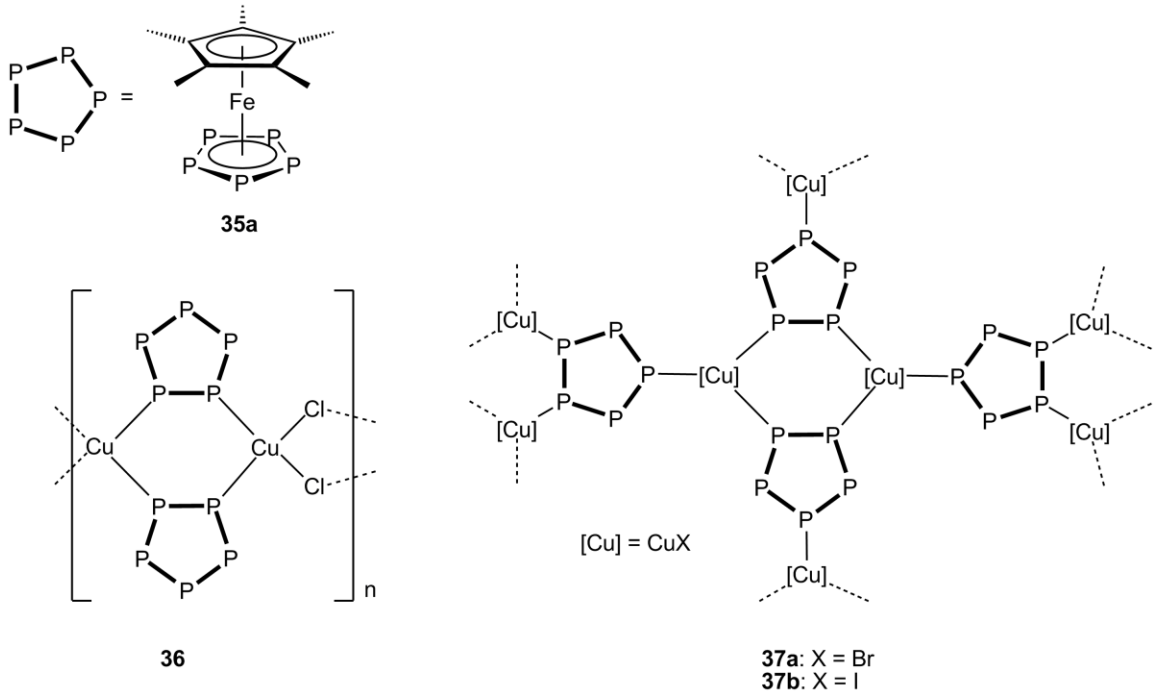

Figure 5. 1D and 2D polymers formed by the reaction of **35a** with copper(I)-halides.

Completely different behavior can be observed when the pentaarsaferrocene **35b** is reacted with CuX (X = Cl, Br, I), which demonstrates the coordination flexibility of E_n ligand complexes. In contrast to the σ-coordination dominated compounds **36** and **37**, the reaction of the pentaarsaferrocene **35b** with CuX (X = Cl, Br) yields 1D polymers that are built up by π-type interactions.[60] The *cyclo*-As_5 ring coordinates to three copper atoms of a six-membered, ruffled $(CuX)_3$ ring in a η^2:η^2:η^2coordination mode to form a discrete monomeric unit. These units are linked together by weak σ-type Cu–As interactions to form infinite strands. A reason for that feature might be the capability of arsenic to realize higher coordination numbers as well as the

poor electron donating character of the lone pairs. Hence, the simultaneous coordination of three copper atoms below the ring plane is more favorable than coordination via the lone pairs.

The most intriguing coordination compounds of P_n ligand complexes may be the spherical supramolecules formed by [Cp*Fe(η^5-P_5)] (**35a**). The first example of this fascinating class of compounds was given by Scheer *et al.* in 2003 by reacting **35a** with CuCl or CuBr under carefully chosen reaction conditions to yield $[Cp^*FeP_5]@[(CuX)_{10}(Cu_2X_3)_5\{Cu(CH_3CN)_2\}_5(Cp^*FeP_5)_{12}]$ (X = Cl (**38a**), Br (**38b**)) (Figure 6).[61] Molecules of **38** are built up by two half shells that consist of alternating *cyclo*-P_5 rings as well as six-membered (Cu_2P_4) rings that are connected by a belt of (Cu_2X_3) and {$Cu(CH_3CN)_2$} units. Altogether the basic framework consists of 90 non-carbon atoms that possesses five-fold molecular symmetry and exhibits a fullerene-like topology. The inner cavity of the spherical clusters is occupied by one molecule of **35a,** which indicates a template effect of the used starting material.

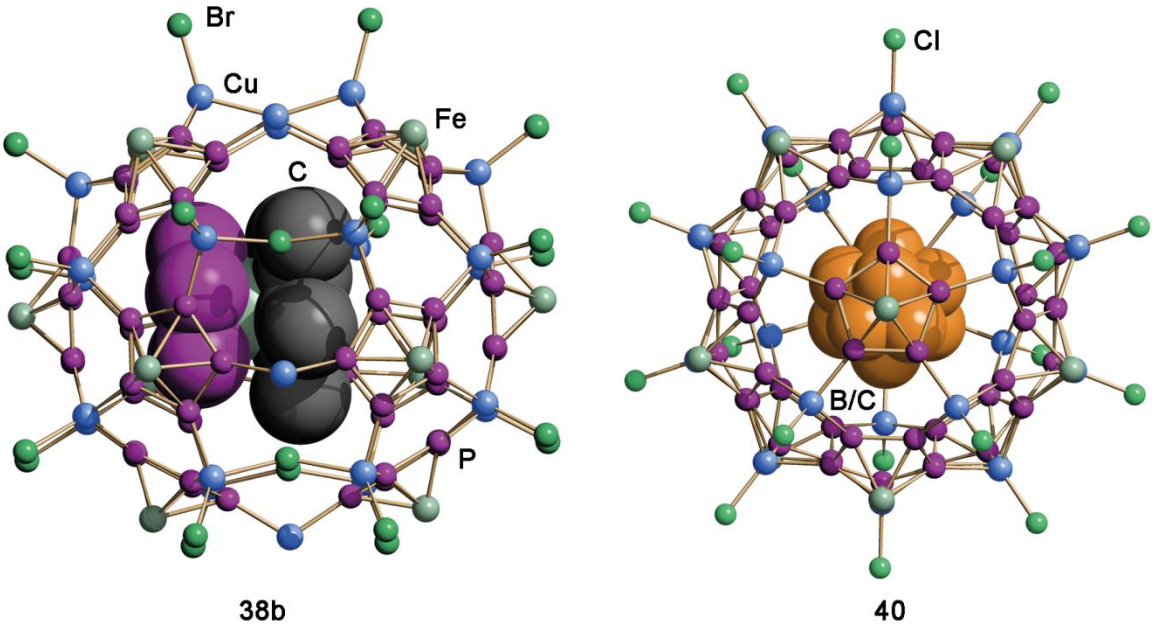

Figure 6. Molecular structures of **38b** und **40** in the crystal. Cp* and (MeCN) ligands as well as hydrogen atoms are omitted for clarity.

By varying the size and symmetry of the used template several other examples of spherical aggregates could be obtained. Using buckminsterfullerene (C_{60}) as template yields the supramolecule $C_{60}@[Cu_{26}Cl_{26}(Cp^*FeP_5)_{13}(H_2O)_2(CH_3CN)_9]$ (**39**), in which the fullerene is encapsulated in a cluster consisting of 99 non-carbon atoms.[62] As the C_{60} template seems to be slightly too large, the shell of **39** is not completely closed. By using the smaller icosahedral carborane *o*-$C_2B_{10}H_{12}$ the spherical cluster $C_2B_{10}H_{12}@[(CuCl)_{20}(Cp^*FeP_5)_{12}]$ (**40**) is obtained (Figure 6).[63] It is completely closed and consists of 80 non-carbon atoms. Compound **40**

possesses icosahedral symmetry and is built up by fused five- and six-membered rings. Hence, it may be viewed as the inorganic analog of the I_h-C_{80} fullerene.

Beside the icosahedral molecules C_{60} and *o*-$C_2B_{10}H_{12}$, molecules with lower symmetry could also be used as templates for the synthesis of spherical supramolecules. The reaction of **35a** with CuCl in the presence of P_4S_3 leads to the formation of P_4S_3@[$(CuCl)_{20}(Cp^*FeP_5)_{12}$] (**41**) which is isostructural to **40**.[64] By using the small P_4 as template, the formation of a novel coordination compound could be observed. The formed molecule P_4@[$(Cp^*FeP_5)_{10}(CuI)_{30}(CH_3CN)_6$] (**42**) is of cuboid shape and consists of two half-shells that are connected by a CuI framework.[65] The P_4 tetrahedron occupies one of these half-shells with a 50 % probability. In contrast to the previously mentioned structures, no six-membered Cu_2P_4 rings can be found in the framework.

2. Research Objectives

While the transition metal mediated degradation of the P_4 tetrahedron is well investigated only a few results for the activation of AsP_3 and yellow arsenic are known to date. Additionally, classical synthetic routes for E_n ligand complexes often involve harsh thermolytic and photolytic conditions which favour the formation of side-products and only grant access to thermodynamically stable compounds in low yields. Furthermore, only a few results describe direct C–P bond formation reactions. Therefore, the objectives of this work are:

- To investigate the reactivity of cyclic (alkyl)-(amino)carbenes towards yellow arsenic;
- To find new ways for the synthesis of *cyclo*-E_4 (E_4 = P_4, AsP_3, As_4) complexes;
- To optimize the synthesis of the bridging P_4 butterfly complex **9b** and to use these optimized reaction conditions for the synthesis of novel E_4 butterfly complexes (E_4 = P_4, AsP_3, As_4);
- To investigate possible routes to direct C–P bond formation reactions with P_4 as the phosphorus source.

The coordination chemistry of *cyclo*-E_n ligand complexes towards Lewis acids, expecially coinage metal cations, is well investigated. In contrast, very little is known about the coordination chemistry and reactivity of bridging butterfly complexes. Hence, the task for this work is:

- To investigate the reactivity of bridging E_4 butterfly complexes as well as their coordination behavior towards Lewis acids.

The coordination behavior of white phosphorus has been surveyed for many years and several examples have been reported that exhibit an intact P_4 tetrahedron as the ligand. In contrast, the coordination of an intact As_4 tetrahedron has not been observed to date. The following objectives arise:

- To investigate the coordination behavior of the intact As_4 tetrahedron towards suitable Lewis acidic metal fragments;
- To investigate the reactivity of such complexes;
- To use yellow arsenic as a template for the formation of spherical aggregates in the [Cp*FeP_5]/CuI system.

3. Results and Discussion

3.1 Reactivity of yellow arsenic towards stable carbenes

In 2007, Bertrand *et al.* demonstrated the potential of stable carbenes for the mild activation of white phosphorus. The reaction of P_4 with a N-heterocyclic carbene (NHC) leads to an initial formation of an NHC-containing tetraphosphatriene, which is not stable.[46] Further fragmentation and reaggregation steps finaly lead to a P_{12} framework stabilized by two NHCs. By using stronger nucleophilic CAACs the group was able to stabilize and characterize the tetraphosphatriene species [(^{Menthyl}CAAC)$_2$P$_4$] (**18**), the *iso*-tetraphosphane [(^{cHex}CAAC)$_3$P$_4$] (**20**) as well as the diphosphene [(^{cHex}CAAC)$_2$P$_2$] (**21**) (equations 2 and 3).[44, 47] All products possess interesting electronic properties in means of delocalized π-systems and possible resonance stabilization.[66] As the tendency to form π-bonds decreases on descending the p-block of the periodic table, it is of special interest to investigate the reactivity of yellow arsenic towards the strongly nucleophilic CAACs.

3.1.1 Reactivity of yellow arsenic towards ^{Menthyl}CAAC (17)

The reaction of two equivalents of the menthyl substituted CAAC (**17**) with one equivalent of As_4 in toluene at room temperature affords the 2,3-diarsabutadiene [(^{Menthyl}CAAC)$_2$As$_2$] (**43**) in moderate yields (equation 5). The reaction mixture features a reversible color change from pale yellow to intense green upon cooling. This thermochromic behavior cannot be observed for solutions of pure **43** and shall be discussed later.

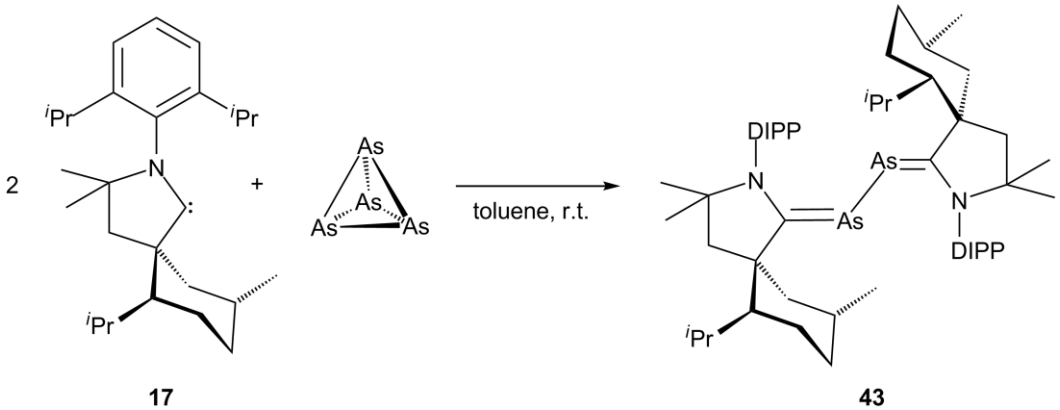

17 **43**

51 %

(5)

Complete removal of the solvent leads to a yellow solid. The crude product can be purified by extraction with hexane followed by crystallization from a concentrated Et_2O solution upon cooling to 4 °C. Compound **43** has good solubility in polar as well as non polar solvents. The ^{1}H and $^{13}C\{^{1}H\}$ NMR spectra (C_6D_6) show numerous superimposed signals due to the highly complex nature of the CAAC. Hence, a meaningful assignment of the signals was not possible (see Figure 62 Appendix). However, four signals for the ^{i}Pr groups of the CAAC can be detected at δ = 3.15, 3.25, 3.37 and 4.12 ppm which are shifted from the corresponding signals in the starting material **17** (three septets or multipletts at δ = 2.11, 2.54 – 2.78 and 3.18 ppm). The field desorption ionisation (FD) mass spectrum shows one peak at *m*/*z* = 912.4 that can be assigned to the molecular ion of **43**.

[(^{Menthyl}CAAC)$_2$As$_2$] (**43**) crystallizes as pale yellow plates and enantiomerically pure in the non-centrosymmetric space group $P2_1$ of the monoclinic crystal system. The asymmetric unit contains two molecules of **43**. The molecular structure of **43** in the crystal is shown in Figure 7.

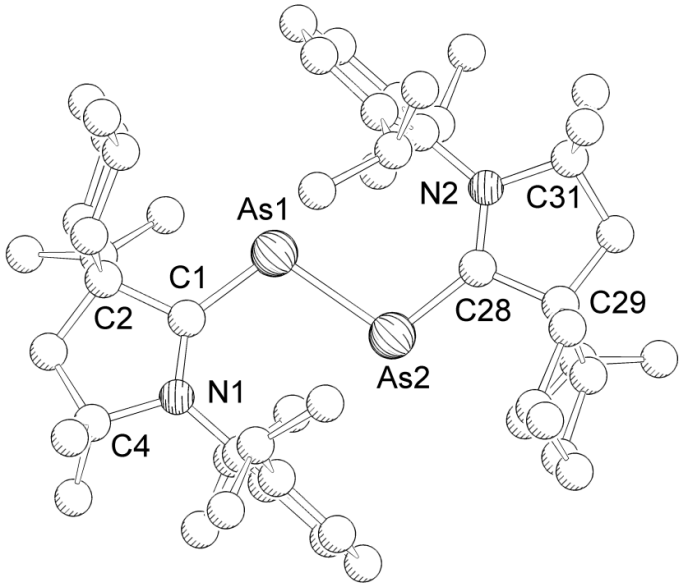

Figure 7. Molecular structure of **43** in the crystal. For clarity reasons only one of the two molecules in the asymmetric unit is depicted and hydrogen atoms are omitted. Selected bond lengths [Å] and angles [°]: As1–As2 2.4423(3), As1–C1 1.856(3), As2–C28 1.859(3), C1–N1 1.371(3), C1–C2 1.549(3), N1–C4 1.509(3), C28–N2 1.364(3), C28–C29 1.556(3), N2–C31 1.508(3), As2–As1–C1 107.24(7), As1–C1–C2 118.5(2), As1–C1–N1 134.4(2), N1–C1–C2 107.0(2), As1–As2–C28 107.59(7), As2–C28–C29 117.6(2), As2–C28–N2 134.2(2), N2–C28–C29 108.0(2).

The crystal structure of **43** reveals a central As_2 unit that is stabilized by two ^{Menthyl}CAACs. The C1–As1–As2–C28 dihedral angle is165.7(1)°. The two CAACs bind to the As_2 unit in an almost coplanar fashion. The carbene carbon atoms show a typical planar geometry for sp^2 hybridized

carbon atoms with sum of angles of 359.9° for C1 and 359.8° for C28. The As1–As2 bond length of 2.4423(3) Å is in the range of an As–As single bond (2.435(4) Å in As_4 determined by electron diffraction,[67] 2.42 Å sum of covalent radii[68]). The C1–As1 and C28–As2 bonds with 1.856(3) Å and 1.859(3) Å, respectively, can be viewed as in between a carbon-arsenic single and double bond (1.96 Å and 1.81 Å, respectively).[68] The C1–N1 and C28–N2 bond lengths of 1.371(3) Å and 1.364(3) Å are slightly shorter than the corresponding C–N bond distances in **18** (1.40(1) Å)[44] and **21** (1.387(9) Å),[47] and lie in between a C–N single and a C–N double bond (1.46 Å and 1.27 Å, respectively).[68] In contrast, the N1–C4 and N2–C31 bonds are with 1.509(3) Å and 1.508(3) Å longer and can be regarded as single bonds. The electronic structure of **43** may best be described by the resonance forms shown in Scheme 4.

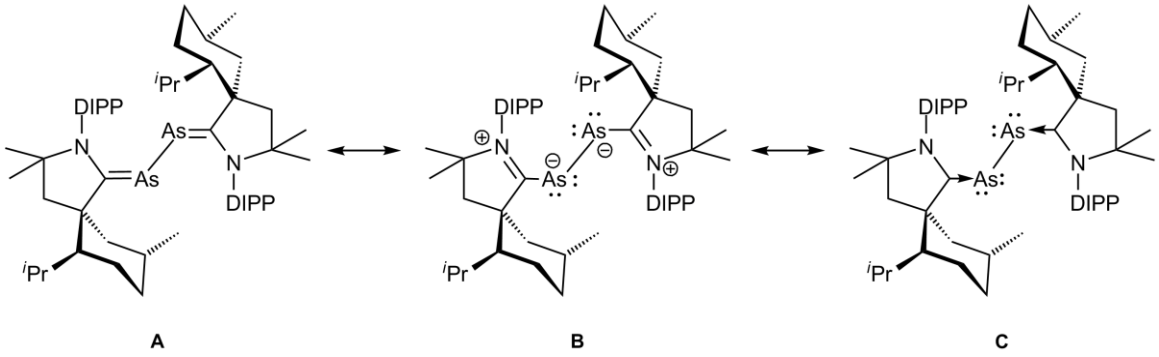

Scheme 4. Canonical forms of [(^{Menthyl}CAAC)$_2$As$_2$] (**43)** that may be described as 2,3-diarsabutadiene (**A**), a charge separated diarsanediid (**B**) or *bis*-arsinidine (**C**).

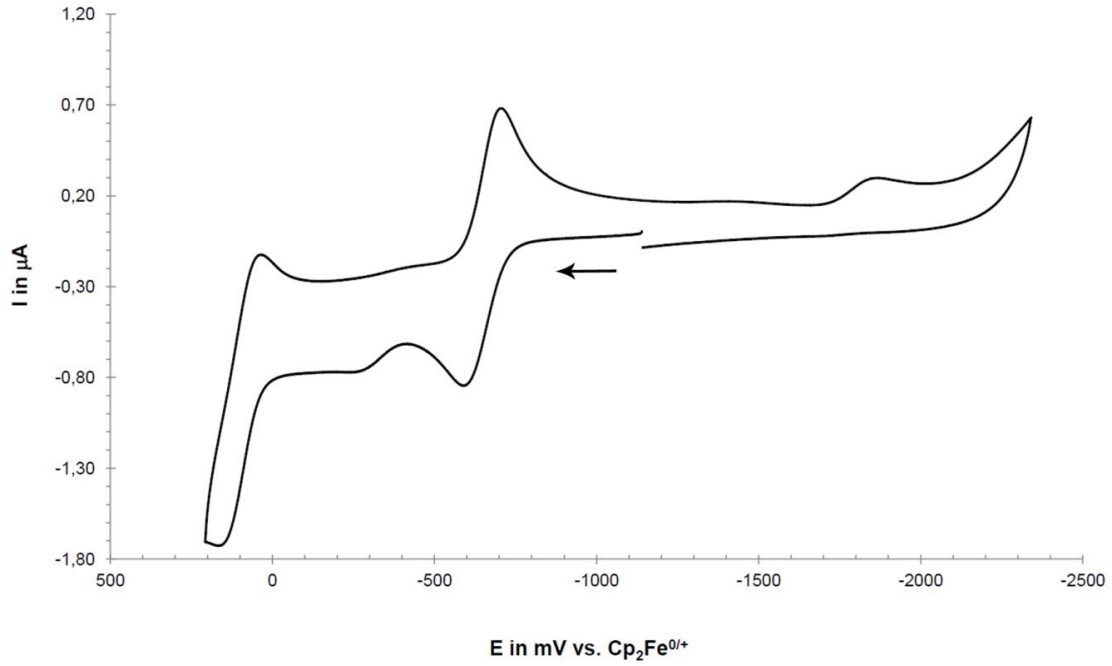

Figure 8. Cyclic voltammogram of **43** in THF containing 0.1 M [NBu_4][PF_6] at 298 K (ν = 100 mV/sec, Pt electrode). Data is referenced with Cobaltocene and specified vs. Ferrocene.

While the double bond nature between the carbene and the As_2 unit demonstrates the 2,3-diarsabutadiene like character of **43** (structure **A**), the shortened C–N bonds point to structure **B**. However, structures **B** and **C** clearly indicate an electron rich As_2 unit because of the donating character of the nitrogen atoms.

The cyclovoltammogram of **43** in THF solution shows a reversible first oxidation at $E_{1/2}$ = -658 mV vs. ferrocene (Figure 8). A second irreversible oxidation can be observed at $E_{1/2}$ = -350 mV. Compared to the corresponding P_2 analogue **21**, which shows a reversible oxidation at -536 mV vs. ferrocene and an irreversible one at 20 mV, **43** is oxidized more easily. It is also noteworthy, that in the forward bias the difference between the peaks of the first and second oxidation is with 308 mV much smaller than the difference of 556 mV observed for **21**. The easier oxidation may be explained as a direct consequence of the lower ionization energy of arsenic compared to phosphorus.[7] Another possible explanation can be given by the resonance forms of **43** (Scheme 4). As the tendency for the formation of double bonds is smaller for arsenic compared to phosphorus, the canonical form **A** is less important for **43** while the forms **B** and **C** with an electron rich As_2 unit are consequently more relevant. Hence, the arsenic derivative should be more electron rich than the P_2 compound and oxidation can be performed more easily. This trend is well reflected by shorter C–N bonds in **43** compared to the P_4 derivatives **18** and **21**.

While the reaction of the stable CAAC **17** with P_4 yields the carbene stabilized P_4 chain **18** (equation 3) its reaction with yellow arsenic leads to the formation of [(^{Menthyl}CAAC)$_2$As$_2$] (**43**). To get a deeper insight in the formation of **43**, DFT calculations at the B3LYP/def2-SVP level of theory were carried out by Dr. Alexey Y. Timoshkin (University of St. Petersburg). The result of these calculations is summarized in Table 1.

Table 1. Reaction energies (ΔE^o_0, kJ mol^{-1}), standard enthalpies (ΔH^o_{298}, kJ mol^{-1}), entropies (ΔS^o_{298}, J mol^{-1}) and Gibbs energies (ΔG^o_{298}, kJ mol^{-1}) for the gas phase processes.

Process	ΔE^o_0	ΔH^o_{298}	ΔS^o_{298}	ΔG^o_{298}
$P_4 \rightarrow 2\ P_2$	171.2	168.2	155.9	121.8
$As_4 \rightarrow 2\ As_2$	202.8	200.2	153.4	154.5
2 CAAC + $P_4 \rightarrow$ (CAAC)$_2$P$_4$ (trans)	-153.4	-135.6	-361.8	-27.8
2 CAAC + $P_4 \rightarrow$ (CAAC)$_2$P$_4$ (cis)	10.1	30.9	-384.3	145.4
2 CAAC + $As_4 \rightarrow$ (CAAC)$_2$As$_4$ (trans)	-69.8	-53.7	-350.3	50.7
2 CAAC + $As_4 \rightarrow$ (CAAC)$_2$As$_4$ (cis)	91.5	110.9	-368.3	220.6
(CAAC)$_2$P$_4$(trans) $\rightarrow$ (CAAC)$_2$P$_2$ + ½ P_2	9.6	7.5	30.7	-1.7
(CAAC)$_2$As$_4$(trans) $\rightarrow$ (CAAC)$_2$As$_2$ + ½ As_2	-8.5	-10.0	25.0	-17.4

For both, P_4 and As_4, the formation of an E_2 (E = P, As) unit is endothermic and therefore not probable. Hence, the reaction is likely to proceed via a successive degradation of the E_4 tetrahedron induced by a nucleophilic attack. The formation of a carbene stabilized E_4 chain is exothermic for phosphorus as well as arsenic but only in case of the trans isomer. The cis isomer is much higher in energy which disfavours its formation. Further fragmentation of $[(CAAC)_2E_4]$ into $[(CAAC)_2E_2]$ units is endothermic for phosphorus but exothermic for arsenic. This may explain why the P_4 chain is stable, while in case of arsenic the formation of **43** is observed.

Additionally, kinetic aspects may influence the reactivity of the $[(CAAC)_2E_4]$ molecules. As the As–As bonds are longer than the corresponding P–P bonds, the steric bulk of the used carbene may not be sufficient to provide a shielding of the As_4 chain which allows further reactions. In contrast, the P_4 chain is sufficiently protected to be isolated. However, the predicted reaction energies also allow an interpretation of the observed thermochromic behavior of the reaction mixture of **43**. The used excess of As_4 used in the reaction mixture is able to shift the equilibrium (equation 6) for the proposed fragmentation of $[(CAAC)_2As_4]$ to the left side. Additionally the cooling of the reaction mixture lowers the influence of entropy. These two factors together with the only slightly negative values for the reaction enthalpy point to the formation of $[(CAAC)_2As_4]$ upon cooling. The observed dark green color also indicates a more conjugated π-system (compare for the dark blue color of **18**) that would be realized in a hypothetical carbene stabilized As_4 chain.

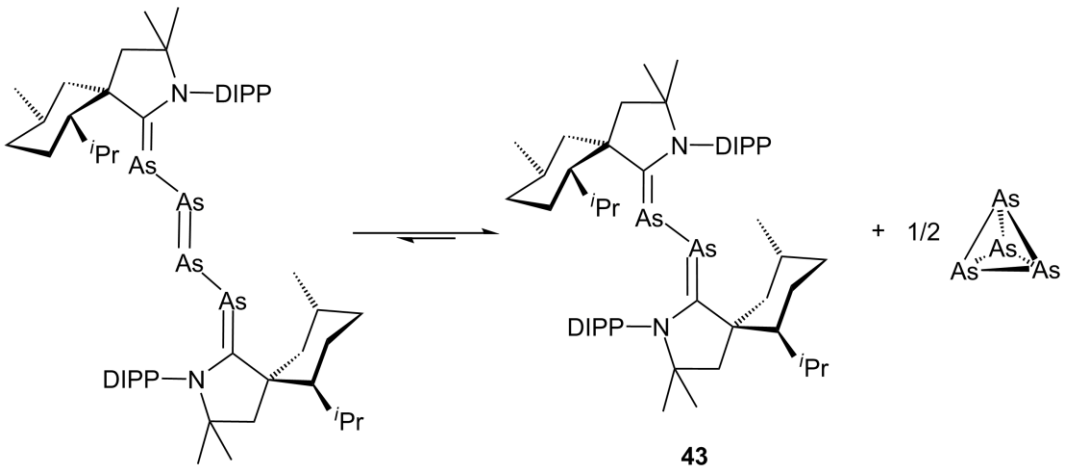

43 (6)

However, compound **43** is the first compound in which an As_2 unit in an end-on binding mode is derived directly from the degradation of As_4. Furthermore, it bears the potential to serve as starting material for the formation of arsenic-centered radicals by the chemical oxidation of **43**.

3.1.2 Reaction of yellow arsenic with ^{cHex}CAAC (19)

Independent of stochiometry, ^{cHex}CAAC (**19**) reacts with As_4 to afford the *iso*-tetraarsane [{^{cHex}CAAC}$_3$As$_4$] (**44**) in moderate yields (equation 7). Compound **44** is purified by extraction with Et_2O and subsequent crystallization. It is soluble in polar as well as non polar solvents.

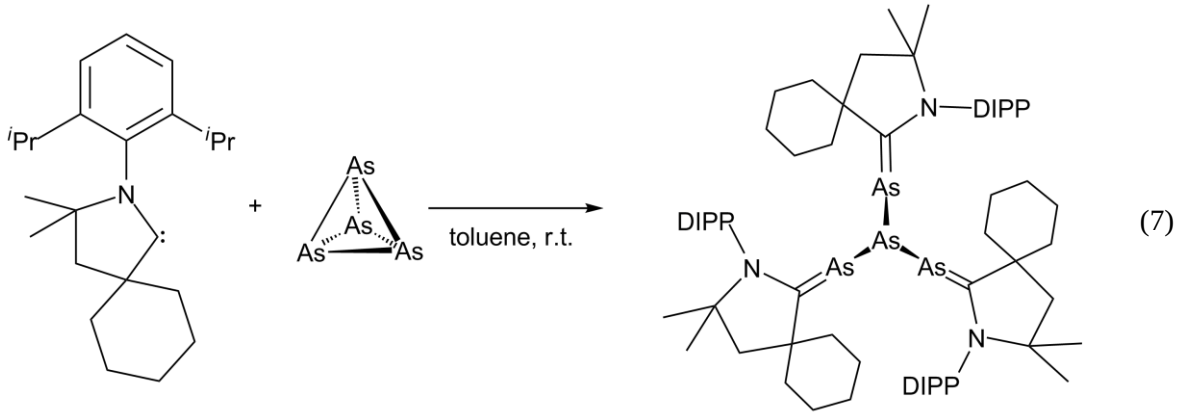

19 **44**

21 %

(7)

The ^{1}H NMR spectrum (C_6D_6) shows several signals that can be assigned to the three ^{cHex}CAAC units (see Figure 64 Appendix). In the ^{13}C{^{1}H} NMR spectrum (C_6D_6) the signal for the carbene carbon appears at δ = 224.5 ppm (Figure 65 Appendix), which is shifted downfield by about 20 ppm compared to the phosphorus derivative **20**, and is shifted upfield by about 85 ppm compared to the starting material **19**. Hence, the shielding of the carbene carbon atoms is less distinct in **44** than in **20**, which is due to a weaker π-bonding between arsenic and the carbene carbon. In the FD mass spectrum the molecular ion peak can be observed at *m*/*z* = 1275.4. Furthermore, a peak at *m*/*z* = 875.7 can be detected that corresponds to the [(^{cHex}CAAC)$_2$As$_3$]$^+$ cation. At *m*/*z* = 326.5 a peak for the protonated species [(^{cHex}CAAC)H]$^+$ appears.

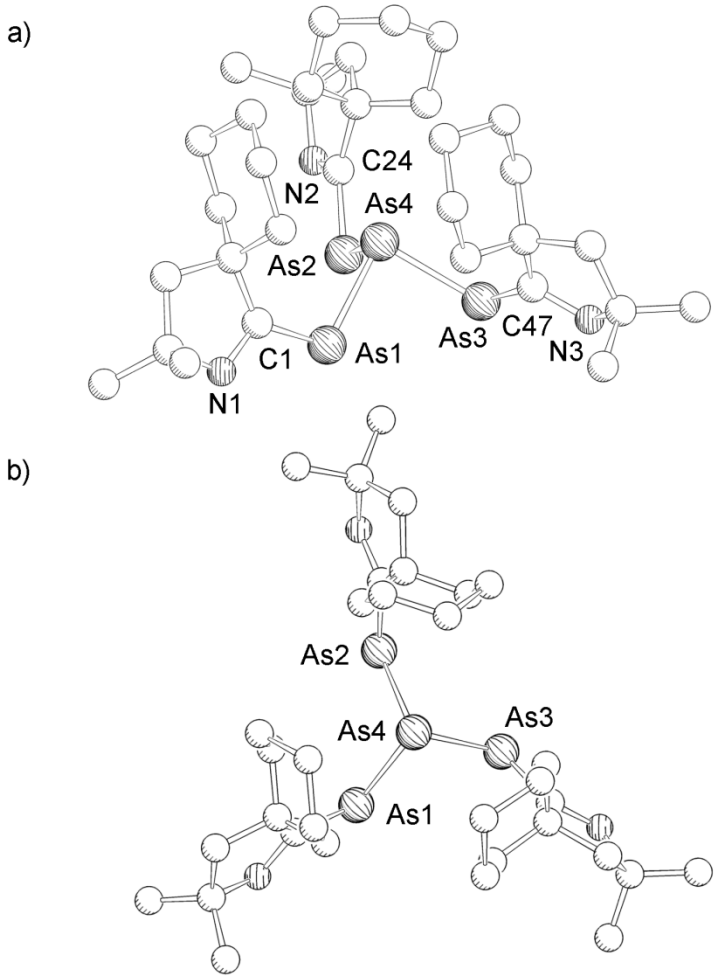

Figure 9. a) side view and b) top view of the molecular structure of **44** in the crystal. Hydrogen atoms as, 2,6-diisopropylphenyl substituents as well as Et_2O molecules are omitted for clarity. Selected bond lengths [Å] and angles [°]: As1–As4 2.4519(2), As2–As4 2.4508(2), As3–As4 2.4480(2), As1–C1 1.863(2), As2–C24 1.866(2), As3–C47 1.862(2), C1–N1 1.361(2), C24–N2 1.356(2), C47–N3 1.358(2), As1–As4–As2 90.40(1), As2–As4–As3 92.24(1), As3–As4–As1 89.29(1).

[(^{cHex}CAAC)$_3$As$_4$] (**44**) crystallizes as pale yellow blocks in the space group $P\bar{1}$ of the triclinic crystal system. The asymmetric unit contains one molecule of **44** together with two molecules of Et_2O. The molecular structure of **44** is depicted in Figure 9 and consists of a tripodal *iso*-tetraarsane that is stabilized by three ^{cHex}CAAC substituents. While the *cyclo*-hexyl groups of the CAAC substituents point towards the central arsenic atom and provide steric shielding, the diisopropylphenylgroups point away from atom As4. The steric protection is in this case large enough to stabilize the molecule, and further fragmentation as discussed in chapter 3.1.1 does not occur.

The angles around the central atom As4 range from 89.29(1)° to 92.24(1)° and deviate only slightly from the expected 90° angle. In contrast to [(^{cHex}CAAC)$_3$P$_4$] (**20**), in which all three angles add up to 90.15(2)°, **44** shows more distortion from a perfect local C_{3v} symmetry. The

As–As bond distances lie in the range between 2.4480(2) Å and 2.4519(2) Å and can be viewed as single bonds. With 1.863(2) Å, 1.866(2) Å and 1.862(2) Å, the As1–C1, As2–C24 and As3-C47 bond lengths compare well to the corresponding bond lengths in **43** and lie in between a single and double bond (1.96 Å and 1.81 Å).[68] The bonds between nitrogen and the carbene carbons are in the range from 1.356(2) Å to 1.361(2) Å and are slightly shorter than in **43** or in the phosphorus derivative **20** (1.368(2) Å to 1.374(2) Å).[47] The electronic structure of **44** may therefore be described analogously to the one of **43** as already discussed in chapter 3.1.1 (Scheme 4).

[(^{cHex}CAAC)$_3$As$_4$] (**44**) is the first compound with an *iso*-tertraarsane unit. While the reaction of the larger ^{Menthyl}CAAC (**17**) with P_4 and As_4 leads to different products, the reaction of ^{cHex}CAAC (**19**) with white phosphorus and yellow arsenic affords analogous compounds. However, the formation of an As_2 unit is not observed. This is in contrast to the reaction of **19** with P_4 in which, beside the formation of [(^{cHex}CAAC)$_3$P$_4$] (**20**), also the P_2 containing compound [(^{cHex}CAAC)$_2$P$_2$] (**21**) is detected (see equation 3). Anyway, the formation of an As_2 unit during the reaction of **19** with As_4 is not precluded but hard to observe due to the poor NMR properties of arsenic.

3.2 Formation of *cyclo*-E_4^{2-} units (E_4 = P_4, AsP_3, As_4) by a quintuply bonded dichromium complex[69]

As the nature of chemical bonding is of fundamental interest, the synthesis of compounds with high bond orders has drawn the attention of many chemists around the world. Especially chromium-chromium multiple bonds are of special interest as they provide very short metal-metal distances. Recently Kempe *et al.* reported the synthesis of [L_2Cr_2] (**45**) (L = (2,6-diisopropylphenyl)-{6-(2,6-dimethylphenyl)-pyridin-2-yl}-amide), which exhibits a formal chromium-chromium quintuple bond.[70] First reactivity studies of **45** towards oxygen and trimethylaluminium reveal its potential for the activation of small molecules. The reaction with $AlMe_3$ leads selectively to a formal oxidative addition of a carbon-aluminium bond to the chromium-chromium quintuple bond accompanied by a reduction of the formal bond order from five to four. Hence, **45** seems to be an ideal reagent for the 2 e^- reduction of E_4 tetrahedra.

3.2.1 The reactivity of $[L_2Cr_2]$ (45) towards white phosphorus

The reaction of $[L_2Cr_2]$ (**45**) with one equivalent of white phosphorus in THF at room temperature leads to the selective cleavage of two bonds of the P_4 tetrahedron and subsequent formation of $[L_2Cr_2(\mu,\eta^{1:1:2:2}\text{-}P_4)]$ (**46**) in excellent yields (equation 8).

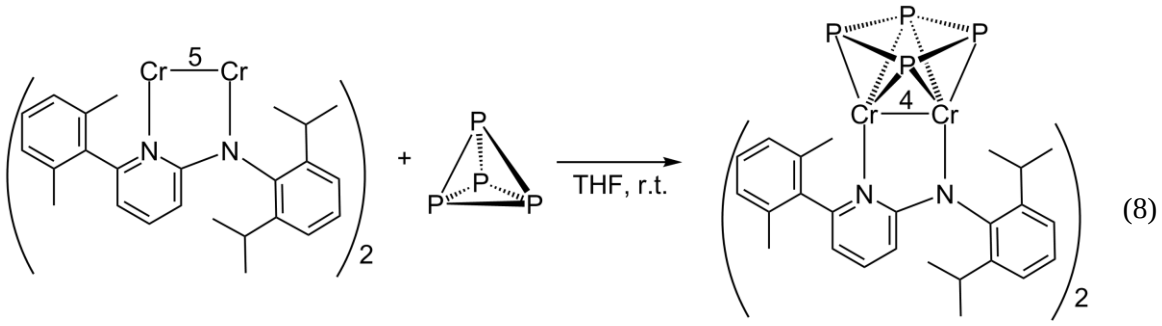

(8)

45 **46**

> 95 %

Compound **46** is isolated as analytically pure substance without further purification from the reaction mixture as dark green solid. It has good solubility in THF and toluene but is sparingly soluble in hexane. Recrystallization from a concentrated THF solution gives **46** as dark green crystals, suitable for X-ray structure analysis.

The ^{1}H and $^{13}C\{^{1}H\}$ NMR spectra (C_6D_6) of **46** show one set of characteristic signals for the amide ligand. The $^{31}P\{^{1}H\}$ NMR spectrum (C_6D_6) reveals two groups of signals at δ = 244.0 ppm and 275.6 ppm with equal integral intensities. In order to evaluate the coupling constants and the underlying spin system a simulation[71] of the spectrum was carried out which points to an AA'MM' spin system (Figure 10). The two pairs of P atoms chemically, but not magnetically equivalent. The result of the simulation is summarized in Table 2. The assignment of the signals is discussed later.

Table 2. Chemical shifts and coupling constants gained from the simulated $^{31}P\{^{1}H\}$ NMR spectrum of **46**.

$\delta_{AA'}$ = 275.5 ppm	$\delta_{MM'}$ = 244.0 ppm	$^{1}J_{A'M}$ = 295.5 Hz
$^{1}J_{A'M'}$ = 253.0 Hz	$^{1}J_{AM'}$ = 296.2 Hz	$^{1}J_{AM}$ = 253.2 Hz
$^{2}J_{MM'}$ = 17.7 Hz	$^{2}J_{AA'}$ = 19.0 Hz	

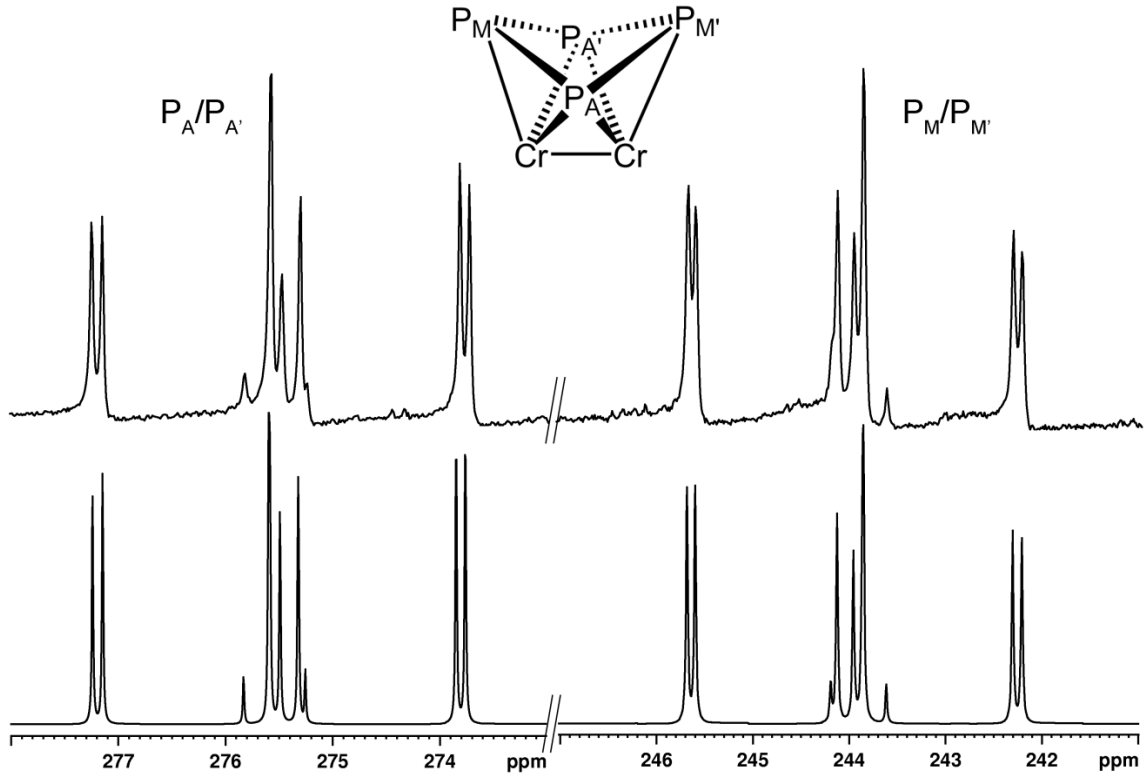

Figure 10. Experimental (C_6D_6, 300 K; top) and simulated (bottom) $^{31}P\{^1H\}$ NMR spectrum of **46**.

$[L_2Cr_2(\mu,\eta^{2:2:1:1}\text{-}P_4)]$ (**46**) crystallizes as dark green needles in the triclinic space group $P\bar{1}$. The asymmetric unit contains one molecule of **46** which structure is shown in Figure 11. The central structural motif in **46** is a nearly square planar *cyclo*-P_4 ring that is located above the Cr_2 unit in a unique $\eta^{1:1:2:2}$ coordination mode. The Cr–P bond distances are larger for the bridging P atoms (P1–Cr1 2.679(1) Å, P1–Cr2 2.687 (1) Å, P3–Cr2 2.678(1) Å, P3–Cr1 2.682(1) Å) than for the terminal ones (P2–Cr2 2.379(1) Å, P4–Cr1 2.362(1) Å). The bond angles within the four-membered ring vary from 86.53(5)° to 91.67(5)° whereupon the larger angles are observed for the bridging phosphorus atoms. The P1–P4 (2.176(1) Å), P1–P2 (2.179(2) Å), P2–P3 (2.168(1) Å), P3–P4 (2.183(2) Å) bonds are shorter than a P–P single bond in P_4 (2.21(2) Å determined by electron diffraction,[72] 2.186(1) – 2.194(1) Å determined by DFT calculations[73]). The Cr1–Cr2 distance of 1.8664(1) Å is lengthened by more than 0.1 Å compared to the starting material (1.750(1) Å[70]), and is indicative for a formal Cr–Cr quadruple bond. This, together with the short P–P bond lengths points to a selective 2 e^- reduction of the P_4 tetrahedron and the formation of a rare *cyclo*-P_4^{2-} ligand.

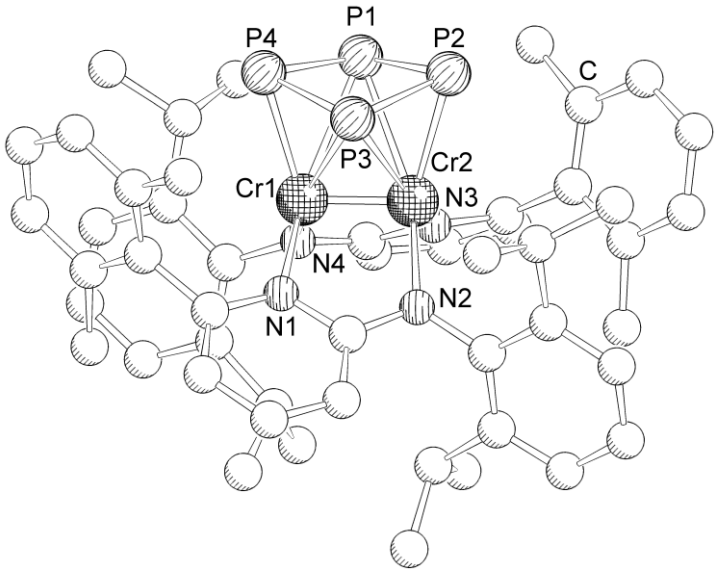

Figure 11. Molecular structure of **46** in the crystal. Hydrogen atoms omitted for clarity. Selected bond lengths [Å] and angles [°]: N1–Cr1 2.029(3), N2–Cr2 2.037(3), N3–Cr2 2.029(3), N4–Cr1 2.036 (3), P1–P4 2.176(1), P1–P2 2.179 (2), P2–P3 2.168(1), P3–P4 2.183 (2), P1–Cr1 2.679(1), P1–Cr2 2.687 (1), P2–Cr2 2.379(1), P3–Cr2 2.678(1), P3–Cr1 2.682(1), P4–Cr1 2.362(1), Cr1–Cr2 1.8664(8), P4–P1–P2 91.55(5), P3–P2–P1 86.85(5), P2–P3–P4 91.67(5), P1–P4–P3 86.53(5).

To understand further the formation of **46**, DFT calculations at the B3LYP/def2-SVP and def2-TZVPP level of theory were carried out by Dr. Alexey Y. Timoshkin (University of St. Petersburg). The reaction of **45** with P_4 to give **46** is predicted to be exothermic by 24 kJ mol^{-1} in the gas phase. Taking into account that the planarization of P_4 requires 335 kJ mol^{-1}, this energy has to be compensated for by the interaction of the planar P_4 unit with **45**. The calculations also predict an elongation of the Cr–Cr bond by 0.098 Å, which is consistent with the experimental value of 0.117 Å. The change of the bonding situation is also exemplified by the alteration of the Wiberg bond index (WBI) that decreases from 4.39 in **45** to 2.91 in **46** indicating the oxidation of the Cr–Cr center by white phosphorus.

3.2.2 The reaction of $[L_2Cr_2]$ (45) with yellow arsenic

The synthesis of $[L_2Cr_2(\mu,\eta^{1:1:2:2}\text{-}As_4)]$ (**47**) is achieved by the reaction of yellow arsenic with one equivalent of $[L_2Cr_2]$ (**45**) in toluene at room temperature (equation 9). Analytically pure **47** can be obtained by crystallization from a concentrated toluene solution upon cooling. Compound **47** is well soluble in THF and toluene but only sparingly soluble in aliphatic solvents.

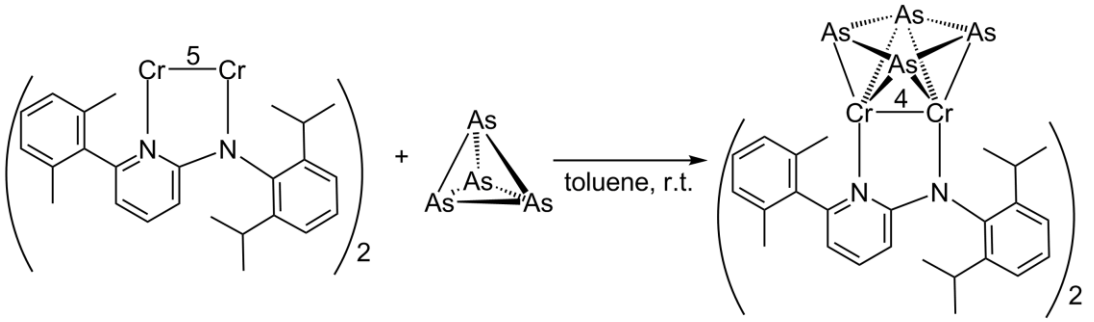

(9)

45 **47**

68 %

The ^{1}H and $^{13}C\{^{1}H\}$ NMR spectra (C_6D_6) of **47** show one characteristic set of signals for ligand L. Compared to **46**, especially the signals for the Me and ^{i}Pr substituents close to the *cyclo*-As_4 ligand are shifted downfield by about 0.1 ppm.

$[L_2Cr_2(\mu,\eta^{1:1:2:2}\text{-}As_4)]$ (**47**) crystallizes as dark green prisms in the space group $P\bar{1}$ of the triclinic crystal system. The asymmetric unit contains one molecule of **47**. Its molecular structure is depicted in Figure 12.

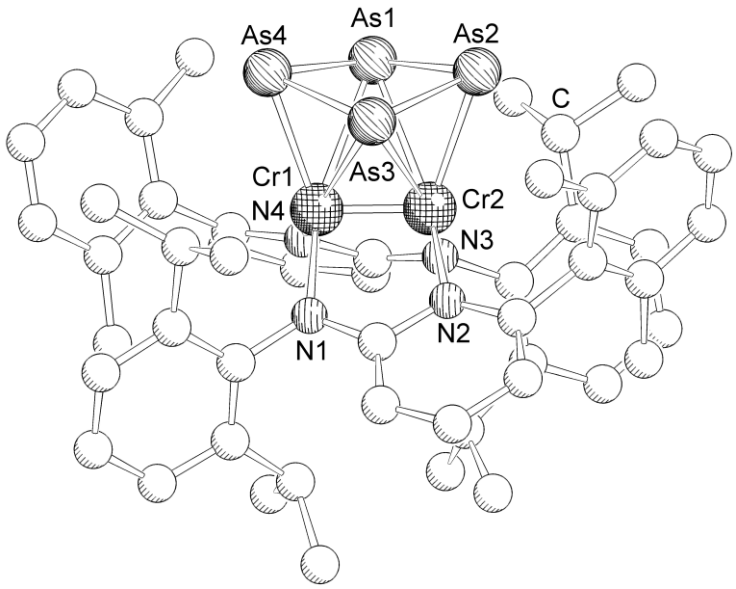

Figure 12. Molecular structure of **47** in the crystal. Hydrogen atoms omitted for clarity. Selected bond lengths [Å] and angles [°]: N1–Cr1 2.031(6), N2–Cr2 2.049(6), N3–Cr2 2.036(5), N4–Cr1 2.045(5), Cr1–As4 2.505(1), Cr1–As3 2.769(1), Cr1–As1 2.786(1), Cr2–As2 2.490(1), Cr2–As3 2.769(1), Cr2–As1 2.779(1), As1–As2 2.398(1), As1–As4 2.405(1), As2–As3 2.406(1), As3–As4 2.388(1), Cr1–Cr2 1.863(2), As2–As1–As4 92.10(4), As1–As2–As3 85.59(4), As4–As3–As2 92.32(4), As3–As4–As1 85.81(4).

Compound **47** is isostructural with **46**, with a *cyclo*-As_4 unit located above the Cr–Cr center in a $\eta^{1:1:2:2}$ coordination mode. By analogy to the phosphorus derivative **46** the terminal Cr–As (Cr1–As4 2.505(1) Å and Cr2–As2 2.490(1) Å) bonds are shorter than the bridging ones (2.769(1) Å - 2.786(1) Å). The bond angles within the *cyclo*-As_4 ligand vary from 85.59(4)° to 92.32(4)° and deviate a little more from a perfect 90° angle than they do in **46**. Hence, the *cyclo*-As_4 unit is slightly more distorted than the *cyclo*-P_4 unit. The As1–As2 (2.398(1) Å), As1–As4 (2.405(1) Å), As2–As3 (2.406(1) Å), As3–As4 (2.388(1) Å) bonds are shorter than an As–As single bond (2.435(4) Å determined by electron diffraction,[72] 2.4372 Å determined via DFT calculations[74]) and the Cr–Cr bond distance is increased from 1.750(1) Å to 1.863(2) Å. The short As–As bonds together with the elongated Cr–Cr bond indicate a 2 e^- reduction of yellow arsenic (as already discussed in chapter 3.2.1) and the subsequent formation of a *cyclo*-As_4^{2-} ligand.

3.2.3 The reaction of $[L_2Cr_2]$ (45) with AsP_3

The reaction of $[L_2Cr_2]$ (**45**) with AsP_3 in THF at room temperature results in the formation of the expected compound $[L_2Cr_2(\mu,\eta^{1:1:2:2}\text{-}AsP_3)]$ (**48**) in good yields (equation 10). It is obtained as greenish brown solid from the reaction mixture after removal of the solvent and washing the residue with small amounts of hexane. It readily dissolves in polar solvents and has poor solubility in aliphatic solvents. Crystallization from a concentrated THF solution affords **48** as greenish brown plates, suitable for X-ray structure analysis.

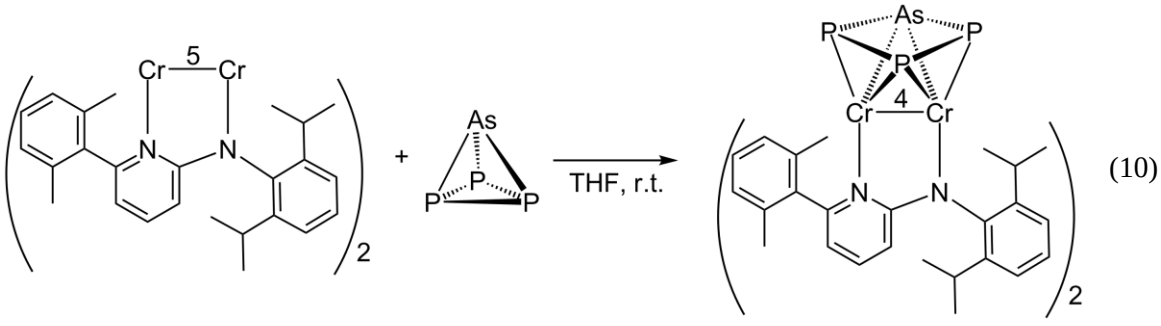

45 **48**

61 % (10)

In the ^1H and $^{13}C\{^1H\}$ NMR spectra (C_6D_6), two sets of signals for the ligand can be observed. While one of the sets shows chemical shifts that are similar to the ones found in **46**, the other one reveals signals that compare well to that of **47**. The presence of two signal sets point to a different chemical and magnetic environment of the ligands, which is the case when one of the bridging positions is occupied by arsenic. In the $^{31}P\{^1H\}$ NMR spectrum (C_6D_6) three doublet of doublets are observed at δ = 255.6 ppm (dd, 1P, $^1J_{PP}$ = 316Hz, $^2J_{PP}$ = 23Hz), 260.6 ppm (dd, 1P,

$^{1}J_{PP}$ = 274Hz, $^{2}J_{PP}$ = 23Hz), 291.0 (dd, 1P, $^{1}J_{PP}$ = 316Hz, $^{1}J_{PP}$ = 274Hz). The signals possess equal integral intensities and the coupling constants reveal an AMN spin system which is in good agreement with the expected C_1 symmetry of the molecule. As arsenic occupies one of the bridging positions (see discussion of crystal structure of **48**) of the *cyclo*-AsP_3 ring, the upfield shifted signals may be assigned to the terminal phosphorus atoms while the downfield shifted signal corresponds to the bridging positions. As the relative chemical shifts observed in **48** are similar to those in the P_4 derivative **46** the assignment of signals may also be used for the $^{31}P\{^{1}H\}$ NMR spectrum of **46**.

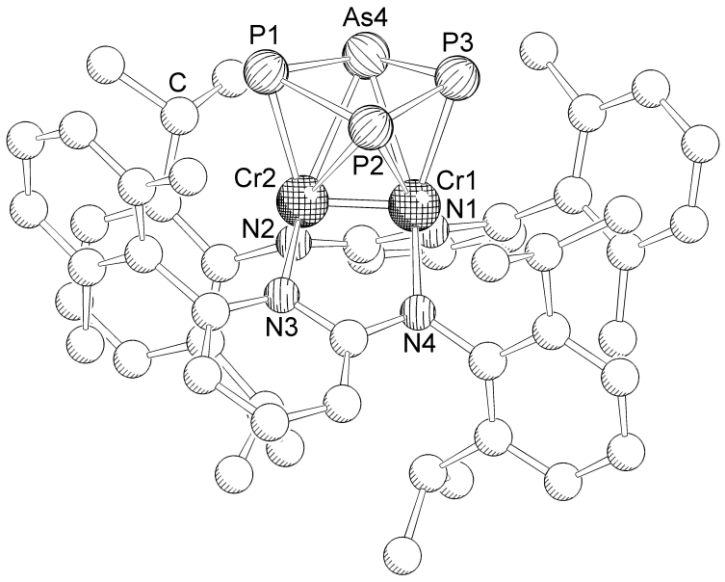

Figure 13. Molecular structure of **48** in the crystal. For clarity reasons only one of the two possible positions of arsenic is shown and hydrogen atoms are omitted. Selected bond lengths [Å] and angles [°]: N1–Cr1 2.031(2), N2–Cr2 2.035(2), N3–Cr2 2.027(2), N4–Cr1 2.035(2), Cr2–P1 2.3814(6), Cr2–P2 2.702(5), Cr1–P2 2.561(5), Cr1–P3 2.3926(8), Cr1–As4 2.76(1), Cr2–As4 2.77(1), P1–P2 2.211(2), P2–P3 2.095(5), P3–As4 2.26(1), As4–P1 2.30(1), Cr1–Cr2 1.8735(5), P1–P2–P3 91.0(2), P2–P3–As4 91.7(3), P3–As4–P1 89.4(4), As4–P1–P2 83.6(3).

$[L_2Cr_2(\mu,\eta^{1:1:2:2}\text{-}AsP_3)]$ (**48**) crystallizes in the triclinic space group $P\bar{1}$ as greenish brown plates. The asymmetric unit contains one molecule of **48**. X-ray structure analysis confirms the exclusive population of the bridging positions by arsenic. While the terminal positions P1 and P3 are only occupied by phosphorus, arsenic is found with a 50 % probability at the positions 2 and 4 (labeling according to Figure 13). The placement of arsenic leads to a distortion of the four-membered ring due to the size difference of the two homologues. The terminal Cr2–P1 (2.3814(6) Å) and Cr1–P3 (2.3926(8) Å) bond lengths compare well to the corresponding bonds in **46**. The average Cr–As bond distance is with 2.77(1) Å in the same range as the Cr–As bond distances in **47**. The divergent Cr1–P2 and Cr2–P2 bond lengths of 2.561(5) Å and 2.702(5) Å

indicate an asymmetric coordination which is also reflected by the P1–P2 and P2–P3 bond distances of 2.211(2) Å and 2.095(5) Å. However, the found Cr1–Cr2 bond length of 1.8735(5) Å is only slightly longer than the ones in **46** and **47** (1.8664(8) Å and 1.863(2) Å, respectively) but can still be viewed as a quadruple bond. Hence, complex **48** is the first example of a *cyclo*-AsP_3^{2-} ligand.

3.2.4 The coordination behavior of $[L_2Cr_2(\mu,\eta^{1:1:2:2}\text{-}P_4)]$ (46) towards $[\{W(CO)_5\}(thf)]$

As **46** bears accessible lone pairs, its reactivity towards Lewis acids was investigated by reacting it with one equivalent of $[W(CO)_5(thf)]$. The reaction proceeds in THF at room temperature within 48 hours to give $[\{L_2Cr_2\}(\mu_3,\eta^{1:1:1:2:2}\text{-}P_4)\{W(CO)_5\}]$ (**49**) in moderate yields (equation 11). It is well soluble in polar solvents like dichloromethane and nearly insoluble in aliphatic solvents. Dark red crystals of **49**, suitable for X-ray structure analysis are obtained from a saturated dichloromethane solution upon cooling.

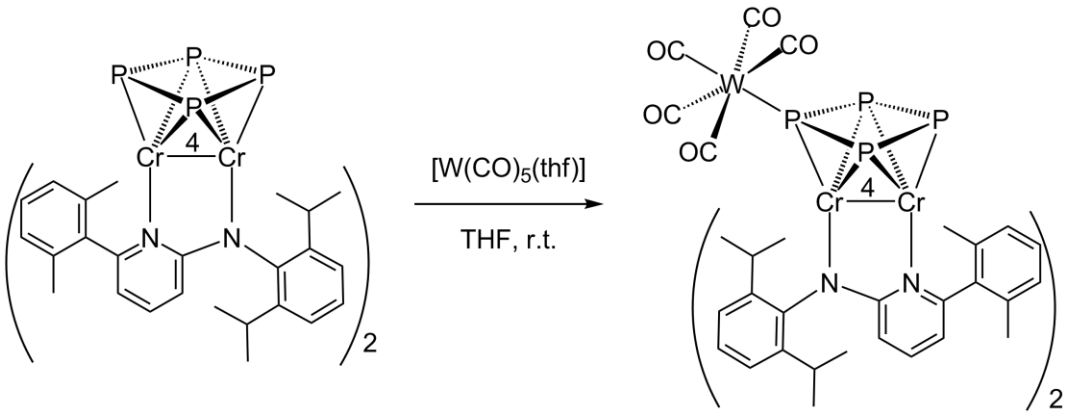

46 **49**

19 % (11)

The ^1H and $^{13}C\{^1H\}$ NMR spectra (CD_2Cl_2) of **49** show characteristic signals for the ligands L that are slightly shifted compared to the signals observed for **46**. In the $^{31}P\{^1H\}$ NMR spectrum (CD_2Cl_2) a broad pseudo triplet is observed at δ = 250 ppm together with a broad singlet between δ = 210 and 230 ppm. The broad signal indicates dynamic behavior in solution which may best be explained by a scrambling of the tungsten carbonyl fragment. Furthermore, the chemical shift of δ = 250 ppm for the non coordinating phosphorus atoms is indicative of coordination of the bridging positions P1 and P3 (Figure 11). To slow down the scrambling of the Lewis acid a variable-temperature (VT) $^{31}P\{^1H\}$ NMR experiment was performed (Figure 14). At 183 K the dynamics of the complex are suppressed and a resolved spectrum can be observed. Due to the low

solubility of **49** at low temperatures no tungsten satellites can be detected. Nevertheless an assignment of the signals can be achieved on the basis of chemical shifts and a simulation[71] of the splitting pattern (Figure 15).

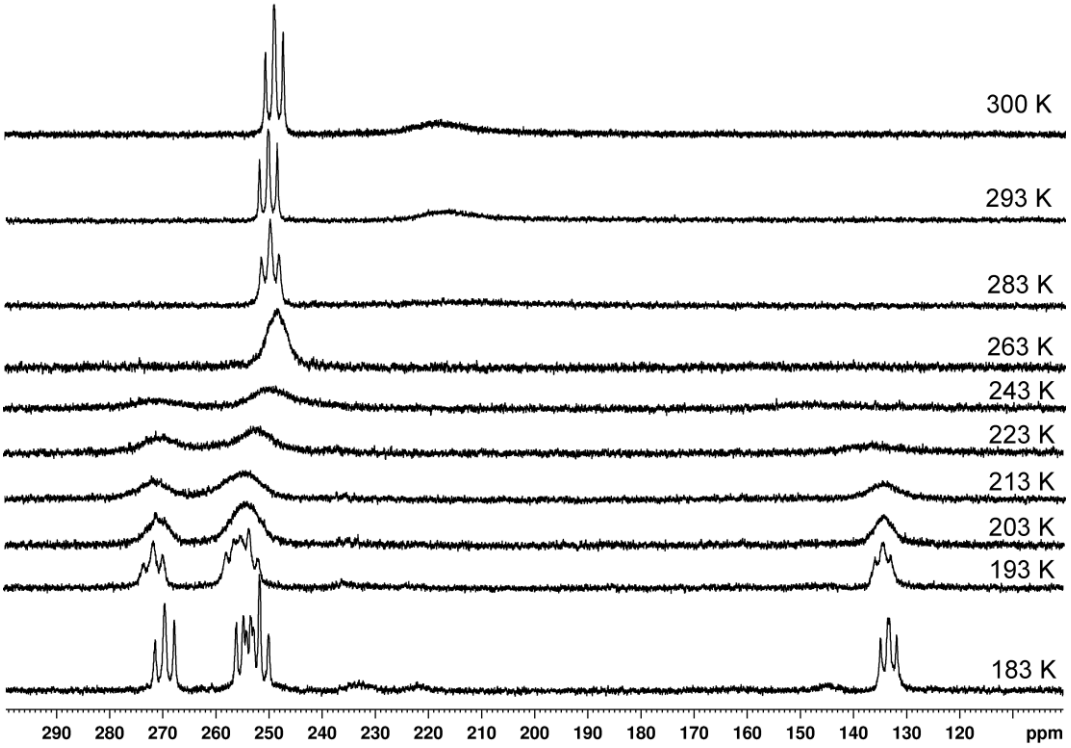

Figure 14. Experimental (CD_2Cl_2) $^{31}P\{^1H\}$ NMR spectra (CD_2Cl_2) of **49** at different temperatures.

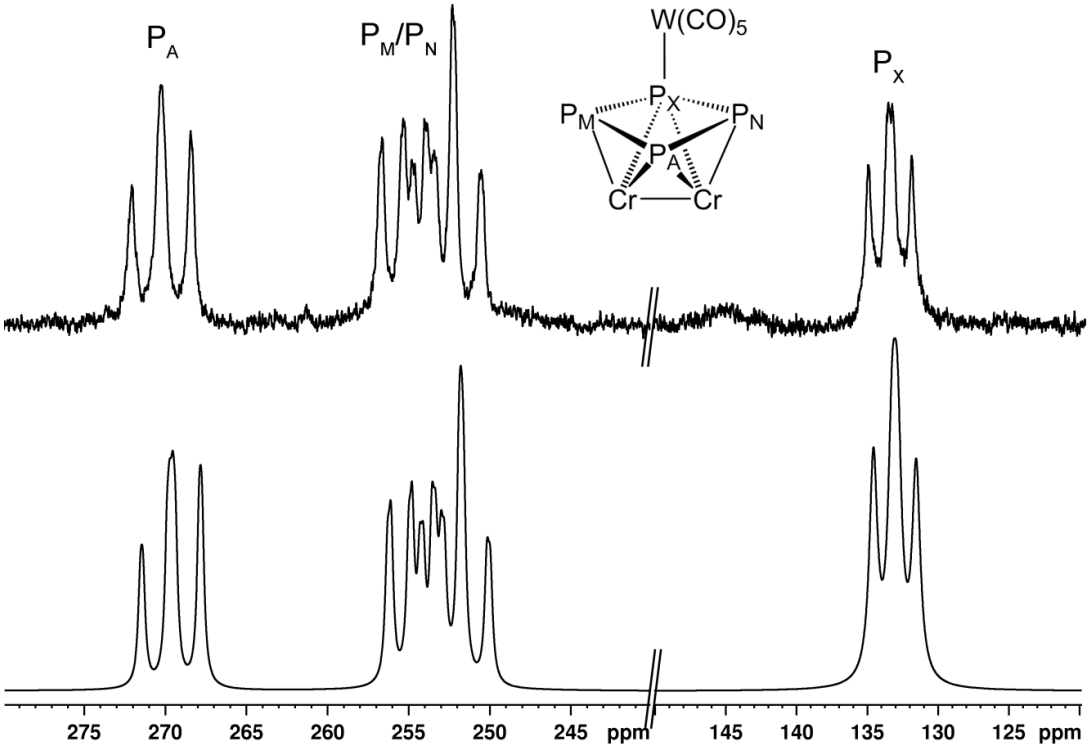

Figure 15. Experimental (CD_2Cl_2, 183 K; top) and simulated (bottom) $^{31}P\{^1H\}$ NMR spectrum of **49**.

In the $^{31}P\{^{1}H\}$ NMR spectrum (CD_2Cl_2) at 183 K three groups of signals arise at δ = 269 ppm, 255 ppm and 133 ppm with a ratio of 1:2:1. Due to its large upfield shift the latter one can be assigned to the phosphorus atom coordinating to the tungsten atom. The signal group at δ = 255 ppm consists of two overlapping signals. It shows a complex splitting pattern and its chemical shift corresponds to the terminal non-coordinating P atoms in **46**. The broadened triplet at δ = 269 ppm is detected in the same range as a non-coordinating bridging P atom in **46**. Hence, the spectrum at low temperatures clearly indicates the coordination of one of the two bridging P atoms to the $[W(CO)_5]$ group. Simulation of the spectrum proves the expected AMNX spin system and affords the associated chemical shifts and coupling constants (Table 3).

Table 3. Chemical shifts and coupling constants from the simulated $^{31}P\{^{1}H\}$ NMR spectrum of **49**.

δ_A = 269.5 ppm	δ_M = 254.6 ppm	δ_N = 251.8 ppm
δ_X = 133.4 ppm	$^{1}J_{AM}$ = 322.0 Hz	$^{1}J_{AN}$ = 267.6 Hz
$^{1}J_{MX}$ = 212.6 Hz	$^{1}J_{NX}$ = 282.7 Hz	$^{2}J_{AX}$ = 25.1 Hz
$^{2}J_{MN}$ = 33.8 Hz		

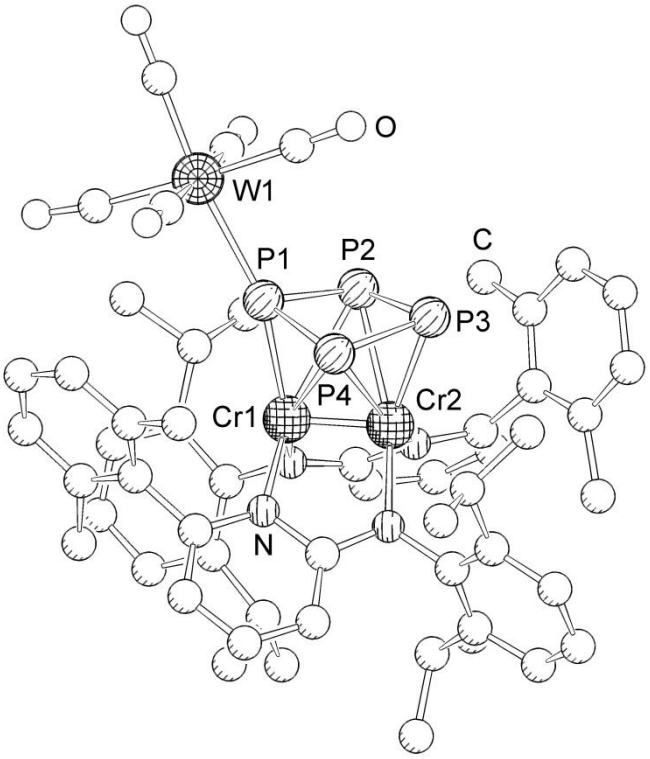

Figure 16: Molecular structure of **49** in the crystal. Hydrogen atoms omitted for clarity. Selected bond lengths [Å] and angles [°]: Cr1–P1 2.3740(7), Cr1–P2 2.7627(8), Cr1–P4 2.7364(9), Cr2–P3 2.3381(8), Cr2–P2 2.6409(8), Cr2–P4 2.6941(8), P1–W1 2.5648(6), P1–P2 2.187(1), P2–P3 2.172(1), P3–P4 2.180(1), P4–P1 2.180(1), Cr1–Cr2 1.9037(6), P1–P2–P3 90.04(4), P2–P3–P4 88.66(4), P3–P4–P1 89.99 (4), P4–P1–P2 88.27(4), Cr1–P1–W1 159.38(4).

[{L_2Cr_2}(μ_3,$\eta^{1:1:1:2:2}$-P_4){$W(CO)_5$}] (**49**) crystallizes as dark red blocks in the space group $P\bar{1}$ of the triclinic crystal system. The asymmetric unit contains one molecule of **49** together with two molecules of dichloromethane. Surprisingly, X-ray structure analysis does not confirm the coordination of the [$W(CO)_5$] fragment by one of the bridging P atoms but shows the coordination of one of the terminal phosphorus atoms (Figure 16). The P–P bond distances vary from 2.172(1) Å to 2.187(1) Å and compare well to the corresponding bond lengths in the starting material **46**. While the Cr1–P1 bond lenth with 2.3740(7) Å compares well to the terminal bonds in **46**, the Cr2–P3 bond is slightly shortened (2.3381(8) Å). All other Cr–P bond lengths are essentially the same as in **46**. The Cr1–Cr2 bond adds up to 1.9037(6) Å and is a little bit longer than in the starting material which may be explained by the electron withdrawing character of the Lewis acid.

NMR investigations and X-ray structure analysis show different constitutional isomers in solution and in the solid state. DFT calculations at the B3LYP/def2-SVP and def2-TZVPP level of theory were carried out to investigate further the bonding situation in **49** as well as the origin of this difference (Dr. Alexey Y. Timoshkin, University of St. Petersburg). Thereafter the reaction of **46** with [$W(CO)_5$(thf)] is exothermic by 93 kJ mol^{-1} in the gas phase. The calculated Cr–Cr distance increases marginally by 0.008 Å (0.037 Å experimentally) which means the quadruple bond is nearly uninfluenced by the coordination. To clarify the discrepancy between the structure in solution and solid state, four isomers on the potential energy surface were calculated (Figure 17).

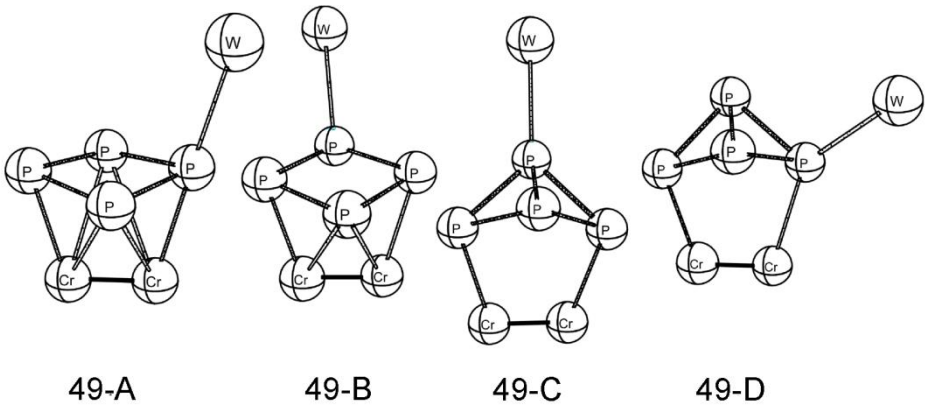

Figure 17. Theoretical isomers of **49**. Carbonyl groups and organic ligands are omitted for clarity.

At the B3LYP/def2-TZVPP level of theory **49-A** is predicted to be lowest in energy while the isomers **49-B**, **49-C** and **49-D** are 12, 53 and 82 kJ mol^{-1} higher in energy, resepctively. By using the smaller def2-SVP basis set, isomer **49-B** is predicted to be 2 kJ mol^{-1} lower in energy compared to **49-A**. However, since the energy difference between **49-A** and **49-B** is quite small, an equilibrium between the isomers is reasonable and explains the observation of different isomers in solution and solid state.

3.3 The selective formation of tetrapnictido-*bicyclo*[1.1.0]butane complexes

The cleavage of one bond of the E_4 tetrahedron (E_4 = P_4, As_4 AsP_3) by a formal 2 e^- reduction leads to the formation of a tetrapnictido-*bicyclo*[1.1.0]butane unit that is often referred to as a butterfly ligand. As butterfly complexes represent the initial intermediates of the E_4 degradation they are interesting research targets in means of their stability, reactivity and coordination behavior. To date, several complexes with this type of ligand have been synthesized (see section 1.2). Unfortunately, the reported complexes are usually obtained in moderate yields as the synthetic routes normally include elevated temperatures which leads to further degradation and reaggregation products.[34, 36-37, 39, 75] Additionally, time consuming chromatographic workup is often needed. Hence, an improvement of the synthetic strategy is desirable that allows enhanced selectivity, higher yields and easier work-up. Furthermore, novel synthetic concepts should be developed that grant access to new butterfly compounds, including transition-metal-stabilized complexes of P_4, AsP_3 and As_4, as well as carbon-substituted molecules derived directly from P_4.

3.3.1 Improved synthetic strategy for [{Cp'''Fe(CO)$_2$}$_2$] (10b) – Synthesis of K[Cp'''Fe(CO)$_2$] (50)

Because of the steric bulk of the Cp''' ligand the direct formation of **10b** by the reaction of Cp'''H with [Fe(CO)$_5$] is not suitable. Therefore in our group a synthetic strategy was developed that uses [Cp'''Fe(CO)$_2$Br] as the key intermediate.[56, 76] It is reduced with [Cp_2Co] to give the desired product [{Cp'''Fe(CO)$_2$}$_2$] (**10b**) in moderate yields. As cobaltocene is a quite weak reducing agent it has to be used in excess together with long reaction times to achieve a complete reduction of [Cp'''Fe(CO)$_2$Br]. The separation of **10b** from unreacted [Cp_2Co] is achieved by coloumn chromatography which limits the batch size and lowers the yields. Therefore the reduction of [Cp'''Fe(CO)$_2$Br] is now performed with KC_8 as reducing agent to give **10b** together with the further reduced complex K[Cp'''Fe(CO)$_2$] (**50**) in good yields within two days (equation 12).

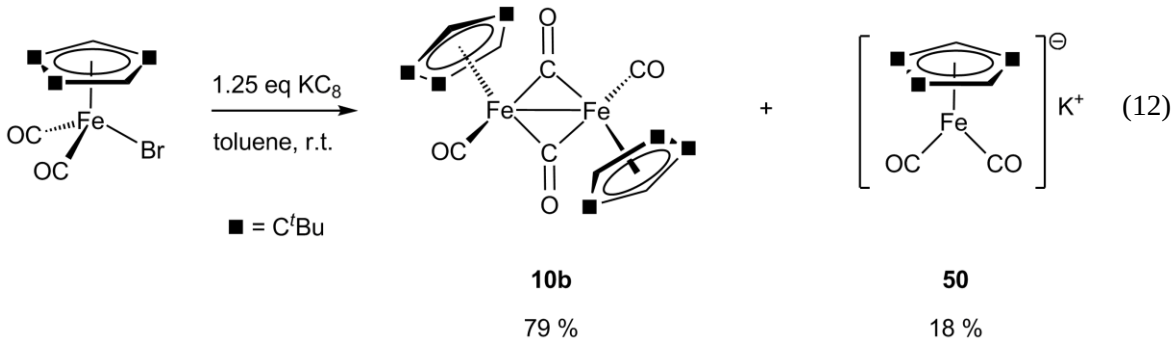

(12)

The two complexes **10b** and **50** are obtained as a mixture that can be filtered from the formed graphite. Extraction of the crude product with acetonitrile gives analytically pure **10b**. The acetonitrile fraction contains mainly the anionic complex **50** together with traces of **10b** that can be removed by washing with hexane. As no column chromatographic work-up is necessary the reaction can be scaled up easily. Additionally, the new synthetic route is faster, affords higher yields and a smaller amount of solvent is needed.

[{Cp'''Fe(CO)$_2$}$_2$] (**10b**) is obtained as brownish purple solid that is well soluble in polar and nonpolar solvents, but only scarcely soluble in acetonitrile. Its ^{1}H NMR spectrum (C_6D_6) shows three sharp singlets at δ = 1.22, 1.51 and 4.53 ppm with a ratio of 9:18:2 that can be assigned to the protons of the Cp''' ligands.[56, 76] The IR spectrum of **10b** reveals three absorption bands at ν = 1955, 1933 and 1753 cm^{-1} for the carbonyl ligands indicating terminal as well as bridging coordination modes.

K[Cp'''Fe(CO)$_2$] (**50**) is isolated as an orange solid that is well soluble in toluene and THF, moderately soluble in acetonitrile and insoluble in hexane. Upon dissolving in halogenated solvents it decomposes. The ^{1}H NMR spectrum (C_6D_6) reveals three slightly broadened singlets for a freely rotating Cp''' ligand at δ = 1.40 (9H), 1.56 (18H) and 4.65 (2H) ppm. In the IR spectrum of **50** two absorption bands at ν = 2001 and 1894 cm^{-1} for the carbonyl ligands can be detected. Compared to the starting material [Cp'''Fe(CO)$_2$Br][76] with carbonyl bands at ν = 2032 and 1970 cm^{-1}, the signals for **50** are red-shifted, which is due to the smaller formal oxidation number of iron and the consequently stronger π backbonding.

3.3.2 Optimized synthesis of [{Cp'''Fe(CO)$_2$}$_2$(μ,$\eta^{1:1}$-P$_4$)] (9b)

The synthesis of **9b** has first been described by Scherer *et al.* in the late 1990s by the short time thermolysis of [{Cp'''Fe(CO)$_2$}$_2$] (**10b**) with white phosphorus in boiling toluene.[37] Due to the elevated temperature during the reaction further decarbonylation reactions occur. Hence, the product has to be purified by coloumn chromatography at -20 °C. The low temperature is needed since **9b** is decarbonylated by silica gel at room temperature. The synthesis is therefore time consuming and only small batches can be handled. Additionally the published yield of 78 % could not be reproduced in our group. Usually **9b** is obtained in 40 – 50 % yield.

Surprisingly, our results show that **10b** reacts immediately with white phosphorus already at room temperature to give the desired butterfly complex **9b** (equation 13). ^{1}H and ^{31}P{^{1}H} NMR experiments clearly show a complete reaction with exclusive formation of **9b**. The formation of

any side product cannot be observed. Hence, no further purification steps are needed. Furthermore the batch size is not limited anymore.

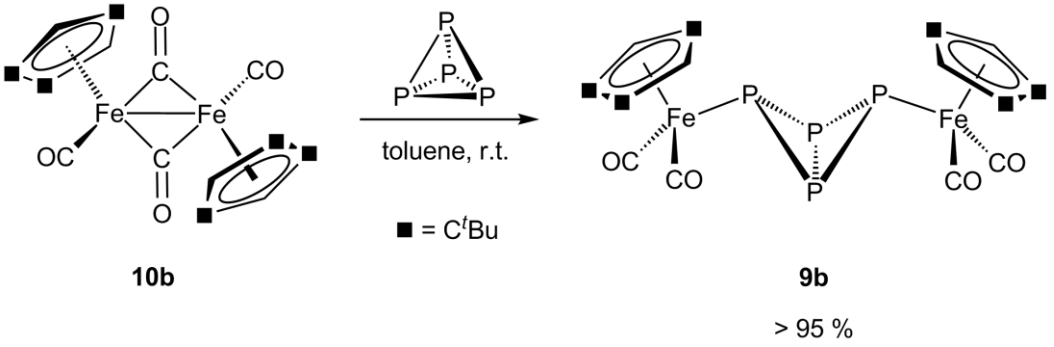

10b **9b**

> 95 %

(13)

[{Cp'''Fe(CO)$_2$}$_2$(μ,$\eta^{1:1}$-P$_4$)] (**9b**) is isolated as brownish orange solid that is readily soluble in polar solvents while only sparingly soluble in aliphatic solvents. In the ^{1}H NMR spectrum (C_6D_6) three sharp singlets for the Cp''' ligand at δ = 1.20 (9H), 1.21 (18H) and 4.64 (2H) ppm can be detected. The ^{31}P{^{1}H} NMR spectrum (C_6D_6) of **9b** shows two characteristic triplets at δ = -81.4 and -325.0 ppm with equal integral intensities. When CD_2Cl_2 is used as solvent for the NMR the the chemical shift of the triplets is slightly changed to δ = -75.2 and -322.3 ppm. The IR spectrum reveals two absorption bands at ν = 2000 and 1950 cm^{-1} for the terminal carbonyl ligands.

The reactivity of **10b** towards white phosphorus may be explained by the formation of metal-centered radicals [Cp'''Fe(CO)$_2$]$^\bullet$ in solution which react readily with the P$_4$ tetrahedron. The underlying monomer/dimer equilibrium of **10b** has been investigated by Sitzmann *et al.* for the derivative [{Cp$^{i\mathrm{Pr}}$Fe(CO)$_2$}$_2$] (Cp$^{i\mathrm{Pr}}$ = C$_5$^{i}Pr$_5$) (**10c**) that is completely dissociated in solution.[38] As the IR spectrum of **10b** in solution shows a resonance for bridging carbonyl ligands, the Cp'''-substituted derivative is not completely dissociated. The reason might be the reduced steric bulk of Cp''' compared to Cp$^{i\mathrm{Pr}}$. However, as the reaction with P$_4$ shifts the equilibrium, only a small amount of [Cp'''Fe(CO)$_2$]$^\bullet$ radical monomers in solution are sufficient to afford a complete reaction.

3.3.3 E_4 butterfly complexes (E_4 = AsP_3, As_4) based on [{Cp'''Fe(CO)$_2$}$_2$] (10b)

While transition-metal-stabilized bridging butterfly complexes are well known for phosphorus, to date no examples for AsP_3 or As_4 exist. In case of As_4 spectroscopic evidence for a bridging butterfly complex could be obtained during the authors diploma thesis.[51] As the optimized synthetic strategy for **9b** is high yielding as well as selective, the concept was used for the activation of AsP_3 and As_4.

3.3.3.1 Synthesis of [{Cp'''Fe(CO)$_2$}$_2$(μ,$\eta^{1:1}$-AsP_3)] (51)

The reaction of **10b** with one equivalent of AsP_3 leads to the immediate formation of the bridging butterfly complex [{Cp'''Fe(CO)$_2$}$_2$(μ,$\eta^{1:1}$-AsP_3)] (**51**) which is isolated as a bright orange solid in excellent yields (equation 14). The ^{1}H and ^{31}P{^{1}H} NMR spectra show a quantitative formation of **51**. It is well soluble in CH_2Cl_2 and toluene but sparingly soluble in aliphatic solvents. Though several attempts were undertaken, no single crystals of **51** suitable for X-ray structure analysis could be obtained to date.

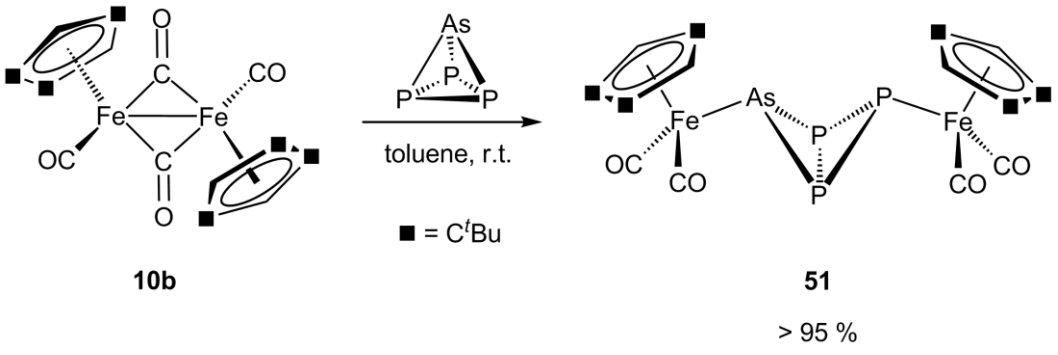

10b **51** > 95 % (14)

In the FD mass spectrum the molecular ion peak at *m*/*z* = 858.1 can be detected beside two peaks at *m*/*z* = 830.2 and 802.1 that correspond to fragments formed by single and double decarbonylation. In the IR spectrum four absorption bands appear at ν = 1998, 1990, 1950 and 1940 cm^{-1} due to the terminal carbonyl ligands. The signals at ν = 1998 and 1950 cm^{-1} are essentially the same than the ones observed for **9b**. The other carbonyl bands are both blue shifted by 10 cm^{-1}.

The ^{1}H NMR spectrum (C_6D_6) of **51** shows two sets of signals for two slightly different Cp''' ligands. The first one consists of three sharp singlets at δ = 1.21 (9H), 1.215 (18H) and

4.60 (2H) ppm, the other one of four singlets at δ = 1.16 (9H), 1.221 (18H), 4.66 (1H) and 4.67 (1H) ppm. The chemical shifts of the first set of signals compares well those found for **9b**, while the second set is slightly shifted. Additionally, in the second set two singlets for the aromatic protons are detected, which indicates magnetically inequivalent environments. In the $^{31}P\{^{1}H\}$ NMR spectrum (C_6D_6) a triplet at δ = -94.2 (1P) ppm and a doublet at δ = -312.0 (2P) ppm with coupling constants of $^{1}J_{PP}$ = 190 Hz can be detected. While the triplet can be assigned to an iron coordinating P atom, the doublet corresponds to the bridgehead P atoms. Hence, arsenic occupies exclusively one of the iron coordinating positions while the non-coordinating positions are solely occupied by phosphorus. This selectivity is consistent with the results obtained by Cummins *et al.* and is a direct consequence of weaker As–P bonds compared to P–P bonds (energy difference of 6 kcal·mol^{-1}).[53]

A similar splitting pattern has been observed by Cummins *et al.* for the butterfly complex [{Ti(N(^{t}Bu)Ar)$_3$}$_2$(μ,$\eta^{1:1}$-AsP$_3$)] (Ar = 3,5-Me$_2$C$_6$H$_3$) with signals at δ = -9.6 and -275.0 ppm.[53] However, the titanium AsP$_3$ butterfly complex could not be isolated so far. The reason is an equilibrium that favours the reactants and only allows a conversion to [{Ti(N(^{t}Bu)Ar)$_3$}$_2$(μ,$\eta^{1:1}$-AsP$_3$)] of about 30 %. In contrast, the reaction of **10b** with AsP$_3$ leads to a quantitative formation of the desired AsP$_3$ butterfly complex. Hence, **51** represents the first isolated and characterized transition metal butterfly complex of AsP$_3$ known to date.

3.3.3.2 Synthesis of [{Cp'''Fe(CO)$_2$}$_2$(μ,$\eta^{1:1}$-As$_4$)] (52)

By analogy to the reactions of [{Cp'''Fe(CO)$_2$}$_2$] (**10b**) with P$_4$ and AsP$_3$, its reaction with As$_4$ leads to the selective formation of the first bridging tetraarsa-*bicyclo*[1.1.0]-butane complex [{Cp'''Fe(CO)$_2$}$_2$(μ,$\eta^{1:1}$-As$_4$)] (**52**) in good yields (equation 15). Compound **52** is obtained as an orange solid that readily dissolves in CH_2Cl_2 and toluene and is moderately soluble in hexane. Single crystals of **52** are obtained from a hexane/toluene (2:1) solution upon cooling to -28 °C.

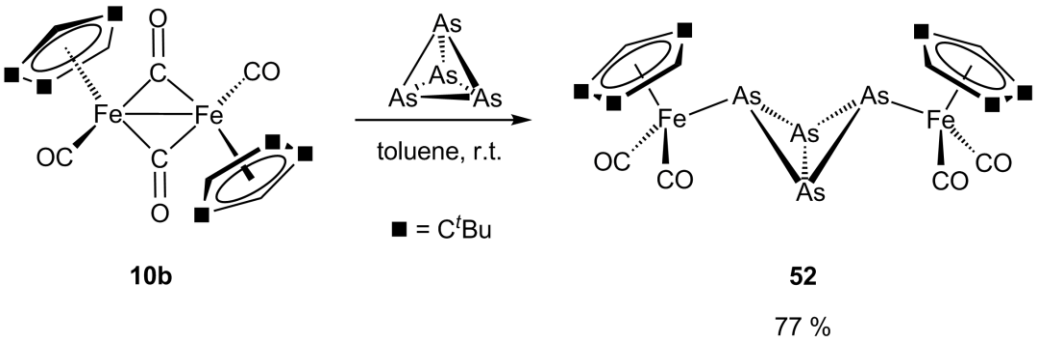

10b **52** 77 % (15)

The FD mass spectrum of **52** reveals only the molecular ion peak at *m*/*z* = 990.0 without any further fragmentation. In the IR spectrum two carbonyl bands can be detected at ν = 1990 and 1940 cm^{-1} that are red-shifted compared to the bands in **9b** by 10 cm^{-1} but compare well to the stretching frequencies in **51**. The red- shift points to an increased electron density at the iron fragments which in turn indicates either a stronger σ-donor or a weaker π-acceptor ability (or both) of the As_4^{2-} butterfly moiety compared to its phosphorus derivative. In the ^{1}H NMR spectrum (C_6D_6) three sharp singlets for the Cp''' ligands are observed at δ = 1.18, 1.23 and 4.66 ppm which compares well to the values of the arsenic bound [Cp'''Fe$(CO)_2$] fragment in **51**.

[{Cp'''Fe$(CO)_2$}$_2$($\mu,\eta^{1:1}$-As_4)] (**52**) crystallizes as orange platelets in the monoclinic space group $P2_1/n$. The asymmetric unit contains one molecule of **52**. X-ray structure analysis confirms the bridging coordination mode of a formal As_4^{2-} moiety between two [Cp'''Fe$(CO)_2$] fragments (Figure 18). The bonds between the coordinating and noncoordinating As atoms lie in the range of 2.449(2) Å and 2.461(3) Å and are slightly longer than the As–As single bonds in As_4 (2.435(4) Å determined by electron diffraction,[67] 2.42 Å sum of covalent radii[68]). In contrast, the As3–As4 bond between the two bridgehead atoms is with 2.405(3) Å shortened compared to As_4. An analogous trend for the E–E bond lengths is found for the P_4 derivative **9b**.[37] The As1···As2 distance of 3.184(2) Å clearly indicates the reduction of the As_4 tetrahedron and consequent cleavage of one As–As bond. However, it is 0.52 Å less than the sum of van der Waals (vdW) radii (3.70 Å) which may be interpreted as weak interaction between the atoms. In **9b** a similar tendency is observed (P–P dist. is 0.64 Å below sum of vdW radii).

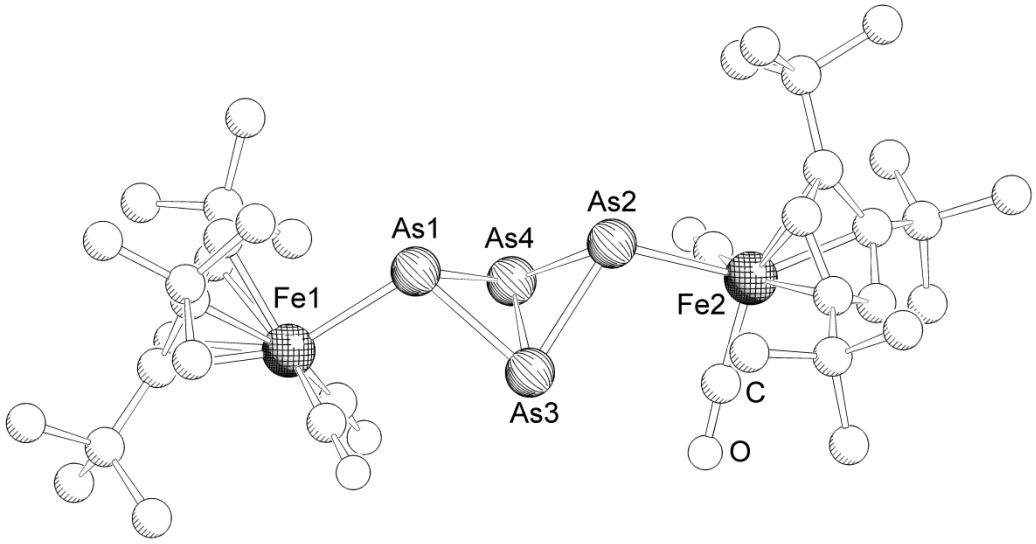

Figure 18. Molecular structure of **52** in the crystal. Hydrogen atoms omitted for clarity. Selected bond lengths [Å] and angles [°]: Fe1–As1 2.443(3), Fe2–As2 2.458(3), As1–As3 2.449(2), As1–As4 2.461(3), As2–As3 2.452(2), As2–As4 2.460(3), As3–As4 2.405(3), As1···As2 3.184(2), As3–As1–As4 58.67(7), As3–As2–As4 58.63(8), As1–As3–As2 81.04(7), As1–As4–As2 80.65(9), As1–As3–As4 60.92(7), As1–As4–As3 60.42(7), As2–As3–As4 60.84(8), As2–As4–As3 60.53(8).

The As3–As1–As4 and As3–As2–As4 bond angles of 58.67(7)° and 58.63(8)° are smaller than the tetrahedral angle of 60° and compare well to the corresponding angles in **9b** (58.12(8)° and 58.42 (8)°). The As1–As3–As2 and As1–As4–As2 angles are with 81.04(7)° and 80.65(9)° smaller than the associated bond angles in **9b** (84.47(9)° and 84.07(9)°) indicating a less distinct opening of the butterfly ligand which compares well to the trend found for the E1···E2 bond distances.

3.3.4 E_4 butterfly complexes ($E_4 = P_4$, AsP_3, As_4) based on $[\{Cp^*Cr(CO)_3\}_2]$ (53)

The thermolysis of $[\{Cp^*Cr(CO)_3\}_2]$ (**53**) with white phosphorus yields the tetrahedrane complex $[\{Cp^*Cr(CO)_2\}(\mu,\eta^{2:2}\text{-}P_2)]$ as well as the *cyclo*-P_3 complex $[\{Cp^*Cr(CO)_2\}(\eta^3\text{-}P_3)]$. It is assumed that the intermediate of this reaction is the butterfly complex $[\{Cp^*Cr(CO)_3\}_2(\mu,\eta^{1:1}\text{-}P_4)]$ (**54**) that undergoes several decarbonylation steps.[77] These are accompanied by a degradation of the bicyclic P_4 framework to finally yield the desired P_2 and *cyclo*-P_3 complexes. The starting material **53** shows a quite long Cr–Cr bond[78] of 3.310(1) Å and dissociates in solution to an extent of about 10 %.[79] The so-formed 17 VE $[Cp^*Cr(CO)_3]$ fragments resemble the 17 VE iron species derived from **10b**. Compound **53** therefore seemed to be an ideal starting material for the formation of chromium-stabilized E_4 butterfly complexes.

3.3.4.1 Synthesis of $[\{Cp^*Cr(CO)_3\}_2(\mu,\eta^{1:1}\text{-}P_4)]$ (54)

The reaction of $[\{Cp^*Cr(CO)_3\}_2]$ (**53**) with white phosphorus at room temperature affords the bridging butterfly complex $[\{Cp^*Cr(CO)_3\}_2(\mu,\eta^{1:1}\text{-}P_4)]$ (**54**) in excellent yields (equation 16). It is isolated as bright orange solid that has good solubility in dichloromethane, moderate solubility in toluene but is only sparingly soluble in hexane. Single crystals of **54** are obtained from a saturated toluene solution upon cooling.

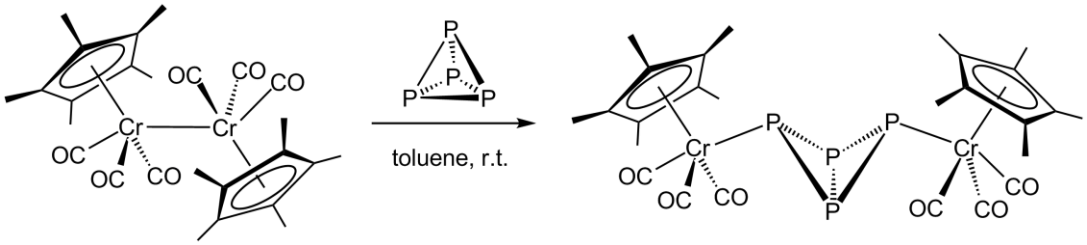

53 **54**

> 95 %

(16)

The ^{1}H NMR spectrum (CD_2Cl_2) of **54** reveals one singlet at δ = 1.83 ppm for the methyl groups of the two freely rotating Cp* ligands. In the $^{31}P\{^{1}H\}$ NMR (CD_2Cl_2) spectrum two triplets at δ = -95.2 ppm and -327.4 ppm with equal intensities are observed. The first one is shifted upfield by about 20 ppm compared to the iron butterfly complex **9b**. This deshielding of the "wing-tip" phosphorus nuclei indicates less electron density on the Cr coordinating P atoms in **54** compared to the Fe coordinating P atoms in **9b**. In the IR spectrum four absorption bands for the terminal CO ligands are detcted at ν = 1983, 1967, 1916 and 1900 cm^{-1}. Compared to the starting material **53** (ν = 1987 and 1877 cm^{-1}) the signals for **54** are blue-shifted suggesting formal oxidation of Cr(I) to Cr(II).

[{Cp*Cr(CO)$_3$}$_2$(μ,$\eta^{1:1}$-P$_4$)] (**54**) crystallizes as orange blocks in the monoclinic space group $P2_1/c$. The asymmetric unit contains one molecule of **54**. X-ray structure analysis shows the expected bridging coordination mode of a P_4 butterfly unit between two {Cp*Cr(CO)$_3$} fragments.

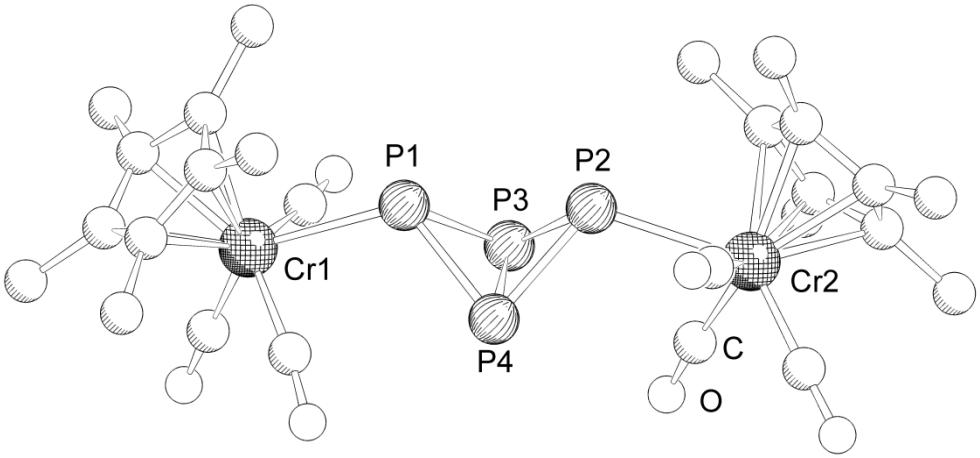

Figure 19. Molecular structure of **54** in the crystal. Hydrogen atoms omitted for clarity. Selected bond lengths [Å] and angles [°]: Cr1–P1 2.529(2), Cr2–P2 2.508(2), P1–P3 2.198(2), P1–P4 2.200(3), P2–P3 2.205(2), P2–P4 2.196(3), P3–P4 2.165(2), P1···P2 2.809(3), P3–P1–P4 58.99(8), P3–P2–P4 58.95(8), P1–P3–P2 79.29(8), P1–P4–P2 79.45 (9), P1–P3–P4 60.55(8), P1–P4–P3 60.47(8), P2–P3–P4 60.32(8), P2–P4–P3 60.74(8).

The bond lengths between the coordinating P atoms P1 and P2 and the non coordinating atoms P3 and P4 vary from 2.196(3) Å to 2.200(3) Å and compare well to a P–P single bond (2.186(1) Å[73] to 2.21(1) Å[72]). In contrast, the P3–P4 bond with 2.165(2) Å is shortened. Compared to **9b** the bond between the bridgehead atoms is elongated (2.151(2) Å for **9b**) while the other P–P bonds are slightly shorter (**9b**: 2.198(3) Å – 2.210(3) Å).[37] The P–P–P bond angles are pretty close to the tetrahedral angle of 60° and compare well to the ones found in **9b**. The only exceptions are the

P1–P3–P2 and P1–P4–P2 angles of 79.29(8)° and 79.45(8)° that are smaller than the corresponding angles in **9b** (84.49(9)° and 84.07(9)°). Consequently, the P1···P2 distance of 2.809(3) Å about 0.15 Å shorter than in **9b** (2.96 Å) pointing to a stronger interaction between the P atoms in **54** compared to **9b** and may be explained by the steric demand of the metal fragments. However, as the $^{31}P\{^{1}H\}$ NMR spectrum of **54** indicates a smaller electron density on the "wing-tip" P atoms compared to **9b**, the shortened P1···P2 distance may also be interpreted as a less effective reductive P–P bond cleavage and therefore a stronger P–P interaction. Hence, the $[Cp^*Cr(CO)_3]$ fragments seem to be less potent electron donors than the $[Cp'''Fe(CO)_2]$ moieties.

3.3.4.2 Synthesis of $[\{Cp^*Cr(CO)_3\}_2(\mu,\eta^{1:1}\text{-}AsP_3)]$ (55)

The quantitative formation of $[\{Cp^*Cr(CO)_3\}_2(\mu,\eta^{1:1}\text{-}AsP_3)]$ (**55**) is achieved by the reaction of $[\{Cp^*Cr(CO)_3\}_2]$ (**53**) with one equivalent of AsP_3 in toluene at room temperature (equation 17). Compound **55** is isolated as bright orange solid that dissolves well in dichloromethane and THF, has moderate solubility in toluene but is almost insoluble in hexane. Single crystals of **55** suitable for X-ray structure analysis are obtained from saturated solutions of **55** upon cooling to 4 °C.

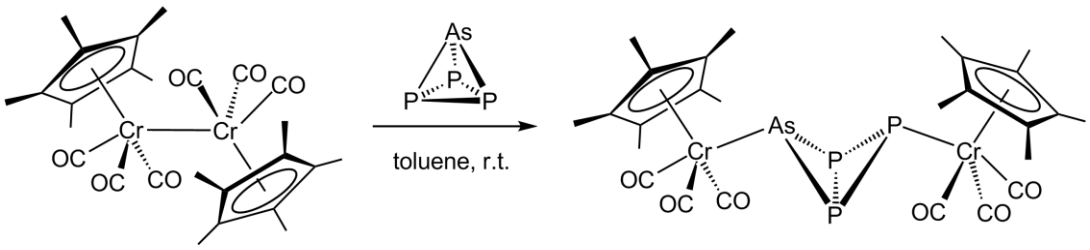

53 **55**

> 95 %

(17)

The ^{1}H NMR spectrum (C_6D_6) of **55** shows two singlets at δ = 1.43 and 1.44 ppm with equal intensities. They can be assigned to the Cp* protons of two slightly different $[Cp^*Cr(CO)_3]$ units, which again indicates the selective cleavage of an As–P bond and exclusive occupation of one of the "wing-tip" positions by arsenic. In the $^{31}P\{^{1}H\}$ NMR spectrum (C_6D_6) a triplet and a doublet are found at δ = -112.9 and -312.9 ppm which show an intensity ratio of 1:2. As observed for the P_4 derivative, the signal at d = -112.9 ppm is upfield shifted by about 20 ppm compared to the iron AsP_3 butterfly complex **51**. The location, splitting pattern and intensity ratio of the signals clearly point to the selective cleavage of an As–P bond.

In the electron spray ionization (ESI) mass spectrometry beside the molecular ion peak at *m*/*z* = 710.1 two peaks at *m*/*z* = 641.1 and 625.1 can be detected. They originate from the

fragments $[M - 2(CO) + O]^+$ and $[M - 3(CO)]^+$. The IR spectrum of **55** reveals three bands at ν = 1980, 1964 and 1897 cm^{-1}, of which the latter one is broadened.

$[\{Cp^*Cr(CO)_3\}_2(\mu,\eta^{1:1}\text{-}AsP_3)]$ (**55**) crystallizes as orange plates in the monoclinic space group *C*2/*c*. The asymmetric unit contains half a molecule of **55**. The "wing-tip" position is occupied by arsenic and phosphorus with a 50 % probability, respectively. The non coordinating position is only occupied by phosphorus (Figure 20).

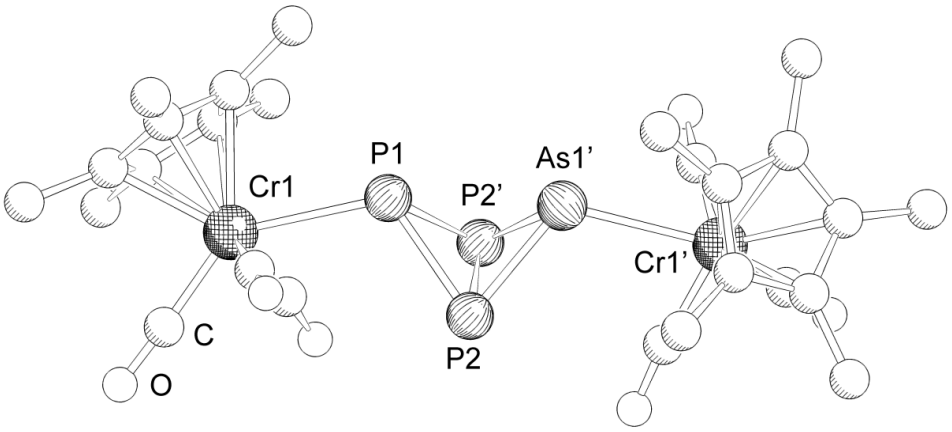

Figure 20. Molecular structure of **55** in the crystal. For clarity reasons only one of the two possible positions of arsenic is shown and hydrogen atoms are omitted. Selected bond lengths [Å] and angles [°]: Cr1–P1 2.606(4), Cr1'–As1' 2.610(2), P1–P2 2.289(3), P1–P2' 2.315(3), As1'–P2 2.259(2), As1'–P2' 2.287(2), P2–P2' 2.1766(7), P1···As1' 2.778(4), P2–P1–P2' 56.42(8), P2–As1–P2' 57.22(5), P1–P2–P2' 62.4(1), As1'–P2–P2' 60.74 (5), P1–P2–As1' 74.8(1).

Due to the disorder of the phosphorus and arsenic atoms, a distinct determination of the P–P and As–P bond lengths is only possible to a certain point. Hence, the stated P–P and As–P bond lengths (Figure 20) between the bridgehead and the "wing-tip" atoms are essentially the same and vary from 2.259(2) Å to 2.315(3) Å, which is in between a P–P single bond (2.21 Å) and As–As single bond (2.435 Å). The P2–P2' bond of 2.1766(7) Å compares well to the corresponding P–P bond in **54** (2.165(2) Å). The P1–P2–As1' bond angle of 74.8(1)° is smaller than in **54**. Consequently, the P1···As1' distance of 2.778(4) Å is also shortened (2.809(3) Å in **54**) pointing to a stronger interaction between the coordinating atoms.

3.3.4.3 Synthesis of $[\{Cp^*Cr(CO)_3\}(\mu,\eta^{1:1}\text{-}As_4)]$ (56)

$[\{Cp^*Cr(CO)_3\}_2(\mu,\eta^{1:1}\text{-}As_4)]$ (**56**) is obtained by the reaction of $[\{Cp^*Cr(CO)_3\}_2]$ (**53**) with yellow arsenic in toluene at room temperature (equation 18). It is isolated as an orange solid in good yields that has good solubility in dichloromethane, moderate solubility in toluene and is sparingly soluble in hexane. It can be recrystallized from a saturated hexane/toluene solution upon

cooling to 4 °C. The initially formed bright orange crystals disappear after one day, and red crystals begin to form that contain **56** as well as its dimerization product (see chapter 3.4.2). So far all attempts to obtain single crystals of pure **56** failed. However, the crude reaction product is analytically pure.

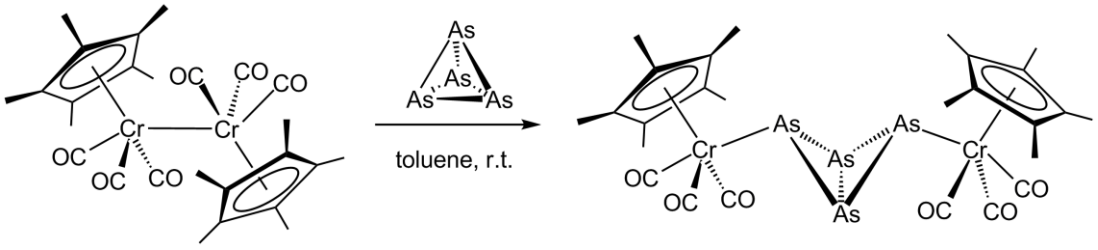

53 **56** (18)

75 %

The ^{1}H NMR spectrum (CD_2Cl_2) of **56** reveals one sharp singlet at δ = 1.84 ppm for the protons of the Cp* ligand. In the ESI mass spectrum three peaks can be detected at *m*/*z* = 749.0, 412.2 and 300.0 that can be assigned to the cationic fragments $[\{Cp^*Cr\}_2As_5]^+$, $[Cp^*CrAs_3]^+$ and $[As_4^+]$, respectively. The molecular ion peak cannot be found. In the IR spectrum three bands at ν = 1977, 1965 and 1904 cm^{-1} appear for the terminal carbonyl ligands.

$[\{Cp^*Cr(CO)_3\}_2(\mu,\eta^{1:1}\text{-}As_4)]$ (**56**) cocrystallizes together with $[\{Cp^*Cr(CO)_3\}_4(\mu,\eta^{1:1:1:1}\text{-}As_8)]$ (vide infra) as red plates in the monoclinic, non-centrosymmetric space group *Pn*. The asymmetric unit contains two molecules of **56** together with one molecule of $[\{Cp^*Cr(CO)_3\}_4(\mu_4,\eta^{1:1:1:1}\text{-}As_8)]$ (*vide infra*) (Figure 21).

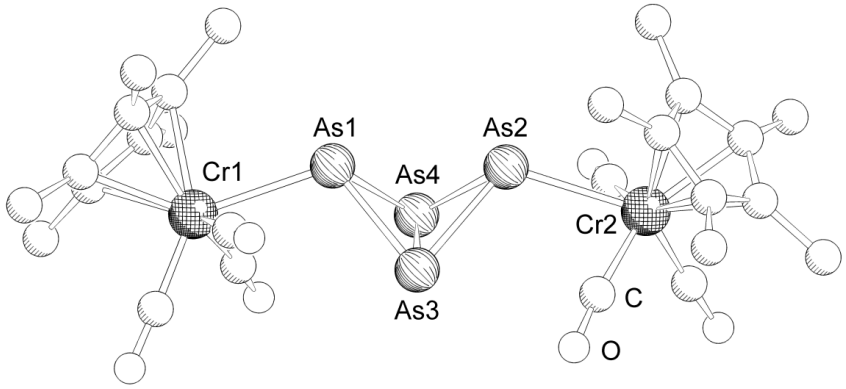

Figure 21. Molecular structure of **56** in the crystal. For clarity resaons only one of the two molecules in the asymmetric unit is depicted and hydrogen atoms as well as the cocrystallized As_8 complex are omitted. Selected bond lengths[Å] and angles [°]: Cr1–As1 2.641(1), Cr2–As2 2.614(1), As1–As3 2.425(1), As1–As4 2.454(1), As2–As3 2.449(1), As2–As4 2.435(1), As3–As4 2.367(1) As1···As2 3.032(1), As3–As1–As4 58.06(3), As3–As2–As4 57.99(3), As1–As3–As2 76.93(4), As1–As4–As2 76.65(4), As1–As3–As4 61.58(3), As1–As4–As3 60.37(4), As2–As3–As4 60.73(4), As2–As4–As3 61.28(3).

The molecular structure of **56** features the typical characteristics of a bridging butterfly complex. The Cr–As bond lengths of 2.641(1) Å and 2.614(1) Å are rather long compared to the Fe–As bond lengths in **52** (2.443(3) Å and 2.458(3) Å) pointing to a weaker metal arsenic interaction. The bond lengths between the coordinating and non-coordinating arsenic atoms range from 2.425(1) Å to 2.454(1) Å, which is in good agreement with an As–As single bond (2.435 Å).[67] The As3–As4 bond is with 2.367(1) Å slightly shorter than the corresponding bond in **52** (2.405(3) Å). The As1–As3–As2 and As1–As4–As2 bond angles of 76.93(4)° and 76.65(4)° are smaller than the associated angles in **52** (81.04(7)° and 80.65(9)°). Hence, the As1···As2 distance of 3.032(1) Å is shortened compared to **52** (3.184(2) Å). The same tendency has already been observed for the P_4 derivatives **9b** and **54** (see section 3.3.4.1).

3.3.5 A novel dinuclear iron complex for the activation of white phosphorus

In the 1990s Scherer *et al.* could show the potential of the dinuclear iron complexes $[\{Cp^RFe(CO)_2\}_2]$ (Cp^R = Cp'' (**10a**), Cp'''(**10b**), Cp^{iPr} (**10c**)) for the activation of white phosphorus and the formation of the corresponding butterfly complexes $[\{Cp^RFe(CO)_2\}_2(\mu,\eta^{1:1}\text{-}P_4)]$ (Cp^R = Cp'' (**9a**)[36], Cp'''(**9b**)[37], Cp^{iPr} (**9c**)[80]). The basic mechanism for these reactions is the formation of 17 VE monomeric iron complexes[81] $[Cp^RFe(CO)_2]$ in solution which then react with P_4. While in case of **10a** the 17 VE species are generated by photolysis of the starting material, **10b** and **10c** already dissociate in solution without further activation. However, the Cp^R ligand has to be sterically demanding to stabilize the radical species. Hence, the reaction of $[\{Cp^*Fe(CO)_2\}_2]$ (**10d**) with P_4 does not yield the desired butterfly complex $[\{Cp^*Fe(CO)_2\}_2(\mu,\eta^{1:1}\text{-}P_4)]$ (**9d**) even under thermolytic or photolytic conditions. In a different approach Jutzi *et al.* were able to obtain contaminated **9d** by the dimerization of the diphosphene $[\{Cp^*Fe(CO)_2\}P{=}PCp^*]$ and subsequent elimination of Cp*.[82] As this synthetic route is time consuming and **9d** is only obtained in low yields, another synthetic strategy would be desirable for its formation. As the relatively small Cp* ligands in **10d** do not provide enough stabilization for the formed radicals, almost no dissociation is observed in solution. In order to enhance the reactivity of the dinuclear iron complex the steric bulk of one of the $[Cp^*Fe(CO)_2]$ fragments is increased by introducing the large Cp''' ligand. The resulting diiron complex $[\{Cp^*Fe(CO)_2\}\{Cp'''Fe(CO)_2\}]$ (**57**) reacts with white phosphorus to yield the butterfly complexes **9b**, **9d** and $[\{Cp^*Fe(CO)_2\}(\mu,\eta^{1:1}\text{-}P_4)\{Cp'''Fe(CO)_2\}]$ (**58**) that can be separated by column chromatography.

3.3.5.1 Synthesis of [{Cp*Fe(CO)$_2$}{Cp'''Fe(CO)$_2$}] (57)

[{Cp*Fe(CO)$_2$}{Cp'''Fe(CO)$_2$}] (**57**) is synthesized via a salt elimination reaction of [Cp*Fe(CO)$_2$Br] with one equivalent of K[Cp'''Fe(CO)$_2$] (**50**) in toluene at room temperature (equation 19). It has good solubility in dichloromethane and toluene but is only moderately soluble in hexane. Crystallization from a hot hexane solution affords **57** in good yields as brownish purple crystals.

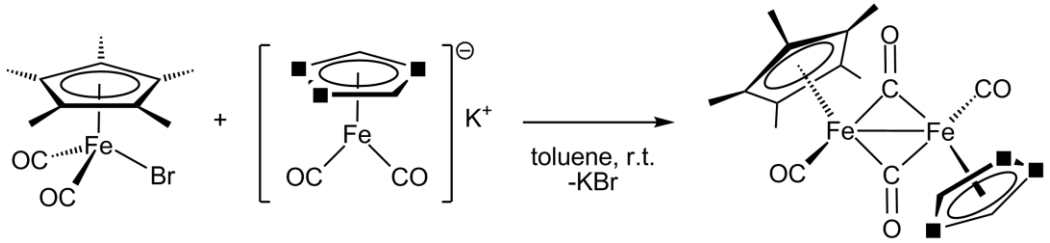

50 ■ = C^{t}Bu **57** 75 % (19)

In the ^{1}H NMR spectrum (C_6D_6) of **57** signals for a freely rotating Cp''' ligand and a Cp* ligand can be observed at δ = 1.34 (9H), 1.49 (18H) and 4.40 (2H) ppm and δ = 1.56 (15H) ppm. The IR spectrum of **57** reveals two absorption bands at ν = 1929 and 1760 cm^{-1}, which lie in a typical range for a terminal as well as a bridging coordination mode of the carbonyl ligands.

[{Cp*Fe(CO)$_2$}{Cp'''Fe(CO)$_2$}] (**57**) crystallizes as green/brown/purple pleochromic plates in the space group $P\bar{1}$ of the triclinic crystal system. The asymmetric unit contains one molecule of **57**.

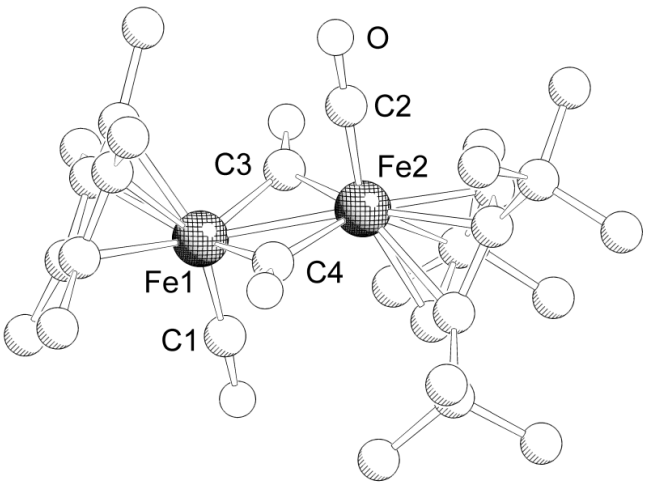

Figure 22. Molecular structure of **57** in the crystal. Hydrogen atoms omitted for clarity. Selected bond lengths[Å] and angles [°]: Fe1–Fe2 2.5494(4), Fe2–Fe1–C1 91.64(6), Fe1–Fe2–C2 95.45(7), C3–Fe1–C4 97.23(8), C3–Fe2–C4 96.40(8), Fe1–C3–Fe2 82.66(7), Fe1–C4–Fe2 82.51(7).

The molecular structure of **57** shows a trans configuration of the two Cp^R ligands and the terminal CO ligands, respectively. The Fe1–Fe2 bond length of 2.5494(4) Å is slightly shorter than the corresponding bond distance in **10d** (2.560(1) Å).[83] Two of the four carbonyl ligands bridge the two iron atoms in an almost coplanar fashion (sum of angles of 358.8°). The terminal carbonyl ligands are located perpendicular to the Fe–Fe bond.

3.3.5.2 The reaction of [{Cp*Fe(CO)$_2$}{Cp'''Fe(CO)$_2$}] (57) with P_4

The reaction of **57** with white phosphorus yields the three bridging butterfly complexes [{Cp'''Fe(CO)$_2$}$_2$($\mu,\eta^{1:1}$-P_4)] (**9b**), [{Cp*Fe(CO)$_2$}($\mu,\eta^{1:1}$-P_4){Cp'''Fe(CO)$_2$}] (**58**) and [{Cp*Fe(CO)$_2$}$_2$($\mu,\eta^{1:1}$-P_4)] (**9d**) in a ratio of about 1:2:1 (equation 20).

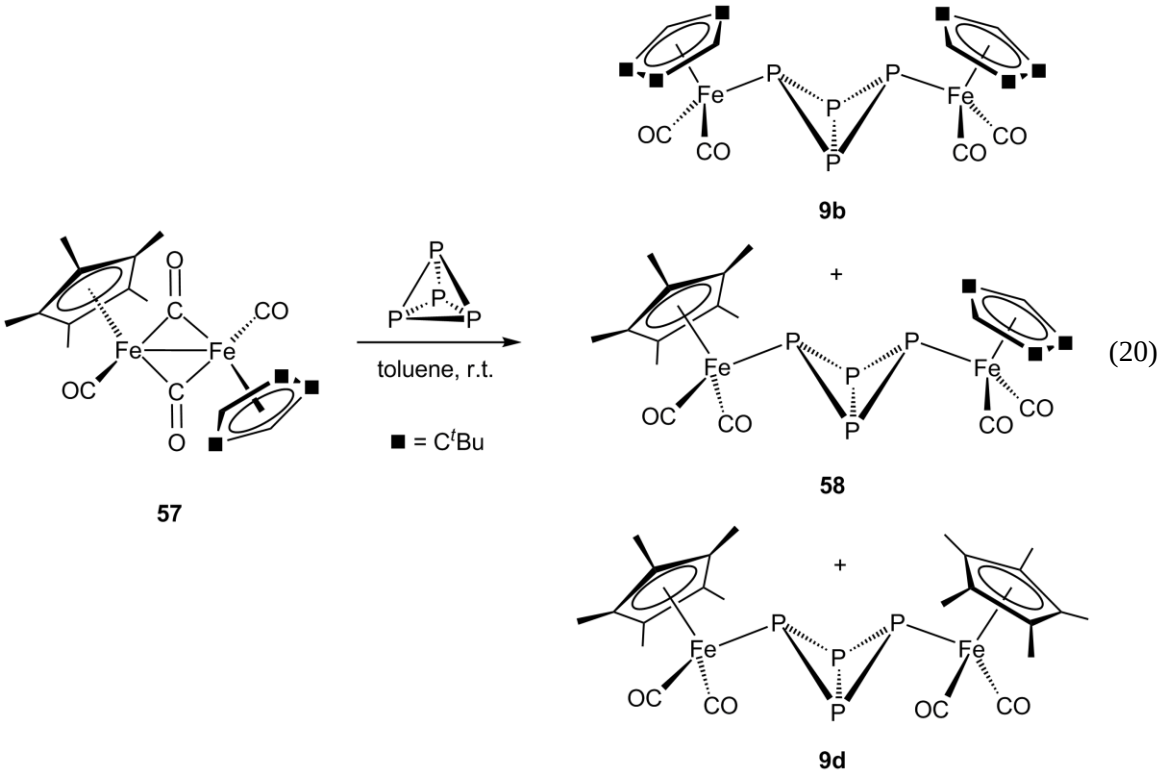

(20)

In the $^{31}P\{^1H\}$ NMR spectrum (CD_2Cl_2) of the reaction mixture two signal groups around δ = -64 ppm and δ = -330 ppm can be detected in a typical range for the "wing-tip" and bridghead P atoms of bridging butterfly complexes (Figure 23). The triplets at δ = -83.3 (2P) and -326.9 (2P) ppm show an associated coupling constant of $^1J_{PP}$ = 187 Hz and can be assigned to **9b**. At δ = -45.1 (2P) and -334.9 (2P) ppm two triplets with a coupling constant of $^1J_{PP}$ = 185 Hz are detected. The chemical shifts as well as the coupling constant compare well to the published data for **9d**.[82] Beside the signals for compounds **9b** and **9d** a triplet at δ = -330.9 (4P) and two doublets of triplets arise at δ = -73.8 (2P) and -56.4 (2P) ppm that are attributed to the mixed

butterfly complex **58**. The observed ABM_2 spin system with a large $^2J_{AB}$ coupling constant of 292 Hz suggests a through space coupling of the two coordinating P atoms which is in accordance with the short P···P distances observed in this class of compounds (see section 3.3.4.1).

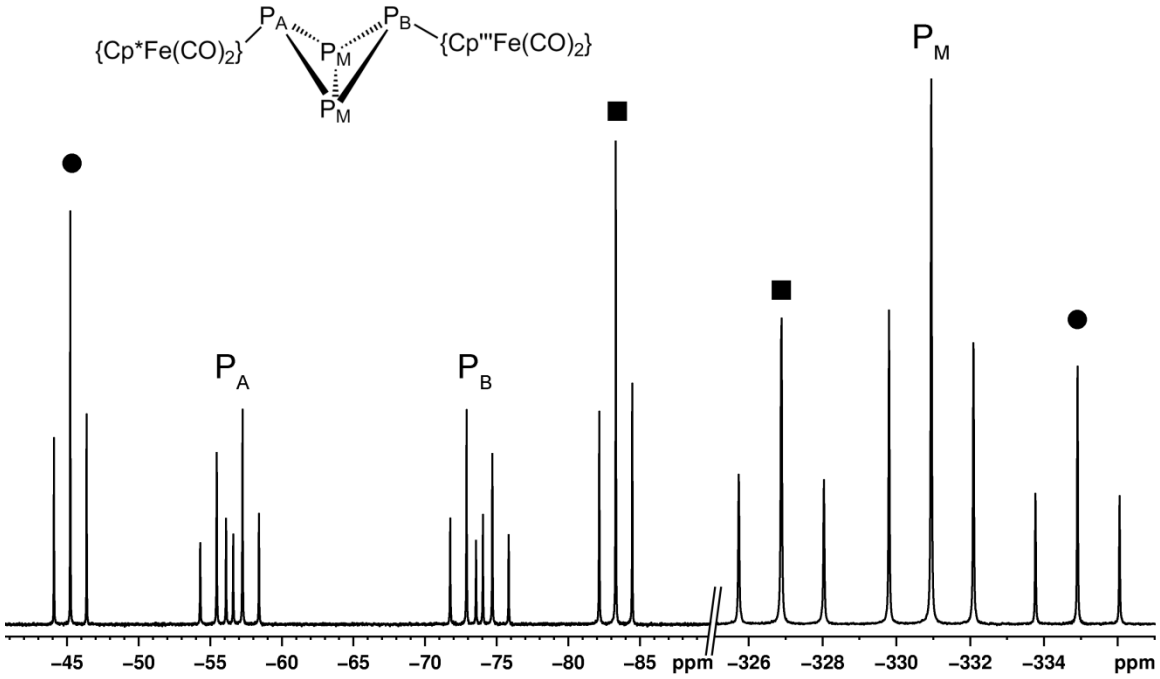

Figure 23. $^{31}P\{^1H\}$ NMR spectrum (CD_2Cl_2, 300 K) of the reaction mixture of **9b** (■), **9d** (●) and **58** (signals are assigned to the ABM_2 spin system).

Separation of the products is possible by column chromatographic workup at -40 °C. Elution with hexane/toluene 5:1 gives an orange fraction which $^{31}P\{^1H\}$ NMR spectrum (C_6D_6) only shows signals at δ = -83.3 (2P) and -326.9 (2P) ppm for pure **9b**. By increasing the polarity of the used eluent (hexane/toluene 1:4) one well-separated orange band is obtained which likely contains pure **58**. Surprisingly, the $^{31}P\{^1H\}$ NMR spectrum (C_6D_6) of the second fraction shows signals for all three butterfly ligands **9b**, **58** and **9d** in a 1:2:1 ratio. This points to a dissociation/association equilibrium in solution which produces a statistical mixture of the three possible products. As the fraction is well separated on the chromatography column, the symmetrization starts to take place after the fraction is collected. Hence, the equilibrium can be utilized for the further formation of **9d** that is separable by subsequent column chromatography.

Finally, THF elutes **9d** as an orange fraction. After removal of the solvent, **9d** is obtained as bright orange solid in 20 % yield (*n.b.* that a maximum yield of 25 % can be achieved). It has good solubility in THF, toluene and CH_2Cl_2 but is sparingly soluble in hexane. This is surprising, since it has been described as "pale brown solid which is moderately soluble in THF".[82] In the ^1H NMR spectrum (CD_2Cl_2) one singlet at δ = 1.44 ppm for the protons of the Cp* ligand can be

detected. The $^{31}P\{^{1}H\}$ NMR spectrum (CD_2Cl_2) shows two sharp triplets at δ = -45.1 (2P) and -334.9 (2P) ppm. In the IR spectrum two absorption bands at ν = 1987 and 1931 cm^{-1} are found, which are similar to the corresponding signals for **9b** (ν = 2000 and 1950 cm^{-1}).

Compound **9d** is highly desirable for the formation of the tri and tetraphosphaferrocenes [Cp*Fe($P_3C_2{}^tBu_2$)] and [Cp*Fe($P_4C{}^tBu$)] which bear a large potential for the synthesis of supramolecular assemblies. The reaction of the mixed dimeric iron complex [{Cp*Fe$(CO)_2$}{Cp'''Fe$(CO)_2$}] (**57**) with white phosphorus provides an elegant method for the synthesis of [{Cp*Fe$(CO)_2$}$_2$(μ,$\eta^{1:1}$-P_4)] (**9d**), which so far could only be obtained contaminated and in low yields but is now easily accessible. Furthermore, the equilibrium of **58** in solution can be utilized to increase the yield of **9d**.

3.3.6 Selective Formation of C–P bonds - A carbon substituted tetraphospha-*bicyclo*-butane

The selective activation of white phosphorus with transition metal complexes or heavy main group elements is well known and a broad variety of compounds could be characterized so far.[23] As the industrial synthesis of organophosphorus compounds usually involves hazardous halogenation steps, the direct incorporation of phosphorus into organic molecules would be of special interest. However, the selective C–P bond formation based on white phosphorus remains challenging. Early results were achieved by the reaction of P_4 with organolithium or organomagnesium compounds to yield complex mixtures of organophosphanides.[84] The reactions are not selective and usually the degradation/reaggregation pathway of the P_n fragments is not well understood. Recently, Bertrand *et al.* showed the potential of stable carbenes for the activation of white phosphorus (c.f. section 1.2).[44, 46-47] The formed products possess direct C–P bonds and the reactions usually work selectively.

However, to the best of our knowledge only three butterfly-like tetraphospha-*bicyclo*-butane molecules with direct C–P bonds are known that are derived from white phosphorus. In the 1980s Fluck *et al.* presented the synthesis of [Mes_2P_4] (**8**) in yields of 4 % by the reaction of LiMes with MesBr in the presence of P_4. More recently Power *et al.* reported on the formation of [{Ar^{Dipp}}$_2P_4$] (**12**) (Ar^{Dipp} = C_6H_3-2,6-(C_6H_3-2,6-$^{i}Pr_2$)$_2$) in a two step synthesis in moderate yields.[40] While the formation of **8** and **12** involves a nucleophilic attack at the P_4 tetrahedron, Cummins *et al.* presented the formation of [Dmp_2P_4] (Dmp = 2,6-$Mes_2C_6H_3$) via a radical reaction for the first time.[85] In this case the carbon radicals are generated *in situ* by the treatment of DmpI

with the Ti(III) complex [Ti(N(^{t}Bu)Ar)$_3$] (Ar = 3,5-$Me_2C_6H_3$). Nevertheless, all presented reactions use sp^2 hybridized carbon reagents. Direct C–P bond formation reactions with sp^3 carbons are not known so far. Furthermore, Sitzmann *et al.* reported on the formation of a pentaisopropylcyclopentadienyl radical from the reaction of the corresponding cyclopentadienylsodium salt and $FeCl_2$.[86] Unfortunately the authors did not give any possible explanation for the radical formation. A possible intermediate could be the dimeric iron(II) complex [{Cp^{iPr}Fe(μ-Cl)}$_2$] for which the derivatives [{Cp^{4iPr}Fe(μ-Br)}$_2$] and [{Cp’’’Fe(μ Br)}$_2$] (**59**) are well known and crystallographically characterized.[87] These 16 VE species should be capable of interacting with P_4 and bear the potential for direct C–P bond formation.

The reaction of white phosphorus with one equivalent of [{Cp’’’Fe(μ-Br)}$_2$] (**59**) in toluene at room temperature leads to the formation of the dinuclear iron complex [{Cp’’’Fe}$_2$(μ,η$^{4:4}$-P_4)] (**16b**) as well as the carbon substituted butterfly compound [Cp’’’$_2$$P_4$] (**60**) (equation 21). The $^{31}P\{^1H\}$ NMR spectrum (C_6D_6) of the reaction mixture shows the quantitative conversion of the used white phosphorus and the exclusive formation of **16b** and **60** in a 1 : 1 ratio. The formation of PBr_3 is not observed. The compounds can be separated by column chromatography. Complex **16b** was identified by ^1H and $^{31}P\{^1H\}$ NMR spectroscopy but not further analyzed. Compound **60** is isolated as colorless solid in moderate yields. It is has good solubility in polar as well as non polar solvents and can be crystallized from a saturated Et_2O solution at room temperature to give single crystals suitable for X-ray structure analysis.

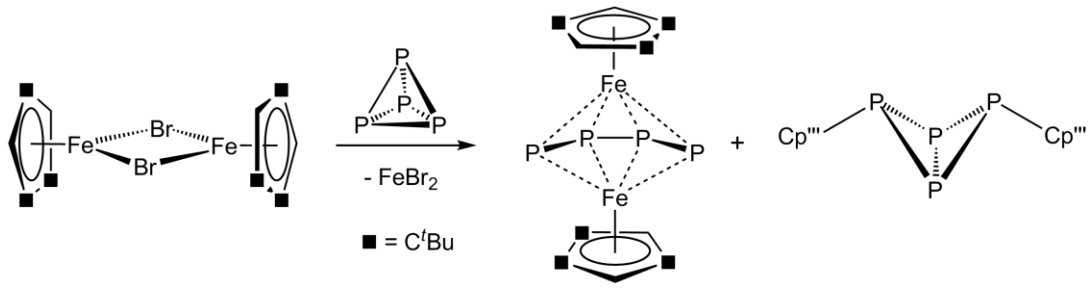

59 **16b** **60** 14 % (21)

In the electron impact ionization (EI) mass spectrometry the molecular ion peak is detected at *m/z* = 590.4. Additionally, peaks are detected at m/z = 533.3 [M^+ - (C_4H_9)], 466.3 [Cp’’’P_4(C_8H_{13})]$^+$, 357.1 [Cp’’’P_4]$^+$, 301.1 [Cp’’P_4]$^+$ that correpsond to several fragmentation products.

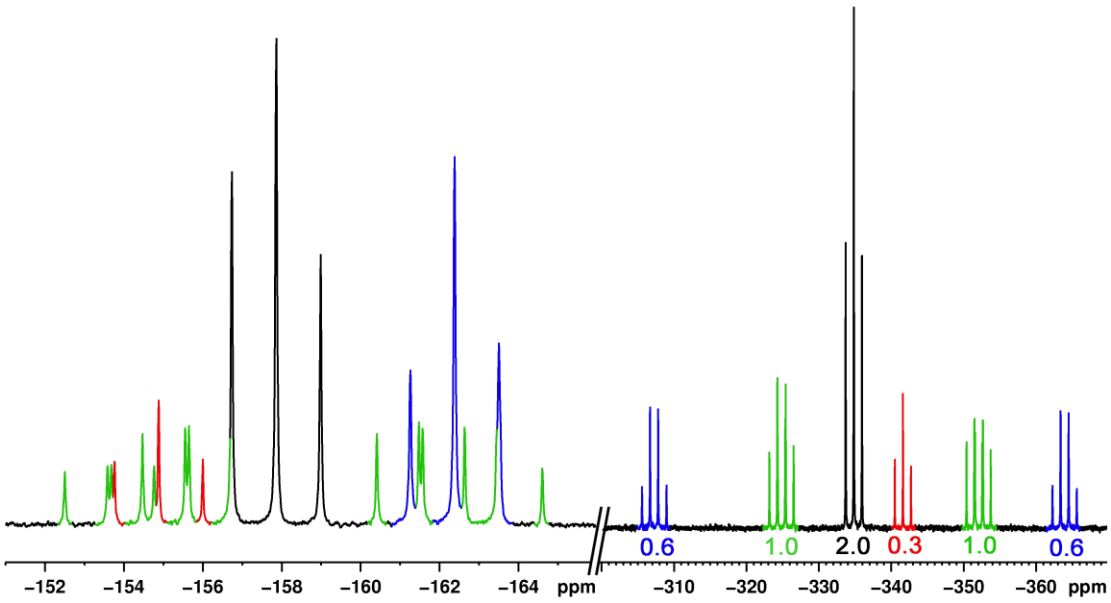

Figure 24. $^{31}P\{^{1}H\}$ NMR (C_6D_6, 300 K) spectrum of **60** with signals for isomers **A** (blue), **B** (red), **C** (black) and **D** (green) (Scheme 5). Relative intensities are given below the signals.

The ^{1}H NMR spectrum (C_6D_6) of **60** shows several singlets between δ = 1.0 and 1.6 ppm, pointing to non equivalent *tert*-butyl groups of a σ-bonding Cp''' substituent. The signals for the ring protons appear between δ = 5.4 – 6.4 ppm and are downfield shifted by about 0.8 ppm compared to a η^5 coordinating Cp''' ligand. In the $^{31}P\{^{1}H\}$ NMR spectrum (C_6D_6) two groups of signals are detected betwen δ = -152 and -165 ppm as well as δ = -304 and -367 ppm each consisting of several more or less overlapping triplets, pseudo quartets or doublet of doublet of doublets (Figure 24). The chemical shift and coupling pattern indicates a tetraphospha-*bicyclo*-butane arrangement. The integral intensity ratio of the upfield-shifted signals, the coupling constants and the splitting pattern point to four isomers that are present in solution (Scheme 5) in a 4 : 1 : 7 : 7 ratio. In order to determine the correlation of the signals of the four isomers a $^{31}P\{^{1}H\}$-$^{31}P\{^{1}H\}$-COSY NMR experiment was performed (see Figure 66 Appendix). The associated chemical shifts, spin systems and coupling constants of the isomers are summarized in Table 4.

All isomers feature C–P bonds between the "wing-tip" P atoms of the butterfly framework and a tertiary C atom of the σ-bound Cp''' substituent. Altogether, three constitutional isomers are detected. While isomers **A** and **C** both exhibit a tertiary carbon atom next to the phosphorus-bound carbon, in isomer **B** the P-bound carbon is neighboured only by secondary carbon atoms. In isomer **D** both substitution patterns of the Cp''' substituent are realized. Isomers **A** and **C** are diastereomers with **A** being the *meso* compound. For isomers **C** and **D** two enantiomeric forms are possible but indistinguishable in the $^{31}P\{^{1}H\}$ NMR spectrum.

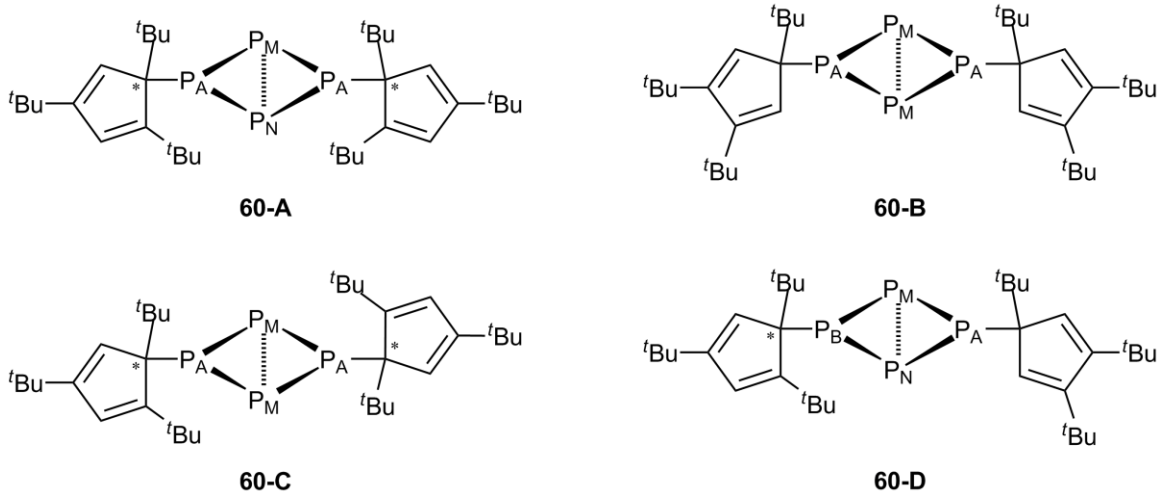

Scheme 5. Isomers of **60** detected in the $^{31}P\{^{1}H\}$ NMR spectrum. Phosphorus atoms are numbered according to the corresponding spin system.

Table 4. Spin system, chemical shift and coupling constants of the four isomers of **60**.

isomer	spin system	chemical shift (multiplicity)	coupling constant
A	A_2MN	δ_A = -163.4 ppm (t)	$^1J_{AM} = {}^1J_{AN}$ = 181 Hz
		δ_M = -307.3 ppm (dt)	$^1J_{MN}$ = 181 Hz
		δ_N = -364.0 ppm (dt)	
B	A_2M_2	δ_A = -154.9 ppm (t)	$^1J_{AM}$ = 181 Hz
		δ_M = –341.6 ppm (t)	
C	A_2M_2	δ_A = -157.9 ppm (t)	$^1J_{AM}$ = 182 Hz
		δ_M = –334.8 ppm (t)	
D	ABMN	δ_A = -154.4 ppm (ddd)	$^1J_{AM} = {}^1J_{BN}$ = 190 Hz
		δ_B = -162.5 ppm (ddd)	$^1J_{AN} = {}^1J_{BM}$ = 175 Hz
		δ_M = -324.8 ppm (dt)	$^1J_{MN}$ = 173 Hz
		δ_N = -352.1 ppm (dt)	$^2J_{AB}$ = 317 Hz

The exclusive presence of isomers that exhibit a C–P bond to a tertiary carbon atom indicates a radical mechanism for the formation of **60**. For the {Cp’’’}• radical several mesomeric formula are possible in which the single electron is either located on a tertiary or on a secondary carbon atom of the ring. As the stability of tertiary radicals is larger than that of secondary ones, their formation is favoured, giving the observed isomers. In contrast, an ionic mechanism requires the

formation of the aromatic cyclopentadienyl anion with a delocalized 6 π electron system. Hence, the tertiary carbon atoms are no longer preferred reaction sites and the formation of C–P bonds to secondary carbon atoms should be formed to a certain extent. This is not observed experimentally, confirming a radical mechanism.

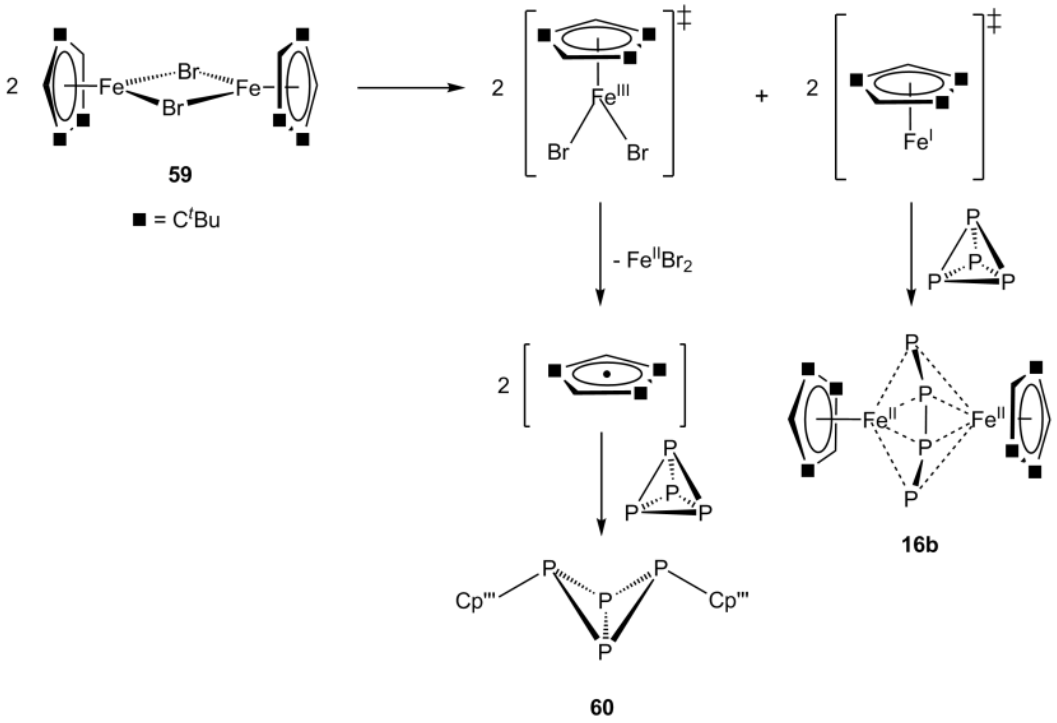

Scheme 6. Proposed reaction pathway for the formation of **16b** and **60**.

The formation of the {Cp’’’}• radical could proceed via a multi step mechanism (Scheme 6). The disproportionation reaction of **59** leads to the transient formation of the complex fragments [Cp’’’Fe] and [Cp’’’FeBr$_2$] with iron in the formal oxidation states +1 and +3, respectively. As this reaction is not observed in solutions of pure **59** or its iodine derivative,[88] a possible interaction between the starting material and P_4 could induce the disproportionation. While the reaction of two equivalents of the [Cp’’’Fe] fragment with P_4 affords **16b**, the Fe(III) species undergoes an electron transfer from the cyclopentadienyl ligand to the iron atom to form the desired (Cp’’’)• radical together with $FeBr_2$, which is found as insoluble by product of the reaction ($FeBr_2$ is oxidized rapidly upon contact with air and moisture and shows a characteristic rusty color). However, detailed EPR investigations should be carried out to get a deeper insight in the radical formation, which could unfortunately not be performed within the scope of this work.

[Cp’’’$_2$P$_4$] (**60**) crystallizes from a saturated Et_2O solution as colorless plates in the monoclinic centrosymmetric space group *Cc*. The asymmetric unit contains two molecules of **60-C** and one molecule of **60-D** that is disordered over two positions (The molecular structure of isomer **60-D** is depicted in Figure 61 Appendix). X-ray structure analysis confirms the expected butterfly

arrangement in a *syn,syn*-configuration. The same configuration is observed for the previously synthesized [{Ar^{Dipp}}$_2P_4$] (**12**).[40] While for **12** also the *syn,anti*-configuration can be observed, in [Mes_2P_4] (**8**) exclusively the *anti,anti*-configuration is found.[35] However, **60** represents the first compound with a direct C–P bond to a sp^3 hybridized carbon atom that could be synthesized directly from white phosphorus.

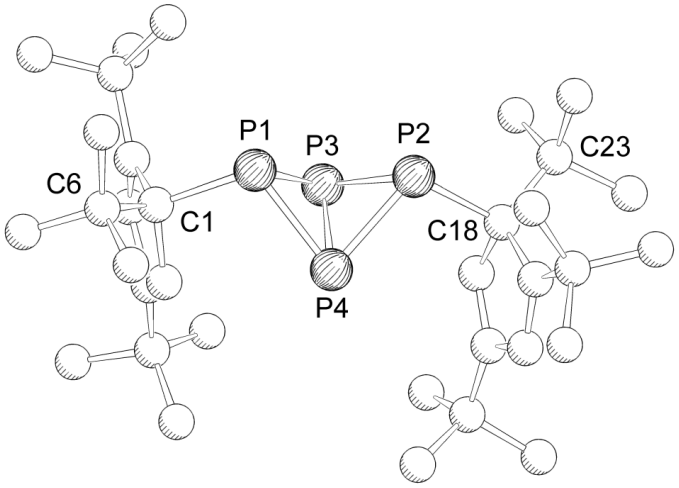

Figure 25. Molecular structure of **60-C** in the crystal. For clarity reasons only one molecule of the asymmetric unit is shown and hydrogen atoms are omitted. Selected bond lengths [Å] and angles [°]: P1–C1 1.948(5), P2–C18 1.947(5), P1–P3 2.182(2), P1–P4 2.233(2), P2–P3 2.231(2), P2–P4 2.201(2), P3–P4 2.154(2), P1···P2 2.828(1), P3–P1–P4 58.37(5), P3–P2–P4 58.13(5), P1–P3–P4 62.00(6), P1–P4–P3 59.63(6), P2–P3–P4 60.24(6), P2–P4–P3 61.63(6), P1–P3–P2 79.70(6), P1–P4–P2 79.25 (6), P3–P1–C1 102.2(2), P4–P1–C1 105.3(1), P3–P2–C18 102.7(1), P4–P2–C18 104.6(1), P1–C1–C6 108.0(3), P2–C18–C23 108.5(3).

The bond lengths of the P_4 framework follow the same trends that have been observed for the previously discussed butterfly complexes. While the bond distances between the wing-tip and bridgehead P atoms are in the range of a P–P single bond (2.182(2) Å – 2.233(2) Å) the P3–P4 bond is with 2.154(2) Å shortened and compares well to the corresponding bonds in **9b** (2.151(2) Å)[37] and **54** (2.165(2) Å). The C1–P1 and C18–P2 bond lengths of 1.948(5) Å and 1.947 (5) Å are longer than the C–P bond lengths in **8** (1.892(8) Å, 1.885(1) Å) and **12** (1.866(3) Å, 1.887(3) Å) which may be due to the steric bulk of the Cp''' ligand. The P1···P2 distance adds up to 2.828(1) Å which is shorter than in **9b** (2.96(1) Å) and slightly longer than in **54** (2.809(3) Å). Consequently, the P1–P3–P2 and P1–P4–P2 angles of 79.70(6)° and 79.25(6)° are smaller than in **9b** (84.49(9)° and 84.07(9)°) but compare well to those of **54** (79.29(8)° and 79.45(9)°).

3.4 Reactivity of tetraarsa-*bicyclo*[1.1.0]butane complexes

The reactivity of P_4 butterfly complexes under thermolytic and photolytic conditions has been investigated by Scherer *et al.* in the late 1990s. Irradiation of $[\{Cp''Fe(CO)_2\}_2(\mu,\eta^{1:1}\text{-}P_4)]$ (**9a**) with UV light leads to a successive decarbonylation of the starting material accompanied by a rearrangement of the P_4 framework.[36] Due to the rather mild reaction conditions all intermediary species could be identified and characterized. In contrast, under thermolytic conditions mainly the fully decarbonylated species $[\{Cp''Fe\}_2(\mu,\eta^{4:4}\text{-}P_4)]$ (**16a**) is formed. Analogous reaction behavior is observed for $[\{Cp'''Fe(CO)_2\}_2(\mu,\eta^{1:1}\text{-}P_4)]$ (**9b**) that shows a complete loss of the carbonyl ligands under thermolytic conditions,[37] while photolysis gives the twofold decarbonylated species $[\{Cp'''Fe\}(\mu,\eta^{4:1}\text{-}P_4)\{Cp'''Fe(CO)_2\}]$ in good yields.[89] However, during the reactivity studies of **9a** and **9b** the formation of P_n ligand complexes with $n > 5$ could not be observed under photolytic conditions.

In contrast, Dahl *et al.* used the diiron complex $[\{Cp^{Me}Fe(CO)_2\}_2]$ (**10e**) ($Cp^{Me} = C_5H_4Me$) with the quite small Cp^{Me} ligand for the formation of a P_8 ligand complex.[90] The photolysis of **10e** together with P_4 afforded $[\{Cp^{Me}Fe(CO)_2\}_2(\mu_4,\eta^{1:1:2:2}\text{-}P_8)\{Cp^{Me}Fe(CO)\}_2]$ (**61**) in 11 % yield that exhibits a P_8 cuneane framework. It was assumed that the reaction proceeds via P_2 intermediates. However, reactivity studies of the dinuclear iron complexes **10b** and **57** with P_4 presented in this work clearly prove the formation of the corresponding butterfly complexes. Hence, compound **61** is likely to be formed via a butterfly intermediate.

In the 1990s Scherer *et al.* reported the synthesis of the two analogous complexes $[\{Cp''Nb\}_2(\mu,\eta^{4:4}\text{-}As_8)]$ and $[\{Cp''Ta\}_2(\mu,\eta^{4:4}\text{-}As_8)]$ which both show a *cyclo*-As_8 framework as central building unit.[91] So far, complexes with As_8 cuneane motif are not known but would be worthwhile synthetic targets. As the As_8 cuneane formation could proceed via butterfly intermediates, the As_4 complexes $[\{Cp'''Fe(CO)_2\}_2(\mu,\eta^{1:1}\text{-}As_4)]$ (**52**) and $[\{Cp^*Cr(CO)_3\}_2(\mu,\eta^{1:1}\text{-}As_4)]$ (**56**) seemed to be perfect precursor compounds for that purpose.

3.4.1 Photolysis of [{Cp'''Fe(CO)$_2$}$_2$(μ,η$^{1:1}$-As$_4$)] (52)

Photolysis of **52** is performed in toluene at room temperature and monitored by IR spectroscopy. After two hours of irradiation, the carbonyl bands of the starting material disappear and new bands can be detected at ν = 1998, 1987, 1952, 1940 and 1898 cm^{-1}. Column chromatographic workup of the reaction mixture affords a dark brown fraction of [{Cp'''Fe(CO)$_2$}(μ,η$^{1:2}$-As$_4$){Cp'''Fe(CO)}] (**62**) and a dark green fraction of [{Cp'''Fe(CO)$_2$}$_2$(μ$_4$,η$^{1:1:2:2}$-As$_8$){Cp'''Fe(CO)}$_2$] (**63**) (equation 22). Complex **62** has good solubility in toluene and CH_2Cl_2 but only moderatesolubility in hexane. Complex **63** is isolated as dark green solid in low yields and dissolves readily in toluene, moderately in hexane but is nearly insoluble in acetonitrile. Single crystals of **63** suitable for X-ray structure analysis are obtained from a hexane/toluene solution upon cooling.

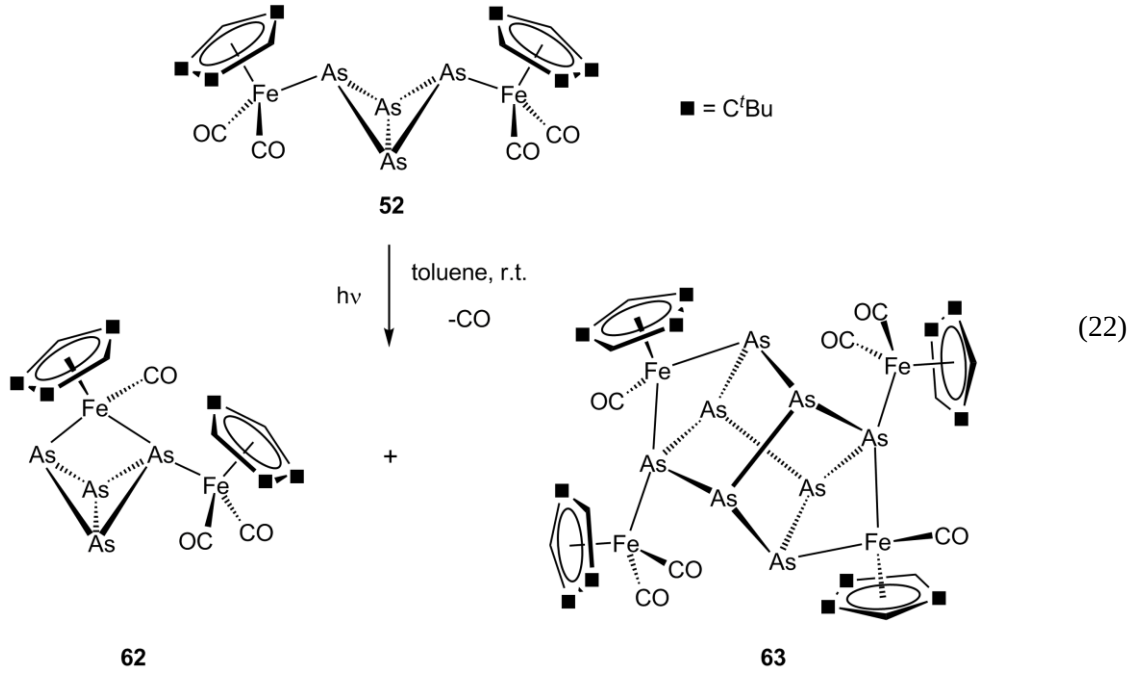

(22)

The IR spectrum of the brown fraction shows three sharp bands in the range of terminal carbonyl ligands. The signals at ν = 1988 and 1939 cm^{-1} compare well to the signals found for the starting material **52** (ν = 1990 and 1940 cm^{-1}) pointing to a [Cp'''Fe(CO)$_2$] moiety. The third signal is observed red-shifted at ν = 1908 cm^{-1} indicating a stronger π-backbonding from the central iron atom which is the case for a [Cp'''Fe(CO)] fragment. The IR spectrum compares well to the one of [{Cp''Fe(CO)$_2$}(μ,η$^{1:2}$-P$_4$){Cp''Fe(CO)}] that derives from **9a** by the loss of one carbonyl ligand (ν = 2008, 1960 and 1900 cm^{-1}).[36] Hence, the brown fraction can be identified as **62**, which exhibits a bridged As$_4$ butterfly framework (Equation 22). All attempts to obtain single

crystals of **62** by cooling solutions of **62** were not succesfull so far. Surprisingly, crystals of **63** were isolated from these solutions.

The IR spectrum of **63** shows three sharp carbonyl bands at ν = 1997, 1954 and 1885 cm^{-1}. While the first two signals are blue-shifted compared to the starting material **52**, the latter one is red-shifted indicating a terminal [Cp'''Fe$(CO)_2$] as well as a bridging [Cp'''Fe(CO)] unit. In the FD mass spectrum the molecular ion peak is observed as base peak at *m*/*z* = 1924.5. An additional peak is observed at *m*/*z* = 925.5 that can be assigned to the triple decker cation [{Cp'''Fe}$_2$$As_5$]$^+$. The ^{1}H NMR spectrum (C_6D_6) of **63** reveals one set of signals for freely rotating Cp''' ligands. Additionally, three singlets with equal intensities (9H) for ^{t}Bu groups and two doublets (1H each) with a small $^4J_{HH}$ coupling constant of 1.8 Hz are detected that can be assigned to a Cp''' ligand with hindered rotation on the NMR timescale. In the $^{13}C\{^1H\}$ NMR spectrum (C_6D_6) three singlets for the carbonyl ligands are found at δ = 213.7, 217.8 and 223.5 ppm.

[{Cp'''Fe$(CO)_2$}$_2$(μ_4,$\eta^{1:1:2:2}$-As_8){Cp'''Fe(CO)}$_2$] (**63**) crystallizes as dark green plates in the triclinic space group $P\bar{1}$. The asymmetric unit contains one molecule of **63** together with two molecules of toluene. The molecular structure of **63** is depicted in Figure 26.

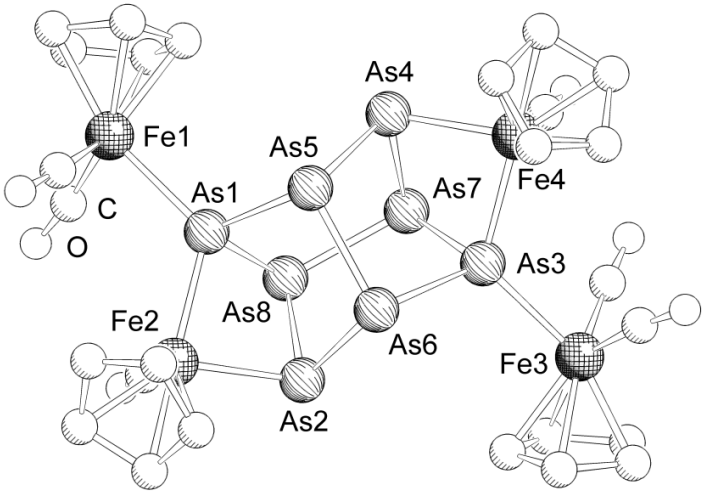

Figure 26. Molecular structure of **63** in the crystal. Hydrogen atoms and ^{tert}Bu groups are omitted for clarity. Selected bond lengths [Å] and angles [°]: Fe1–As1 2.4675(6), Fe2–As1 2.4253(5), Fe2–As2 2.4067(6), Fe3–As3 2.4692(6), Fe4–As3 2.4205(5), Fe4–As4 2.4213(6), As1–As5 2.4562(4), As1–As8 2.4557(4), As2–As6 2.4356(4), As2–As8 2.4323(4), As3–As6 2.4607(4), As3–As7 2.4499(4), As4–As5 2.4423(4), As4–As7 2.4317(5), As5–As6 2.4299(4), As7–As8 2.4348(5), As5–As1–As8 97.73(2), As6–As2–As8 98.29(2), As6–As3–As7 97.37(2), As5–As4–As7 98.44(2), As1–As5–As4 101.85(1), As1–As5–As6 93.99(2), As4–As5–As6 100.85(2), As2–As6–As3 101.28(1), As2–As6–As5 101.64(2), As3–As6–As5 94.74(1), As3–As7–As4 79.00(1), As3–As7–As8 108.27(2), As4–As7–As8 103.96(2), As1–As8–As2 78.90(1), As1–As8–As7 108.24(2), As2–As8–As7 103.57(2).

X-ray structure analysis of **63** reveals an As_8 cuneane framework coordinating two terminal [Cp'''Fe$(CO)_2$] and two bridging [Cp'''Fe(CO)] fragments. Hence, complex **63** is isostructural with the P_8 cuneane complex **61** of Dahl *et al.* Considering one positive charge for every iron moiety, the As_8 ligand has an overall charge of -4. Hence it is valence isoelectronic to the well known realgar As_4S_4. The Fe–As bonds vary from 2.4067(6) Å to 2.4692(6) Å whereupon the bonds to the terminal iron fragments are longer than the bonds to the bridging ones. The Fe1–As1 and Fe3–As3 bond lengths (2.4675(6) Å and 2.4692(6) Å) also compare well to the Fe–As bond distances in **52** (2.443(3) Å and 2.458(3) Å). The As–As bond lengths range from 2.4317(5) Å to 2.4607(4) Å which is typical for As–As single bonds (2.435(4) Å[67]). The smallest As–As–As bond angles are found for As3–As7–As4 (79.00(1)°) and As1–As8–As2 (78.90(1)°) which is due to the bridging [Cp'''Fe(CO)] iron moieties contracting the coordinating arsenic atoms. Furthermore, the As–As_{coord}–As angles for the coordinating arsenic atoms are smaller than the bond angles around the four non coordinating arsenic atoms.

While irradiation of the phosphorus butterfly complex **9b** leads to the loss of two carbonyl ligands with preservation of the P_4 framework, the arsenic butterfly complex **52** is decarbonylated only once and an additional aggregation process is observed. The formation of **63** is likely to proceed via the dimerization of **62**, which is indicated by the same Fe/As ratio and the same coordination modes of the iron moieties. Additionally, **63** crystallizes from solutions of pure **62**. An analogous reaction pattern may also be assumed for the above mentioned photolytic reaction of [{$Cp^{Me}Fe(CO)_2$}$_2$] (**10e**) with P_4 to yield the P_8 cuneane complex **61**.[90] In both cases the steric bulk of the used Cp^R ligand seems to play an important role for the formation of the E_8 cuneane (E = P, As) framework. While in the case of **9b** the bulky Cp''' ligand prevents any P–P interactions and therefore inhibits aggregation processes, the small Cp^{Me} ligand is not bulky enough to shield the corresponding butterfly complex and/or the mono decarbonylated species. Hence the formation of the P_8 cuneane **61** is observed. In case of arsenic, the used Cp''' ligand provides enough steric shielding to make the As_4 butterfly complex **52** stable. The loss of one carbonyl ligand leads to the bridged butterfly complex **62** in which the As_4 butterfly framework is not sufficiently shielded by the two [Cp'''Fe$(CO)_n$] (n = 1 or 2) fragments. Hence, intermolecular As–As interactions are possible which leads to the dimerzation product **63**.

3.4.2 Dimerization of [{Cp*Cr(CO)$_3$}$_2$(μ,η$^{1:1}$-As$_4$)] (56)

In contrast to [{Cp'''Fe(CO)$_2$}$_2$(μ,η$^{1:1}$-As$_4$)] (**52**) which is stable in solution, its chromium derivative **56** dimerizes to afford the As$_8$ cuneane complex [{Cp*Cr(CO)$_3$}$_4$(μ$_4$,η$^{1:1:1:1}$-As$_8$)] (**64**) already at room temperature (equation 23). As mentioned in chapter 3.3.4.3, attempts to recrystallize **56** leads to bright orange crystals that disappear within one day and red crystals form that contain **56** cocrystallized with **64**. Stirring a solution of **56** in THF at room temperature leads to color change from orange to red. The As$_8$ cuneane complex **64** is obtained as a dark-red solid that is well soluble in polar solvents and moderately soluble in hexane. Single crystals of **64** suitable for X-ray structure analysis are obtained from a THF solution upon cooling.

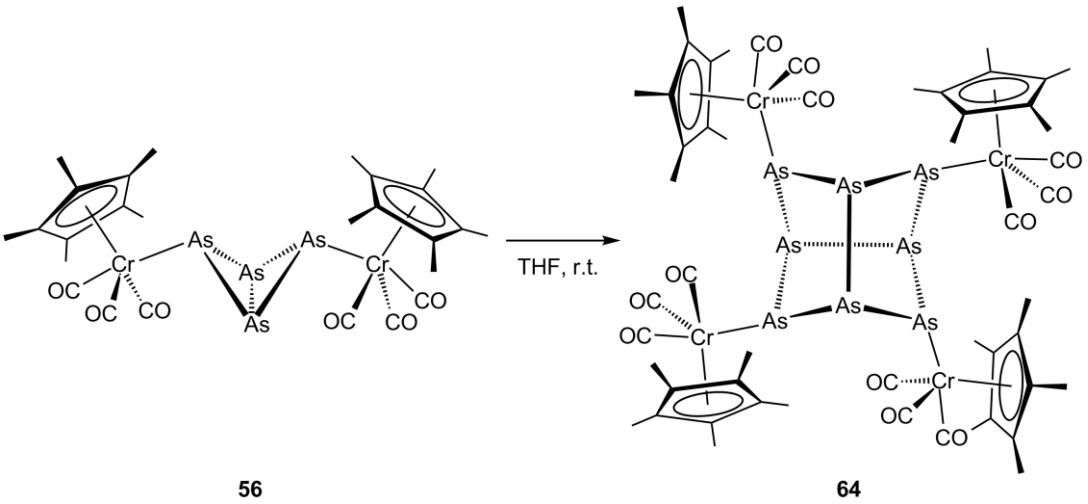

(23)

The IR spectrum of the reaction mixture reveals two broadened signals in the solid state at ν = 1973 and 1902 cm^{-1} and three bands in CH_2Cl_2 solution at ν = 1978, 1966 and 1905 cm^{-1} that appear in the same range as the signals for **56** ($\nu(CH_2Cl_2)$ =1977, 1965, 1904 cm^{-1}, (ν(KBr) = 1969, 1956, 1894 cm^{-1}). The ^{1}H NMR spectrum (CD_2Cl_2) shows one signal at δ = 1.84 ppm for the Cp* ligands. Interestingly, the signal is not shifted compared to the starting material **56** which points to a similar magnetic environment of the Cp* ligands in **56** and **64**.

[{Cp*Cr(CO)$_3$}$_4$(μ$_4$,η$^{1:1:1:1}$-As$_8$)] (**64**) crystallizes as dark red blocks in the tetragonal space group $I4_1/a$. The asymmetric unit contains two molecules of **64** together with one molecule of THF. The molecular structure of **64** is depicted in Figure 27.

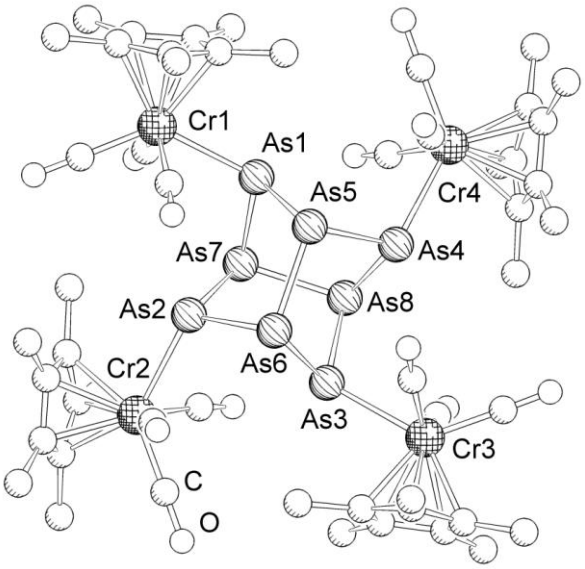

Figure 27. Molecular structure of **64** in the crystal. Hydrogen atoms are omitted for clarity. Selected bond lengths [Å] and angles [°]: Cr1–As1 2.608(1), Cr2–As2 2.628(1), Cr3–As3 2.626(1), Cr4–As4 2.635(1), As1–As5 2.4356(8), As1–As7 2.4246(8), As2–As6 2.4267(8), As2–As7 2.4412(8), As3–As6 2.4423(8), As3–As8 2.4266(8), As4–As5 2.4229(8), As4–As8 2.4470(8), As5–As6 2.4600(8), As7–As8 2.4543(8), As5–As1–As7 98.18(3), As6–As2–As7 98.02(3), As6–As3–As8 98.56(3), As5–As4–As8 97.82(3), As1–As5–As4 91.84(3), As1–As5–As6 106.58(3), As4–As5–As6 96.38(3), As2–As6–As3 90.39(3), As2–As6–As5 96.19(3), As3–As6–As5 106.45(3), As1–As7–As2 90.69(3), As1–As7–As8 96.12(3), As2–As7–As8 107.41(3), As3–As8–As4 91.00(3), As3–As8–As7 95.16(3), As4–As8–As7 107.27(3).

The central building unit in **64** is an As_8 cuneane framework which may again be seen as an As_8^{4-} ligand. In contrast to **63**, which shows two terminal and two bridging iron fragments, all [Cp*Cr(CO)$_3$] moieties are terminally coordinated. The Cr–As bond distances vary from 2.608(1) Å to 2.635(1) Å and compare well to the Cr–As bond lengths in **56** (2.641(1) Å and 2.614(1) Å). The As–As bond distances vary from 2.4229(8) Å to 2.4600(8) Å and are in the range of As–As single bonds (2.435 Å).[67] The longest bonds are found for As5–As6 and As7–As8 (2.4600(8) Å and 2.4543(8) Å). Surprisingly, these elongated bonds between the non-coordinating As atoms cannot be observed for the iron derivative **63**. The As_{coord}–$As_{non\text{-}coord}$–As_{coord} angles (91.84(3)°, 90.39(3)°, 90.69(3)°, 91.00(3)°) are about 5° – 15° smaller than the other As–As–As bond angles which is again not the case for **63** and is a result of the different coordination mode of the As_8 cuneane unit in **64** compared to **63**.

The formation of **64** may proceed via a direct dimerization of the butterfly complex **56** which is in contrast to the stable iron derivative **52**. The reason for the enhanced dimerization tendency might be the small steric bulk of the [Cp*Cr(CO)$_3$] fragment compared to the large [Cp'''Fe(CO)$_2$] unit. Hence, intermolecular As–As interactions are already possible for the butterfly complex **56** and no initial decarbonylation is necessary for the dimerzation process as is the case for **52**.

3.5 E_4 butterfly complexes (E = P_4, AsP_3, As_4) as chelating ligands for transition metal lewis acids

Since the isolation of the first transition-metal-stabilized bridging P_4 butterfly complex **9b**, its reactivity under thermolytic and photolytic conditions as well as its reactivity towards various alkynes has been investigated intensively.[37, 80, 92] In contrast, its coordination behavior towards Lewis acids has only been scarcely studied (see chapter 1.4, Scheme 3).[56, 89] The reported compounds do not contain intact **9b** units but show rearranged P_4 frameworks due to decarbonylation and P–P bond cleavage reactions.

However, the three coordinate "wing-tip" phosphorus atoms in **9b** should bear accessible lone pairs for the interaction with Lewis acids. Hence, the butterfly complex itself could be used as bidentate ligand with small bite angle but large steric bulk. To confirm this assumption the frontier molecular orbitals of the model complex [{$CpFe(CO)_2$}$_2$($\mu,\eta^{1:1}$-P_4)] were calculated by Dr. Gábor Balázs (University of Regensburg) using DFT methods at the BP86/def-SVP level of theory.

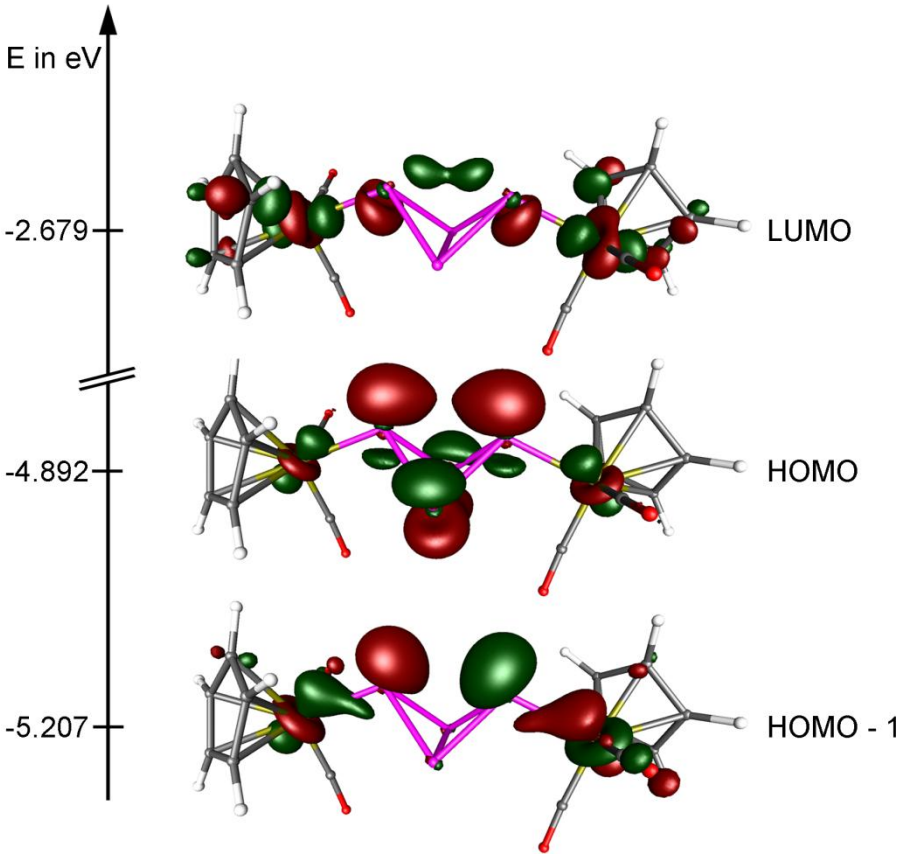

Figure 28. Illustration of the HOMO (highest occupied molecular orbital), HOMO–1 and LUMO (lowest unoccupied molecular orbital) of the model complex [{$CpFe(CO)_2$}$_2$($\mu,\eta^{1:1}$-P_4)] calculated at the BP86/def-SVP level of theory.

The HOMO (highest occupied molecular orbital) as well as the HOMO–1 are mainly localized at the P_4 framework as well as the iron atoms. The HOMO contains contributions from the lone pairs at the "wing-tip" P atoms and shows a bonding overlap between the two "bridgehead" P atoms. The HOMO–1 may be seen as a combination of the lone pairs at the "wing-tip" P atoms and a Fe d-orbital with a slight antibonding character with respect to the Fe–P bond. However, the position of the filled orbitals should allow an appreciable interaction between the "wing-tip" P atoms of the butterfly complex and a Lewis acid. Additionally, the LUMO (lowest unoccupied molecular orbital) can be found in between the two "wing-tip" phosphorus atoms which could allow backbonding from the Lewis acid to the butterfly complex.

Table 5. Summary of isolated compounds in which the butterfly complex acts as chelating ligand for the used Lewis acid.

complex	**Lewis acid**	**product successfully characterized by**			
		X-ray structure	$^{31}P\{^1H\}$ NMR	IR	ESI MS
	½ Cu^+	✓	✓	✓	
9b	½ Ag^+	✓	✓	✓	✓
M = Fe	$\{(PPh_3)Au\}^+$	✓	✓	✓	✓
$E_4 = P_4$	$\{(MeCN)Cu\}^+$	✓	✓	✓	
	$FeBr_2$	✓		✓	
54	½ Cu^+	✓	✓	✓	
M = Cr	½ Ag^+	✓	✓	✓	✓
$E_4 = P_4$	$\{(PPh_3)Au\}^+$	✓	✓	✓	✓
51	½ Cu^+		✓	✓	✓
M = Fe	½ Ag^+	✓	✓	✓	✓
$E_4 = AsP_3$	$\{(PPh_3)Au\}^+$		✓	✓	✓
55	½ Cu^+	✓	✓	✓	
M = Cr	½ Ag^+	✓	✓	✓	✓
$E_4 = AsP_3$	$\{(PPh_3)Au\}^+$	✓	✓	✓	✓
52	½ Cu^+	✓		✓	✓
M = Fe	½ Ag^+	✓		✓	✓
$E_4 = As_4$					
56					
M = Cr	½ Ag^+	✓		✓	✓
$E_4 = As_4$					

In order to evaluate the ligand properties of the butterfly complexes $[\{Cp^RM(CO)_n\}_2(\mu,\eta^{1:1}\text{-}E_4)]$ (Cp^R = Cp''', M = Fe, n = 2; Cp^R = Cp*, M = Cr, n = 3; $E_4 = P_4$, AsP_3, As_4) (see chapter 3.3), they were reacted with the group 11 cations $[Cu(MeCN)_4]^+[BF_4]^-$, $Ag^+PF_6^-$ and

$[(PPh_3)Au(tht)]^+[PF_6]^-$ that contain weakly coordinating anions. Additionally, the coordination behavior of **9b** towards the neutral Lewis acid $FeBr_2$·dme was investigated. In almost all cases the respective E_4 butterfly complex acts as a chelating ligand. The reactions are selective and the formation of side products is not observed in the NMR spectra of the reaction mixtures. Given yields refer to the isolated, crystalline material. The products were characterized by X-ray structure analysis, $^{31}P\{^1H\}$NMR spectroscopy, IR spectroscopy and ESI mass spectrometry and are discussed in the following chapters. Table 5 summarizes the performed experiments.

3.5.1 P_4 butterfly complexes as chelating ligands

3.5.1.1 Coordination behavior towards monovalent copper cations

The reaction of two equivalents of $[\{Cp'''Fe(CO)_2\}_2(\mu,\eta^{1:1}\text{-}P_4)]$ (**9b**) or $[\{Cp^*Cr(CO)_3\}_2(\mu,\eta^{1:1}\text{-}P_4)]$ (**54**) with one equivalent of $[Cu(MeCN)_4]^+[BF_4]^-$ leads to the selective formation of $[\{\{Cp'''Fe(CO)_2\}_2(\mu_3,\eta^{1:1:1:1}\text{-}P_4)\}_2Cu]^+[BF_4]^-$ (**65**) and $[\{\{Cp^*Cr(CO)_3\}_2(\mu_3,\eta^{1:1:1:1}\text{-}P_4)\}_2Cu]^+[BF_4]^-$ (**66**), respectively (Equation 24). In both cases an immediate color change from bright orange to red can be observed during the reaction. The $^{31}P\{^1H\}$ NMR spectra of the reaction mixtures show a quantitative formation of the respective compound. The reaction of **9b** with $[Cu(MeCN)_4]^+[BF_4]^-$ in a 1 : 1 stochiometry affords the monoadduct $[\{Cp'''Fe(CO)_2\}_2(\mu_3,\eta^{1:1:2}\text{-}P_4)\{Cu(MeCN)\}]^+[BF_4]^-$ (**67**) which shows a dynamic behavior in solution. The stochiometry dependency will be discussed in detail later on. Compounds **65** and **66** are isolated as red solids that have good solubility in dichloromethane and THF but are insoluble in hexane. Single crystals of the compounds suitable for X-ray structure analysis are obtained by slow diffusion of hexane into a THF solution of **65** or **66**, respectively.

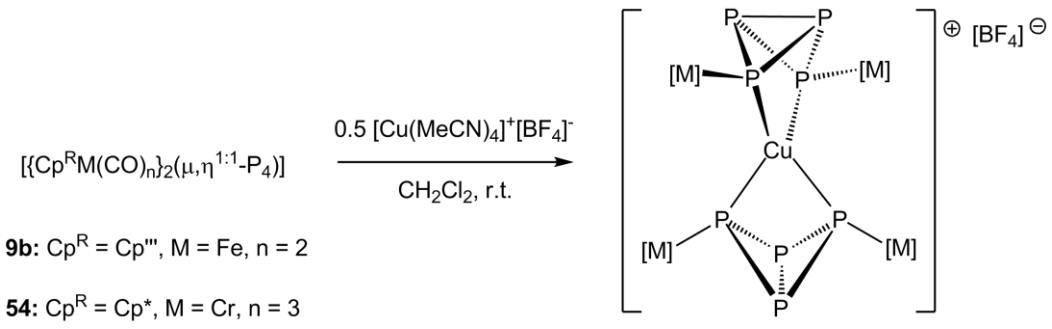

(24)

In the positive ion ESI mass spectrum of **65** the base peak is detected at *m*/*z* = 1131.4 and corresponds to the fragment [**9b** + $\{Cp'''Fe(CO)\}]^+$. Additionally a peak is detected at

m/z = 1103.6 that can be assigned to [**9b** + {Cp'''Fe}]$^+$. The unusual fragmentation pattern and the absence of copper-containing fragments indicate a rather weak Cu–P interaction in complex **65**. The IR spectrum (KBr) of **65** reveals three broad carbonyl bands at ν = 2008, 1960, 1930 cm^{-1}. Compared to the starting material **9b**, the signals are blue-shifted by about 10 cm^{-1} pointing to stronger C–O bonds and consequently weaker π-backbonding. This can be explained readily by an electron-withdrawing effect of the coordinated copper(I) cation. The ^{1}H NMR spectrum (CD_2Cl_2) of **65** shows three sharp singlets at δ = 1.42, 1.44 and 4.82 ppm for the freely rotating Cp''' ligands. In the $^{31}P\{^1H\}$ NMR spectrum (CD_2Cl_2) two triplets of an A_2M_2 spin system at δ = -81.2 and -282.0 ppm ($^1J_{PP}$ = 181 Hz) appear that correspond to the "wing-tip" and the bridgehead phosphorus atoms of the butterfly complex, respectively. While the first one is shifted upfield compared to the signal in **9b** the latter one is shifted downfield (**9b**: δ = -75.2 and -322.3 ppm). Additionally, the signals show a broadening at their base indicating more complicated spin system. Hence, VT NMR investigations were performed to shed more light in the spin system of **65** (Figure 67 Appendix). Upon cooling to 193 K, the chemical shift of both signals is nearly unchanged. While the triplet at δ = -81.2 ppm is only slightly broadened, the upfield shifted signal at δ = -282.0 ppm shows severe line broadening at 213 K ($\omega_{1/2}$ = 443 Hz) and is only detected as a broad singlet ($\omega_{1/2}$ = 795 Hz) at 193 K. The broadening of the upfield shifted signal seems to be a result of a hindered rotation of the Cp''' ligands. However, the VT NMR spectra do not allow a further analysis of the spin system of **65**.

The IR spectrum (KBr) of **66** shows three broad signals at ν = 1990, 1932 and 1913 cm^{-1} for terminal CO ligands. They are slightly blue-shifted compared to **54**, indicating a decrease of the electron density at the Cr atoms. In the ^{1}H NMR spectrum (CD_2Cl_2) one singlet for the methyl protons of the Cp* ligand is observed at δ = 1.94 ppm. The $^{31}P\{^1H\}$ NMR spectrum (CD_2Cl_2) shows two triplets at δ = -89.1 and -284.4 ppm that are typical for a P_4 butterfly arrangement. In contrast to **65**, both signals are shifted downfield compared to the starting material **54** (δ = -95.2 ppm and -327.4 ppm). The signals are broadened at their base, pointing again on a spin system of higher order that is not resolved.

$[\{\{Cp'''Fe(CO)_2\}_2(\mu_3,\eta^{1:1:1:1}\text{-}P_4)\}_2Cu]^+[BF_4]^-$ (**65**) crystallizes as red plates in the triclinic space group $P\bar{1}$. The asymmetric unit contains one molecule of **65** together with two molecules of THF. X-ray structure analysis confirms the expected chelating coordination of the copper(I) cation by two molecules of **9b** (Figure 29) via their "wing-tip" P atoms. The central Cu^+ is coordinated in a distorted tetrahedral way.

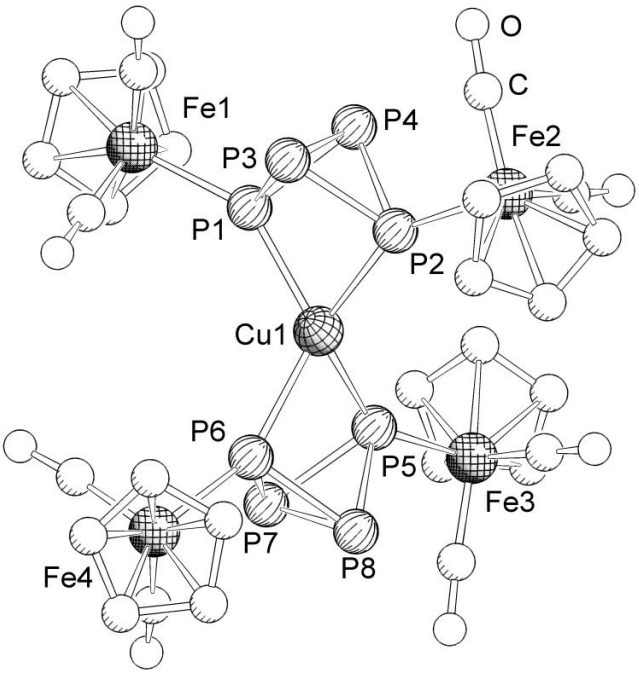

Figure 29. Molecular structure of **65** in the crystal. Hydrogen atoms, ^{tert}Bu groups as well as the $[BF_4]^-$ counter ion are omitted for clarity. Selected bond lengths [Å] and angles [°]: Cu1–P1 2.3630(8), Cu1–P2 2.4268(8), Cu1–P5 2.3737(8), Cu1–P6 2.4266(8), Fe1–P1 2.3059(8), Fe2–P2 2.3248(8), Fe3–P5 2.3122(8), Fe4–P6 2.3380(8), P1–P3 2.221(1), P1–P4 2.210(1), P2–P3 2.217(1), P2–P4 2.227(1), P3–P4 2.176(1), P5–P7 2.214(1), P5–P8 2.218(1), P6–P7 2.230(1), P6–P8 2.213(1), P7–P8 2.175(1), P1···P2 2.833(1), P5···P6 2.846(1), P1–Cu1–P2 72.51(3), P1–Cu1–P5 136.62(3), P1–Cu1–P6 123.15(3), P2–Cu1–P5 124.65(3), P2–Cu1–P6 138.98(3), P5–Cu1–P6 72.71(3), P1–P3–P2 79.34(4), P1–P4–P2 79.36(4), P5–P7–P6 79.63(4), P5–P8–P6 79.93(4).

The planes defined by the atoms P1–P2–Cu1 and P5–P6–Cu1 generate a dihedral angle of 73.94(4)° which means the two butterfly complexes are twisted from a perfect perpendicular arrangement. The Cu–P bond lengths vary from 2.3630(8) Å to 2.4268(8) Å. This is slightly longer than in the archetypal compound $[(dppe)_2Cu]^+[ClO_4]^-$ (2.259(2) Å to 2.301(2) Å)[93] but compares well to the bond lengths in the dppm containing compound $[(dppm)(POP)Cu]^+[BF_4]^-$ (POP = bis[2-(diphenylphosphino)phenyl]ether) with 2.333(3) Å and 2.425(4) Å.[94] The Fe–P bond distances are in the range from 2.3059(8) Å to 2.3380(8) Å and are shorter than in the starting material **9b** (2.348(2) Å and 2.355(2) Å).[37] A reason for this might be the contribution of the HOMO-1 for the coordination of the copper cation. As this MO has an antibonding character with respect to the Fe–P bond, the electron withdrawing effect of the Lewis acid strengthens the Fe–P bond and decreases the bond length. While the P–P bonds between the coordinating and non-coordinating P atoms are essentially the same as those in **9b**, the P3–P4 and P7–P8 bonds with 2.176(1) Å and 2.175(1) Å are shorter than the corresponding bond in **9b** (2.209(2) Å). The P1···P2 and P5···P6 distances add up to 2.833(1) Å and 2.846(1) Å, respectively and are shorter than the associated distance in **9b** (2.96 Å). This means the butterfly framework is contracted by

the interaction with the copper cation. However, the bite angles in **65** are small at 72.51(3)° and 72.71(3)°, and compare well to the dppm bite angle in $[(dppm)(POP)Cu]^+[BF_4]^-$ (73.3(1)°). As the bite angle as well as the Cu–P bonds in $[(dppm)(POP)Cu]^+[BF_4]^-$ and **65** are very similar, the butterfly complex **9b** may be regarded as sterically demanding, inorganic dppm analogue.

$[\{\{Cp^*Cr(CO)_3\}_2(\mu_3,\eta^{1:1:1:1}\text{-}P_4)\}_2Cu]^+[BF_4]^-$ (**66**) crystallizes as red blocks in the triclinic space group $P\bar{1}$. The asymmetric unit contains one molecule of **66**. X-ray structure analysis shows the coordination of one Cu(I)-cation by two butterfly complexes **54** (Figure 30).

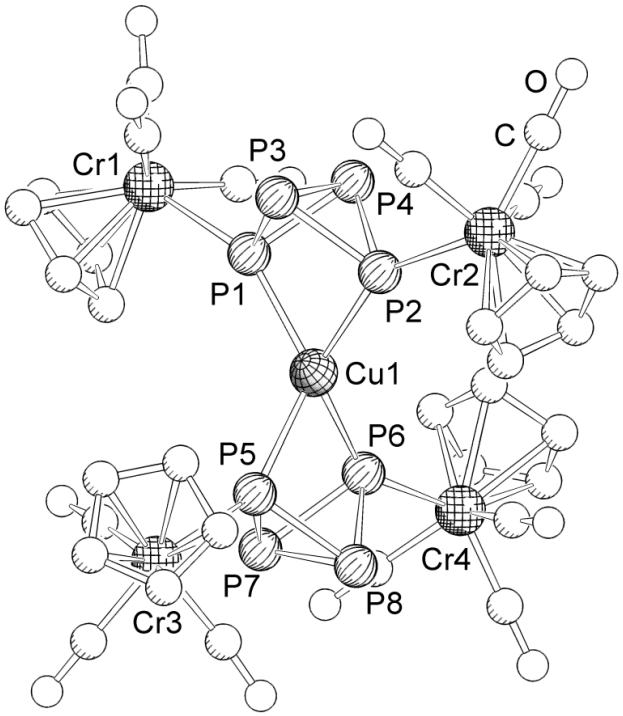

Figure 30. Molecular structure of **66** in the crystal. Methyl groups as well as the $[BF_4]^-$ counter ion are omitted for clarity. Selected bond lengths [Å] and angles [°]: Cu1–P1 2.4005(7), Cu1–P2 2.4151(7), Cu1–P5 2.4551(7), Cu1–P6 2.3742(6), Cr1–P1 2.5118(6), Cr2–P2 2.5266(6), Cr3–P5 2.5269(6), Cr4–P6 2.4931(6), P1–P3 2.2233(8), P1–P4 2.2035(8), P2–P3 2.2154(8), P2–P4 2.2125(9), P3–P4 2.1767(9), P5–P7 2.2043(8), P5–P8 2.2341(8), P6–P7 2.2274(8), P6–P8 2.2057(8), P7–P8 2.1786(7), P1···P2 2.8568(8), P5···P6 2.8481(8), P1–Cu1–P2 72.78(2), P1–Cu1–P5 127.35(2), P2–Cu1–P5 131.68(2), P2–Cu1–P6 130.08(2), P5–Cu1–P6 72.26(2), P1–P3–P2 80.12(3), P1–P4–P2 80.62(3), P5–P7–P6 79.98(3), P5–P8–P6 79.80(3).

The angle between the planes defined by the atoms Cu1–P1–P2 and Cu1–P5–P6 is with 86.67(3)° larger than the corresponding angle in **65** but still indicative for the distorted tetrahedral coordination environment of the central copper cation. A reason for this might be the smaller steric bulk of the $[Cp^*Cr(CO)_3]$ moiety compared to the $[Cp'''Fe(CO)_2]$ fragment. The Cu–P bond distances vary from 2.3742(6) Å to 2.4551(6) Å, which compares well to the corresponding bond lengths in **65** and $[(dppm)(POP)Cu]^+[BF_4]^-$. The Cr–P bond lengths (2.4931(6) Å to

2.5269(6) Å) are essentially the same as those in **54**. The P–P bond lengths between the coordinating and non-coordinating P atoms (2.2035(8) Å to 2.2341(8) Å) are slightly longer compared to those in **54** (2.196(3) Å to 2.205(2) Å) which is also the case for the P3–P4 and P7–P8 bonds (2.1767(9) Å and 2.17868(7) Å compared to the bridgehead P–P bond in **54** (2.165(2) Å). Surprisingly, the P1···P2 and P5···P6 distances of 2.8568(8) Å and 2.8481(8) Å are longer than the corresponding distance in the butterfly complex **54** with 2.8081(3) Å, which is in contrast to the observation for the iron derivative **65** in which the bond distance is shorter than in the starting material **9b**. However, the found P–P bond lengths as well as P···P distances are essentially the same as those in **65**, which is also the case for the angles around the central copper cation. Hence, the stabilizing $[Cp^{R}M(CO)_n]$ (Cp^{R} = Cp''', M = Fe, n = 2; Cp^{R} = Cp*, M = Cr, n = 3) fragments only play a minor role for the interaction between the P_4 butterfly ligand and the Cu^{+} cation and the resulting coordination geometry does not depend on the $[Cp^{R}M(CO)_n]$ moiety. The bite angles (72.78(2)° and 72.26(2)°) in **66** are essentially the same than in **65**.

While the reaction of $[Cu(MeCN)_4]^{+}[BF_4]^{-}$ with two equivalents of **9b** leads to the formation of **65** in which all acetonitrile ligands have been replaced by two chelating butterfly complexes, the reaction with only one equivalent of **9b** leads to the formation of $[\{Cp'''Fe(CO)_2\}_2(\mu_3,\eta^{1:1:2}\text{-}P_4)\{Cu(MeCN)\}]^{+}[BF_4]^{-}$ (**67**) in which three acetonitrile ligands are substituted by one butterfly complex (Equation 25). Compound **67** is isolated as reddish orange solid that has good solubility in dichloromethane and THF but is only sparingly soluble in hexane. Single crystals of **67** suitable for X-ray structure analysis can be obtained by slow diffusion of hexane into a saturated solution of **67** in dichloromethane.

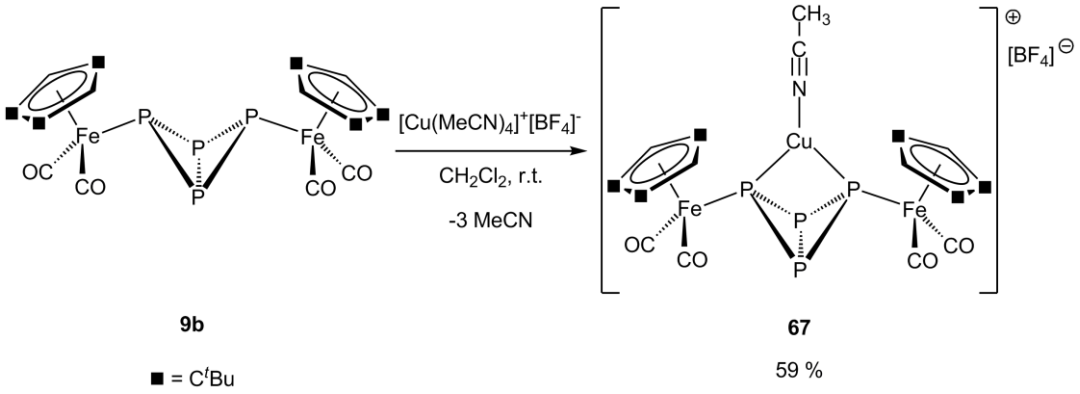

(25)

The positive ion ESI mass spectrum of **67** reveals one peak at *m*/*z* = 1103.6 that corresponds to the cationic fragment [**9b** + {Cp'''Fe}]$^{+}$. The absence of copper containing fragments in the ESI mass spectrum has also been observed for the bis chelate complex **65**. In the IR spectrum (KBr)

four absorption bands for the terminal carbonyl ligands are observed at ν = 2009, 2000, 1962 and 1956 cm^{-1}. The signals are blue shifted compared to **9b** which is due to the electron withdrawing effect of the Lewis acid. At ν = 2285 cm^{-1} one weak band appears for the terminal acetonitrile ligand. In the ^{1}H NMR spectrum (CD_2Cl_2) of **67** one typical set of signals for the Cp''' ligands are detected. Additionally, a sharp singlet for the coordinating acetonitrile ligand appears at δ = 2.36 ppm which is only slightly shifted compared to the starting material $[Cu(MeCN)_4]^+[BF_4]^-$ (δ = 2.15 ppm).[95] The $^{31}P\{^{1}H\}$ NMR spectrum (CD_2Cl_2) of pure **67** at room temperature reveals two broad signals at δ = -71.0 ($\omega_{1/2}$ = 608 Hz) and -317.2 ppm ($\omega_{1/2}$ = 625 Hz) indicating dynamic behavior in solution. Furthermore, two sharp triplets at δ = -80.9 and -282.0 ppm are observed which can be assigned to complex **65**. The intensity ratio of the signals (**67** : **65**) is about 12 : 1. Taking into account that that complex **65** bears two butterfly ligands while complex **67** only bears one, the molar ratio of the mono- and bis chelate complex is about 24 : 1. After six hours, the molar ratio is lowered to about 14 : 1 and does not change further upon time. Hence, a dynamic ligand exchange takes place in solution (Scheme 7) which will be outlined after the discussion of the X-ray structure analysis.

$[\{Cp'''Fe(CO)_2\}_2(\mu_3,\eta^{1:1:2}\text{-}P_4)\{Cu(MeCN)\}]^+[BF_4]^-$ (**67**) crystallizes as reddish orange blocks in the monoclinic space group $P2_1/c$. The asymmetric unit contains one molecule of **67**. X-ray structure analysis shows the coordination of a central Cu(I) cation by one molecule of **9b** as well as one acetonitrile ligand (Figure 31).

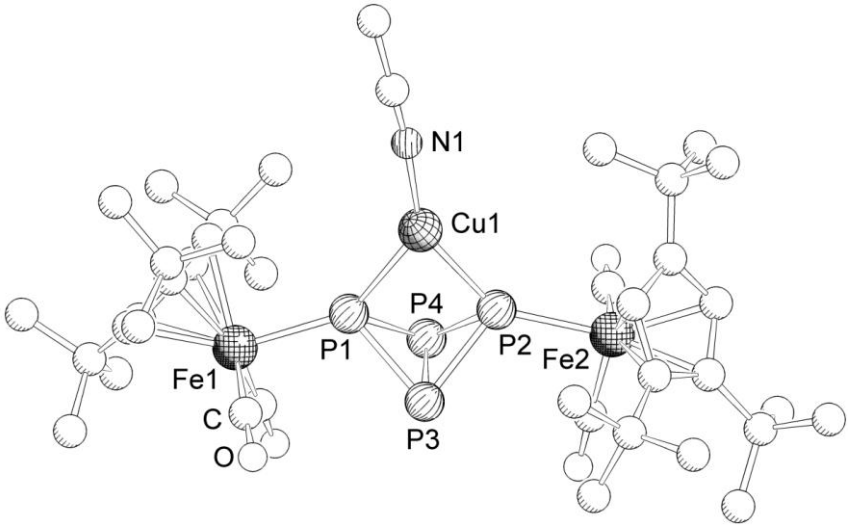

Figure 31. Molecular structure of **67** in the crystal. Hydrogen atoms as well as the $[BF_4]^-$ counter ion are omitted for clarity. Selected bond lengths [Å] and angles [°]: Cu1–P1 2.3224(7), Cu1–P2 2.2891(6), Cu1–N1 1.897(2), Fe1–P1 2.2928(6), Fe2–P2 2.2845(6), P1–P3 2.2196(8), P1–P4 2.2261(8), P2–P3 2.2263(8), P2–P4 2.2189(8), P3–P4 2.1792(8), P1···P2 2.8135(8), P1–Cu1–P2 75.19(2), P1–Cu1–N1 136.23(7), P2–Cu1–N1 148.37(7), P1–P3–P2 78.52(3), P1–P4–P2 78.54(3).

The central copper cation shows a trigonal-planar coordination environment. The sum of angles around the Cu1 atom is 359.8°. The P1–Cu1–N1 angle is 136.23(7)°, and hence smaller than the P2–Cu1–N1 angle of 148.37(7)°, pointing to a slightly distorted coordination. However, the P1–Cu1–P2 bond angle of 75.19(2)° is larger than the corresponding angles in **65** (72.51(3)° and 72.71(3)°). Additionally, the Cu1–P1 and Cu1–P2 bond lengths of 2.3224(7) Å and 2.2891(6) Å are shorter than the associated bond lengths in **65** (2.3630(8) Å, 2.4268(8) Å, 2.3737(8) Å and 2.4266(8) Å). Hence, the copper cation is coordinated more tightly by the butterfly complex, which also explains the larger P1–Cu1–P2 bond angle. A reason for this might be the reduced steric bulk on one side of the central Cu atom which allows a better interaction between the Lewis acid and **9b**. While the P–P bond lengths as well as the P1···P2 distance compare well to the corresponding distances in **65**, the Fe–P bond lengths (2.2928(6) Å and 2.2845(6) Å) are shorter than in **65** (2.3059(8) Å, 2.3248(8) Å, 2.3122(8) Å and 2.3380(8) Å). This indicates either a stronger contribution of the HOMO-1 of **9b** to the bonding or might also be explained by the reduced steric bulk provided by the MeCN ligand.

To further investigate the equilibrium of **67** in solution a $^{31}P\{^{1}H\}$ VT NMR spectrum was recorded at 193 K revealing a total of five signals at δ = -11.4 ppm (br s, $\omega_{1/2}$ = 609 Hz), -72.4 ppm (t, $^{1}J_{PP}$ = 176 Hz), -283.3 ppm (br s, $\omega_{1/2}$ = 800 Hz), -300.0 ppm (t, $^{1}J_{PP}$ = 177 Hz) and -316.3 ppm (t, $^{1}J_{PP}$ = 177 Hz) (Figure 68 Appendix). The integral intensity ratio of the signals is 1 : 3 : 1 : 1 : 2 pointing to three species in solution. The signal with an integral intensity of 3 is a result of two overlapping signals with integral intensities of 2 and 1. The signals at δ = -72.4 and -283.3 ppm can be assigned to complex **65** ($^{31}P\{^{1}H\}$ VT NMR (193 K) δ = -81.2 ppm (t, $^{1}J_{PP}$ = 181 Hz) and -282.0 ppm (br s)). The discrepancy of the chemical shift of the downfield shifted signal can be explained by the presence of acetonitrile. Furthermore, the chemical shifts of the triplets at δ = -72.4 and -316.3 ppm compare well to the broad signals found in the room temperature spectrum of **67**. They are therefore assigned to the monochelate complex **67**.

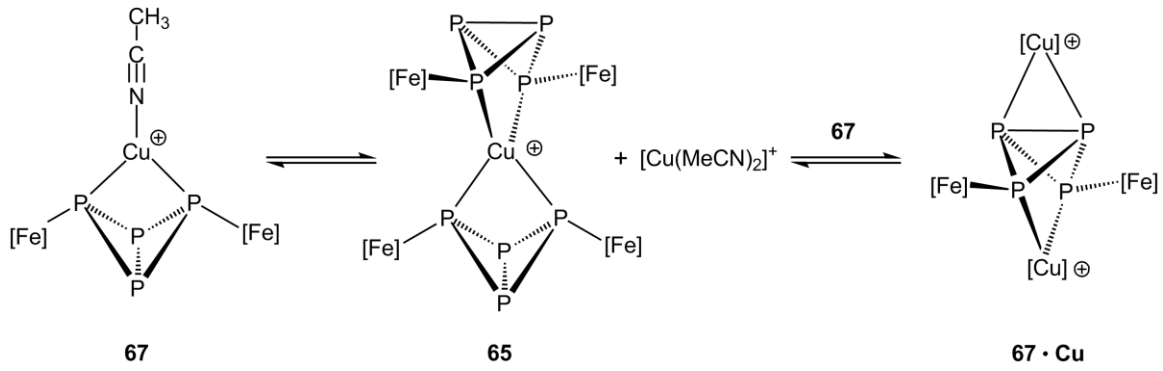

Scheme 7. Proposed equilibrium of **67** in solution and the suggested structure of **67·Cu** ([Fe] = [Cp'''Fe(CO)$_2$] and [Cu] = [Cu(MeCN)$_n$]).

The formation of **65** from two molecules of **67** formally affords the release of a $[Cu(MeCN)_2]^+$ fragment which acts as a Lewis acid in solution and can interact with both complexes **65** or **67**. The resulting product gives rise to the signals at δ = -11.4 and -300.0 ppm. To clarify the nature of these signals, the butterfly complex **9b** was reacted with two equivalents of $[Cu(MeCN)_4]^+[BF_4]^-$ and a $^{31}P\{^1H\}$ NMR spectrum was recorded. The $^{31}P\{^1H\}$ NMR spectrum (CD_2Cl_2) at room temperature shows two triplets δ = -31.0 and -305.6 ppm with a coupling constant of $^1J_{PP}$ = 194 Hz which is evocative of the two unassigned signals in the $^{31}P\{^1H\}$ NMR spectrum of **67** at 193 K. The discrepancy in the chemical shift is most likely a result of the different temperatures during the measurement and the amount of acetonitrile in solution. Furthermore, the line broadening leads to slightly different coupling constants. Hence, **67** is likely to undergo a ligand exchange reaction in solution which affords the bis chelate complex **65** as well as $[\{Cp'''Fe(CO)_2\}_2(\mu_4,\eta^{1:1:1:1:2}\text{-}P_4)\{Cu(MeCN)\}\{Cu(MeCN)_2\}]^{2+}[BF_4]^-_2$ (**67·Cu**). Unfortunately, in the course of this thesis, **67·Cu** could not be further characterized. However, for sterical reasons, the coordination of the $[Cu(MeCN)_2]^+$ via the bridgehead P atoms of the butterflyframework seems reasonable but has to be proven by X-ray structure analysis.

3.5.1.2 Coordination behavior towards monovalent silver cations

The reaction of $AgPF_6$ with two equivalents of **9b** or **54** yields the two complexes $[\{\{Cp'''Fe(CO)_2\}_2(\mu_3,\eta^{1:1:1:1}\text{-}P_4)\}_2Ag]^+[PF_6]^-$ (**68**) and $[\{\{Cp^*Cr(CO)_3\}_2(\mu_3,\eta^{1:1:1:1}\text{-}P_4)\}_2Ag]^+[PF_6]^-$ (**69**), respectively (Equation 26). The $^{31}P\{^1H\}$ NMR spectra (CD_2Cl_2) of the reaction mixtures shows quantitative formation of the respective compound. Compounds **68** and **69** are obtained as orange solids that have good solubility in dichloromethane and THF, but are insoluble in hexane. Crystals of **68** and **69** suitable for X-ray structure analysis were obtained by slow diffusion of hexane into solutions of the respective compound in THF.

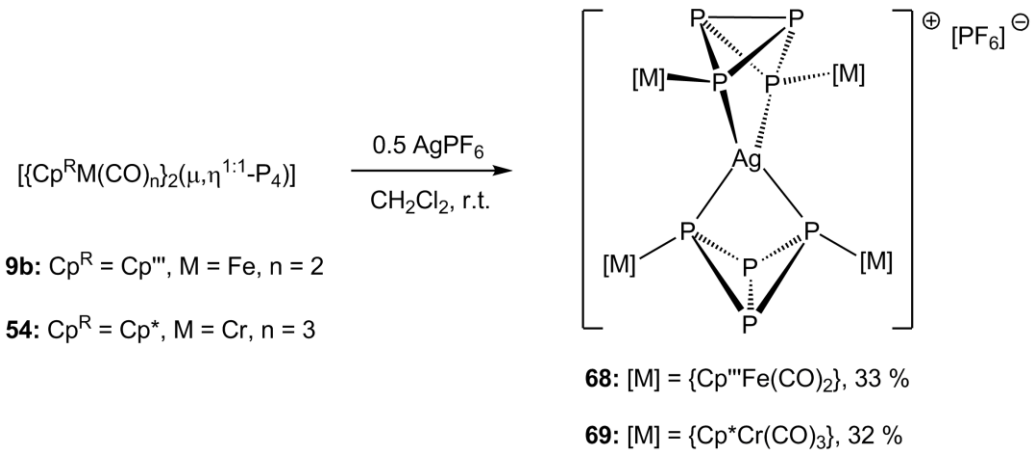

(26)

In the positive ion ESI mass spectrum of **68** the molecular ion peak is detected as the base peak at *m*/*z* = 1736.2. Additionally, peaks are detected at *m*/*z* = 1709.0, 1679.0 and 1651.2 that can be assigned to the cationic fragments $[M^+ - CO]$, $[M^+ - 2CO]$ and $[M^+ - 3CO]$, respectively. The IR spectrum (KBr) of **68** reveals two strong absorption bands at ν = 2006 and 1961 cm^{-1} for the terminal carbonyl ligands. Compared to **9b** the signals are blue-shifted, which has already been observed for the analogous Cu species **65** (see section 3.5.1.1). In the ^1H NMR spectrum (CD_2Cl_2) of **68** three sharp singlets for the ^{t}Bu groups and the aromatic protons of the Cp''' ligands are observed. The $^{31}P\{^1H\}$ NMR spectrum (CD_2Cl_2) shows the characteristic septet for the $[PF_6]^-$ counterion. Furthermore it reveals a sharp triplet at δ = -305.0 ppm (2 P) for the bridghead P atoms as well as two overlapping doublets of triplets at δ = -63.8 ppm (2 P). The downfield-shifted signal corresponds to the coordinating phosphorus atoms with a triplet splitting due to the coupling with the bridghead P atoms ($^1J_{PP}$ = 191 Hz) and two doublet splittings with coupling constants of $^1J_{P^{109}Ag}$ = 158 Hz and $^1J_{P^{107}Ag}$ = 138 Hz. The ratio of these coupling constants corresponds perfectly to the ratio of the gyromagnetic ratios of ^{109}Ag and ^{107}Ag, which both possess a spin of ½ and show a natural abundance of about 48 % and 52 %, resepctively. Hence, the doublet splitting originates from a coupling of the coordinating phosphorus atoms with the two NMR active silver nuclei. An analogous coupling has been observed by Sadler *et al.* for the complex $[Ag(dppe)_2]^+[NO_3]^-$ with coupling constants of $^1J_{P^{109}Ag}$ = 266 Hz and $^1J_{P^{107}Ag}$ = 231 Hz.[96]

In the positive ion ESI mass spectrum of **69** the molecular ion peak is detected at m/z = 1441.2. The IR spectrum (KBr) reveals four absorption bands at ν = 1998, 1988, 1935, 1918 cm^{-1}, which are blue-shifted by about 15 cm^{-1} compared to the butterfly complex **54**. In the ^1H NMR spectrum (CD_2Cl_2) one sharp singlet for the Cp* ligands is observed. In analogy to the previously discussed compound **68**, the $^{31}P\{^1H\}$ NMR spectrum (CD_2Cl_2) of **69** shows a septet for the $[PF_6]^-$ counterion as well as a triplet at δ = -310.3 ppm and two superimposed doublet of triplets at δ = -68.6 ppm. The $^1J_{PP}$ = 200 Hz coupling constant is only slightly larger than that of **68**. In contrast, the silver phosphorus coupling constants of $^1J_{P^{109}Ag}$ = 144 Hz and $^1J_{P^{107}Ag}$ = 125 Hz are smaller than in **68**.

$[\{\{Cp'''Fe(CO)_2\}_2(\mu_3,\eta^{1:1:1:1}\text{-}P_4)\}_2Ag]^+[PF_6]^-$ (**68**) crystallizes as orange plates in the monoclinic space group *Cc*. The asymmetric unit contains one molecule of **68** together with 3.5 molecules of THF. $[\{\{Cp^*Cr(CO)_3\}_2(\mu_3,\eta^{1:1:1:1}\text{-}P_4)\}_2Ag]^+(PF_6)^-$ (**69**) crystallizes as orange plates in the tetragonal space group *P*4/*n*. The asymmetric unit contains a quarter of a molecule of **69**.

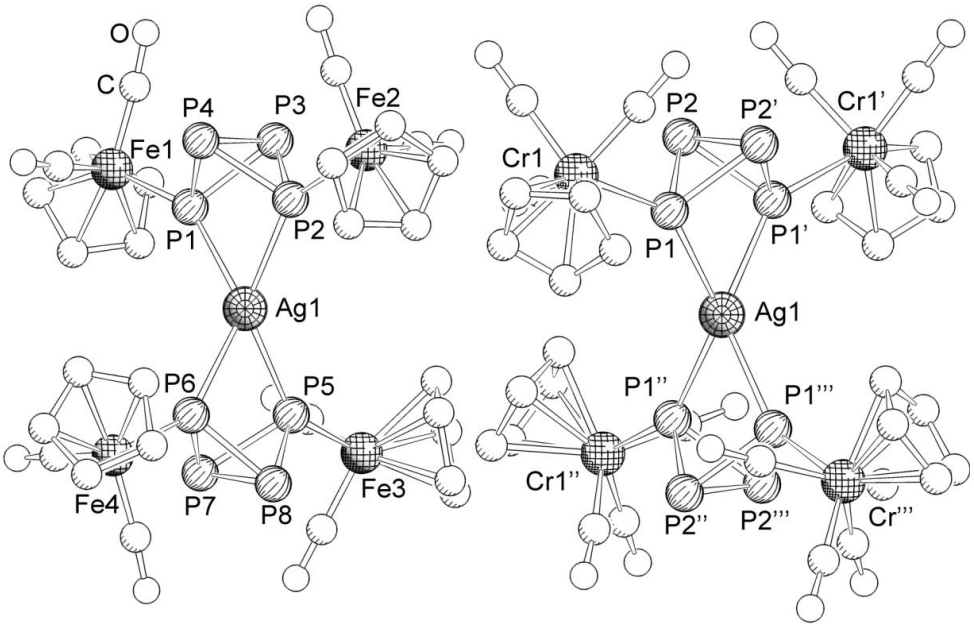

Figure 32. Molecular structure of **68** (left) and **69** (right) in the crystal. Hydrogen atoms, methyl- and ^{t}Bu groups as well as $[PF_6]^-$ counterions are omitted for clarity. Selected bond lengths [Å] and angles [°]: **68:** Ag1–P1 2.6342(8), Ag1–P2 2.5882(8), Ag1–P5 2.6110(9), Ag1–P6 2.6162(9), Fe1–P1 2.3012(4), Fe2–P2 2.2986(9), Fe3–P5 2.303(1), Fe4–P6 2.303(1), P1–P3 2.220(1), P1–P4 2.218(1), P2–P3 2.219(1), P2–P4 2.221(1), P3–P4 2.183(2), P5–P7 2.225(1), P5–P8 2.219(1), P6–P7 2.212(1), P6–P8 2.221(1), P7–P8 2.174(1), P1···P2 2.885(1), P5···P6 2.850(1), P1–Ag1–P2 67.07(2), P1–Ag1–P5 130.22(3), P1–Ag1–P6 129.34(3), P2–Ag1–P5 137.19(3), P2–Ag1–P6 139.68(3), P5–Ag1–P6 66.08(3); **69:** Ag1–P1 2.6102(6), Cr1–P1 2.4713(7), P1–P2 2.2023(9), P1–P2' 2.222(1), P2–P2' 2.181(1), P1···P1' 2.854(1), P1–Ag1–P1' 66.27(2), P1–Ag1–P1'' 134.52(2).

In both cases X-ray structure analysis confirms the chelating coordination of a central silver cation by two molecules of **9b** and **54**, respectively, resulting in a distorted tetrahedral coordination environment (Figure 32). While in **68** the planes defined by the atoms P3–P4–Ag1 and P7–P8–Ag1 generate a dihedral angle of 88.45(5)°, the corresponding planes in **69** are perfectly perpendicular to each other. The P1–Ag1–P2 and P5–Ag1–P6 angles of 67.07(2)° and 66.08(3)° in **68** as well as the P1–Ag1–P1' angle of 66.27(2)° in **69** are smaller than the corresponding angles in **65** (72.51(3)° and 72.71(3)°) and **66** (72.78(2)° and 72.26(2)°) due to a larger metal phosphorus distance. The Ag–P distances in **68** (2.5882(8) Å to 2.6342(8) Å) and **69** (2.6102(6) Å) are slightly longer than in $[Ag(dppe)_2]^+[NO_3]^-$ (2.438(3) Å to 2.527(3) Å).[97] However, the longer Ag–P distances in **68** and **69** compared to the Cu–P distances in **65** and **66** reduce the steric crowding and allows a less distorted coordination environment of the central atom. The distances between the coordinating P atoms in **68** (2.885(1) Å and 2.850(1) Å) and **69** (2.854(1) Å) compare well to the corresponding distances in **65**, **66** and **67**. This is also the case for the observed P–P bond lengths, which show typical tendencies for P_4 butterfly ligands.

3.5.1.3 Coordination behavior towards monovalent gold cations

The reaction of $[(PPh_3)Au(tht)]^+[PF_6]^-$ (tht = tetrahydrothiophene) with one equivalent of **9b** or **54** leads to the formation of $[\{Cp'''Fe(CO)_2\}_2(\mu_3,\eta^{1:1:1:1}\text{-}P_4)\{Au(PPh_3)\}]^+[PF_6]^-$ (**70**) and $[\{Cp^*Cr(CO)_3\}_2(\mu_3,\eta^{1:1:1:1}\text{-}P_4)\{Au(PPh_3)\}]^+[PF_6]^-$ (**71**), respectively, accompanied by a loss of the tht ligand (Equation 27). The $^{31}P\{^1H\}$ NMR spectra of the reaction mixtures clearly show quantitative formation of the desired complexes. Compounds **70** and **71** are isolated as orange solids that have good solubility in dichloromethane and THF but are insoluble in hexane. Single crystals are obtained by slow diffusion of hexane into a saturated solution of the respective compound in THF (**70**) or CH_2Cl_2/THF (**71**).

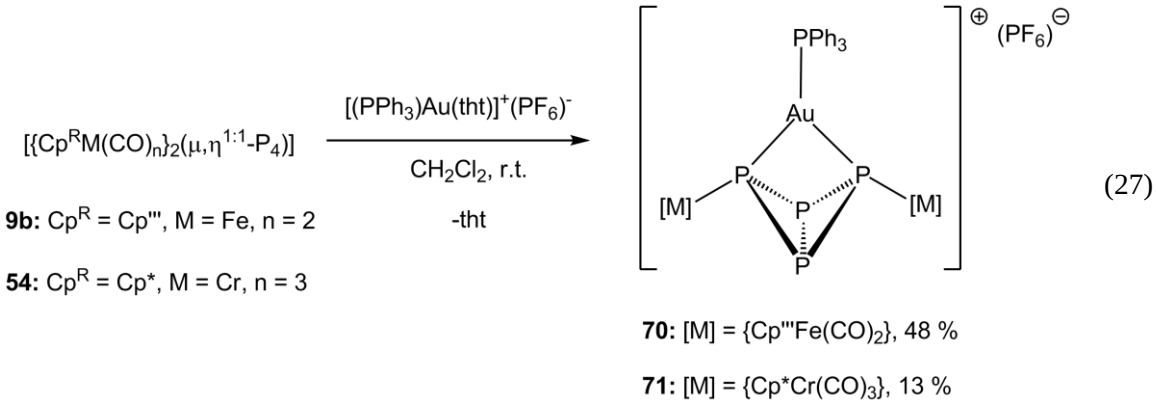

(27)

In the positive ion ESI mass spectrum of **70** a peak is detected at *m*/*z* = 1245.8 that corresponds to the doubly charged molecular ion dimer $[M_2]^{2+}$ as well as the base peak for $[(PPh_3)_2Au]^+$ at *m*/*z* = 721.2. The IR spectrum (KBr) shows four strong absorption bands for terminal carbonyl ligands at ν = 2030, 2008, 1966 and 1944 cm^{-1} which show a blue shift of about 30 cm^{-1} compared to **9b**. In the ^1H NMR spectrum (CD_2Cl_2) of **70** a typical set of signals for the Cp''' ligands is observed together with a broad multiplet at δ = 7.55 - 7.65 ppm, which corresponds to the protons of the PPh_3 ligand. The $^{31}P\{^1H\}$ NMR spectrum (CD_2Cl_2) of **70** reveals, beside the septet for the counterion, three signals of an AM_2X_2 spin system. The signal for the PPh_3 ligand is found at δ = 42.5 ppm as a triplet with $^2J_{AM}$ = 111 Hz. The signal for the coordinating P atoms of the chelating butterfly complex appears as a doublet of triplets at δ = -22.9 ppm with coupling constants of $^1J_{MX}$ = 192 Hz and $^2J_{AM}$ = 111 Hz. Finally, the bridgehead phosphorus atoms are detected at δ = -299.2 ppm with associated coupling constant.

The positive ion ESI mass spectrum of **71** reveals the molecular ion peak $[M]^+$ at m/z = 1125.3. The base peak is found at *m*/*z* = 721.2 and corresponds to the cationic fragment $[(PPh_3)_2Au]^+$. In the IR spectrum (KBr) five signals are observed at ν = 2004, 1991, 1948, 1932 and 1916 cm^{-1} which are blue-shifted by about 20 cm^{-1} compared to **54**. The ^1H NMR spectrum (CD_2Cl_2) shows

one characteristic singlet for the Cp* ligands at δ = 1.75 ppm as well as a multiplet for the PPh_3 ligand at δ = 7.46 - 7.66 ppm. In the $^{31}P\{^1H\}$ NMR spectrum (CD_2Cl_2) of **71** a triplet is found at δ = 44.1 ppm ($^1J_{AM}$ = 103 Hz) which can be assigned to the PPh_3 ligand. The P atoms of the butterfly complex appear as a doublet of triplets at δ = -16.8 ppm and a triplet δ = -302.6 ppm with a coupling constant of $^1J_{MX}$ = 206 Hz. The chemical shift as well as the coupling constants compare well to those in **70**.

$[\{Cp'''Fe(CO)_2\}_2(\mu_3,\eta^{1:1:1:1}\text{-}P_4)\{Au(PPh_3)\}]^+[PF_6]^-$ (**70**) crystallizes as orange plates in the monoclinic space group $P2_1/n$. The asymmetric unit contains one molecule of **70**. $[\{Cp^*Cr(CO)_3\}_2(\mu_3,\eta^{1:1:1:1}\text{-}P_4)\{Au(PPh_3)\}]^+[PF_6]^-$ (**71**) crystallizes as orange bars in the orthorhombic space group *Pccn* with one molecule of **71** in the asymmetric unit. In both cases only small crystals of the respective compound could be obtained and X-ray structure analysis turned out to be challenging. As crystals of **71** decomposed during the measurement only low quality data could be collected for this compound. However, X-ray structure analysis proves in both cases the chelating coordination of a $[Au(PPh_3)]^+$ cation by one molecule of **9b** or **54**, respectively (Figure 33 and Figure 34).

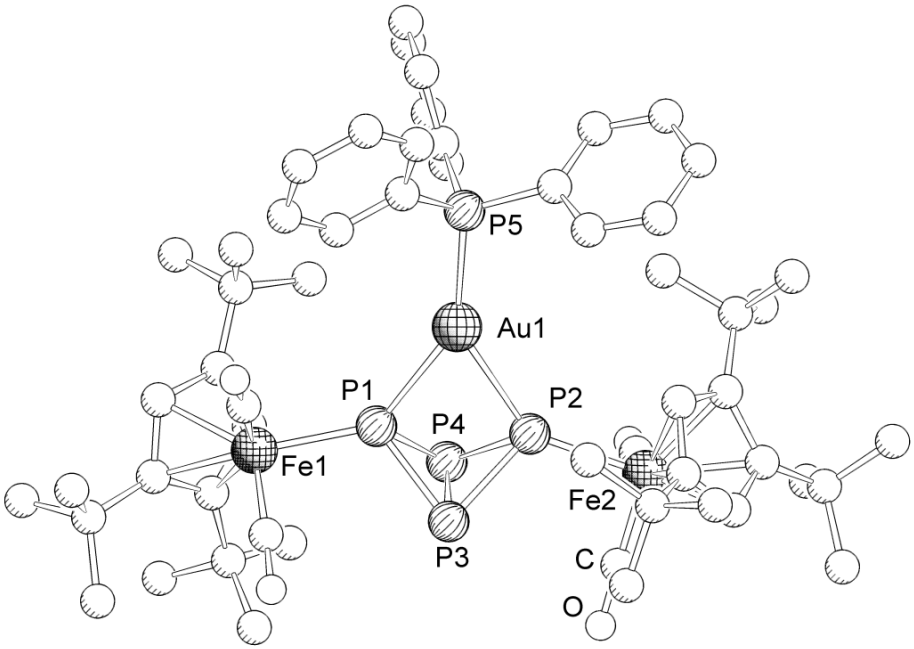

Figure 33. Molecular structure of **70** in the crystal. Hydrogen atoms and the $[PF_6]^-$ counterion are omitted for clarity. Selected bond lengths [Å] and angles[°]: Au1–P1 2.480(2), Au1–P2 2.557(2), Au1–P5 2.292(3), Fe1–P1 2.282(3), Fe2–P2 2.270(3), P1–P3 2.204(3), P1–P4 2.210(3), P2–P3 2.220(3), P2–P4 2.224(3), P3–P4 2.183(3), P1···P2 2.823(3), P1–Au1–P2 68.16(7), P1–Au1–P5 146.84(8), P2–Au1–P5 144.65(8).

The central motif in **70** is a gold(I) cation with a trigonal planar coordination environment. Two of the coordination sites are occupied by the "wing-tip" P atoms of the butterfly complex **9b**, the

third one by a PPh_3 ligand. The sum of the angles around the Au^+ cation adds up to 359.7°, indicating an almost perfect planar arrangement. The P1–Au1–P2 bond angle of 68.16(7)° is slightly larger than the corresponding angles in the silver compound **68** (67.07(2)° and 66.08(3)°) but smaller than in the copper derivatives **65** (72.51(3)° and 72.71(3)°) and **67** (75.19(2)°). The Au1–P1 and Au2–P2 bond lengths are with 2.480(2) Å and 2.557(2) Å in between the observed metal phosphorus bond lengths for the silver- and copper derivatives **65** and **68**, which is consistent with the observed tendency for the P–M–P bond angles. A similar coordination geometry can be observed in $[\{o\text{-}B_{10}H_{10}C_2(PPh_2)_2\}Au(PPh_3)]^+[ClO_4]^-$ which also exhibits one chelating ligand as well as one terminal PPh_3 group.[98] While the Au–P bond lengths for the chelating ligand are, at 2.405(1) Å and 2.417(1) Å, shorter than the corresponding bonds in **70**, the Au–P bond to the terminal PPh_3 moiety is at 2.318(1) Å slightly longer than the Au1–P5 bond in **70** (2.292(8) Å). The Fe1–P1 and Fe2–P2 bond lengths of 2.282(3) Å and 2.270(3) Å are shorter than the Fe–P bond lengths in **65** (2.3059(8) Å - 2.3380(8) Å) and **68** (2.2986(9) Å - 2.303(1) Å), but compare well to the Fe–P bond distances in **67** (2.2928(6) Å and 2.2845(6) Å) which also exhibits one σ-donor ligand at the central atom. The P–P bond lengths are in a typical range for butterfly ligands and compare well to the bond distances found in the previously discussed compounds.

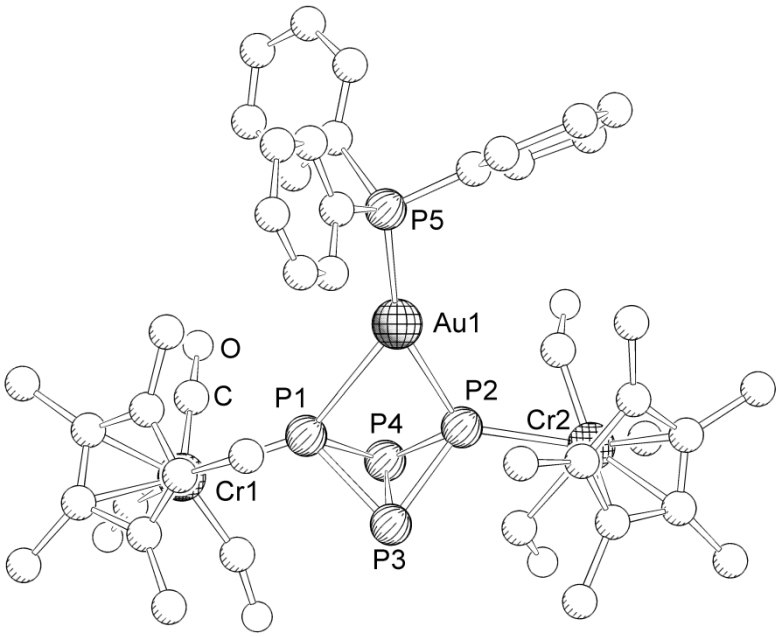

Figure 34. Molecular structure of **71** in the crystal. Hydrogen atoms and $[PF_6]^-$ counterion are omitted for clarity.

Due to the poor quality of the crystals and the X-ray structure analysis of **71** a detailed discussion of bond lengths and angles is not appropriate. However, the basic framework is similar to that found for **70**. Surprisingly, the Cp* ligands of the $\{Cp^*Cr(CO)_3\}$ moieties point in the same direction which could so far not be observed for any of the related compounds.

3.5.1.4 Coordination behavior towards iron(II) bromide

In the last years chelate complexes of iron(II) halides have drawn interest because of their use as catalysts in different processes. Gibson *et al.* investigated the use of $[(R_2EC_2H_4ER_2)FeX_2]$ (E = N, P; X = Cl, Br; R = alkyl or aryl) complexes as catalysts for the controlled polymerization of styrenyl and acrylate monomers.[99] Moreover, Tyler *et al.* reported on the catalytic activity of $[(dppe)_2FeCl_2]$ for the direct generation of ammonia from hydrogen and dinitrogen.[100] However, to the best of our knowledge no structurally characterized compounds are known, which exhibit a chelating, phosphorus-containing ligand with small bite angle such as dppm. As the bite angle greatly influences the catalytic activity the synthesis and characterization iron(II) complexes with small bite angle chelating ligands is of scientific interest.[101]

The reaction of $[FeBr_2{\cdot}dme]$ with one equivalent of the butterfly complex **9b** leads to the formation of $[\{Cp'''Fe(CO)_2\}_2(\mu_3,\eta^{1:1:1:1}\text{-}P_4)\{FeBr_2\}]$ (**72**) accompanied by a color change from bright orange to dark red (Equation 28). The $^{31}P\{^1H\}$ NMR spectrum of the reaction mixture shows no signals for **9b** anymore indicating a quantitative conversion. Complex **72** is obtained as dark red solid that has good solubility in THF, toluene and dichloromethane. Single crystals of **72** suitable for X-ray structure analysis are obtained from a saturated solution of **72** in CH_2Cl_2 upon cooling.

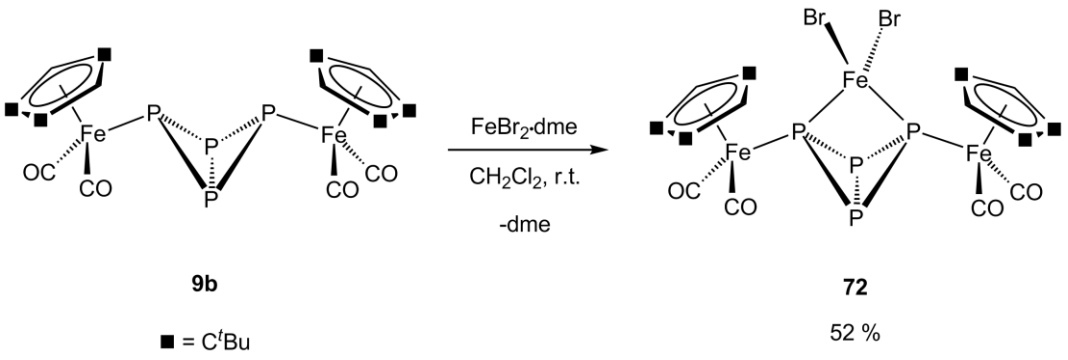

(28)

In the EI mass spectrum of **72** peaks can be detected at *m*/*z* = 1283.3, 1253.4 and 733.3 that corrrespond to the cationic fragments $[\{Cp'''Fe(CO)_2\}_3P_8]^+$, $[\{Cp'''Fe(CO)_2\}_3P_8 - CO - 2H]^+$ and $[\{Cp'''Fe\}_2P_5]^+$. The unusual fragmentation pattern may be a result of the harsh ionization method. A bromine-containing fragment could not be observed. The IR spectrum (KBr) shows two strong absorption bands at ν = 2029 and 1983 cm^{-1} which are about 30 cm^{-1} blue-shifted compared to **9b**. The ^1H NMR spectrum (CD_2Cl_2) shows several broad signals indicating the paramagnetic character of the sample. Hence, no signals could be observed in the $^{31}P\{^1H\}$ NMR spectrum (CD_2Cl_2). To further investigate the magnetic behavior of complex **72** the Evans method

was used to determine the effective magnetic moment and the number of unpaired spins.[102] Complex **72** possesses an effective magnetic moment of μ_{eff} = 6.1 μ_B, which is larger compared to the complexes [($R_2PC_2H_4PR_2$)$FeCl_2$] (R = alkyl or aryl) (μ_{eff} = 5.0 – 5.5 μ_B)[99] and corresponds to about five unpaired electrons. This value is higher than the expected four unpaired electrons for **72** (tetrahedral coordinated high-spin Fe^{2+} complex with an $e^3t_2^3$ configuration[103]) which may be explained by the inaccuracy of the Evans method and shall be clarified by variable-temperature magnetic susceptibility measurements.

[{Cp'''Fe$(CO)_2$}$_2$(μ_3,$\eta^{1:1:1:1}$-P_4)$FeBr_2$] (**72**) crystallizes as dark red plates in the monoclinic space group $P2_1/n$. The asymmetric unit contains one molecule of **72** together with two molecules of dichloromethane. X-ray structure analysis confirms the chelating coordination of a $FeBr_2$ unit by one molecule of **9b** (Figure 35).

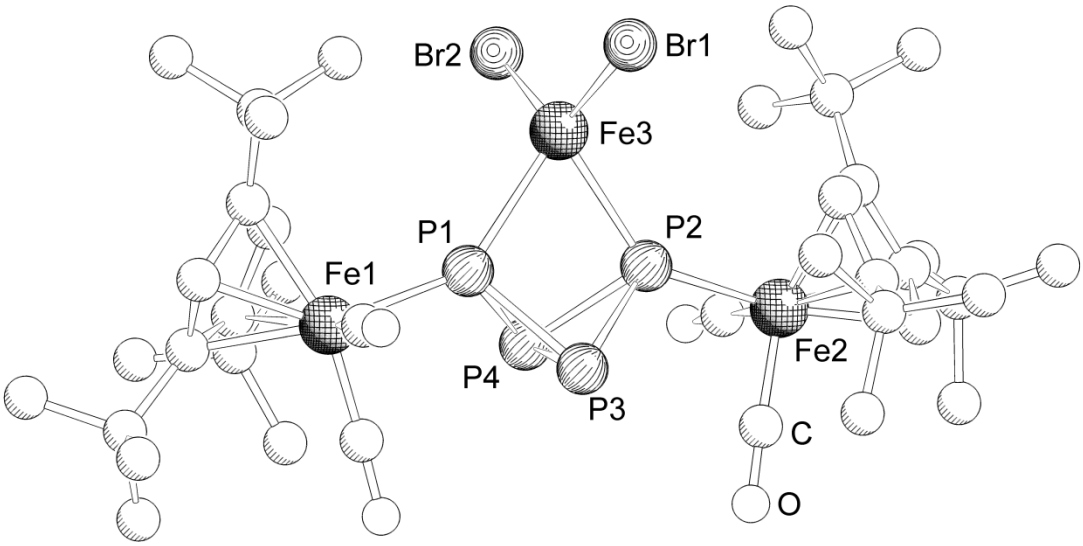

Figure 35. Molecular structure of **72** in the crystal. Hydrogen atoms are omitted for clarity. Selected bond lengths [Å] and angles [°]: Br1–Fe3 2.3872(5), Br2–Fe3 2.3798(6), Fe1–P1 2.2861(8), Fe2–P2 2.2634(7), Fe3–P1 2.4823(8), Fe3–P2 2.4364(7), P1–P3 2.210(1), P1–P4 2.222(1), P2–P3 2.221(1), P2–P4 2.206(1), P3–P4 2.191(1), P1···P2 2.831(1) Br1–Fe3–Br2 119.95(2), Br1–Fe3–P1 121.80(3), Br1–Fe3–P2 112.95(2), Br2–Fe3–P1 109.59(2), Br2–Fe3–P2 111.93(2), P1–Fe3–P2 70.27(3).

The Lewis acidic Fe3 atom in **72** is coordinated by two terminal bromine atoms and the two "wing-tip" phosphorus atoms of the butterfly ligand **9b** in a distorted tetrahedral manner. The planes defined by the atoms Fe3–Br1–Br2 and Fe3–P1–P2 draw an angle of 85.35(2)° which deviates from perfect 90°. The P1–Fe3–P2 bond angle of 70.27(3)° compares well to the corresponding bond angles in the previously discussed chelate complexes. However, it is smaller than the P–Fe–P bond angle in [($Cy_2PC_2H_4PCy_2$)$FeCl_2$] (83.91(5)°) which chelating ligand exhibits a two-membered chain between the coordinating P atoms. The Fe3–P1 and Fe3–P2 bond

lengths (2.4823(8) Å and 2.4364(7) Å) compare well to those found in [($Cy_2PC_2H_4PCy_2$)$FeCl_2$] (2.461(1) Å and 2.466(1) Å).[99] The Br1–Fe3 and Br2–Fe3 bond lengths of 2.3872(5) Å and 2.3798(6) Å as well as the Br1–Fe3–Br2 bond angle of 119.95(2)° are almost the same as the corresponding distances and angles in the complex [(^{t}BuNC_2H_2N^{t}Bu)$FeBr_2$] (2.367(2) Å and 118.53(8)°).[99] The P–P and Fe–P bond lengths compare well to the ones of **67** and **70** that exhibit a similar coordination environment of the Lewis acid and nicely exemplifies the potential of **9b** to serve as small bite angle chelate ligand for various Lewis acids.

3.5.1.5 Concluding remarks

The P_4 butterfly complexes **9b** and **54** are able to act as chelating ligands with small bite angles for cationic as well as neutral Lewis acids, and may be regarded as inorganic dppm derivatives. Most of the complexes are stable as solids as well as in solution and can be well characterized by NMR and IR spectroscopy due to the presence of phosphorus atoms and carbonyl ligands (Table 6). Furthermore, the complexes [{Cp'''$Fe(CO)_2$}$_2$($\mu,\eta^{1:1:2}$-P_4){Cu(MeCN)}]$^+$[BF_4]$^-$ (**67**) with a labile acetonitrile ligand and [{Cp'''$Fe(CO)_2$}$_2$($\mu,\eta^{1:1:2}$-P_4)$FeBr_2$] (**72**), bearing substitutable halides, could have large potential as building blocks for the formation of organometallic self-assembled polymers and frameworks. Furthermore, the large steric bulk of the butterfly complexes together with their small bite angle could make them interesting ligands for catalytic applications.

Table 6. Selected spectroscopic data and averaged bond angles and distances for P_4 butterfly compounds **9b** and **54** and their chelate complex products with different Lewis acids.

complex	ν_{CO} [cm^{-1}]	$\delta_{P coord.}$ [ppm]	∢**(PMP)** [°]	***d*(MP)** [Å]	***d*(M'P)** [Å]
9b M' = Fe	2000, 1950	-75.2	-	-	2.351
65 M' = Fe, M = Cu	2008, 1960, 1930	-81.2	72.61	2.397	2.320
68 M' = Fe, M = Ag	2006, 1961	-63.8	66.58	2.612	2.301
70 M' = Fe, M = Au	2030, 2008, 1966, 1944	-22.9	68.16	2.518	2.276
67 M' = Fe, M = Cu	2009, 2000, 1962, 1956	-81.0	75.19	2.305	2.289
72 M' = M = Fe	2029, 1983	-	70.27	2.459	2.275
54 M' = Cr	1983, 1967, 1916, 1900	-95.2	-	-	2.519
66 M' = Cr, M = Cu	1990, 1932, 1913	-89.1	72.75	2.411	2.515
69 M' = Cr, M = Ag	1998, 1988, 1935, 1918	-68.6	66.27	2.610	2.471
71 M' = Cr, M = Au	2004, 1991, 1948, 1932, 1916	-16.8	-	-	-

The IR spectra of the chelate complexes show absorption bands that are blue-shifted relative to the respective butterfly complexes due to an electron withdrawing effect of the Lewis acids. In case of **9b** the bands are shifted by about 10 cm^{-1} when copper(I) or silver(I) cations are used and about 30 cm^{-1} when the Lewis acid is either $[Au(PPh_3)]^+$ or the neutral $FeBr_2$. For **54** the copper(I) complex shows the smallest shift of about 10 cm^{-1} while the signals of the silver(I) and gold(I) complexes are shifted by about 15 – 20 cm^{-1}. This is counterintuitive since the hardest Lewis acid Cu^+ has the smallest electron withdrawing effect whereas the soft Lewis acids Au^+ and $FeBr_2$ have the largest. A similar tendency is found for the chemical shift of the coordinating phosphorus atoms of the butterfly ligands in the $^{31}P\{^1H\}$ NMR spectrum. In general, deshielding (high-field shift) of the nucleus indicates small electron density while shielding (low-field shift) is often

observed for electron-rich systems in which the nuclei are influenced by surrounding bonding and non-bonding electrons. The strongest deshielding effect is observed for the chelate complexes of $[Au(PPh_3)]^+$ while the complexes with copper(I) show only a small high-field shift compared to **9b** (complex **66**) or even a shielding of the coordinating P atoms (complexes **65** and **67**). This behavior indicates a complicated orbital interaction rather than just a simple electrostatic attraction. While gold and iron may possess orbitals with suitable energies for the interaction with the respective butterfly complex, the positive charge on the copper(I) cations increases their orbital energies leading to a weaker interaction.

The M'–P bond distances in the chelate complexes are generally shorter than in the respective starting material. The shortest M'–P bond lengths with **9b** as ligand are found for **70** and **72** with $[Au(PPh_3)]^+$ and $FeBr_2$ as Lewis acid, the longest in the bis chelate complex **65** with Cu^+ as central cation. A possible reason for this effect could be the contribution of the HOMO-1 (see Figure 28) of **9b** for the coordination of the Lewis acid. As this orbital has an antibonding character with respect to the Fe–P bond, a withdrawing of electrons from this orbital should shorten the bond.

The M–P bond distances are shortest for the copper(I) complexes and longest for the silver(I) derivatives which is in good agreement with the different atom sizes of the coinage metals. As a direct consequence, the P–M–P bond angles are the largest for the copper(I) complexes and the smallest for the silver(I) ones.

3.5.2 AsP_3 butterfly complexes as chelating ligands

Transition metal phosphine complexes have proven to be useful catalysts for several processes including hydrogenation or carbonylation reactions.[104] The substitution of phosphorus by other group 15 elements changes the characteristics of the ligand through the bite angle and the resulting electronic properties. Hence, the synthesis of heterobidentate ligands that exhibit phopshorous as well as arsenic donor atoms moved into the focus of interest.[104-105] However, to date only few structurally characterized examples for tetrahedral Cu(I), Ag(I) or Au(I) complexes with large bite angle P, As-heterobidentate ligands exist.[106] Furthermore, these complexes show an interesting fluxional behavior with labile M–As bonds. As P_4 butterfly complexes are able to act as bidentate ligands with small bite angle, it was of great interest to also investigate the ligand properties of the AsP_3 butterfly complexes $[\{Cp'''Fe(CO)_2\}_2(\mu,\eta^{1:1}\text{-}AsP_3)]$ (**51**) and $[\{Cp^*Cr(CO)_3)\}_2(\mu,\eta^{1:1}\text{-}AsP_3)]$ (**55**) towards monovalent coinage metal cations.

3.5.2.1 Coordination behavior towards monovalent copper cations

The reaction of $[Cu(MeCN)_4]^+[BF_4]^-$ with two equivalents of **51** or **55** leads to the formation of the chelate complexes $[\{\{Cp'''Fe(CO)_2\}_2(\mu_3,\eta^{1:1:1:1}\text{-}AsP_3)\}_2Cu]^+[BF_4]^-$ (**73**) and $[\{\{Cp^*Cr(CO)_3\}_2(\mu_3,\eta^{1:1:1:1}\text{-}AsP_3)\}_2Cu]^+[BF_4]^-$ (**74**), respectively (Equation 29). The $^{31}P\{^1H\}$ NMR spectra of the reaction mixtures indicate a complete consumption of the respective starting material. Compounds **73** and **74** are obtained as reddish orange solids that have good solubility in THF and dichloromethane but are insoluble in hexane. So far, single crystals of **73** could not be obtained. However, the product was purified by washing with hexane to remove all traces of acetonitrile leading to analytically pure **73**. Single crystals of **74** suitable for X-ray structure analysis are obtained by slow diffusion of hexane into a solution of **74** in THF.

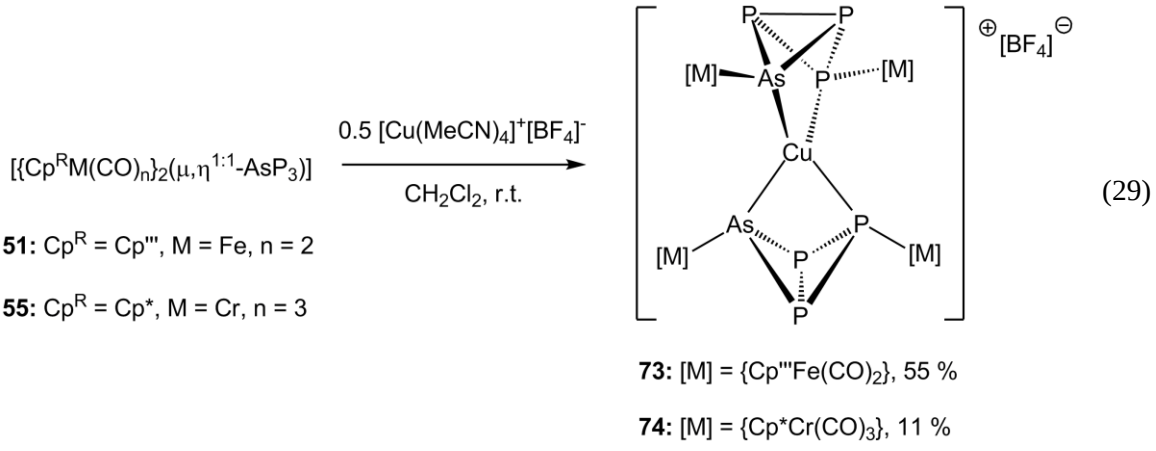

(29)

In the positive ion ESI mass spectrum of **73** the molecular ion peak $[M]^+$ is detected at *m*/*z* = 1780.0. Additionally a peak is found at *m*/*z* = 1724.0 that corresponds to $[M - 2CO]^+$ as well as the base peak at *m*/*z* = 1175.5 that can be assigned to the fragment $[\mathbf{51} + \{Cp'''Fe(CO)\}]^+$. The IR spectrum (KBr) reveals three bands at ν = 2008, 1993 and 1959 cm^{-1} that are blue-shifted compared to the starting material **51** (ν = 1998, 1990, 1950 and 1940 cm^{-1}). In the ^1H NMR spectrum (CD_2Cl_2) of **73** several overlapping singlets are observed between δ = 1.38 – 1.46 ppm. Additionally a sharp as well as a broad singlet are detected at δ = 4.80 and δ = 4.83 ppm, respectively. The integral intensity ratio of the signals is 27:1:1 which corresponds to the expected ratio for the Cp''' ligands. Hence, the ^1H NMR spectrum either indicates several Cp''' bearing species in solution and/or points to a hindered rotation of the Cp''' ligand of one species.

In the $^{31}P\{^1H\}$ NMR spectrum (CD_2Cl_2) (Figure 36) two signals are detected for complex **73**. At δ = -96.9 ppm a broad triplet appears that exhibits a fine structure pointing to a high-order spin system. Additionally, a multiplet is detected around δ = –273.4 ppm. The two signals show an integral intensity ratio of 1 : 1.7 which differs from the expected intensity ratio 1 : 2 for the AsP_3 moieties by 0.3. Hence, the broad triplet might be interpreted as two superimposed signals that correspond to coordinating P atoms with similar coordination environments. In addition, a doublet of doublets is found around δ = -269.4 ppm with coupling constants of *J* = 141 Hz and *J* = 193 Hz which belongs to a second species in solution. The chemical shift points to non-coordinating P atoms and the signals show an an integral intensity of 0.3 which compares well to the "missing" intensity for the signals of **73**. However, the sharp doublet of doublets points to a simple AMM' spin system which could correspond to the species $[\{Cp'''Fe(CO)_2\}_2(\mu_3,\eta^{1:1:1:1}\text{-}AsP_3)\{Cu(MeCN)\}]^+$ which is present in solution due to a slight excess of $[Cu(MeCN)_4]^+$.

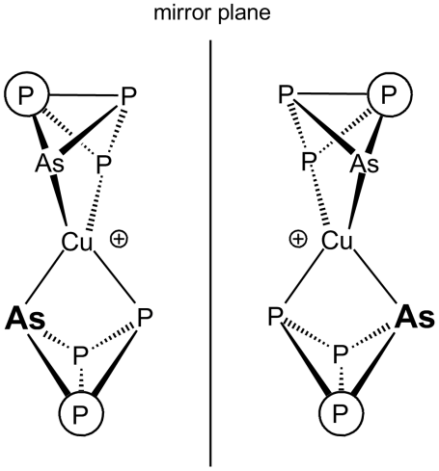

Scheme 8. Possible enantiomeric forms of the central building unit of **73**. The encircled phosphorus atoms point to the same side as the coordinating arsenic atom of the second AsP_3 butterfly framework.

The signals around δ = -96.9 and -273.4 ppm result from a high-order spin system that was not observed for the complexes **65** and **66**. The reason for this is the introduction of arsenic atoms at two of the four coordinating positions of the chelate complex. Hence, the symmetry directly around the central copper atom is lowered to C_{2v}. Additionally, the chelating coordination has to be considered as a restrictive condition which leads to a C_1 symmetry of the $Cu(AsP_3)_2$ core. As the steric bulk of the [Cp'''Fe(CO)$_2$] moieties disables rotation of the bidentate ligands, the relative orientation of the arsenic atoms to each other is fixed. Hence, image and mirror image cannot be superimposed which makes complex **73** a "chiral-at-metal"[107] compound with two possible enantiomers. However, they are indistinguishable using NMR spectroscopy. Furthermore, the two bridghead phosphorus atoms of the AsP_3 butterfly framework are magnetically inequivalent due to perpendicular orientation of the second AsP_3 butterfly framework which leads to an AA'MM'NN' spin system for complex **73** (Scheme 8). Simulation of the spectrum affords the corresponding chemical shifts and coupling constants (Figure 36,Table 7).[71]

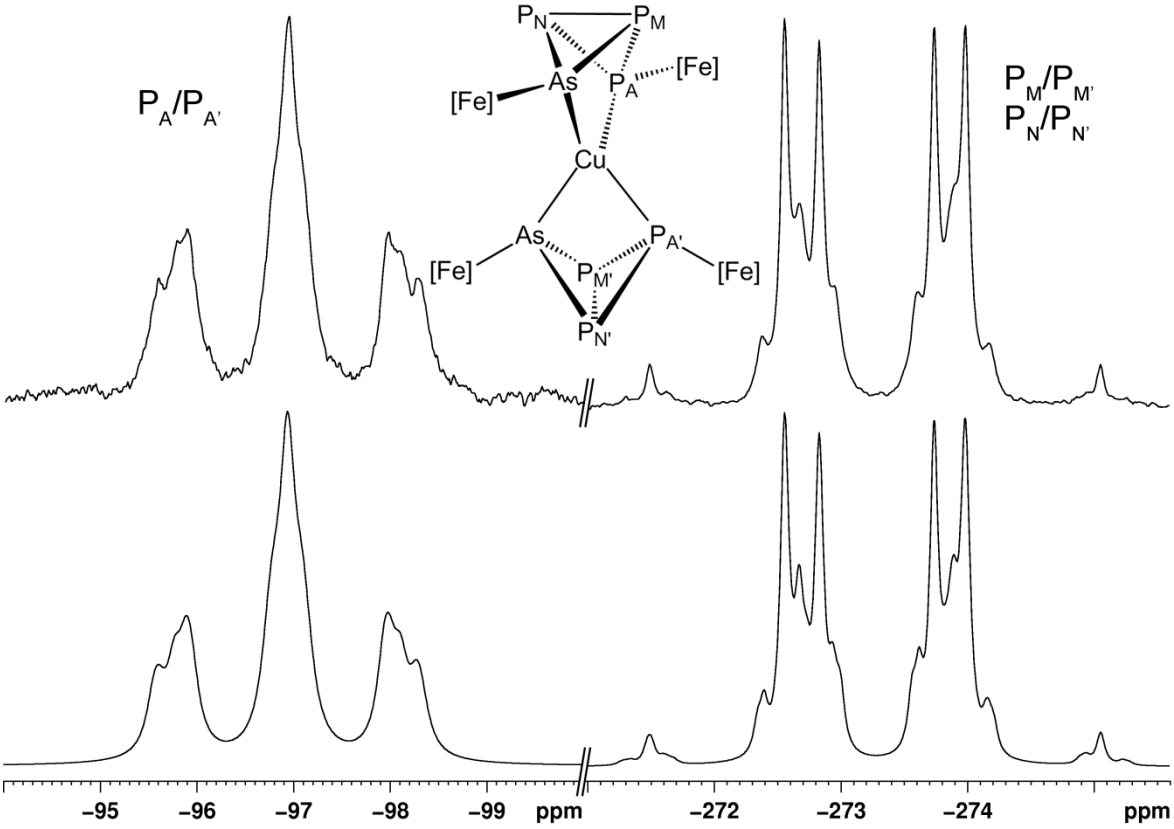

Figure 36. Sections of the experimental (CD_2Cl_2, top) and simulated (bottom) $^{31}P\{^1H\}$ NMR spectrum of complex **73**.

Table 7. Chemical shifts and coupling constants from the simulated $^{31}P\{^{1}H\}$ NMR spectrum of **73**.

δ_A = -97.0 ppm	$\delta_{A'}$ = -96.9 ppm	δ_M = -272.9 ppm
$\delta_{M'}$ = -272.9 ppm	δ_N = -273.7 ppm	$\delta_{N'}$ = -273.7 ppm
$^{1}J_{AM}$ = 192 Hz	$^{1}J_{AN}$ = 187 Hz	$^{1}J_{MN}$ = 171 Hz
$^{1}J_{A'M'}$ = 193 Hz	$^{1}J_{A'N'}$ = 187 Hz	$^{1}J_{M'N'}$ = 175 Hz
$^{2}J_{AA'}$ = 53 Hz		

The IR spectrum (KBr) of **74** shows three bands at ν = 1996, 1979 and 1910 cm^{-1} of which the latter is broadened. Compared to the starting material **55** (ν = 1980, 1964 and 1897 cm^{-1}) the signals are blue-shifted by about 15 cm^{-1}. The ^{1}H NMR spectrum (CD_2Cl_2) reveals two singlets at δ = 1.94 and 1.95 ppm for the Cp* ligands depending on wether the [Cp*Cr(CO)$_3$] moiety is coordinated by phosphorus or arsenic. This behavior has already been observed for the free butterfly complex **55** (see section 3.3.4.2).

In the $^{31}P\{^{1}H\}$ NMR spectrum (CD_2Cl_2) of crystalline **74** two sets of signals are observed. The broad triplet at δ = -104.9 ppm corresponds to the coordinating phosphorus atoms of the AsP_3 butterfly framework. Around δ = -275 ppm a symmetrical multiplet is detected, as well as several signals that might be interpreted as a doublet of doublets (Figure 37). The integral intensity ratio of the two signal groups is about 1 : 2.8 which differs from the expected 1 : 2 ratio. Hence, other species than **74** seem to exist in solution, which could be the result of dissociation processes. However, the coordination of the copper(I) cation by two molecules of **55** results in a C_1 symmetric coordination environment of the central atom which has already been discussed for complex **73** (Scheme 8). As a consequence, a high-order AA'MM'NN' spin system is observed for which the corresponding chemical shifts and coupling constants were estimated by the simulation of the experimental spectrum (Table 8).[71] The chemical shifts and coupling constants obtained by the simulation of the spectrum compare well to the ones found for **73**.

Table 8. Chemical shifts and coupling constants from the simulated $^{31}P\{^{1}H\}$ NMR spectrum of **74**.

δ_A = -104.9 ppm	$\delta_{A'}$ = -105.0 ppm	δ_M = -273.0 ppm
$\delta_{M'}$ = -273.0 ppm	δ_N = -277.6 ppm	$\delta_{N'}$ = -277.6 ppm
$^{1}J_{AM}$ = 197 Hz	$^{1}J_{AN}$ = 199 Hz	$^{1}J_{MN}$ = 173 Hz
$^{1}J_{A'M'}$ = 199 Hz	$^{1}J_{A'N'}$ = 196 Hz	$^{1}J_{M'N'}$ = 173 Hz
$^{2}J_{AA'}$ = 61 Hz		

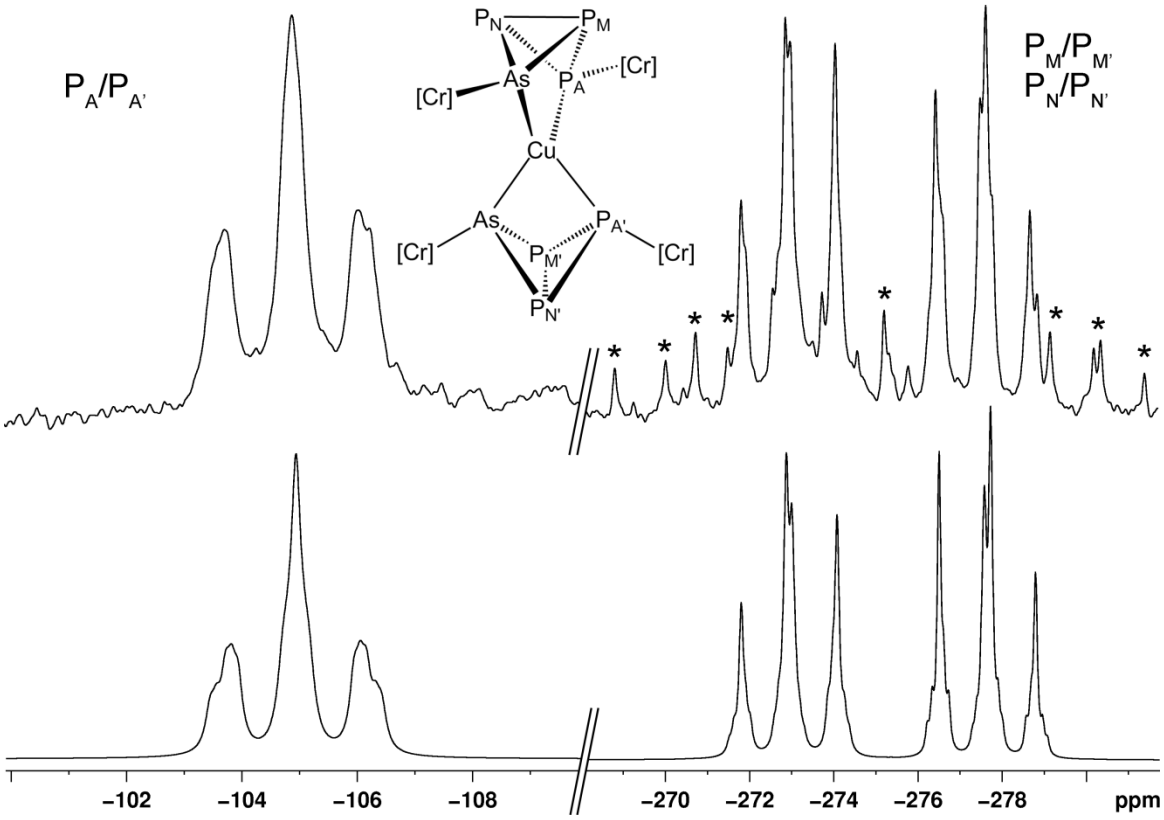

Figure 37. Sections of the experimental (CD_2Cl_2, top) and simulated (bottom) $^{31}P\{^1H\}$ NMR spectrum of **74**. Signals marked with an asterisk may belong to dissociation products which are formed in solution.

$[\{\{Cp^*Cr(CO)_3\}_2(\mu_3,\eta^{1:1:1:1}\text{-}AsP_3)\}_2Cu]^+[BF_4]^-$ (**74**) crystallizes as orange bars in the triclinic space group $P\bar{1}$. The asymmetric unit contains one molecule of **74**. X-ray structure analysis confirms the expected chelating coordination of a Cu(I) cation by two molecules of **55** (Figure 38). The copper(I) cation in **74** is coordinated by two heterobidentate AsP_3 butterfly complexes **55** in a distorted tetrahedral way. The "wing-tip" positions of the butterfly frameworks are either occupied by phosphorus or arsenic, leading to an allocation disorder. During the refinement process the occupancy of phosphorus and arsenic was refined freely but the P/As atom positions and displacement parameters had to be restrained to be the same. The result of the occupancy refinement is summarized in Table 9.

Table 9. Occupancy of phosphorus and arsenic at the respective positions of **74**. Labeling according to Figure 38.

	position			
atom	**1**	**2**	**5**	**6**
P	43 %	57 %	39 %	61 %
As	57 %	43 %	61 %	39 %

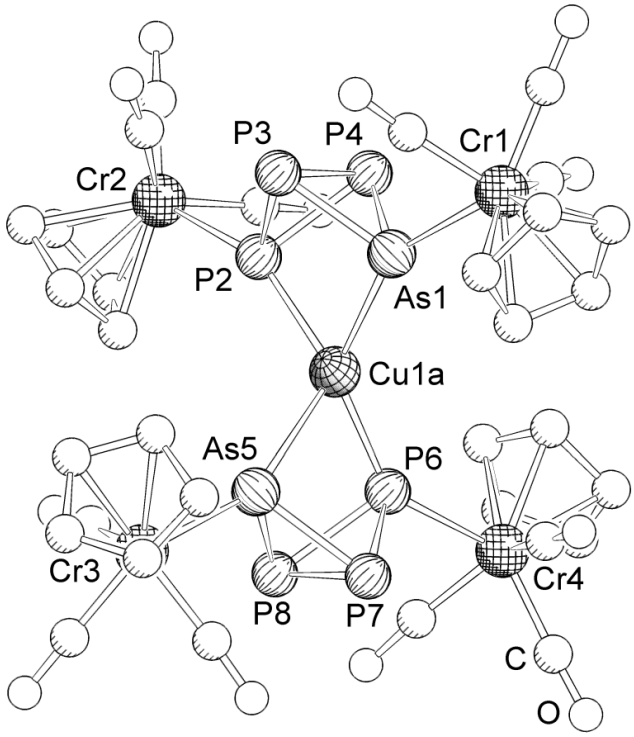

Figure 38. Molecular structure of **74** in the crystal. For clarity reasons methyl groups and the $[BF_4]^-$ counterion are omitted. Additionally, only one of the four copper positions and only one possible occupancy combination of arsenic are depicted. Selected bond lengths [Å] and angles [°]: As1–Cr1 2.564(2), P2–Cr2 2.553(2), As5–Cr3 2.565(2), P6–Cr4 2.533(2), Cu1a–As1 2.473(8), Cu1a–P2 2.372(7), Cu1a–As5 2.678(7), Cu1a–P6 2.250(7), As1–P3 2.284(2), As1–P4 2.277(3), P2–P3 2.278(2), P2–P4 2.269(3), P3–P4 2.210(3), As5–P7 2.304(2), As5–P8 2.286(2), P6–P7 2.270(3), P6–P8 2.292(2), P7–P8 2.207(2), As1···P2 2.947(2), As5···P6 2.939(2), As1–Cu1a–P2 74.9(2), As1–Cu1a–As5 120.5(3), As1–Cu1a–P6 133.6(3), P2–Cu1a–As5 118.5(3), P2–Cu1a–P6 142.2(3), As5–Cu1a–P6 72.6(2).

As a result of the used restraints used during the allocation refinement, the bond lengths between the "wing-tip" atoms E1, E2, E5 and E6 (E = P, As) and the bridgehead P atoms are similar and range from 2.269(3) Å to 2.304(2) Å. Hence, they can be viewed as in between a P–P and an As–P single bond (2.22 Å and 2.32 Å, respectively).[68a] The bonds between the bridgehead P atoms P3–P4 and P7–P8 are with 2.210(2) Å and 2.207(2) Å in the normal range of a P–P single bond. While the E1···E2 and E5···E6 distances of 2.947(2) Å and 2.939(1) Å are elongated compared to the corresponding distance in **55** (2.778(4) Å), the Cr–E distances range from 2.565(2) Å to 2.533(2) Å and are shorter than in **55** (2.606(4) Å and 2.610(2) Å). Both effects have also been observed for the P_4 derivative **66**.

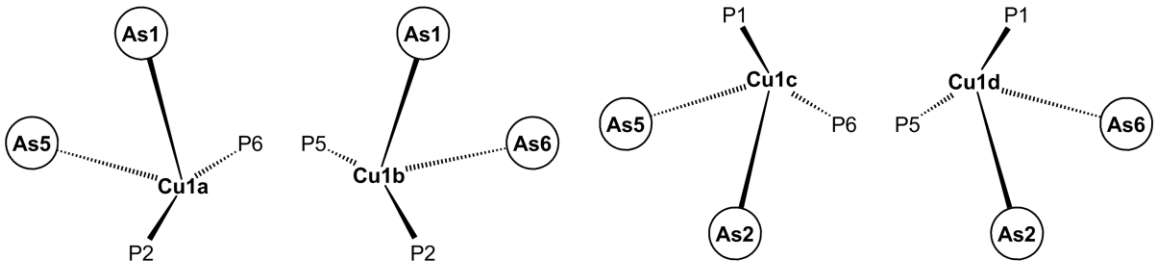

Scheme 9. Schematic view of the disordered central copper atom Cu1 due to the location of the two arsenic atoms. Labeling according to Figure 38.

However, the allocation disorder of the arsenic atoms leads to a disorder of the central copper atom. In the crystal, four different occupancy combinations of the two arsenic atoms are possible. As Cu–As bonds are longer than Cu–P bonds, the copper cation occupies four different positions, depending on where the arsenic atoms of the butterfly frameworks are located (Scheme 9). In Figure 38, the position of Cu1 is depicted for arsenic occupying the positions E1 and E5. Hence, the As1–Cu1a and As5–Cu1a bond lengths of 2.473(8) Å and 2.678(7) Å are longer than the P2–Cu1a and P6–Cu1a bond lengths of 2.372(7) Å and 2.250(7) Å. Furthermore, the Cu–P bond lengths are shorter than the corresponding bond lengths in the P_4 derivative **66** (2.3742(6) Å to 2.4551(7) Å). Hence, the introduction of arsenic at one of the coordinating positions of the bidentate butterfly complexes leads to a slipped coordination of the central atom and allows a stronger P–Cu interaction. Compared to the "classic" chelate complex $[Cu_2(diphars)_2]^{2+}$ (diphars = $Ph_2AsC_2H_4P(Ph)C_2H_4P(Ph)C_2H_4AsPh_2$)[106a] (Cu–P 2.255(3) Å – 2.304(4) Å, Cu–As 2.397(2) Å – 2.463(2) Å) the Cu–E bond lengths in **74** are slightly elongated. The bite angles of 74.9(2)° and 72.6(2)° in **74** are smaller than in $[Cu_2(diphars)_2]^{2+}$ (87.2(1)° to 89.5(1)°) and qualify the AsP_3 butterfly complex as chelating complex with small bite angle.

3.5.2.2 Coordination behavior towards monovalent silver cations

The reaction of $AgPF_6$ with two equivalents of **51** or **55** leads to the formation of the chelate complexes $[\{\{Cp'''Fe(CO)_2\}_2(\mu_3,\eta^{1:1:1:1}\text{-}AsP_3)\}_2Ag]^+[PF_6]^-$ (**75**) and $[\{\{Cp^*Cr(CO)_3\}_2(\mu_3,\eta^{1:1:1:1}\text{-}AsP_3)\}_2Ag]^+[PF_6]^-$ (**76**), respectively (equation 30). The $^{31}P\{^1H\}$ NMR spectra of the reaction mixtures show a quantitative product formation. Complexes **75** and **76** are isolated as orange solids that have good solubility in dichloromethane and THF but insoluble in hexane. They can be crystallized by slow diffusion of hexane into solutions of the respective compound in THF.

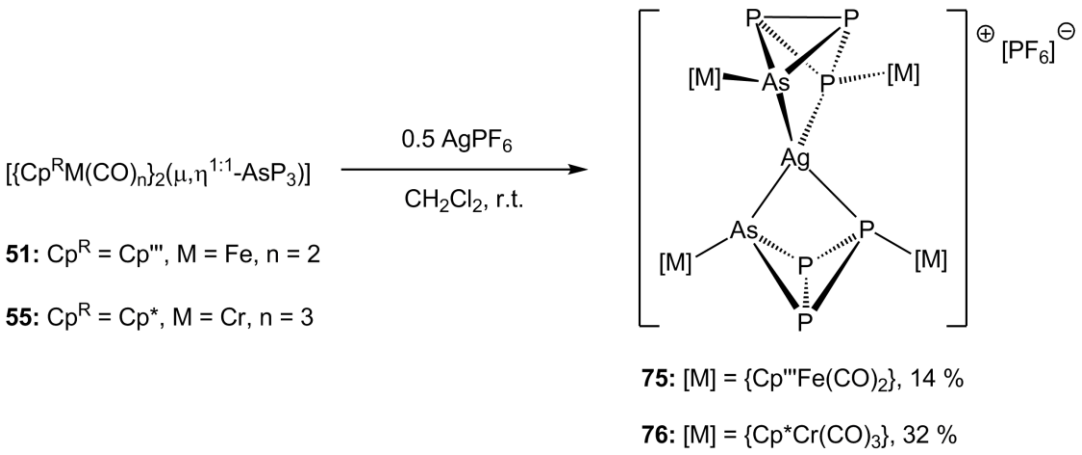

(30)

In the positive ion ESI mass spectrum of **75** a peak is detected at *m*/*z* = 1768.7 that can be assigned to the cationic fragment [M^+ - 2CO]. Additional peaks are found at *m*/*z* = 1147.7 and 831.2 that correspond to the cations $[\{Cp'''Fe(CO)_2\}_2AsP_3\{Cp'''Fe\}]^+$ and $[\{Cp'''Fe(CO)_2\}AsP_3\{Cp'''Fe(CO)\}]^+$. The IR spectrum (KBr) shows three absorption bands at ν = 2009, 1993, 1959 cm^{-1} that compare well to the bands found in **73** (ν = 2008, 1993 and 1958 cm^{-1}) and are blue-shifted compared to the starting material **51** (ν = 1998, 1990, 1950 and 1940 cm^{-1}). The ^1H NMR spectrum (CD_2Cl_2) of **75** shows two sets of signals consisting of three singlets each. They can be assigned to the Cp''' ligands of two slightly different [Cp'''Fe$(CO)_2$] fragments, one coordianted by phosphorus, the other one by arsenic. The same observation has already been made for the starting material **51**. In the $^{31}P\{^1H\}$ NMR spectrum (CD_2Cl_2) beside the signal for the $[PF_6]^-$ counterion two signal groups centered at δ = -85.3 ppm and δ = -294.0 ppm are detected that are best described as a combination of signals of two AM_2 spin systems. At δ = -85.3 ppm a broadened doublet of triplets with coupling constants of $^1J_{AM}$ = 200 Hz and $^1J_{PAg}$ = 305 Hz can be found. The signal can be assigned to the coordinating P atoms of both butterfly frameworks. However, due to the broadening of the signal only one averaged J_{AgP} coupling is observed. Additionally two doublets with coupling constants of $^1J_{PP}$ = 200 Hz are observed at δ = -293.9 and -294.1 ppm, respectively, that correspond to the bridgehead P atoms of two butterfly frameworks. A coupling of the bridgehead atoms, which is the case in the copper derivative **73**, is not observed. Hence, the spectrum is best interpreted as two superimposed AM_2 spin systems with isochrone bridgehead phosphorus nuclei.

In the positive ion ESI mass spectrum of **76** the molecular ion peak [M^+] is found as base peak at *m*/*z* = 1528.4. The IR spectrum (KBr) shows three absorption bands at ν = 1998, 1979 and 1916 cm^{-1} of which the latter one is broadened. All three bands compare well to the bands found in the copper derivative **74** (ν = 1996, 1979 and 1910 cm^{-1}) and are blue-shifted compared to the AsP_3 butterfly complex **55** (ν = 1980, 1964 and 1897 cm^{-1}). The ^1H NMR spectrum (CD_2Cl_2) of

76 reveals two sharp singlets at δ = 1.91 and 1.92 ppm with equal integral intensities that can be assigned to the protons of the Cp* ligands. The presence of two singlets has already been observed for the starting material **55** and can be explained by two different {Cp*Cr(CO)$_3$} groups, one coordinated by phosphorus and one by arsenic. In the $^{31}P\{^1H\}$ NMR spectrum (CD_2Cl_2) beside the septet for the $[PF_6]^-$ counterion two signals of a high-order spin system are detected around δ = -92 and -298 ppm with an integral intensity ratio of 1 : 2. Simulation of the spectrum afforded the exact chemical shifts, coupling constants and proved an AA'MM'NN' spin system (Figure 39, Table 10). The downfield shifted signal shows an additional doublet splitting due to the coupling with the I = ½ nuclei ^{107}Ag and ^{109}Ag (natural abundance of about 48 : 52).

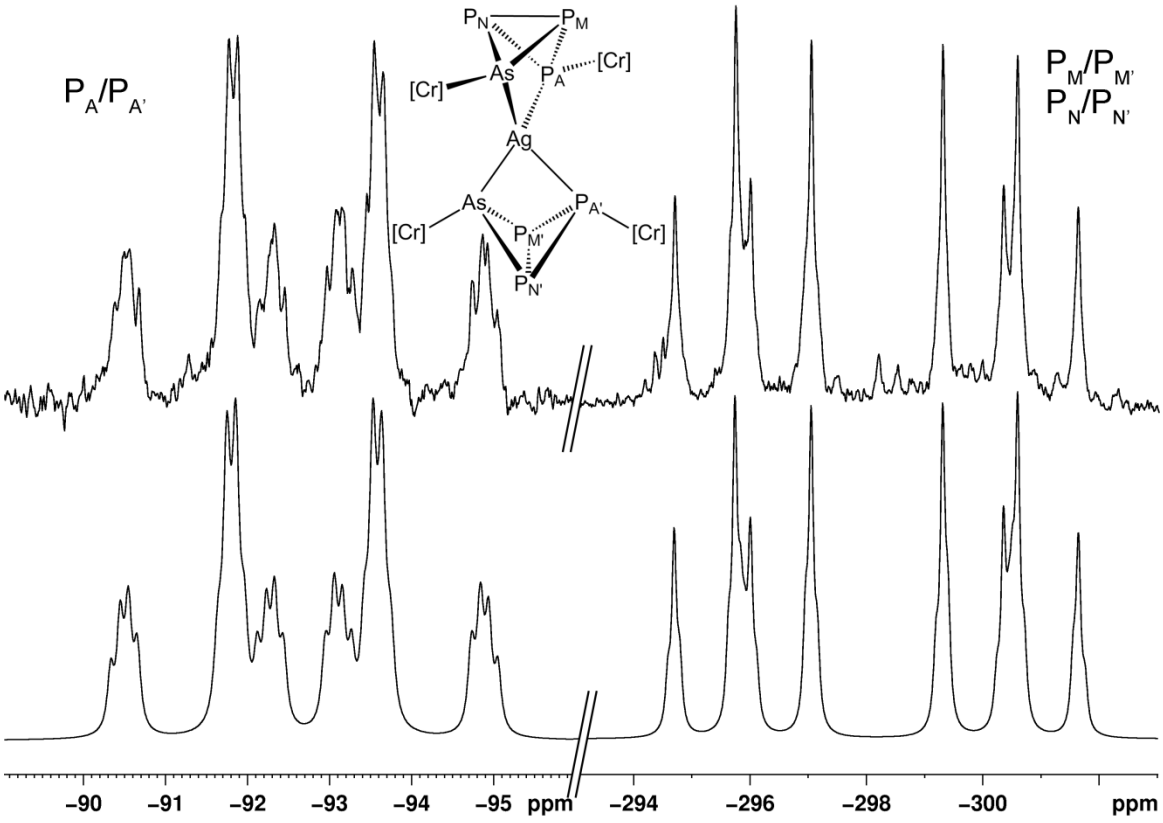

Figure 39. Experimental (CD_2Cl_2, top) and simulated (bottom) $^{31}P\{^1H\}$ NMR spectrum of **76**.

However, as no other signals are observed, dissociation processes do not seem to take place. This is in contrast to the observations for the copper derivative **74** in which several additional signals are observed that could derive from dissociation processes. Hence, the coordination of a silver(I) cation by two molecules of **55** seems to be more favorable than the coordination of a copper(I) cation. On the one hand this could be a result of a decreased steric repulsion of the butterfly ligands due to a larger central atom. On the other hand the interaction between the AsP_3 ligand and the rather soft silver(I) action could be more favorable than the coordination of the harder copper(I) cation. Furthermore, the $^1J_{AgP}$ coupling constants in **75** (ca. 305 Hz) and **76** are (267 Hz

to 310 Hz) are about 140 Hz larger than in the corresponding P_4 derivatives (**68**: 138 Hz and 158 Hz; **69**: 125 Hz and 144 Hz) and even larger than in $[Ag(dppe)_2]^+[NO_3]^-$ (231 Hz and 266 Hz)[96] pointing to a stronger Ag–P interaction.

Table 10. Chemical shifts and coupling constants from the simulated $^{31}P\{^1H\}$ NMR spectrum of **76**.

δ_A = -92.7 ppm	$\delta_{A'}$ = -92.7 ppm	δ_M = -295.9 ppm
$\delta_{M'}$ = -295.9 ppm	δ_N = -300.4 ppm	$\delta_{N'}$ = -300.4 ppm
$^1J_{AM}$ = 212 Hz	$^1J_{AN}$ = 208 Hz	$^1J_{MN}$ = 167 Hz
$^1J_{A'M'}$ = 214 Hz	$^1J_{A'N'}$ = 209 Hz	$^1J_{M'N'}$ = 167 Hz
$^2J_{AA'}$ = 34 Hz	$^1J(^{107}AgP_A)$ = 273 Hz	$^1J(^{109}AgP_A)$ = 310 Hz
$^1J(^{107}AgP_{A'})$ = 267 Hz	$^1J(^{109}AgP_{A'})$ = 305 Hz	

$[\{\{Cp'''Fe(CO)_2\}_2(\mu_3,\eta^{1:1:1:1}\text{-}AsP_3)\}_2Ag]^+[PF_6]^-$ (**75**) crystallizes as orange plates in the monoclinic space group *Cc*. The asymmetric unit contains one molecule of **75** together with four molecules of THF. $[\{\{Cp^*Cr(CO)_3\}_2(\mu_3,\eta^{1:1:1:1}\text{-}AsP_3)\}_2Ag]^+[PF_6]^-$ (**76**) crystallizes as orange blocks in the triclinic space group $P\bar{1}$. The asymmetric unit contains one molecule of **76** together with 1.5 molecules of THF. X-ray structure analysis shows the coordination of a central silver(I) cation by two molecules of **51** or **55**, respectively, in a distorted tetrahedral way (Figure 40).

The coordinating positions of the AsP_3 butterfly units show an allocation disorder of phosphorus and arsenic. The P/As occupancy was refined freely while the P/As atom positions and displacement parameters had to be restrained to be the same. Hence, the bond lengths between the "wing-tip" and the bridgehead atoms (**75**: 2.29 Å average, **76**: 2.27 Å average) are in between a P–P and an As–P single bond (2.22 Å and 2.32 Å, respectively)[68a] and compare well to the observed bond lengths in the copper derivative **74** (2.28 Å average). The bonds between the bridgehead P atoms of the *bicyclic* framework are with 2.210(2) Å and 2.202(2) Å (complex **75**) as well as 2.195(3) Å and 2.166(3) Å (complex **76**) slightly shortened which is typical for the butterfly arrangement. As observed for complex **74**, four position combinations of the two arsenic atoms relative to each other are possible, which consequently leads to four possible positions for the central silver atom (analogously to Scheme 9). The observed Ag1a–P bond lengths (**75**: 2.48 Å average, **76**: 2.40 Å average) are shorter than the corresponding Ag–P bond lengths in the P_4 derivatives **68** (2.61 Å average) and **69** (2.61 Å) which compares well to the shortening of the Cu–P bond lengths in **74** and rationalize the large $^1J_{AgP}$ coupling constants found in the $^{31}P\{^1H\}$ spectrum. Furthermore, the observed Ag–E bond lengths compare well to the bond lengths in $[Ag_2(diphars)_2]^{2+}$ (Ag–P 2.465(5) Å – 2.490(5) Å, Ag–As 2.578 – 2.608(3) Å),[106a] the bite angles (**75**: 66.3(1)° and 67.5(2)°, **76**: 66.7(1)° and 67.8(1)°) are smaller than in the organic derivative (84.1(1)° – 85.4(1)°).

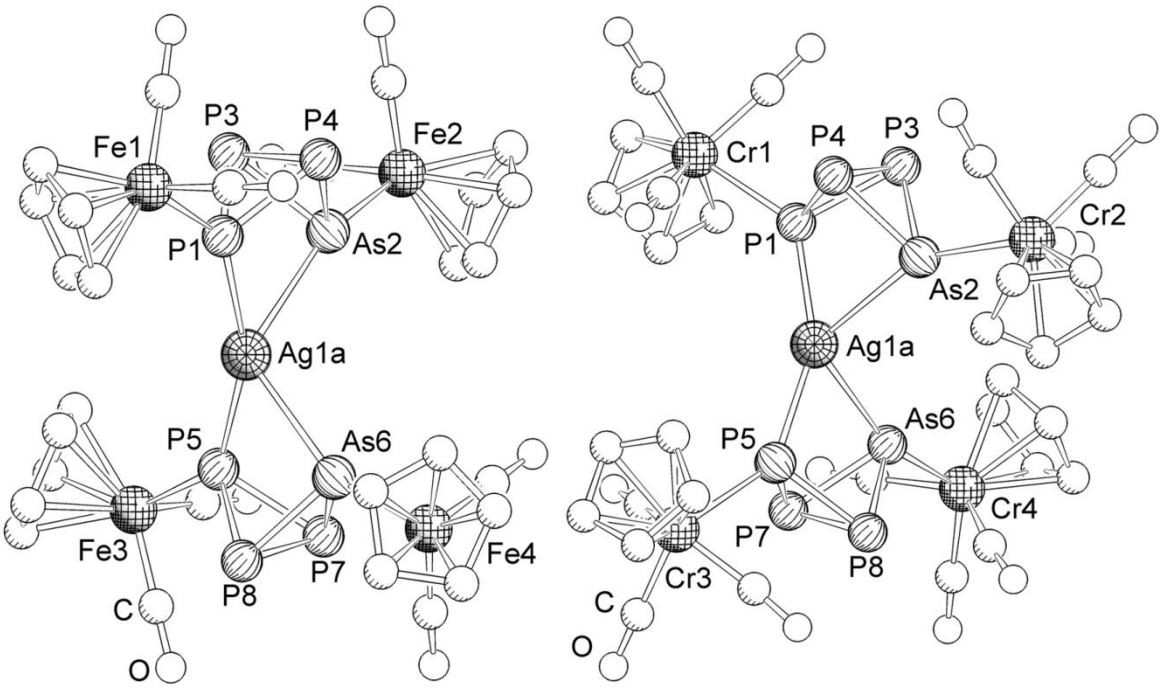

Figure 40. Molecular structure of **75** (left) and **76** (right) in the crystal. For clarity reasons protons, ^{tert}butyl groups, methyl groups, solvent THF and the $[PF_6]^-$ counterions are omitted. Additionally, only one of the four silver positions and only one possible occupancy combination of arsenic are depicted, respectively. Selected bond lengths [Å] and angles [°]: **75**: Ag1a–P1 2.458(3), Ag1a–As2 2.892(4), Ag1a–P5 2.506(5), Ag1a–As6 2.749(7), P1–P3 2.275(1), P1–P4 2.271(1), As2–P3 2.305(1), As2–P4 2.310(1), P3–P4 2.210(2), P5–P7 2.287(1), P5–P8 2.295(1), As6–P7 2.294(1), As6–P8 2.287(1), P7–P8 2.202(2), P1···As2 2.950(1), P5···As6 2.924(1), Fe1–P1 2.338(1), Fe2–As2 2.362(1), Fe3–P5 2.365(1), Fe4–As6 2.336(1), P1–Ag1a–As2 66.3(1), P1–Ag1a–P5 155.3(2), P1–Ag1a–As6 134.7(1), As2–Ag1a–P5 120.1(1), As2–Ag1a–As6 113.0(1), P5–Ag1a–As6 67.5(2). **76**: Ag1a–P1 2.384(3), Ag1a–As2 2.880(3), Ag1a–P5 2.413(3), Ag1a–As6 2.918(3), P1–P3 2.279(2), P1–P4 2.240(2), As2–P3 2.277(2), As2–P4 2.289(2), P3–P4 2.195(3), P5–P7 2.254(2), P5–P8 2.280(2), P6–P7 2.273(2), P6–P8 2.294(2), P7–P8 2.166(3), P1···As2 2.921(1), P5···As6 3.003(1), Cr1–P1 2.521(1), Cr2–As2 2.561(1), Cr3–P5 2.550(1), Cr4–As6 2.549(1), P1–Ag1a–As2 66.65(6), P1–Ag1a–P5 153.7(1), P1–Ag1a–As6 128.2(1), As2–Ag1a–P5 133.8(1), As2–Ag1a–As6 106.8(1), P5–Ag1a–As6 67.81(7).

However, it is noteworthy that the P1–Ag1a–P5 bond angles in **75** and **76** (155.3(2)° and 153.7(1)°, respectively) are larger than all other E–Ag1a–E (E = P, As) bond angles in the molecules. Hence, the coordination environment of the silver cation in both molecues seems to be distorted towards a strong linear coordination of Ag1a by the two coordinating P atoms P1 and P5 which corresponds well to the shortening of the Ag1a–P bonds in **75** and **76** compared to the P_4 derivatives. Hence, weakened Ag–As interactions are compensated with strengthened Ag–P interactions

3.5.2.3 Coordination behavior towards monovalent gold cations

The reaction of $[(PPh_3)Au(tht)]^+[PF_6]^-$ with one equivalent of **51** or **55** leads to the the formation of the chelate complexes $[\{Cp'''Fe(CO)_2\}_2(\mu_3,\eta^{1:1:1:1}\text{-}AsP_3)\{Au(PPh_3)\}]^+[PF_6]^-$ (**77**) and $[\{Cp^*Cr(CO)_3\}_2(\mu_3,\eta^{1:1:1:1}\text{-}AsP_3)\{Au(PPh_3)\}]^+[PF_6]^-$ (**78**), respectively (Equation 31). The $^{31}P\{^1H\}$ NMR spectra of the reaction mixtures shows a quantitative product formation. Both complexes are obtained as reddish orange solids that have good solubility in THF or dichloromethane but are insoluble in hexane. Single crystals suitable for X-ray structure analysis could so far only be obtained from **78** by slow diffusion of hexane into a saturated solution of **78** in a mixture of THF/dichloromethane.

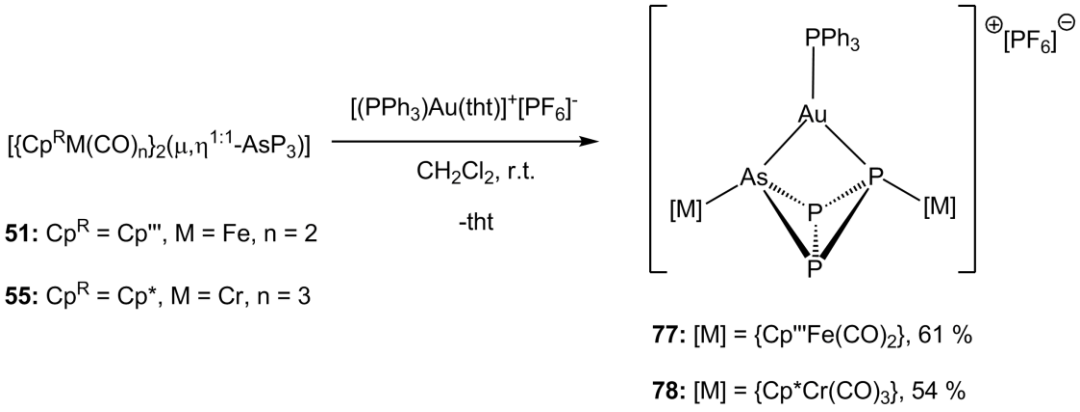

51: Cp^R = Cp''', M = Fe, n = 2

55: Cp^R = Cp*, M = Cr, n = 3

77: [M] = {Cp'''Fe(CO)$_2$}, 61 %

78: [M] = {Cp*Cr(CO)$_3$}, 54 %

(31)

In the ESI mass spectrum of **77** the molecular ion peak $[M^+]$ is detected as base peak at *m*/*z* = 1317.6. Furthermore, two peaks are detected at *m*/*z* = 944.4 and 721.3 that can be assigned to the cationic fragments $[(\mathbf{51})_2Au - CO]^{2+}$ and $[(PPh_3)_2Au]^+$. The IR spectrum (KBr) shows four bands at ν = 2018, 1990, 1973 and 1947 cm^{-1} that are blue-shifted compared to the starting material **51** (ν = 1998, 1990, 1950 and 1940 cm^{-1}). The ^1H NMR spectrum (CD_2Cl_2) reveals two sets of signals for two different Cp''' ligands, which compares well to the ^1H NMR spectrum of the startng material **51**. Additionally a multiplet for the phenyl protons of the PPh_3 ligand is detected around δ = 7.57 ppm. However, in the $^{31}P\{^1H\}$ NMR spectrum (CD_2Cl_2), beside the signal for the counterion, three signals of an AMX_2 spin system are observed. At δ = 41.2 ppm a doublet with a $^2J_{AM}$ = 248 Hz coupling constant is detected that can be assigned to the PPh_3 ligand. Surprisingly, the coupling constant is more than twice the corresponding $^2J_{PP}$ coupling in the P_4 derivative **70** ($^2J_{AM}$ = 111 Hz) pointing to a stronger interaction between the gold cation and the "wing-tip" phosphorus atom. The signal for the "wing-tip" phosphorus atom appears as a doublet of triplets at δ = -49.6 ppm ($^2J_{AM}$ = 248 Hz, $^1J_{MX}$ = 213 Hz), the signal for the bridgehead P atoms as a sharp doublet at δ = -287.3 ppm ($^1J_{MX}$ = 213 Hz).

In the ESI mass spectrum of **78** the molecular ion peak [M^+] is detected at *m*/*z* = 1169.3 beside peaks at *m*/*z* = 983.3 and 721.2 for the cationic fragments $[(PPh_3)_3Au]^+$ and $[(PPh_3)_2Au]^+$. In the IR spectrum (KBr) five bands are observed at ν = 2009, 1980, 1946, 1933 and 1904 cm^{-1} which are blue-shifted compared to the butterfly complex **55** (ν = 1980, 1964 and 1897 cm^{-1}). The ^1H NMR spectrum (CD_2Cl_2) of **78** reveals two singlets at δ = 1.68 and 1.88 ppm for two different Cp* ligands as well as a multiplet for the phenyl groups of the PPh_3 ligand. It is noteworthy that the difference in the chemical shift of the Cp* signals is $\Delta\delta$ = 0.2 ppm, i.e. about twenty times higher than in the starting material **55** ($\Delta\delta$ = 0.01 ppm) pointing to magnetically more different [Cp*Cr(CO)$_3$] units. In the $^{31}P\{^1H\}$ NMR spectrum (CD_2Cl_2) three signals of an AMX_2 spin system are observed as well as a septet for the counterion. In contrast to the spectrum of **77**, the $^2J_{AM}$ coupling is not resolved and broad signals are observed at room temperature which can be overcome by cooling the sample to 193 K. The resulting spectrum shows an AMX_2 spin system which compares well to the spectrum of **77**. The signal for the PPh_3 ligand appears as a doublet ($^2J_{AM}$ = 241 Hz) at δ = 41.9 ppm. The signals for the P atoms of the butterfly framework appear as a doublet of triplets ($^2J_{AM}$ = 235 Hz, $^1J_{MX}$ = 229 Hz) at δ = -45.8 ppm as well as doublet ($^1J_{MX}$ = 224 Hz) at δ = -291.5 ppm. As already observed for **77**, the $^2J_{AM}$ coupling constant is larger than in the P_4 derivative **71** ($^2J_{AM}$ = 103 Hz) pointing to a stronger P–P interaction and hence a stronger Au – P interaction.

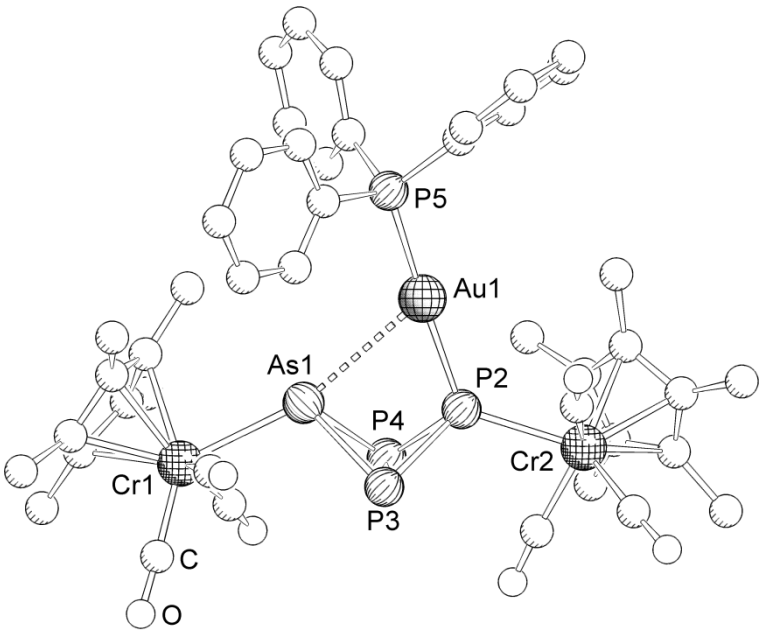

Figure 41. Molecular structure of **78** in the crystal. Hydrogen atoms as well as the $[PF_6]^-$ counterion are omitted for clarity. Selected bond lengths [Å] and angles [°]: Au1–As1 3.097(1), Au1–P2 2.337(2), Au1–P5 2.301(2), Cr1–As1 2.621(1), Cr1–P2 2.443(2), As1–P3 2.353(2), As1–P4 2.334(2), P2–P3 2.215(2), P2–P4 2.205(2), P3–P4 2.215(2), As1···P2 3.013(3), As1–Au1–P2 65.60(4), As1–Au1–P5 116.86(4), P2–Au1–P5 175.31(6).

$[\{Cp^*Cr(CO)_3\}_2(\mu_3,\eta^{1:1:1:1}\text{-}AsP_3)\{Au(PPh_3)\}]^+[PF_6]^-$ (**78**) crystallizes as orange wedges in the monoclinic space group *C*2/*c*. The asymmetric unit contains one molecule of **78**. X-ray structure analysis confirms the expected chelating coordination of the $[(PPh_3)Au]^+$ cation by one molecule of **55** (Figure 41). Surprisingly, no occupancy disorder of phosphorus and arsenic at the "wing-tip" positions of the AsP_3 butterfly framework is observed. This means that arsenic is exclusively found at the position As1 which allows a precise As–P bond length determination. The As1–P3 and As1–P4 bond lengths are with 2.353(2) Å and 2.334(2) Å slightly longer than an As–P single bond (2.32 Å).[68a] The coordination geometry of the central gold atom may best be described as a linear coordination by the two phosphorus atoms P2 and P5 with an additional weak As1–Au1 interaction. The three atoms draw a P2–Au1–P5 bond angle of 175.31(6)° which only deviates marginally from the perfect 180°. The Au1–P2 bond length of 2.337(2) Å is at least 0.1 Å shorter than the corresponding Au–P bond lengths in the P_4 derivatives **70** (2.480(2) Å and 2.557(2) Å) and **71** (2.79(1) Å and 2.43(1) Å) pointing to a stronger interaction. Furthermore, the Au1···As1 bond distance of 3.097(1) Å is only about 0.4 Å shorter than the sum of the van der Waals radii (3.51 Å)[108] indicating an only weak interaction. While the Au1–P2 bond length of 2.337(2) Å compares well to the Au–P bond lengths in $[Au_2(diphars)_2]^{2+}$ (2.333(3) Å to 2.375(3) Å),[106a] the Au···As distance of 3.097(1) Å is nearly 0.5 Å longer than in $[Au_2(diphars)_2]^{2+}$ (2.543(1) Å to 2.637(3) Å). Hence, complex **78** may be regarded as in-between a usual linear coordinated gold(I) cation and a gold(I) chelate complex. The resulting C_1 symmetry of the molecule might be the reason for the absence of the occupancy disorder. Additionally, the lowered symmetry also explains the large difference in the chemical shift of the Cp* ligands in the ^{1}H NMR spectrum of **78** compared to the starting material **55**.

3.5.2.4 Concluding remarks

The AsP_3 butterfly complexes **51** and **55** are able to act as small bite angle chelate ligands for monovalent coinage metal cations. The IR spectra of the resulting chelate complexes show blue-shifted absorption bands due to the electron withdrawing effect of the Lewis acidic cations, and they compare well to the spectra of the corresponding P_4 derivatives. The $^{31}P\{^1H\}$ NMR spectra of the Cu(I) and Ag(I) complexes reveal high-order spin systems due to the low symmetry of the complexes. Furthermore, the $^{31}P\{^1H\}$ NMR spectra of the silver complexes **75** and **76** clearly indicate a stronger Ag–P interaction than in the P_4 derivatives. X-ray structure analysis of the investigated copper and silver compounds **74**, **75** and **76** show an allocation disorder of the coordinating P and As atoms. Consequently the central atom is disordered over four positions. The coordination geometry around the copper and silver cations can be described as distorted tetrahedral with a tendency towards a linear coordination by the two "wing-tip" P atoms of the butterfly ligands. Furthermore, the observed M–P bond (M = Cu, Ag) lengths are shorter than in

the P_4 derivatives. In contrast, no allocation or positional disorder is observed in the gold compound **78** resulting in a linear coordination environment of the central Au(I) cation, with an only weak Au–As interaction. Hence, **78** may be seen as extreme case of the M–P bond shortening observed for **74**, **75** and **76** and nicely demonstrates the preferred coordination of the group 11 metal cation by phosphorus rather than arsenic.

3.5.3 As_4 butterfly complexes as chelating ligands

In the late 1950s Ahrland *et al.* reported on a generally weaker donor character of arsane ligands compared to their phosphane derivatives.[109] This trend is nicely exemplified by the increased dissociation tendency of arsane complexes of copper(I) compared to the corresponding phosphane complexes.[110] This can also be observed for chelating arsane and phosphane ligands.[111] Hence, the coordination behavior of the As_4 butterfly complexes [{Cp'''Fe(CO)$_2$}$_2$(μ,$\eta^{1:1}$-As_4)] (**52**) and [{Cp*Cr(CO)$_3$}$_2$(μ,$\eta^{1:1}$-As_4)] (**56**) towards coinage metal cations moved into the focus of interest.

3.5.3.1 Coordination behavior towards monovalent copper cations

The reaction of two equivalents of [{Cp'''Fe(CO)$_2$}$_2$(μ,$\eta^{1:1}$-As_4)] (**52**) with $[Cu(MeCN)_4]^+[BF_4]^-$ leads to the formation of [{{Cp'''Fe(CO)$_2$}$_2$(μ_3,$\eta^{1:1:1:1}$-As_4)}$_2$Cu]$^+$[BF_4]$^-$ (**79**) in moderate yields (Equation 32). Complex **79** is obtained as dark red solid that has good solubility in dichloromethane or THF but is insoluble in hexane. Crystals of **79** are obtained by slow diffusion of hexane into a solution of **79** in THF.

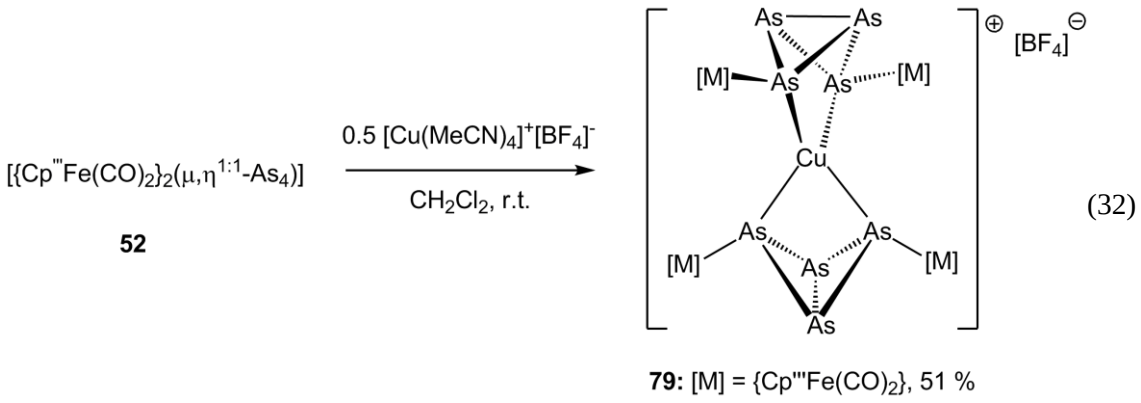

(32)

In contrast, the reaction of [{Cp*Cr(CO)$_3$}$_2$(μ,$\eta^{1:1}$-As_4)] (**56**) with $[Cu(MeCN)_4]^+[BF_4]^-$ did not lead to the desired chelate complex but afforded the dimerized As_8 cuneane complex [{Cp*Cr(CO)$_3$}$_4$(μ,$\eta^{1:1:1:1}$-As_8)] (**64**). This indicates a weak interaction between the As_4 butterfly complex **56** and the copper(I) cation accompanied by partial dissociation in solution. As a consequence, a certain amount of non-interacting **56** is present in solution which is not stable and reacts with itself to afford the dimerization product **64** (see section 3.4.2). However, the same weak interaction may also be the case for **79** but the stability of the As_4 butterfly complex **52** under ambient conditions allows the crystallization of the chelate complex.

In the ESI mass spectrum of **79** the molecular ion peak cannot be found. Instead, several peaks are detected that correspond to fragmentation products. The peak at *m*/*z* = 1961.2 corresponds to the threefold decarbonylated species $[M - 3\ CO]^+$. Additional peaks at *m*/*z* = 1614.0 and 1586.1 indiacte the presence of the copper-containing species $[\{Cp'''Fe\}_3As_8Cu(CO)_3]^+$ and $[\{Cp'''Fe\}_3As_8Cu(CO)_2]^+$. The IR spectrum (KBr) reveals two sharp absorption bands at ν = 1991 and 1953 cm^{-1} of which only the latter one is blue-shifted by 10 cm^{-1} compared to the starting material **52**. This is in contrast to the blue-shifted of both absorption bands in the P_4 derivative $[\{\{Cp'''Fe(CO)_2\}_2(\mu,\eta^{1:1:2}\text{-}P_4)\}_2Cu]^+[BF_4]^-$ (**65**) and points to a weaker interaction between the As_4 butterfly complex and the copper(I) cation. In the ^1H NMR spectrum (CD_2Cl_2) of **79** three signals are observed at δ = 1.42 ppm and 1.44 ppm as well as δ = 4.83 ppm for the ^{tert}butyl groups and the aromatic protons of the Cp''' ligands.

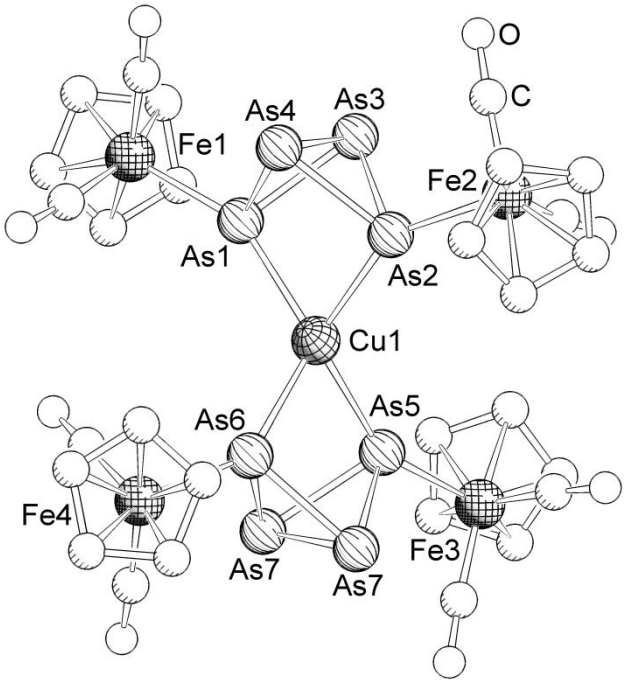

Figure 42. Molecular structure of **79** in the crystal. Hydrogen atoms, ^{tert}buytl groups as well as the $[BF_4]^-$ counterion are omitted for clarity. Selected bond lengths [Å] and angles [°]: Cu1–As1 2.4988(5), Cu1–As2 2.4616(4), Cu1–As5 2.4945(5), Cu1–As6 2.4559(4), Fe1–As1 2.4294(4), Fe2–As2 2.4087(4), Fe3–As5 2.4147(5), Fe4–As6 2.4033(4), As1–As3 2.4402(3), As1–As4 2.4603(4), As2–As3 2.4490(4), As2–As4 2.4468(4), As3–As4 2.4087(4), As1···As2 3.0790(4), As5–As7 2.4484(3), As5–As8 2.4582(4), As6–As7 2.4558(4), As6–As8 2.4373(4), As7–As8 2.4076(4), As5···As6 3.0599(4), As1–Cu1–As2 76.74(1), As1–Cu1–As5 139.15(2), As1–Cu1–As6 120.98(2), As2–Cu1–As5 121.51(2), As2–Cu1–As6 131.61(2), As5–Cu1–As6 76.36(1).

$[\{\{Cp'''Fe(CO)_2\}_2(\mu_3,\eta^{1:1:1:1}\text{-}As_4)\}_2Cu]^+[BF_4]^-$ (**79**) crystallizes as dark red to purple plates in the triclinic space group $P\bar{1}$. The asymmetric unit contains one molecule of **79** together with two

molecules of THF. X-ray structure analysis shows a central copper(I) cation that is coordinated by two As_4 butterfly complexes **52** in a distorted tetrahedral way (Figure 42). The planes defined by the atoms Cu1–As1–As2 and Cu1–As5–As6 draw an angle of 74.53(1)° which is only slightly larger than the corresponding angle in the P_4 derivative **65** (73.94(4)°). The As1–Cu1–As2 and As5–Cu1–As6 bond angles of 76.74(2)° and 76.36(1)° are larger than the P–Cu–P bond angles in **65** (72.51(3)° and 72.71(3)°) due to the larger As_4 butterfly ligand. The Cu–As bonds range from 2.4559(4) Å to 2.4988(5) Å and compare well to the Cu–As bond lengths found for the AsP_3 chelate complex $[\{\{Cp^*Cr(CO)_3\}_2(\mu_3,\eta^{1:1:1:1}\text{-}AsP_3)\}_2Cu]^+[BF_4]^-$ (**74**) (2.473(8) Å and 2.678(7) Å), but are about 0.1 Å longer than the Cu–As bonds in the chelate complex $[(pdma)_2Cu]^+$ (pdma = $C_6H_4(AsMe_2)_2$) (2.360(1) Å).[112] A reason for this might be the large steric bulk of the As_4 butterfly complex compared to the rather small pdma ligand. The As–As bonds between the "wing-tip" and the bridgehead arsenic atoms are in the range from 2.4373(3) Å to 2.4603(3) Å and the bonds between the bridgehead atoms average to 2.408(2) Å. This is nearly unchanged compared to the starting material **52** (2.449(2) Å to 2.461(3) Å and 2.405(3) Å). In contrast, the As1···As2 and As5···As6 distances of 3.0790(4) Å and 3.0599(4) Å are shorter than the As···As distance in **52** (3.184(3) Å) due to the coordination of the Lewis acid. The Fe–As bond lengths vary from 2.4033(4) Å to 2.4294(4) Å and are shorter than the Fe–As bonds in **52** (2.443(3) Å to 2.458(3) Å). This is in good agreement with the shortening of the M–P bond (M = Fe, Cr) in the P_4 chelate complexes dicussed in chapter 3.5.1 and indicates a contribution of the HOMO-1 orbital (see Figure 28) for the coordination of the copper(I) cation.

3.5.3.2 Coordination behavior towards monovalent silver cations

Reaction of $AgPF_6$ with two equivalents of $[\{Cp'''Fe(CO)_2\}_2(\mu,\eta^{1:1}\text{-}As_4)]$ (**52**) or $[\{Cp^*Cr(CO)_3\}_2(\mu,\eta^{1:1}\text{-}As_4)]$ (**56**) leads to the formation of the two chelate complexes $[\{\{Cp'''Fe(CO)_2\}_2(\mu_3,\eta^{1:1:1:1}\text{-}As_4)\}_2Ag]^+(PF_6)^-$ (**80**) and $[\{\{Cp^*Cr(CO)_3\}_2(\mu_3,\eta^{1:1:1:1}\text{-}As_4)\}_2Ag]^+(PF_6)^-$ (**81**), respectively, in moderate to good yields (Equation 33). The formation of by-products was not observed. However, the concurrent dimerization reaction of **56** could be the reason for the lower yields of **81**. Both complexes are isolated as orange solids that have good solubility in THF and dichloromethane but are insoluble in hexane. Crystals suitable for X-ray structure analysis are obtained by slow diffusion of hexane into saturated solutions of **80** in THF and **81** in a mixture of THF/dichloromethane.

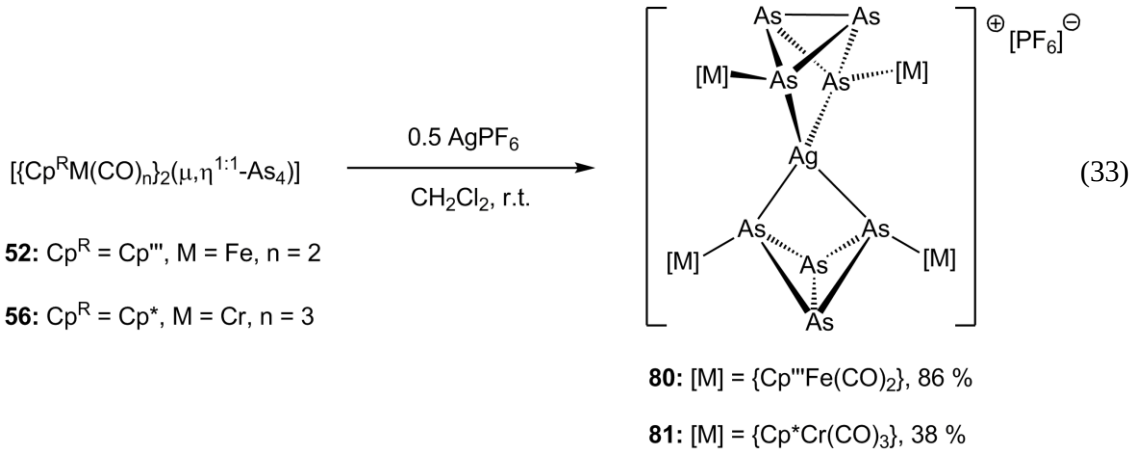

(33)

In the ESI mass spectrum of **80** at *m*/*z* = 1943.7 a peak for the dicationic fragment $[\{Cp'''Fe\}_4As_8Ag_2 - 2\ Me + 2\ H]_2^{2+}$ is detected as well as a peak at *m*/*z* = 1849.7 corresponding to the monocation $[\{Cp'''Fe\}_3As_8Ag_2(CO)_6]^+$. A peak for the molecular ion is not detected. In the IR spectrum (KBr) two strong absorption bands are observed at ν = 1998 and 1954 cm^{-1} that are both blue-shifted compared to **52** (ν = 1990 and 1940 cm^{-1}). This is different from the blue-shift in the copper derivative **79** in which only one band is shifted and points to a slightly stronger interaction between **52** and the silver(I) cation. In the ^1H NMR spectrum (CD_2Cl_2) of **80** three sharp singlets at δ = 1.39, 1.43 and 4.80 ppm for freely rotating Cp''' ligands are found.

The ESI mass spectrum of **81** reveals the molecular ion peak $[M]^+$ at *m*/*z* = 1793.1. In the IR spectrum (KBr) two broad absorption bands are detected at ν = 1982 and 1906 cm^{-1} which are slightly blue-shifted compared to **56** (ν = 1977, 1965 and 1904 cm^{-1}). In the ^1H NMR spectrum

(CD_2Cl_2) of **81** one sharp singlet for the Cp* ligands is observed at δ = 1.91 ppm which is slightly shifted compared to **56** (δ = 1.84 ppm).

The blue shift in the IR spectrum as well as sharp signals in the ^{1}H NMR spectra of **80** and **81** point to rather stable chelate complexes of the As_4 butterfly complexes with monovalent silver cations.

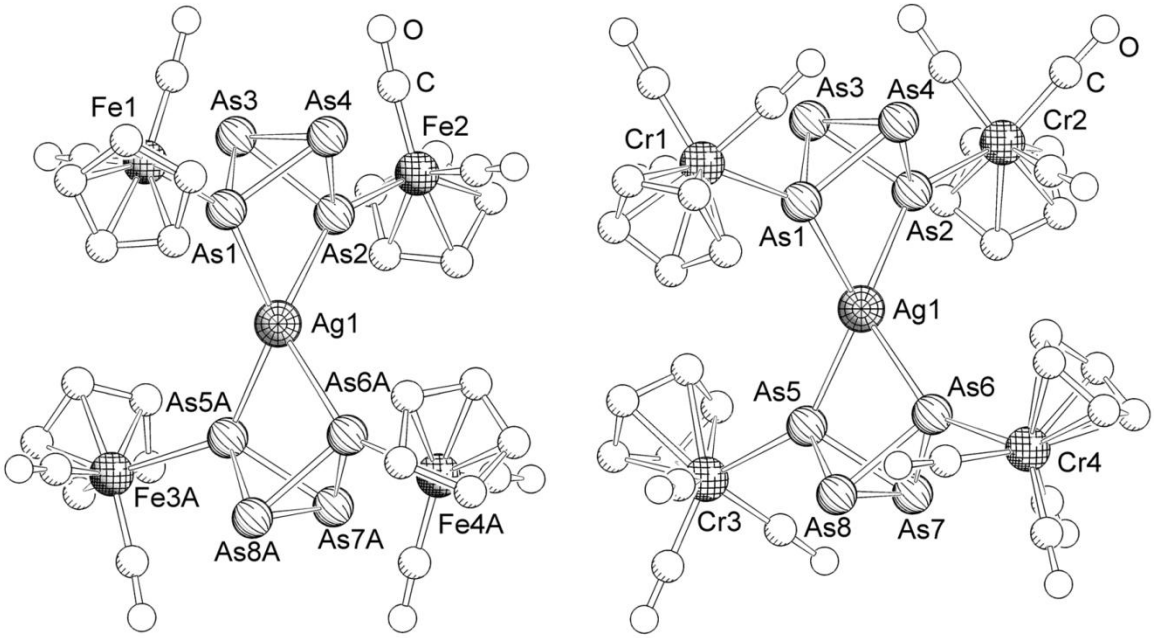

Figure 43. Molecular structure of **80** (left) and **81** (right) in the crystal. For clarity reasons, protons, ^{tert}butyl groups, methyl groups as well as $[PF_6]^-$ counterions are omitted and only one of the two positions of the disordered As_4 butterfly ligand in **80** is shown. Selected bond lengths [Å] and angles [°]: **80**: Ag1–As1 2.664(1), Ag1–As2 2.664(1), Ag1–As5A 2.622(3), Ag1–As6A 2.736(3), Fe1–As1 2.382(1), Fe2–As2 2.383(1), Fe3A–As5A 2.401(3), Fe4A–As6A 2.390(3), As1–As3 2.442(1), As1–As4 2.445(1), As2–As3 2.446(1), As2–As4 2.443(1), As3–As4 2.411(1), As1···As2 3.086(1), As5A–As7A 2.448(3), As5A–As8A 2.446(3), As6A–As7A 2.441(3), As6A–As8A 2.456(3), As7A–As8A 2.402(2), As5A···As6A 3.074(4), As1–Ag1–As2 70.78(2), As1–Ag1–As5A 135.93(6), As1–Ag1–As6A 134.05(6), As2–Ag1–As5A 130.97(6), As2–Ag1–As6A 126.08(6), As5A–Ag1–As6A 69.97(8); **81**: Ag1–As1 2.646(1), Ag1–As2 2.716(1), Ag1–As5 2.674(1), Ag1–As6 2.676(1), Cr1–As1 2.551(1), Cr2–As2 2.587(1), Cr3–As5 2.589(1), Cr4–As6 2.586(1), As1–As3 2.431(1), As1–As4 2.453(1), As2–As3 2.447(1), As2–As4 2.445(1), As3–As4 2.416(1), As1···As2 3.083(1), As5–As7 2.449(1), As5–As8 2.439(1), As6–As7 2.456(1), As6–As8 2.432(1), As7–As8 2.419(1), As5···As6 3.110(1), As1–Ag1–As2 70.19(3), As1–Ag1–As5 129.98(3), As1–Ag1–As6 132.07(3), As2–Ag1–As5 137.52(3), As2–Ag1–As6 127.48(3), As5–Ag1–As6 71.09(3).

$[\{\{Cp'''Fe(CO)_2\}_2(\mu_3,\eta^{1:1:1:1}\text{-}As_4)\}_2Ag]^+[PF_6]^-$ (**80**) crystallizes as red-orange bars in the triclinic space group $P\bar{1}$. The asymmetric unit contains one molecule of **80** together with four molecules of THF. $[\{\{Cp^*Cr(CO)_3\}_2(\mu_3,\eta^{1:1:1:1}\text{-}As_4)\}_2Ag]^+[PF_6]^-$ (**81**) crystallizes as red-orange blocks in the triclinic space group $P\bar{1}$. The asymmetric contains unit one molecule of **81**. X-ray structure analysis shows in both cases the chelating complexation of a silver(I) cation by two molecules of **52** and **56**, respectively (Figure 43). In the case of **80** one of the two As_4 butterfly ligands is disordered over two positions.

The central building unit in both complexes **80** and **81** is a silver(I) cation that is coordinated by two As_4 butterfly complexes in a distorted tetrahedral way. For complex **80** the planes defined by the atoms Ag1–As1–As2 and Ag1–As5A–As6A draw an angle of 87.89(5)°, indicating an almost perpendicular arrangement of the two chelating complexes **52**. In case of **81** the corresponding angle is, at 83.34(4)°, a little smaller. The Ag–As bond lengths in complex **80** vary from 2.622(3) Å to 2.736(3) Å, in complex **81**, they are in the range from 2.646(1) Å to 2.716(1) Å. This compares well to the Ag–As bond lengths found in the "classic" chelate complex $[\{O((CH_2)_2AsPh_2)_2\}_2Ag]^+$ (2.614(1) Å to 2.638(1) Å).[113] The As–As bond lengths in both complexes are in the normal range for an As_4 butterfly arrangement and are nearly unchanged compared to the starting materials **52** and **56**. The As–Ag–As bond angles (70.78(2)° and 69.97(8)° for **80**; 70.19(3)° and 71.09(3)° for **81**) are smaller than the As–Cu–As bond angles in the copper derivative **79** (76.74(2)° and 76.36(1)°) which is due to the longer Ag–As bonds. The distances between the "wing-tip" arsenic atoms (3.086(1) Å and 3.074(3) Å for **80**; 3.083(1) Å and 3.110(1) Å in **81**) compare well to the distances found in **79** (3.0790(4) Å and 3.0599(4) Å). In case of complex **80** they are shortened with respect to the starting material **52** (3.184(3) Å) but elongated in case of complex **81** (**56**: 3.032(1) Å). Hence, the coordination geometry around the silver(I) cation is nearly the same for **80** and **81** and seems to be independent of the $[Cp^RM(CO)_n]$ moiety (Cp^R = Cp''', M = Fe, n = 2; Cp^R = Cp*, M = Cr, n = 3).

3.6 Stabilization of yellow arsenic in the coordination sphere of transition metals

In the late 1970s Sacconi *et al.* succeeded in the synthesis of $[(np_3)Ni(\eta^1\text{-}P_4)]$ (**1**)[24] (np_3 = Tris(2-diphenylphosphinoethyl)amine) as the first complex bearing an intact P_4 tetrahedron as ligand. During the following years several other complexes were reported that exhibit vertex coordinated P_4 tetrahedra (c.f. section 1.2, Figure 1). In 2002, Krossing and co-workers reported the first homoleptic phosphorus complex $[Ag(\eta^2\text{-}P_4)_2]^+[pftb]^-$ (**5a**) (pftb = $Al\{OC(CF_3)_3\}_4$) in which the P_4 tetrahedron binds to the silver(I) cation via a P–P bond.[30] Theoretical calculations indicate only a weak interaction between the P_4 tetrahedra and Ag^+ that is dominated by electrostatic attraction. Hence, the use of the weakly coordinating anion $[pftb]^-$ is crucial for the formation of **5a**. This is nicely exemplified by the reaction of white phosphorus with $Ag^+[GaCl_4]^-$.[32] The resulting product $[Ag(\eta^2\text{-}P_4)(GaCl_4)]$ adopts a polymeric structure in the solid state that is characterized by several strong Ag^+–$[GaCl_4]^-$ interactions.

In contrast to white phosphorus, its heavier congener yellow arsenic is light-sensitive in solution as well as in the solid state and decomposes to metallic grey arsenic. In addition, small traces of grey arsenic accelerate the decomposition of As_4 even under the exclusion of light. Hence, yellow arsenic cannot be stored as is possible for white phosphorus and stochiometric reactions are hard to perform. Yellow arsenic is generated from grey arsenic at 750 °C. The emerging As_4 is taken away in a constant flow of argon carrier gas which is discharged in a solvent.[114] However, due to the high temperatures needed for the As_4 generation, the method is limited to high boiling solvents such as toluene, xylene or decalin. Additionally, the obtained solutions contain grey arsenic which favours the decomposition of the dissolved As_4. Due to the time consuming generation of As_4 together with the instability of the molecule only few results regarding its reactivity are known.[21, 69, 74] Furthermore, no complexes have been reported to date that contain intact As_4 tetrahedra as ligands.

It was therefore of interest whether the As_4 tetrahedron can be used as a ligand for suitable Lewis acids and if these compounds could be used as "easy to handle" As_4 synthons. Preliminary results regarding the coordination behavior of the pentaarsaferrocene $[Cp^*Fe(\eta^5\text{-}As_5)]$ (**35b**) towards copper(I) halides showed a preferred coordination of an As–As bond instead of the arsenics lone pairs.[60] Hence, by analogy to the synthesis of **5a**, the weakly coordinated silver(I) compound[115] $[Ag(CH_2Cl_2)]^+[pftb]^-$ was chosen for the reaction with As_4.

3.6.1 Coordination behavior of As_4 towards $[Ag(CH_2Cl_2)]^+[pftb]^-$

The reaction of freshly prepared yellow arsenic with $[Ag(CH_2Cl_2)]^+[pftb]^-$ leads to the formation of the first homoleptic silver arsenic complex $[Ag(\eta^2\text{-}As_4)_2]^+[pftb]^-$ (**82**) in excellent yields (equation 34) which exhibits two intact As_4 tetrahedra as ligands. Complex **82** is obtained as an air- and moisture-sensitive colorless solid that has good solubility in dichloromethane, moderate solubility in toluene and is insoluble in hexane. It can be stored at -30 °C under an argon atmosphere without decomposition. Surprisingly, complex **82** does not decompose upon heating to at least 50 °C and is light stable. Crystals suitable for X-ray structure analysis were grown by cooling a saturated solution of **82** in dichloromethane to -78 °C.

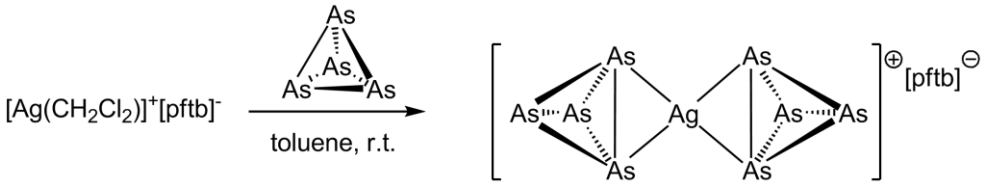

82

80 - 90 %

(34)

The ESI mass spectrum of **82** shows one peak in the anion mode for the $[pftb]^-$ anion at m/z = 967.2. In the cation mode, the molecular ion peak $[M^+]$ is detected at m/z = 706.3. Additionally two peaks are found at m/z = 447.5 and 406.4, the latter being the base peak. They correspond to the cationic fragments $[AgAs_4 + MeCN]^+$ and $[AgAs_4]^+$, respectively. The Raman spectrum of **82** in the solid state reveals three bands at ν = 210, 265 and 343 cm^{-1} that compare well to the DFT calculated Raman bands of the complex at ν = 206, 208, 228, 260, 261 and 339 cm^{-1} with the one at 228 cm^{-1} being the least intense. However, the Raman spectrum also resembles the experimental spectrum of molecular As_4 in solid state (ν = 193 (two-fold degenerate), 250 and 341 cm^{-1})[18] as well as the calculated spectrum of As_4 in the gas phase (ν = 203 (two-fold degenerate), 259 (three-fold degenerate) and 349 cm^{-1}). The similar number and position of Raman active bands of As_4 and **82** indicate a rather weak interaction between the silver(I) cation and the As_4 tetrahedron. Characteristic signals for the $[pftb]^-$ anion are found in the $^{13}C\{^1H\}$, ^{19}F and ^{27}Al NMR spectra (CD_2Cl_2). However, ^1H as well as $^{13}C\{^1H\}$ NMR spectra indicate small impurities of toluene that could not be removed.

$[Ag(\eta^2\text{-}As_4)_2]^+[pftb]^-$ (**82**) crystallizes as colorless blocks in the monoclinic space group $P2_1/c$. The asymmetric unit contains one molecule of **82**. X-ray structure analysis shows the expected side-on coordination of two intact As_4 tetrahedra to a silver(I) cation (Figure 44).

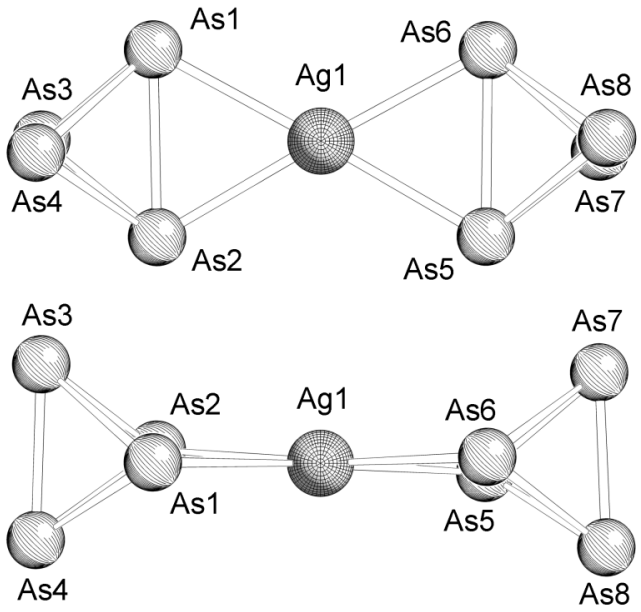

Figure 44. Top (above) and side (below) view of the cationic part of **82** in the crystal. Selected bond lengths [Å] and angles [°]: Ag1–As1 2.626(2), Ag1–As2 2.616(2), Ag1–As5 2.620(2), Ag1–As6 2.611(2), As1–As2 2.585(2), As1–As3 2.396(2), As1–As4 2.389(2), As2–As3 2.380(2), As2–As4 2.384(2), As3–As4 2.423(2), As5–As6 2.569(2), As5–As7 2.387(2), As5–As8 2.385(2), As6–As7 2.383(2), As6–As8 2.378 (2), As7–As8 2.419(2), As1–Ag1–As2 59.10(6), As5–Ag1–As6 58.83(5), As1–Ag1–As6 122.79(5), As2–Ag1–As5 119.61(5).

The planes defined by the atoms Ag1–As1–As2 and Ag1–As5–As6 deviate only 9° from perfect coplanarity leading to a local D_2 symmetry around the central silver atom. The Ag–As bond lengths vary from 2.611(2) Å to 2.626(2) Å and are shorter than the Ag–As bonds in $[\{Cp^*Mo(CO)_2As_3\}_4Ag_2]^{2+}[pftb]^-_2$ (2.665(1) Å to 2.828(1) Å)[116] which also exhibits a side-on coordinating As–As bond. The coordinating As1–As2 and As5–As6 bonds are with 2.585(2) Å and 2.569(2) Å elongated by about 0.14 Å compared to the As–As bond in As_4 (2.435 Å determined by electron diffraction[67] and 2.4372 Å specified by DFT calculations[74]). While the bond lengths between the coordinating and non-coordinating As atoms vary from 2.378(2) Å to 2.396(2) Å and are shorter than in As_4, the As3–As4 and As7–As8 bonds with 2.423(2) Å and 2.419(2) Å compare well to the ones in yellow arsenic. However, the shortening of the bonds between the coordinating and non-coordinating arsenic atoms may be seen as a result of the polarizing effect of the silver(I) cation. The electron withdrawing effect leads to a slightly positive partial charge on the coordinating atoms that consequently attract the electron rich non-coordinating atoms. A similar tendency is also observed for the P_4 derivative **5a**.[30]

In order to gain a deeper insight into the bonding situation of **82** as well as its stability compared to **5a** detailed DFT and CCSD(T) calculations were performed by Prof. Dr Marek Sierka

(University of Jena). Structure optimization for the cationic complexes $[Ag(\eta^2\text{-}E_4)_2]^+$ (E = P, As) leads to two conformational isomers with D_{2h} and D_{2d} symmetry (Figure 45). While the two conformers are virtually isoendergonic for **82**, quantum chemical calcuations predict a slight preference for **5a** (Table 11). The result of the X-ray structure analysis of **82** shows a local D_2 symmetry which may be due to packing effects.

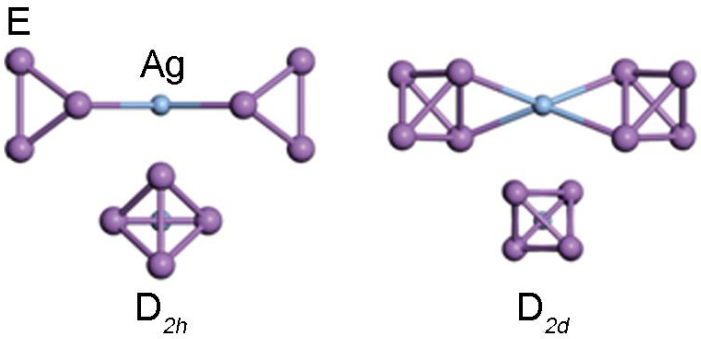

Figure 45. Conformational isomers of $[Ag(X_4)_2]^+$ (X = P, As).

Table 11. Relative energies of the conformational isomers $[Ag(\eta^2\text{-}E_4)_2]^+$ (kJ·mol-1). The imaginary frequencies of first-order saddle points are given in parantheses.

E	**D_{2h}**	**D_{2d}**
As	0.00 (3.1*i*)	0.14
P	0.00 (8.8*i*)	-1.06

In addition, the observed bond length variation in the coordinated As_4 tetrahedra is well reflected by the result of the structure optimization. Table 12 summarizes the experimentally observed, as well as the calculated bond lengths of the molecules $[Ag(\eta^2\text{-}E_4)_2]^+$ and E_4 (E = P, As).

Table 12. Calculated bond lengths [Å] in $[Ag(E_4)_2]^+$ and E_4 (E = As, P). Numbering of atoms according to Figure 44.

bond	As_4	$[Ag(As_4)_2]^+$ (calc)	$[Ag(As_4)_2]^+$ (exp)	P_4	$[Ag(P_4)_2]^+$ (calc)
E1-E2	2.454	2.638	2.569-2.585	2.204	2.364
E1-E3		2.443	2.378-2.396		2.191
E3-E4		2.483	2.419-2.423		2.236
Ag-E1		2.706	2.611-2.626		2.614

In general, the calculated bond lengths in the molecules $[Ag(\eta^2\text{-}E_4)_2]^+$ are overestimated compared to the experimentally obtained ones. However, theory predicts an elongation of the coordinating As1–As2 bond of about 0.18 Å which is slightly larger than the experimental value (0.14 Å) and is similar to the predicted elongation of the coordinating P–P bond in **5a** (0.16 Å). The calculated bond lengths As1–As3 and As3–As4 deviate only slightly from the calculated bond lengths in As_4 with the As1–As3 bond being shorter than the As3–As4 bond, which is in agreement with the experimental molecular structure.

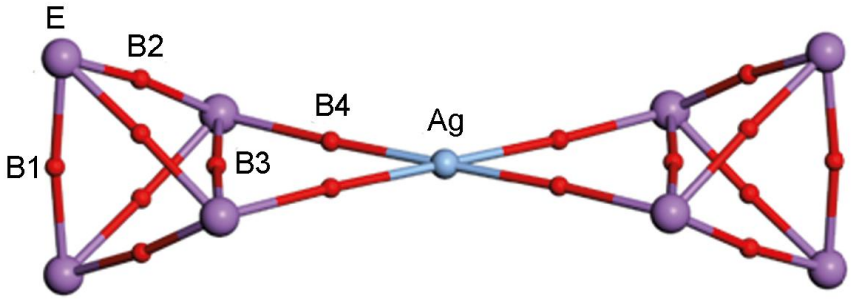

Figure 46. Bond critical points (BCP) in the cations $[Ag(\eta^2\text{-}E_4)_2]^+$ indicated by the red balls (labeled as B1 – B4).

Table 13. Properties of symmetry distinct bond critical points in E_4 and $[Ag(E_4)_2]^+$ (X = As, P) as shown in Figure 46; ρ_b - electron density, $\Delta\rho_b$ - Laplacian of the electron density, ε_b - bond elipticity, H_b - total electronic energy density.

BCP	**E = As**				**E = P**			
	ρ_b	$\Delta\rho_b$	ε_b	H_b	ρ_b	$\Delta\rho_b$	ε_b	H_b
E_4	0.076	-0.004	0.04	-0.029	0.105	-0.073	0.04	-0.054
$Ag(E_4)_2^+$								
B1	0.076	-0.008	0.02	-0.028	0.101	-0.063	0.01	-0.050
B2	0.078	-0.005	0.08	-0.030	0.109	-0.087	0.05	-0.058
B3	0.055	0.036	0.53	-0.015	0.077	0.027	0.31	-0.029
B4	0.048	0.063	0.38	-0.010	0.053	0.080	0.51	-0.012

To further evaluate the nature of bonding in $[Ag(\eta^2\text{-}E_4)_2]^+$ (E = P, As) the bond critical points (BCP) in **82**, **5a** and in the free E_4 tetrahedra were calculated using the atoms in molecule (AiM) approach (Figure 46 and Table 13). As can be seen in Table 13, the P_4 and As_4 molecules show similar bonding properties. The relatively large values of the electron density (ρ_b), the negative

values of the Laplacian of the electron density ($\Delta\rho_b$) along with the negative total electronic energy density (H_b) at the BCPs confirm the covalent character of the E–E bonds in free P_4 and As_4. In addition, small values of the bond elipticity, ε_b, indicate cylindrical symmetry of the E–E bonds. Upon formation of $[Ag(E_4)_2]^+$ only the properties of the BCP of the bond between the coordinating E atoms (B3, Figure 46) show significant changes. The decrease of ρ_b along with increase of $\Delta\rho$ confirms the expected depletion of the electron density upon coordination to Ag^+. Surprisingly, this depletion occurs only at the B3 BCP and not at other BCPs. This demonstrates only a moderate change in the electronic structures of the E_4 moieties upon complex formation. In addition, the properties of the BCPs clearly indicate an intact As–As bond in **82**.

Table 14. Calculated reaction Gibbs free energies at 293.15 K in the gas phase and in CH_2Cl_2 solution ($kJ \cdot mol^{-1}$) (Reaction energies are obtained from single-point CCSD(T) energy calculations on the DFT (B3LYP-QZVPP) optimized structures)

reaction	**E = As**		**E = P**	
	$\Delta G_{(g)}$	$\Delta G_{(l)}$	$\Delta G_{(g)}$	$\Delta G_{(l)}$
$[Ag(E_4)_2]^+ \rightarrow [Ag(E_4)]^+ + E_4$	118.3	-	107.5	-
$[Ag(E_4)]^+ \rightarrow Ag^+ + E_4$	180.1	-	149.5	-
$[Ag(E_4)_2]^+ + CH_2Cl_2 \rightarrow [Ag(E_4)(CH_2Cl_2)]^+ + E_4$	47.9	39.5	32.7	30.8
$[Ag(E_4)(CH_2Cl_2)]^+ + CH_2Cl_2 \rightarrow [Ag(CH_2Cl_2)_2]^+ + E_4$	66.3	55.7	40.0	37.9

Finally, the corresponding Gibbs free energies for the first and second dissociation of the cations $[Ag(\eta^2\text{-}E_4)_2]^+$ (E = P, As) were calculated in gas phase and in CH_2Cl_2 solution at 293.5 K to evaluate the stability of the two complexes. For complex **82** and complex **5a**, the dissociation is endergonic in gas phase and in solution. Surprisingly, the cations $[Ag(\eta^2\text{-}As_4)_2]^+$ and $[Ag(\eta^2\text{-}As_4)]^+$ are more stable than its phosphorus derivatives by 10 – 20 kJ mol^{-1}. The reason for this might be the larger polarizability of the As_4 tetrahedron compared to its lighter congener and hence a stronger interaction with the Lewis acidic Ag(I) cation. This also indicates a mainly electrostatic interaction between Ag^+ and the E_4 tetrahedra.

3.6.2 $[Ag(\eta^2\text{-}As_4)_2]^+[pftb]^-$ (82) as As_4 transfer agent

The Raman spectrum of **82** as well as theoretical calculations clearly indicate the coordination of two intact As_4 tetrahedra to the central silver(I) cation. Additionally, the complex is light-stable, storable and readily soluble in small amounts of polar solvents such as dichloromethane which makes it a perfect storage material for yellow arsenic. Hence, the reactivity of **82** towards halogenated and soluble transition metal compounds moved into the focus of interest. The reaction of $[Ag(\eta^2\text{-}As_4)_2]^+[pftb]^-$ (**82**) with a halide-containing transition metal salt L_nMX should lead to the formation of insoluble AgX (X = Cl, Br, I) accompanied by the release of As_4 and the generation of the corresponding metal cation L_nM^+. This cation is capable of interacting with the released yellow arsenic. Hence, compound **82** can be utilized as unique As_4 transfer material which allows stochiometric reactions.

The salt metathesis reaction of $[Ag(\eta^2\text{-}As_4)_2]^+[pftb]^-$ (**82**) with one equivalent of $[(PPh_3)AuCl]$ leads to the precipitation of beige-colored AgCl and the formation of $[(PPh_3)Au(\eta^2\text{-}As_4)]^+[pftb]^-$ (**83**) in good yields (Equation 35). Complex **83** is obtained as a pale yellow solid that has good solubility in dichloromethane but insoluble in hexane. Crystals suitable for X-ray structure analysis were obtained by diffusion of hexane into a saturated solution of **83** in dichloromethane at -28 °C.

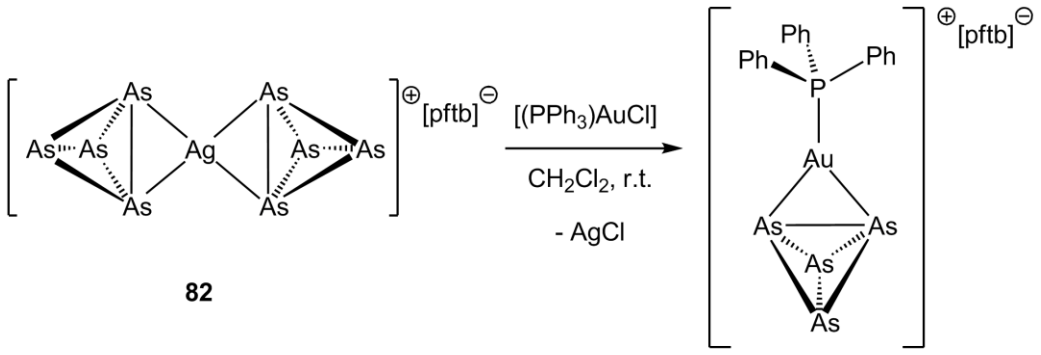

82 **83**

70 %

(35)

In the ESI mass spectrum of **83** in anion mode one peak at *m*/*z* = 967.2 is detected that corresponds to the $[pftb]^-$ counterion. In cation mode only one peak is observed at *m*/*z* = 721.2 which can be assigned to the cation $[(PPh_3)_2Au]^+$. Arsenic-containing fragments are not found, probably due to the lability of **83**. In the ^1H and $^{13}C\{^1H\}$ NMR spectrum (CD_2Cl_2) of **83** typical signals for the PPh_3 ligand are detected. In the $^{31}P\{^1H\}$ NMR spectrum (CD_2Cl_2) one singlet for the PPh_3 moiety appears at δ = 45.6 ppm. Compared to the starting material $[(PPh_3)AuCl]$ the

signal is shifted downfield by about 21 ppm. In the ^{19}F NMR spectrum (CD_2Cl_2) one singlet for the $[pftb]^-$ ion is found at δ = -75.6 ppm. Unfortunately, due to fluorescence of the sample, no Raman spectrum of **83** could be recorded.

$[(PPh_3)Au(\eta^2\text{-}As_4)]^+[pftb]^-$ (**83**) crystallizes as pale yellow bars in the triclinic space group $P\bar{1}$ with two molecules of **83** in the asymmetric unit. The molecular structure of the cationic part of the complex is depicted in Figure 47.

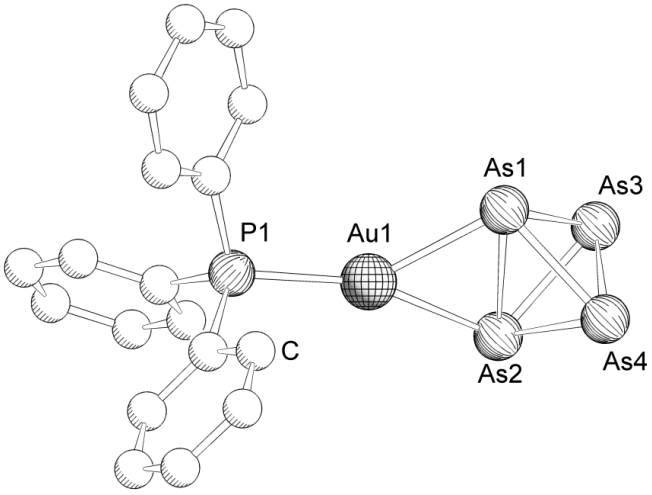

Figure 47. Molecular structure of the cationic part of one of the two molecules of **83** in the asymmetric unit. Hydrogen atoms are omitted for clarity. Selected bond lengths [Å] and angles [°]: Au1–As1 2.5358(6), Au1–As2 2.5514(5), Au1–P1 2.3136(9), As1–As2 2.6162(8), As1–As3 2.4072(7), As1–As4 2.4093(9), As2–As3 2.4009 (8), As2–As4 2.3935(7), As3–As4 2.421(1), As1–Au1–As2 61.90(2), As1–Au1–P1 138.69(3), As2–Au1–P1 159.34(3).

The central building unit of the cation in **83** is a twofold coordinated gold(I) cation with one coordination site occupied by a PPh_3 ligand and the second one by a side-on coordinating As_4 tetrahedron. The angle between P1, Au1 and the midpoint of the As1–As2 bond indicates with 169.65(2)° a slightly distorted linear coordination geometry. The Au–As bond lengths of 2.5358(6) Å and 2.5514(5) Å are shorter than the Ag–As bond lengths in **82** (2.611(2) Å to 2.626(2) Å) which is due to the smaller single bond radius of gold compared to silver.[68a] As a consequence, the As1–Au1–As1 bond angle (61.90(2)°) is a little larger than the As–Ag–As bond angles in **82** (59.10(5)° and 58.83(6)°). The As1–As2 bond (2.6162(8) Å) is elongated by about 0.18 Å compared to free As_4 which is slightly more than the bond elongation observed in **82** (0.14 Å). While the As–As bond lengths between the coordinating and non-coordinating arsenic atoms (2.3935(7) Å to 2.4093(9) Å) are shortened compared to the bond lenths in As_4 (2.435 Å to 2.4372 Å), the As3–As4 bond length (2.421(1) Å) is nearly unchanged. The same tendency has already been observed for the silver derivative **82**.

In order to evaluate the bonding situation in **83**, detailed DFT and CCSD(T) calculations were performed by Prof. Dr. Marek Sierka (University of Jena). Table 15 shows the comparison of calculated and experimental As–As and Au–As bond lengths in $[(PPh_3)Au(\eta^2\text{-}As_4)]^+$ which are in good agreement. Furthermore, the As–As bond lengths compare well to those calculated for $[Ag(\eta^2\text{-}As_4)_2]^+$. The elongation of the coordinating As–As bond is slightly overestimated by theory (0.21 Å) compared to the experimental value of 0.18 Å. In agreement with experimental data the Au–As bonds in $[(PPh_3)Au(\eta^2\text{-}As_4)]^+$ are slightly shorter than the Ag–As bond lengths in $[Ag(\eta^2\text{-}As_4)_2]^+$.

Table 15. Calculated bond lengths [Å] in $[(PPh_3)Au(As_4)]^+$. The numbering of the atoms is taken from Figure 47.

bond	(calc)	(exp)
As1-As2	2.663	2.616
As1-As3	2.448–2.449	2.394–2.409
As3-As4	2.478	2.421
Au-As1	2.622–2.623	2.536–2.551

Additionally, an analysis of the BCPs using the AiM method clearly indicates an intact As_4 tetrahedron coordinating to the $[PPh_3Au]^+$ cation (Figure 48). The obtained values are similar to those calculated for $[Ag(\eta^2\text{-}As_4)_2]^+$ pointing to an analogue bonding situation.

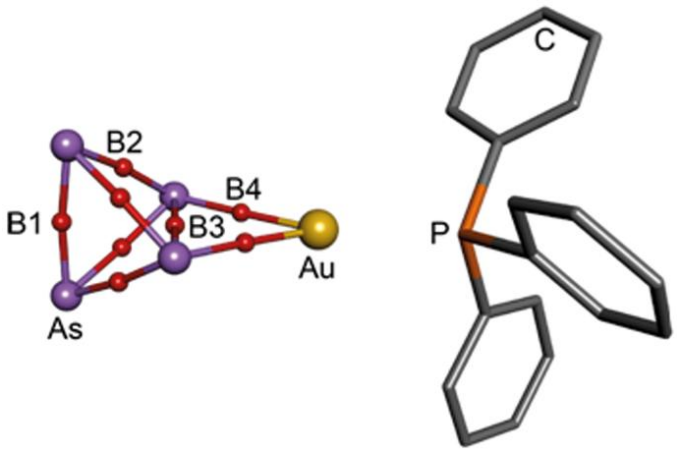

Figure 48. Bond critical points (BCP) in the cation $[(PPh_3)Au(\eta^2\text{-}As_4)]^+$ indicated by the red balls (labeled as B1 – B4).

3.6.3 $[Cp^*Ru(dppe)(\eta^1\text{-}As_4)]^+$ - A cationic complex bearing an intact end-on coordinating As_4 tetrahedron

In general, white phosphorus and yellow arsenic can coordinate to a Lewis acid via the filled σ-orbitals of an E–E (E = P, As) bond or via the lone pairs that are located at the vertices of the E_4 tetrahedron. For P_4 the coordination via the lone pairs is long known and several examples have been reported to date.[24-25, 117] Additionally, Peruzzini *et al.* could demonstrate the activated character of the vertex coordinating P_4 tetrahedron which opened new reaction pathways in phosphorus chemistry.[28-29, 118] In contrast, the η^1-coordination is unfavorable for arsenic (compare the basicity of phosphanes and arsanes).[7] As the stabilization of As_4 in a side-on coordination mode proved to be successful, the synthesis of a complex with an intact, end-on coordinating As_4 tetrahedron moved into the focus of interest.

Because of their easy accessibility, the complexes $[Cp^*M(L_2)]^+$ (M = Fe, Ru, Os; L = PPh_3, ½ dppe) were chosen as starting material for the vertex coordination of As_4. In order to evaluate the most promising candidate for that purpose the reaction energies of the above mentioned complexes with P_4 and As_4 for different combinations of M and L_2 were calculated by Dr. Alexey Y. Timoshkin (University of St. Petersburg) for gas phase conditions at the B3LYP/def2-SVP level of theory (Table 16).

Table 16. Reaction energies $\Delta E°_0$, standard enthalpies $\Delta H°_{298}$ and Gibbs energies $\Delta G°_{298}$ in $kJ{\cdot}mol^{-1}$ as well as standard entropies $\Delta S°_{298}$ in $J{\cdot}K^{-1}{\cdot}mol^{-1}$ for the reactions $[Cp^*M(L_2)]^+ + E_4 \rightleftarrows [Cp^*M(L_2)E_4]^+$ in the gas phase.

L	E	M	$\Delta E°_0$	$\Delta H°_{298}$	$\Delta S°_{298}$	$\Delta G°_{298}$
PPh_3	P_4	Fe	-35.5	-28.3	-173.7	23.5
		Ru	-70.7	-62.7	-193.3	-5.1
		Os	-75.0	-67.6	-193.9	-9.7
PPh_3	As_4	Fe	-10.9	-4.4	-162.2	44.0
		Ru	-40.1	-33.1	-176.8	19.6
		Os	-40.4	-34.0	-177.0	18.8
½ dppe	P_4	Fe	-41.4	-34.1	-169.1	16.3
		Ru	-75.3	-68.2	-181.5	-14.1
		Os	-87.6	-80.4	-185.5	-25.0
½ dppe	As_4	Fe	-75.1	-75.5	-19.9	-65.6
		Ru	-42.9	-39.3	-190.1	17.4
		Os	-51.7	-48.0	-196.5	10.5

The stability of the products $[Cp^*M(L_2)(\eta^1\text{-}E_4)]^+$ (E = P, As) is generally lower for the arsenic derivatives than for the phosphorus derivatives, which is in contrast to the stability of the side-on complexes **5a** and **82**, for which the arsenic complex **82** is more stable. The tendency for the formation of the desired product also depends on the used metal as well as the co-ligand L and increases in the series Fe < Ru < Os and $(PPh_3)_2$ < dppe. Surprisingly, in case of $[Cp^*M(dppe)As_4]^+$ the iron derivative seems to be more stable than the related ruthenium or osmium compounds. Additionally, the complex [Cp*Fe(dppe)Cl] has already been successfully used for the vertex coordination of P_4 and AsP_3.[27, 53] Hence it was initially chosen for the end-on coordination of As_4.

By analogy to the published procedure, [Cp*Fe(dppe)Cl] was reacted with yellow arsenic and subsequently treated with the halide abstractor $NaBPh_4$ to replace the strongly coordinating Cl^- counterion. However, the reaction did not afford the desired product but led to an oxidation of the Fe(II) complex and the formation of the Fe(III) complex $[Cp^*Fe(dppe)Cl]^+(BPh_4)^-$ (Equation 36) together with an orange precipitate. Most likely, this precipitate is a mixture of sodiumpolyarsenides which are formed by the reduction of As_4.

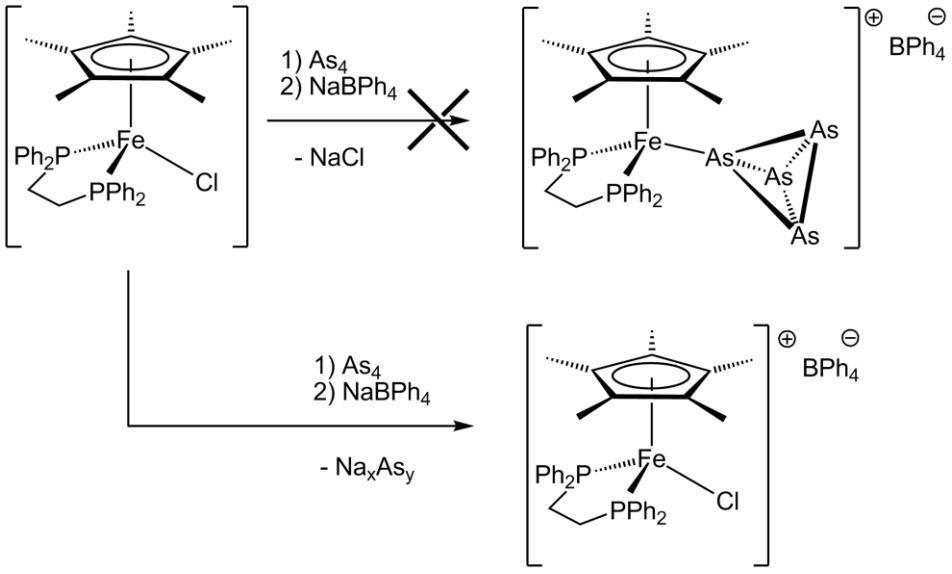

(36)

In order to avoid the oxidation of the starting material upon the reaction with As_4 the more robust ruthenium derivative [Cp*Ru(dppe)Cl] was chosen for the reaction with yellow arsenic. However, the performed calculations predict a positive Gibbs free energy for the related reaction (Table 16). Hence, more detailed calculations for the reaction of $[Cp^*Ru(dppe)]^+$ with As_4 were carried out that account for solvent and temperature influences.

Table 17. Calculated reaction energies $\Delta E°_0$, standard enthalpies $\Delta H°_{298}$ and Gibbs energies in kJ mol^{-1}, standard entropies $\Delta S°_{298}$ in $J·K^{-1}·mol^{-1}$ (PCM corrected for CH_2Cl_2 solution) as well as the corresponding equilibrium constants at 298 K and 243 K for the equlibrium reaction $[Cp*Ru(dppe)]^+ + E_4 \rightleftarrows [Cp*Ru(dppe)(\eta^1\text{-}As_4)]^+$.

E	$\Delta E°_0$	$\Delta H°_{298}$	$\Delta S°_{298}$	$\Delta G°_{298}$	$\Delta S°_{298}$	$\Delta G°_{298}$	K_{298}	K_{243}
	gas phase				solution			
P	-75.3	-68.2	-181.5	-14.1	-91.5	-40.9	$1.48·10^7$	$7.5·10^9$
As	-42.9	-39.3	-190.1	17.4	-100.1	-9.5	45.3	$1.6·10^3$

While for phosphorus the formation of $[Cp*Ru(dppe)(\eta^1\text{-}P_4)]^+$ is exothermic in gas phase as well as in solution, the analogous reaction for arsenic is endothermic in the gas phase but slightly favored in solution due to the increased values of entropy. However, the corresponding equilibrium constant K_{298} is quite small and indicates a dissociation of the desired complex to about 14 % at ambient conditions. Hence, a considerable amount of unstable yellow arsenic is always present in solution which shifts the equilibrium to the left side upon decomposition. This effect can be overcome by lowering the temperature to 243 K which increases the equilibrium constant to $1.6·10^3$ and promotes the product formation. However, as yellow arsenic is only sparingly soluble at low temperatures a direct synthesis of the end-on As_4 complex by the reaction of $[Cp*Ru(dppe)]^+$ with As_4 is not appropriate. Therefore, the As_4 transfer reagent $[Ag(\eta^2\text{-}As_4)_2]^+[pftb]^-$ (**82**) was chosen as As_4 source for the synthesis of the target molecule.

The reaction of [Cp*Ru(dppe)Cl] with one equivalent of $[Ag(\eta^2\text{-}As_4)_2]^+[pftb]^-$ (**82**) at -30 °C leads to a color change from orange to red accompanied by the formation of a pale precipitate of AgCl and affords $[Cp*Ru(dppe)(\eta^1\text{-}As_4)]^+[pftb]^-$ (**84**) in good yields (Equation 37). Complex **84** is obtained as dark red solid that has good solubility in dichloromethane but is nearly insoluble in hexane. Crystals of **84** suitable for X-ray structure analysis were obtained by slow diffusion of hexane into a saturated solution of **84** in dichloromethane at -28 °C.

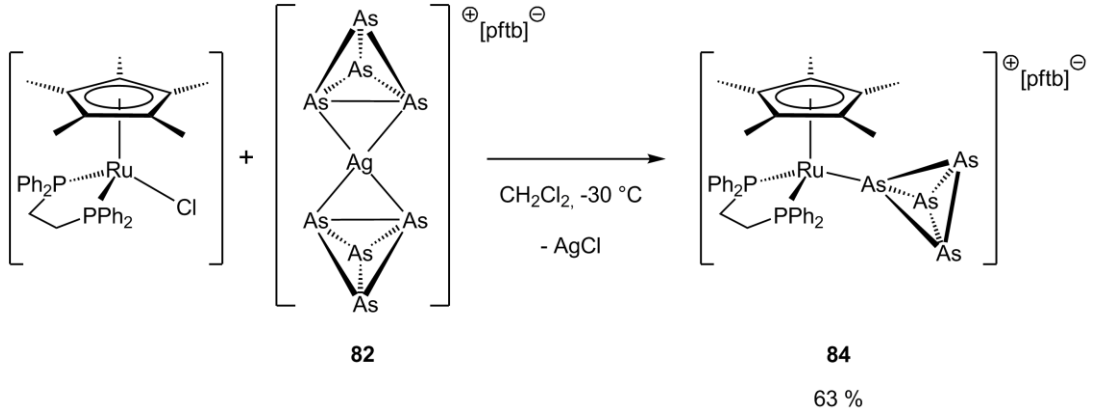

82 **84** 63 % (37)

In the ESI mass spectrum of **84** in anion mode, the $[pftb]^-$ ion is detected at *m*/*z* = 967.2. In cation mode one peak is observed at *m*/*z* = 635.1 that corresponds to the cationic fragment $[Cp^*Ru(dppe)]^+$. Any arsenic containing fragments are not found which indicates the weak interaction between As_4 and the ruthenium cation. In the ^1H NMR spectrum (CD_2Cl_2) the signal for the Cp* protons appears as a triplet at δ = 1.52 ppm ($^4J_{HP}$ = 1.52 Hz) due to the coupling with the P atoms of the dppe ligand. In addition, the signals for the methylene and phenyl protons of the dppe ligand appear as multiplets around δ = 2.4 and δ = 7.4 ppm, respectively. In the $^{31}P\{^1H\}$ NMR spectrum (CD_2Cl_2) of **84** a singlet for the dppe ligand is detected at δ = 69.9 ppm which is shifted upfield by about 6.4 ppm compared to the starting material [Cp*Ru(dppe)Cl] (δ = 76.3 ppm).[119] The $^{19}F\{^1H\}$ NMR spectrum (CD_2Cl_2) reveals one sharp singlet at δ = -75.6 ppm for the $[pftb]^-$ counterion.

$[Cp^*Ru(dppe)(\eta^1\text{-}As_4)]^+[pftb]^-$ (**84**) crystallizes as orange hexagonal plates in the triclinic space group $P\bar{1}$. The asymmetric unit contains one molecule of **84** together with half a molecule of dichloromethane. X-ray structure analysis reveals an intact As_4 tetrahedron that coordinates to the $[Cp^*Ru(dppe)]^+$ fragment in a unique end-on coordination mode (Figure 49).

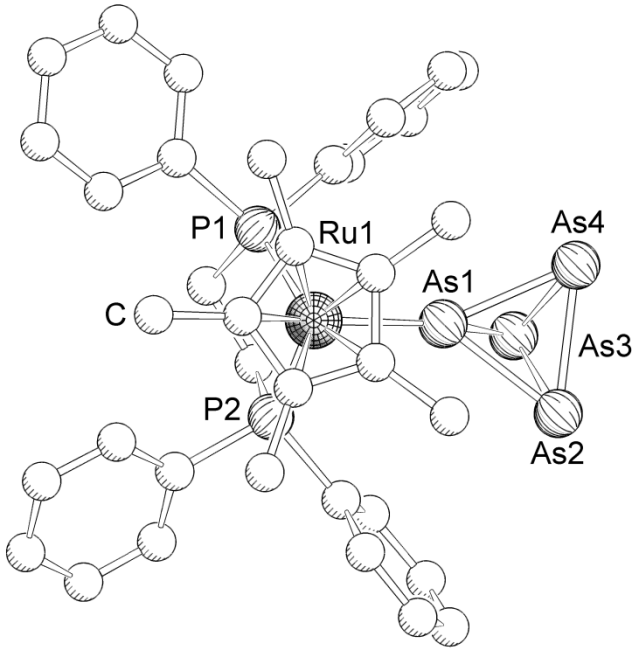

Figure 49. Molecular structure of the cationic part of **84** in the crystal. Hydrogen atoms are omitted for clarity. Selected bond lengths [Å] and angles [°]: Ru1–As1 2.4023(8), Ru1–P1 2.316(1), Ru1–P2 2.329(1), As1–As2 2.376(2), As1–As3 2.386(1), As1–As4 2.380(1), As2–As3 2.438(2), As2–As4 2.431(2), As3–As4 2.431(2); As2–As1–As3 61.60(5), As2–As1–As4 61.48(5), As3–As1–As4 61.34(4).

The Ru1–As1 bond length of 2.4023(8) Å is shorter than Ru–As bond distances in complexes of the strong σ-donor and weak π-acceptor ligand $AsPh_3$ (2.412 Å in $[CpRu(CO)(AsPh_3)Cl]$,[120] 2.442 Å and 2.449 Å in $[Cp^*Ru(AsPh_3)_2Cl]$[121] and 2.435 Å in $[CpRu(MeCN)_2(AsPh_3)]^+$ [122]). The As–As bond distances between the coordinating arsenic atom As1 and the three non-coordinating As atoms vary from 2.376(2) Å to 2.386(1) Å and are shortened compared to the As–As bond lengths in yellow arsenic (2.435 Å determined by electron diffraction[67] and 2.4372 Å specified by DFT calculations[74]). In contrast, the bond lengths between the basal arsenic atoms (2.431(2) Å – 2.438(2) Å) compare well to those in As_4. A similar trend has been found for the P_4 derivative.[27]

The As_4 tetrahedron in **84** is sterically shielded by the Cp* ligand as well as two of the four phenyl substituents of the dppe ligand. Together, these moieties form a tetrahedral shaped binding pocket in which the As_4 tetrahedron is embedded. However, the distances between the planes defined by the atoms As1, As2 and As3 as well as As1, As3 and As4 and the corresponding phenyl planes are in the range of 3.197(1) Å and 3.936(1) Å indicating only minor interactions ($\sum_{vdWradii}$(C and As) = 3.55 Å).[108]

To evaluate the nature of bonding in the cationic part of **84** detailed DFT calculations were performed.

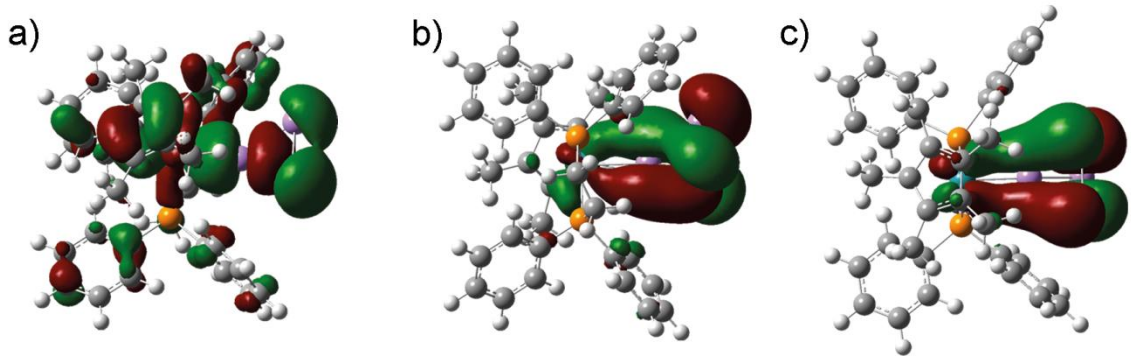

Figure 50. Selected molecular orbitals for the complex cation of **84**. a) σ-type interaction; b) and c) π-type interactions between the As_4 tetrahedron and $\{Cp^*Ru(dppe)\}^+$.

The Wiberg bond index (WBI) of 0.606 for the Ru1–As1 bond indicates a dative single bond between the As_4 tetrahedron and the cationic ruthenium fragment. The isosurfaces of the molecular orbitals indicate an As_4 ligand as being a σ-donor (Figure 50 a)) and π-donor/-acceptor ligand (Figure 50 b) and c)). In case of the π-type MOs, the respective orbitals are distributed over the whole As_4 ligand and are bonding with respect to the the coordinating atom As1 and the non-coordinating atoms As2, As3 and As4, respectively. Referring to the bonds between the basal arsenic atoms, the π-MOs show an antibonding character. This is in good agreement with the

shortened bond lengths between As1 and As2/As3/As4, respectively, as well as the understated bonds between the basal arsenic atoms. The MO distribution is also in good agreement with the short Ru1–As1 bond. Due to the additional π-interactions, the Ru–As bond in **84** is shortened compared to the correpsonding bonds in $AsPh_3$ ruthenium complexes which are mainly characterized by σ-donor interactions.

3.6.4 Coordination behavior of $[Cp^*Ru(dppe)(\eta^1\text{-}As_4)]^+[pftb]^-$ (84)

To further investigate the coordination behavior of the intact As_4 tetrahedron, the reactivity of **84** towards a second cationic ruthenium fragment was investigated. In case of the end-on coordinating P_4 complexes $[CpM(PPh_3)_2(\eta^1\text{-}P_4)]^+$ a bridging $\eta^1{:}\eta^1$ coordination mode of the P_4 unit is observed upon addition of a second $[CpM(PPh_3)_2]^+$ (M = Ru, Os) moiety.[28-29, 117-118] Surprisingly, the reaction of $[Cp^*Ru(dppe)(\eta^1\text{-}As_4)]^+[pftb]^-$ (**84**) with one equivalent of *in-situ* generated $[CpRu(PPh_3)_2]^+[pftb]^-$ does not lead to the expected $\eta^1{:}\eta^1$ coordination of an intact As_4 tetrahedron but to a bond cleavage of one As–As bond to afford the dinuclear complex $[\{Cp^*Ru(dppe)\}(\mu,\eta^{1:3}\text{-}As_4)\{CpRu(PPh_3)\}]^{2+}[pftb]^-_2$ (**85**) in good yields (Equation 38). Complex **85** is isolated as a red-brown solid that has good solubility in dichloromethane but is insoluble in hexane. Single crystals of **85** were obtained by diffusion of hexane into a saturated solution of **85** in dichloromethane at -28 °C.

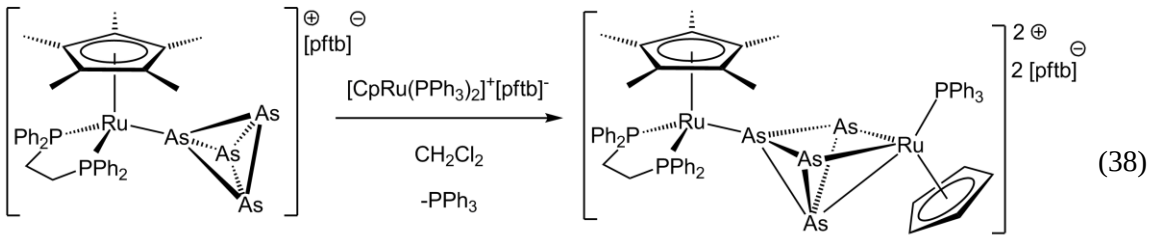

84 **85** 57 % (38)

The positive ion ESI mass spectrum of **85** shows two peaks at *m*/*z* = 710.1 and 1450.4 that can be assigned to the cationic fragments $[\{Cp^*Ru(dppe)\}As_4\{CpRu(PPh_3)\}]^{2+}\cdot(Me_2CO)$ and $[\{Cp^*Ru(dppe)\}As_4\{CpRu(PPh_3)\}]^{+}\cdot(MeCO_2Et)$. The acetone ($Me_2CO$) and ethylacetate ($MeCO_2Et$) molecules originate from sample preparation. The $^{31}P\{^1H\}$ NMR spectrum (CD_2Cl_2) of the crude reaction mixture shows two sharp singlets at δ = 72.7 ppm and δ = 32.9 ppm as well as a broad signal at δ = 12.4 ppm with an integral intensity ratio of 2:1:1. While the singlet at δ = 72.7 ppm can be assigned to the dppe ligand in **85** (δ = 69.9 ppm for **84**), the signal at

δ = 32.9 ppm corresponds to a ruthenium bound PPh_3 ligand (compare for $[\{CpRu(PPh_3)_2\}_2(\mu,\eta^{1:1}\text{-}P_4)]^{2+}$ with δ = 38.3 ppm).[28] The broad signal at δ = 12.35 ppm originates from free PPh_3 indicating the loss of one phosphane ligand from the starting material $[CpRu(PPh_3)_2]^+$. This PPh_3 abstraction has already been stated for the ruthenium catalyzed formation of α,β-unsaturated ketones.[123]

$[\{Cp^*Ru(dppe)\}(\mu,\eta^{1:3}\text{-}As_4)\{CpRu(PPh_3)\}]^{2+}[pftb]^-_2$ (**85**) crystallizes as brown bars in the triclinic space group $P\bar{1}$ with one molecule of **85** in the asymmetric unit. X-ray structure analysis reveals the coordination of the basal As_3 unit of the η^1-As_4 ligand to a $[CpRu(PPh_3)]$ fragment and the cleavage of an As–As bond (Figure 51).

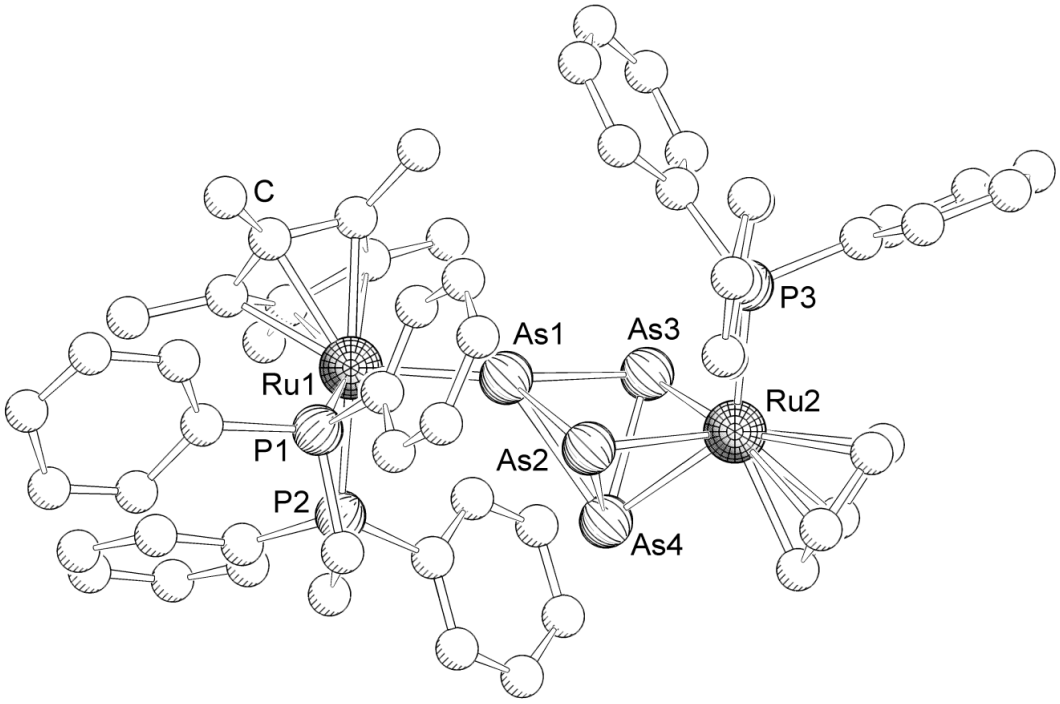

Figure 51. Molecular structure of the cationic part of **85** in the crystal. Hydrogen atoms are omitted for clarity. Selected bond lengths [Å] and angles [°]: Ru1–As1 2.356(1), Ru2–As2 2.458(1), Ru2–As3 2.459(1), Ru2–As4 2.549(1), As1–As2 2.403(1), As1–As3 2.443(1), As1–As4 2.621(1), As2–As4 2.459(2), As3–As4 2.424(1); As2–As1–As3 87.74(4), As1–As3–Ru2 92.32(4), As1–As2–Ru2 93.29(4), As2–Ru2–As3 86.16(3), As1–As4–Ru2 86.27(4), As2–As4–As3 86.91(5).

The central building unit in **85** is a five-membered As_4Ru cluster core with an additional η^1-coordinated $[Cp^*Ru(dppe)]^+$ fragment. The cluster is formally derived by an insertion of the 14 VE fragment $[CpRu(PPh_3)]^+$ into the As2–As3 bond together with an additional coordination of As4 to Ru2. The cluster core itself may best be described as an As_4Ru nido cluster (according to the Wade Mingos rules). Hence, it is formally derived from an octahedral core with one vacant vertex. The As1–As2, As1–As3, As3–As4 and As2–As4 bond lengths (2.403(1) Å, 2.443(1) Å,

2.424(1) Å and 2.459(1) Å, respectively) compare well to the As–As bond lengths in As_4 (2.4372 – 2.435 Å).[67, 74] In contrast, the As1–As4 bond is with 2.621(1) Å elongated. A similar tendency can be observed for the Ru–As bonds in the cluster core. While the Ru2–As2 and Ru2–As3 bond lengths (2.458(1) Å and 2.459(1) Å) are almost the same, the Ru2–As4 bond (2.549(1) Å) is elongated. The bond angles between opposing atoms (e.g. As2 and As3) of the cluster core vary from 86.16(3)° to 93.29(4)° and are reminiscent of the native octahedral arrangement. The Ru1–As1 bond of 2.356(1) Å is shortened compared to the Ru–As bond lengths in the starting material **84** (2.4023(8) Å) and is the shortest Ru–As bond for monodentate arsenic ligands known so far. Shorter bonds have only been realized with bidentate arsenic ligands or in cluster compounds.[124]

The reason for the different reactivity of $[Cp^*Ru(dppe)(\eta^1\text{-}As_4)]^+[pftb]^-$ (**84**) towards $[CpRu(PPh_3)_2]^+$ compared to end-on P_4 complexes might be the weaker As–As bonds (36 kcal·mol^{-1}) compared to a P–P single bond (47 kcal·mol^{-1}) in the E_4 tetrahedron (E = P, As).[53] Hence, the insertion of a $[CpRu(PPh_3)]^+$ fragment into an E–E bond is easier for arsenic than for phosphorus. Additionally, the metallic character and therefore the tendency for cluster formation is more pronounced for arsenic.

3.6.5 $[Ag(\eta^2\text{-}As_4)_2]^+[pftb]^-$ (82) as an As_4 storage material – Reversible As_4 binding

Due to the lack of stability, the knowledge about yellow arsenic is still limited. To date, only few results regarding the reactivity of As_4 are known and first examples about its coordination behavior are presented in this work. As it decomposes at ambient conditions, especially upon exposure to light, yellow arsenic is not storable. Hence, a light-stable storage medium for As_4 would be desirable from which a targeted release of yellow arsenic would allow for more sophisticated reactions. The homoleptic arsenic complex $[Ag(\eta^2\text{-}As_4)_2]^+[pftb]^-$ (**82**) is light- as well as thermally-stable up to at least 50 °C and can be stored without decomposition. Hence, it matches most of the requirements for an As_4 storage material. In addition, it turned out to be a potent As_4 transfer agent for halogenated substrates which themselves serve as stabilizing Lewis acids for the As_4 tetrahedron. However, Krossing *et al.* could demonstrate that the interaction between the soft Lewis base P_4 and the hard Lewis acid Li^+ is very weak and the formation of complexes of the type $Li^+(P_4)_n$ is not observed.[30] Additionally, the lithium salt of the weakly coordinating anion $[pftb]^-$ is only sparingly soluble in dichloromethane or THF.

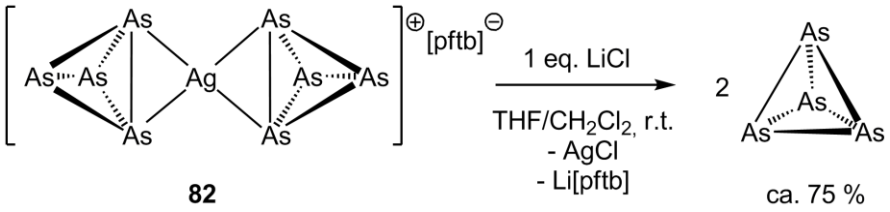

82 (39)

The targeted release of As_4 from **82** could be achieved by the addition of LiCl (Equation 39). The so induced salt metathesis yields silver(I) chloride together with Li[pftb] which both precipitate from the reaction mixture while As_4 remains dissolved. Upon addition of LiCl (THF solution) to a solution of **82** in dichloromethane the immediate formation of grayish precipitate is observed as well as a color change to pale yellow.

In order to monitor the reversible coordination of As_4 to the silver(I) cation challenging ^{75}As NMR investigations were carried out in cooperation with Dr. Maria Neumeier from the research group of Prof. Dr. Ruth Gschwind (University of Regensburg) (Figure 52).[125]

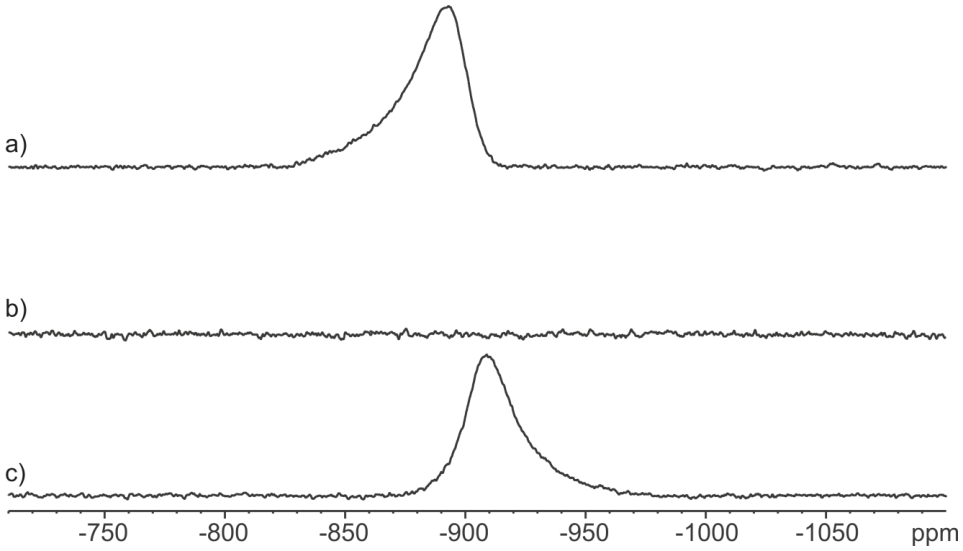

Figure 52. ^{75}As NMR spectra at 300 K of a) conventionally prepared solution of As_4 (CD_2Cl_2/toluene), b) complex **82** (CD_2Cl_2) and c) As_4 generated from the reaction of **82** with LiCl (CD_2Cl_2/THF).

The ^{75}As NMR spectrum (CD_2Cl_2) of conventionally prepared yellow arsenic[114] shows one broad signal (Figure 52a) at δ = -892 ppm ($\omega_{1/2}$ = 2090 Hz) which is reminiscent of the chemical shift of AsP_3 in the ^{75}As MAS NMR spectrum (δ = -962 ppm).[53] In contrast, no signal is observed for the arsenic complex $[Ag(\eta^2\text{-}As_4)_2]^+[pftb]^-$ (**82**) in the range between δ = 0 to -1200 ppm (Figure 52b). However, after addition of LiCl again a broad signal is observed at δ = -908 ppm ($\omega_{1/2}$ = 2364 Hz) that can be assigned to free As_4 (Figure 52c). The remarkable line broadening of the signals is due to very short spin-lattice relaxation times of ^{75}As, mainly influenced by the quadrupole relaxation

mechanism.[126] Even though the ^{75}As nucleus with a natural abundance of 100 %, I = ½ and a 145 times higher receptivity than ^{13}C[108] should be easily observable in the ^{75}As NMR spectrum, the severe line broadening makes the observation of signals challenging. However, in case of symmetrical arsenic compounds in low viscosity solvents the observation of signals in the ^{75}As NMR spectrum is possible.[127] The local C_{3v} symmetry of the arsenic atoms in As_4 is obviously enough to make the molecule detectable. In contrast, no signal is observed for **82** due to the lowered local symmetry of the arsenic nuclei. Hence, the observation of a signal in the ^{75}As NMR spectrum after the addition of LiCl clearly indicates the presence of free As_4 and proves the targeted release of yellow arsenic from **82**.

As_4 solutions obtained by this method contain approximately 75 % of the initially employed arsenic (see section 4.8.5). Additionally, they show a remarkable light stability (> 4h) which may be a result of the salt metathesis. Presumably, impurities of grey arsenic co-precipitate during the formation of AgCl which frees the solution from any polymerization seeds. The straightforward release procedure can be done within twenty minutes and only small amounts of solvent are needed. In contrast to the conventional synthesis, also low boiling solvents such as dichloromethane can be used and the obtained solutions have two to four times higher concentrations.[1] Hence, $[Ag(\eta^2\text{-}As_4)_2]^+[pftb]^-$ (**82**) can be used as economic and effective As_4 storage material that could open new ways in the chemistry of As_4.

[1] conventional As_4 solutions in toluene: $c(As_4) \approx 3.7 \cdot 10^{-3}$ mol L^{-1}; As_4 solutions made from **82**: $c(As_4) \approx 1.5 \cdot 10^{-2}$ mol L^{-1}.

3.7 As_4 as a template for the formation of spherical aggregates

In the last decade, our group succeeded in the synthesis of a plethora of spherical, self assembled supramolecules from the reaction of [Cp*Fe(η^5-P_5)] (**35a**) with CuX and CuX_2 (X = Cl, Br, I).[61c, 62-63, 65, 128] These spherical molecules usually contain a guest molecule which is encapsulated by an inorganic [{Cp*Fe(η^5-P_5)}$_x$($CuX)_y$] framework and serves as a template for the formation of the supramolecule. An indication for that template effect is the symmetry of the inorganic framework which resembles the one of the guest molecule. In case of $C_2B_{10}H_{12}$@[$(CuCl)_{20}$($Cp^*FeP_5)_{12}$] (**40**) the icosahedral symmetry of the template carborane is also found for the [$(CuCl)_{20}$($Cp^*FeP_5)_{12}$] scaffold.[63] In contrast, the encapsulation of the tetrahedral P_4 molecule did not lead to a spherical molecule with tetrahedral symmetry but to the formation of P_4@[$(Cp^*FeP_5)_{10}$($CuI)_{30}$ ($CH_3CN)_6$] (**42**) which is of cuboid shape.[65] So far only one example of a P_4 guest molecule inside a tetrahedral shaped host complex has been reported.[129] However, in this case the host complex is not formed by a template controlled reaction. All attempts to use yellow arsenic as template for the formation of spherical aggregates failed due to the instability of As_4 and the low concentrations of conventionally prepared As_4 solutions. However, solutions of yellow arsenic released from [Ag(η^2-$As_4)_2$]$^+$[pftb]$^-$ (**82**) (see section 3.6.5) show a remarkable stability. Hence they bear a large potential for the synthesis of spherical molecules with tetrahedral As_4 as template.

3.7.1 A cuboid-shaped supramolecular aggregate

The reaction (layering technique) of [Cp*Fe(η^5-P_5)] (**35a**) with two equivalents of CuI in the presence of freshly released As_4 from **82** affords single crystals of the supramolecule As_4@[{Cp*Fe(η^5-P_5)}$_{10}$$Cu_{30}I_{30}$($MeCN)_6$] (**86**) (Equation 40). However, the desired complex is only obtained in low yields (< 0.1 mg) due to the concurrent formation of the polymeric compounds [{Cp^*FeP_5}$CuI]_n$ (**37b**)[59] and [{Cp^*FeP_5}$Cu_3I_3]_n$[65] which were identified by X-ray structure analysis. Hence, beside X-ray structure determination of **86** no further characterization could be performed.

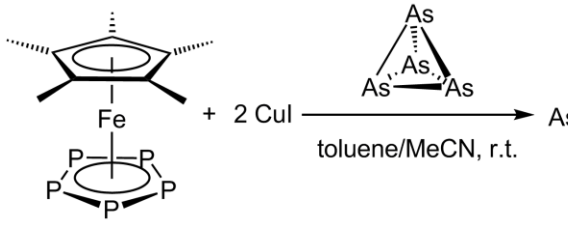

(40)

As_4@[{Cp*Fe(η^5-P_5)}$_{10}$$Cu_{30}I_{30}$(MeCN)$_6$] (**86**) crystallizes as red laths in the monoclinic space group $P2_1/n$. The asymmetric unit contains one molecule of **86** together with four molecules of acetonitrile. It is isostructural with its P_4 containig derivative **42**[65] and shows an As_4 tetrahedron that is encapsulated in an inorganic framework (Figure 53).

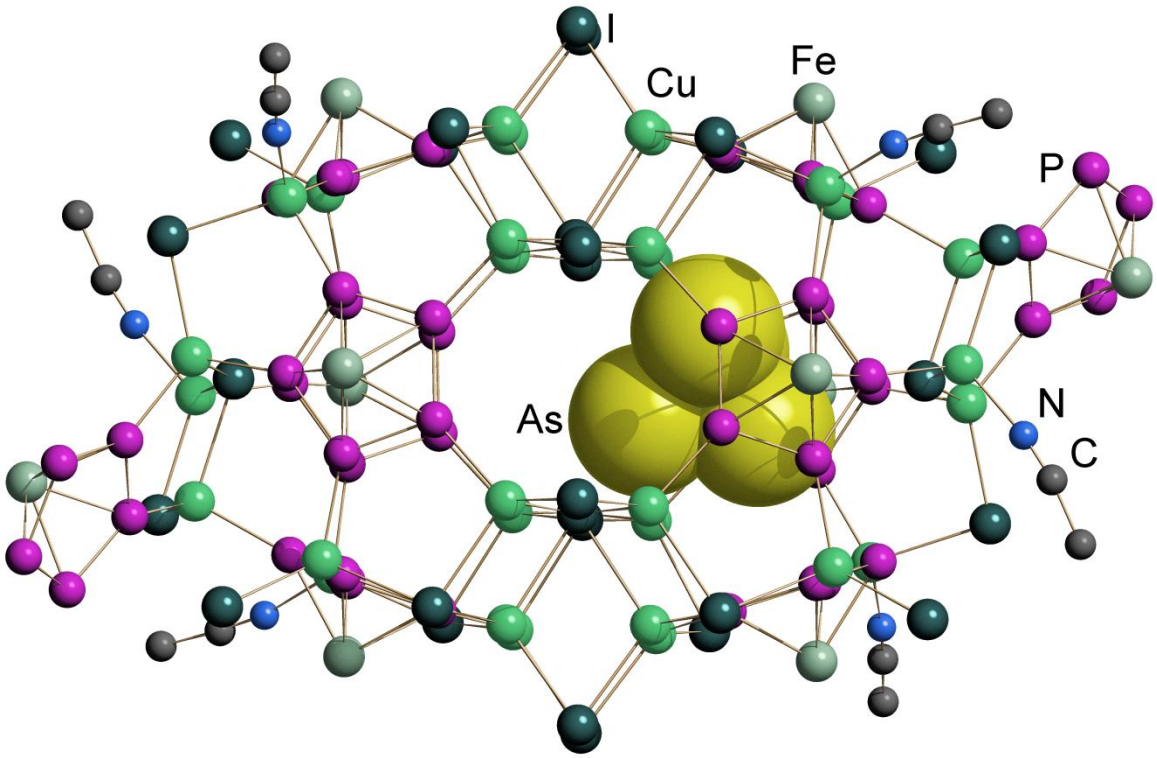

Figure 53. Molecular structure of **86** in the crystal. For clarity reasons, Cp* ligands, hydrogen atoms as well as non-coordinating MeCN molecules are omitted and only one of the possible positions of the As_4 tetrahedron is depicted. Selected bond lengths [Å]: As1a–As2a 2.373(9), As1a–As4a 2.38(1), As1a–As3a 2.380(9), As2a–As4a 2.38(1), As2a–As3a 2.382(9), As3a–As4a 2.37(1).

Molecule **86** is of cuboid shape and consists of two half shells that are connected by a copper iodide scaffold. The belt region is formed by four {$Cu_4(\mu_4$-I)(μ_3-I)(μ_2-I)$_3$} units which exhibit a bowl-like geometry. They connect four pentaphosphaferrocene units of every half shell, that coordinate to the bowls in a 1,2-coordination mode. The four *cyclo*-P_5 ligands are connected with each other in the 3,5-position by two {CuI} and two {Cu(MeCN)} units in an alternating way (Figure 54). While both connecting {CuI} units are additionally linked to an iodine atom of the {Cu_4I_5} moieties, only one of the two {Cu(MeCN} units is connected with the belt region. The other one is attached to a capping {$Cu_2(\mu_2$-I)$_2$(MeCN)CuI} framework which consists of a four-membered *cyclo*-Cu_2I_2 ring and one exocyclic CuI group. The three copper atoms are linked to three of the four pentaphosphaferrocene units. Hence, three of the four *cyclo*-P_5 rings exhibit a 1,2,3,4,5-coordination mode while one shows a 1,2,3,4-coordination mode. One of the two copper atoms of the Cu_2I_2 ring bears an additional acetonitrile ligand, while the other one, together with

the exocyclic copper atom is attached to an additional pentaphosphaferrocene moiety with a 1,2-coordination pattern. Hence, the inorganic framework of **86** consists of 100 atoms.

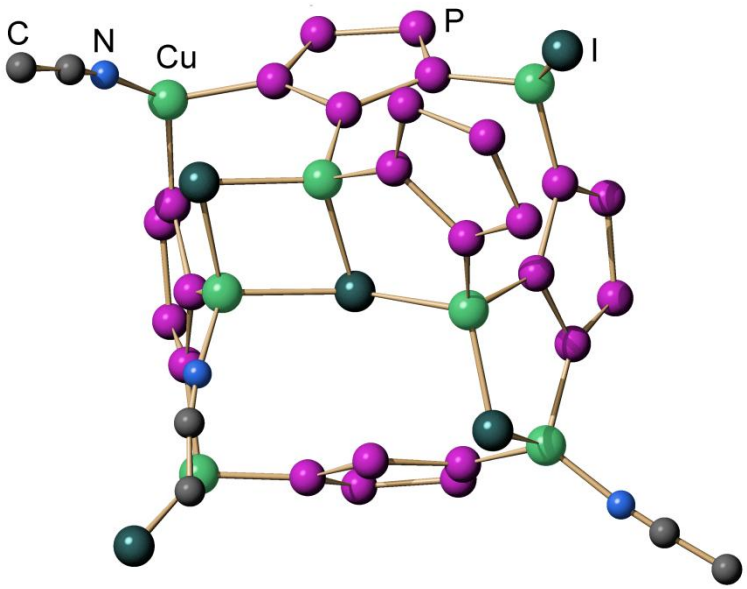

Figure 54. One of the half shells of **86**. Cp*Fe moieties and hydrogen atoms are omitted for clarity.

The distance between two opposing *cyclo*-P_5 units within a half shell is about 4.9 Å, the length of the inner cavity is about 10.3 Å.[130] The opposing (μ_4-I) atoms of the belt region are about 4 Å away from each other. Hence, the inner cavity of **86** is constricted, resulting in two separated voids. The encapsulated As_4 tetrahedron can be found in each of these voids with a 50 % probability. In addition, it shows an orientational disorder over two positions with occupancy factors of 15 % and 35 %. Due to this disorder an accurate bond length determination of the the As–As bonds is not possible. However, the obtained As–As bond lengths (2.37(1) Å to 2.38(1) Å) are significantly shorter than the bond lengths in As_4 (2.435 Å determined by electron diffraction[67] and 2.4372 Å specified by DFT calculations[74]). This could be a result of the low temperature of 123 K during the X-ray structure determination compared to the high temperature during electron diffraction experiment (758 K). A similar shortening of the As–As bonds has been observed for As_4 tetrahedra that are embedded in a [{Cp*FeP_5}$_2$$Cu_2Cl_2$] matrix.[65]

3.7.2 A tetrahedral matryoshka doll

Surprisingly, the formation of another spherical aggregate could be observed during the reaction of [Cp*Fe(η^5-P_5)] (**35a**) with two equivalents of CuI in the presence of As_4 when an excess of LiCl was used for the release of yellow arsenic (Equation 41). Beside red laths of **86** as well as crystals of known polymeric compounds, small red-brown tetrahedral shaped crystals of $\{Z_4As_4\}@[\{Cp^*Fe(\eta^5\text{-}P_5\}_{12}Cu_{51}I_{56}(MeCN)_3]^-Z^+$ (**87**) (Z = light atom) were identified.

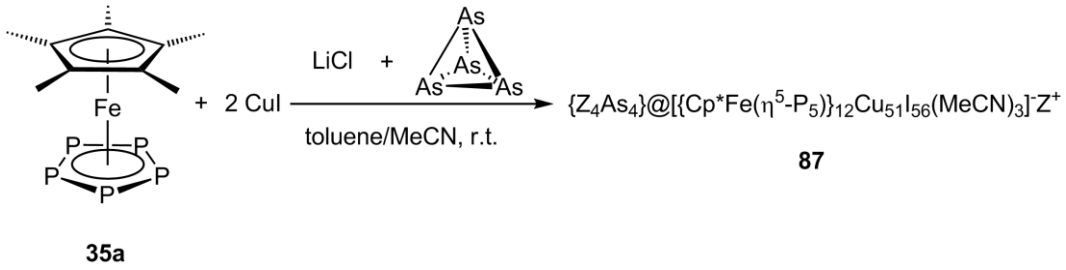

(41)

$\{Z_4As_4\}@[\{Cp^*Fe(\eta^5\text{-}P_5\}_{12}Cu_{51}I_{56}(MeCN)_3]^-Z^+$ (**87**) crystallizes in the cubic space group $P2_13$ with one third of the molecule **87** in the asymmetric unit. X-ray structure reveals a C_{3v} symmetric supramolecule that consists of 12 pentaphosphaferrocene units as well as 51 copper and 56 iodine atoms adding up to 167 atoms in the inorganic framework (Figure 55). The inner cavity is occupied by one As_4 tetrahedron as well as light atoms Z which are disordered over several positions which will be discussed in detail later on.

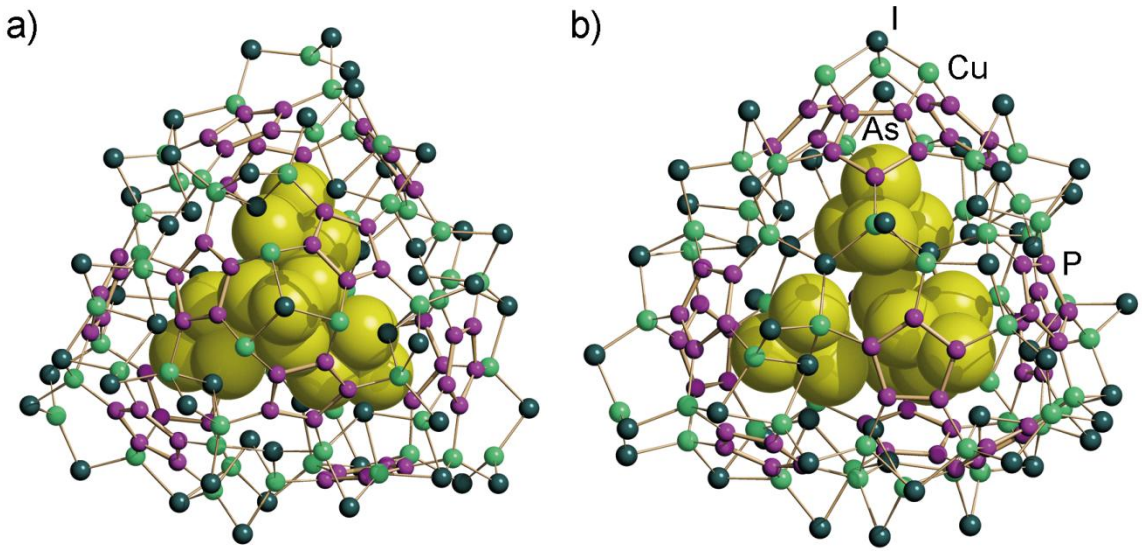

Figure 55. Molecular structure of **87** in the crystal shown a) along the three fold rotation axis and b) from the side. Cp*Fe moieties, acetonitrile ligands as well as atoms Z are omitted for clarity.

The four vertices of the supramolecule can be categorized into one apical and three basal vertices. The apical vertex is formed by a pyramidal {$Cu_3(\mu_3\text{-}I)$} unit that bridges three pentaphosphaferrocene molecules (Figure 56a). Alternatively, it may be described as three condensed five-membered *cyclo*-{P_2Cu_2I} rings. Hence, the isolated pentagon rule is not fulfilled. Additionally, the three copper atoms of the pyramidal {$Cu_3(\mu_3\text{-}I)$} unit bear one acteonitrile each that point towards the apical iodine atom. The three *cyclo*-P_5 rings are additionally linked to six {$Cu_3(\mu_2\text{-}I)_3$} units that exhibit a ladder like motif. The {Cu_3I_3} ladders are connected to each other by three bridging iodine atoms resulting in seven-membered *cyclo*-{$P_2Cu_2I_2Cu$} and eight membered *cyclo*-{CuP_4Cu_2I} rings.

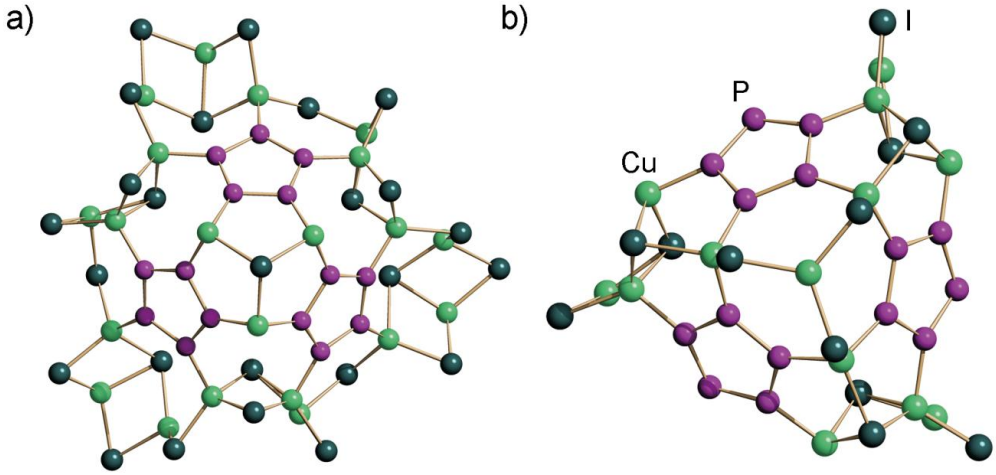

Figure 56. Top view on the a) apical and b) basal vertices of the inorganic framework of **87**. Cp*Fe moieties and acetonitrile ligands are omitted for clarity.

The three basal vertices are formed by an almost trigonal planar {CuI_3} scaffold that is extended by three copper atoms. This {Cu_4I_3} building block connects three pentaphosphaferrocene molecules (Figure 56b). Alternatively, it may be described as three condensed seven-membered *cyclo*-{$P_2Cu_2I_2Cu$} moeties. The three *cyclo*-P_5 rings are additionally linked to each other by three *cyclo*-{Cu_2I_2} units that are part of {Cu_3I_3} ladders. This results in a belt like scaffold of condensed five-membered *cyclo*-{P_2Cu_2I} and *cyclo*-P_5 units.

The outer edge length of the molecule is about 21.3 Å between the apical iodine atom and a basal copper atom and about 22.5 Å between the basal copper atoms.[130] The inner cavity of the molecule (defined by the centers of gravity of the three P_2 edges pointing to the vertex, see Figure 56) exhibits an almost perfect tetrahedral shape (Figure 57) with an edge length of about 12.9 Å. The axial diameter of 10.5 Å compares well to the diameter found in {Cp^*FeP_5}@[{Cp^*FeP_5}$_{12}Cu_{25}Br_{25}(MeCN)_{10}$] (**38**)[61b] (13.2 Å) as well as C_{60}@[{Cp^*FeP_5}$_{13}Cu_{26}Cl_{26}(H_2O)_2(MeCN)_9$] (**39**)[62] (13.5 Å). [130] However, a tetrahedral shaped cavity has not been observed so far.

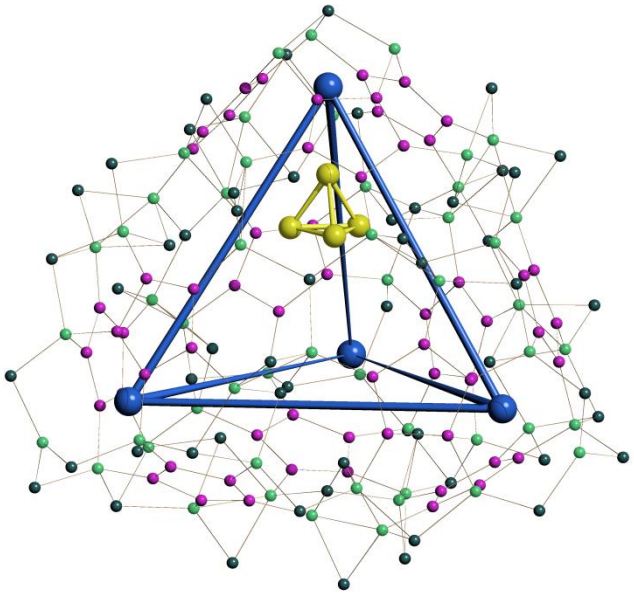

Figure 57. Representation of the tetrahedral shaped cavity of **87** and one of the four positions of the encapsulated As_4 tetrahedron.

The supramolecule **87** contains one molecule of As_4 which is disordered over the four vertices of the tetrahedral shaped inner cavity. Each position is occupied with a probability of 25 % (Figure 58). One of the four vertices of the partially occupied As_4 tetrahedra points exactly towards the vertex of the cavity (Figure 57). The As–As bond lengths range from 2.328 Å to 2.388 Å which compares well to the As–As bond lengths found in **86** (2.37 Å to 2.38 Å).

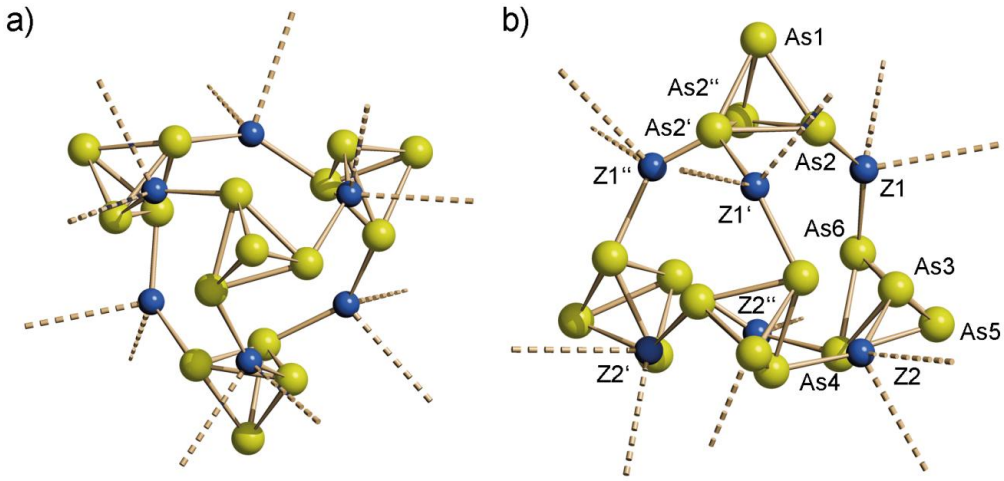

Figure 58. Representation of the four possible positions of the disordered As_4 tetrahedron as well as the six possible positions of the light atom Z inside the cavity of **87**. Dashed bonds indicate interactions with iodine atoms of the outer CuI framework. Selected bond lengths [Å]: As1–As2 2.363, As2–As2’ 2.382, As3–As6 2.382, As3–As4 2.328, As3–As5 2.383, As6–As4 2.388, As6–As5 2.351, As4–As5 2.366, Z1–As2 2.228, Z1–As6 2.279, Z2–As3 2.234, Z2–As4’ 2.217, Z–I 3.03 to 3.10.

During the structure refinement, beside the positions of the disordered As_4 tetrahedron, additional electron density for a light atom (about two electrons) is found at six positions (two positions in the asymmetric unit are multiplied by the C_3 axis) in between the arsenic atoms As3 and As4' as well as As2 and As6. Hence, the light atoms Z are located on the six edges of the tetrahedral shaped cavity. The Z–As distances vary from 2.217 Å to 2.234 Å. Additional interactions (3.03 Å to 3.10 Å) with iodine atoms of the outer CuI framework lead to a distorted tetrahedral coordination environment of the atoms Z. However, to further evaluate the nature of Z the following ancillary conditions have to be considered: a) The formation of **87** is only observed when an excess of Li^+ cations is present in solution; b) as the CuI framework consists of 51 copper atoms and 56 iodine atoms five additional positive charges are needed to fulfill electroneutrality. Hence, the light atoms Z could be interpreted as Li^+ cations. Structure refinement leads to a total of four lithium cations inside the cavity of **87** that are disordered over six positions with an occupancy factor of 2/3 at each position. Hence, the As_4 tetrahedron interacts with at least one lithium cation. This is surprising since it was postulated that the interaction between the hard Lewis acid Li^+ and the soft Lewis basic E_4 (E = P, As) tetrahedra is too weak to observe $[Li_x(E_4)_y]^{x+}$ adducts in solution or in gas pahse.[30] An additional Li position is located 3.7 Å above the apical iodine atom which leads to a total of five lithium cations in **87** and a neutral charge balance. The lithium is embedded in between the three acetonitrile ligands and is stabilized by several Li–(MeCN) interactions (Figure 59). However, to verify the lithium positions, strong high-angle X-ray data has to be obatined which allows the precise localization of light atoms during crystal structure refinement.

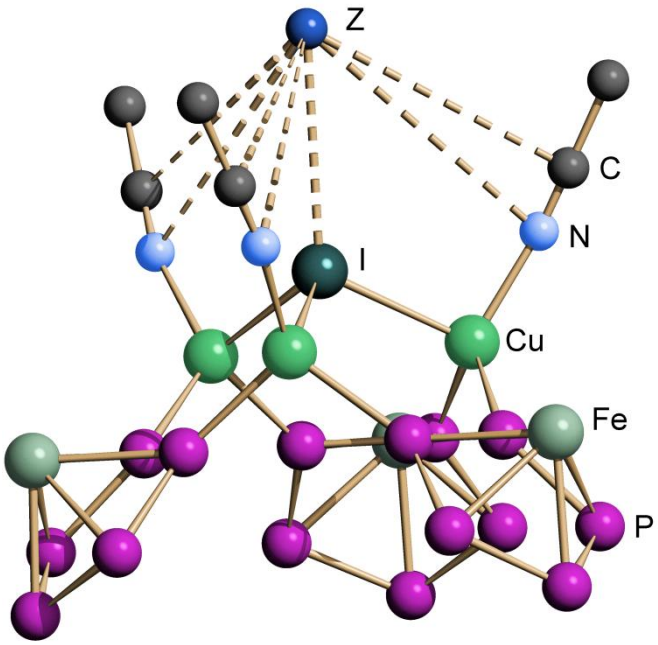

Figure 59. Apical section of **87** with coordinated light atom position Z. Hydrogen atoms and Cp* ligands are omitted for clarity.

In order to verify the nature of Z as lithium cations, crystals of **87** were separated from most of the polymeric byproducts ([{Cp*FeP_5}CuI]$_n$ (**37b**)[59] and [{Cp*FeP_5}Cu_3I_3]$_n$[65]) by flotation. Due to the small size and number of product crystals a complete separation from microcrystalline side products was not possible. The crystals were washed six times with THF (6 × 5 ml) to remove last traces of LiCl (solubility of LiCl in THF: 21 mg ml^{-1}). A ^{7}Li NMR spectrum (pyridine-d_5) of the residual solid was recorded that showed one sharp singlet at δ = 4.23 ppm. The pyridine breaks down the molecular framework of the polymeric and spherical compounds. Hence, only fragments or pyridine coordinated cations can be detected in solution. However, the signal in the ^{7}Li NMR spectrum clearly indicates the presence of lithium cations in solution which could stem from compound **87**. Anyway, as no pure sample of **87** could be obtained so far, the signal in the ^{7}Li NMR spectrum is no final proof but at least a strong hint for Z being lithium cations.

However, compound **87** is the first example of a self assembled CuX/Cp*FeP_5 (X = Cl, Br, I) supramolecule in which the three-fold symmetry of the encapsulated molecule is also found in the supramolecular host complex. Hence, it nicely demonstrates the template effect of the guest molecule. Moreover, the symmetry of the As_4 guest molecule can also be found for the inner cavity which is unprecedented to date. Interestingly, the macroscopic shape of the crystals (compound **87** crystallizes as reddish tetrahedra) is also reminiscent of the As_4 template.

4. Experimental Section

4.1 General remarks

4.1.1 Preparative procedures

All manipulations were performed using standard Schlenk and dry-box techniques under an atmosphere of dry argon or dinitrogen. Traces of oxygen and moisture were removed from the inert gas by passing them over BASF R 3-11 ($CuO/MgSiO_3$) catalyst, through concentrated H_2SO_4 and over coarsely granulated silica gel, in that order.

All solvents were degassed and distilled from appropriate drying agents under an atmosphere of dinitrogen prior to use. Boling the solvents under reflux for at least four hours preceded the distillation process. Hexane was distilled from Na/K alloy, toluene from Na, Et_2O, THF and dme from Na/benzophenone, CH_2Cl_2 from CaH_2 and CH_3CN from $CaCl_2$. The deuterated solvents C_6D_6 and CD_2Cl_2 were degassed and dried in the aforementioned manner. After distillation, C_6D_6 was additionally stored over molecular sieve (4 Å) which had previously been dried for two hours under high vacuum at 100 °C.

Diatomaceous earth was routinely stored at 110 °C prior to use, then dried in vacuum wit the aid of a heat gun. Silical gel 60 (particle size: 0.063 – 0.2 mm) used for the column chromatography was heated under vacuum (3 d, 10^{-3} mbar, 230 °C) prior to use.

4.1.2 Starting materials

The following substances were prepared according to literature procedures: ^{Mentyhl}CAAC (**17**),[131] ^{cHex}CAAC (**19**),[131] $[W(CO)_5(thf)]$,[132] Cp'''H,[133] Cp'''Na,[76] $[FeBr_2(dme)]$,[76] $[Cp'''Fe(CO)_2Br]$,[76], $[Cr(CO)_3(MeCN)_3]$,[134] $[Cp^*Cr(CO)_3H]$,[135] $[\{Cp^*Cr(CO)_3\}_2]$ (**53**),[79] $[Cp^*Fe(CO)_2Br]$,[136] $[\{Cp'''FeBr\}_2]$,[87] $[(PPh_3)AuCl]$,[137] $[(PPh_3)Au(tht)](PF_6)$,[138] $[Ag(CH_2Cl_2)][pftb]$,[115] $[Cp^*Ru(dppe)Cl]$,[119] Tl[pftb][139] and $[Cp^*Fe(\eta^5\text{-}P_5)]$ (**35a**).[57] The compounds (^{Menthyl}CAACH$^+$Cl$^-$·HCl)[131] and (^{cHex}CAACH$^+$Cl$^-$·HCl)[131] (Prof. Dr. Guy Betrand, University of California, Riverside, USA), $[L_2Cr_2]$ (**45**)[140] (Prof. Dr. Rhett Kempe and Dr. Awal Noor, University of Bayreuth), AsP_3[52, 141] (Prof. Dr. Christopher C. Cummins, Dr. Brandi M. Cossairt and Alexandra Velian, MIT, USA), $[CpRu(PPh_3)_2Cl]$[142] (Prof. Dr. Maurizio Perruzini,

Prof. Dr. Piero Stoppioni and Stefano Seniori Constatini, University of Florence, Italy) were kindly donated by the persons given in parantheses. The following compounds were obtained from commercial suppliers: CuI, $[Cu(MeCN)_4](BF_4)$, $AgPF_6$. White phosphorus (P_4) was sublimed and stored under argon in the dark. Solutions of yellow arsenic (As_4) in toluene,[114] $[\{Cp'''Fe(CO)_2\}_2]$ (**10b**),[76] and $[\{Cp'''Fe(CO)_2\}_2(\mu,\eta^{1:1}\text{-}P_4)]$ (**9b**)[37] were prepared by modified literature procedures as detailed below.

4.1.3 Characterization methods

Solution NMR spectra were recorded at the NMR department of the University of Regensburg using a Bruker Avance 300, 400 or 600 (^{75}As NMR) spectrometer. Samples are referenced against TMS (^{1}H, ^{13}C), 1 M LiCl in D_2O (^{7}Li), $CFCl_3$ (^{19}F), 85% H_3PO_4 (^{31}P) and $KAsF_6$ (^{75}As) as external standards. Chemical shifts are reported in ppm, according to the δ-scale, the coupling constants *J* in Hz. The NMR spectra were processed using the TopSpin 2.1 program (Bruker). Simulations of NMR spectra were performed using the WIN-DAISY module in the TopSpin 2.1 software (Bruker). The ^{75}As NMR studies were performed by Dr. Maria Neumeier (Universität Regensburg) in the research group of Prof. Dr. Ruth Gschwind.

EI MS, LIFD MS and ESI MS spectra were measured by the MS department of the University of Regensburg using a Finnigan MAT 95 (LIFD), Finnigan MAT SSQ 710A (EI) and a ThermoQuest Finnigan TSQ 7000 (ESI) spectrometer. The identity of the observed fragments was assigned according to the mass/charge (*m*/*z*) ratio, the isotope pattern and comparison of the experimental signals with simulated ones, which were generated by the ChemDraw Ultra 10.0 software (Cambridge Soft).

IR spectra were recorded on a VARIAN FTS-800 FT-IR spectrometer as KBr discs or in solution.

Raman spectra were measured on a Varian Fourier transform RAMAN module coupled on a Varian FTS 7000e spectrometer equipped with a Nd:Yag laser (excitation wavelength λ = 1064 nm) and a liquid nitrogen cooled germanium detector in the research group of Prof. Dr. Arno Pfitzner (Universität Regensburg). Samples for Raman spectroscopy were sealed in glass capillaries of 1.5 mm outer diameter. The resolution was 2 cm^{-1}. The spectra were processed with the Varian Resolutions Pro software.

Cyclic voltametry experiments were performed with the aid of M.Sc. Eric Mädl in the own research group.

Elemental analyses were performed at the microanalytical laboratory of the University of Regensburg on a Vario EL III instrument.

4.1.4 Theoretical calculations

Dr. Alexey Y. Timoshkin (University of St. Petersburg, Russia) performed the DFT (density functional theory) calculations on the following compounds (used functional and basis sets are given in prantheses): **18** and **43** (B3LYP[143] and def2-SVP[144]), **46** and **49** (B3LYP and def2-SVP or def2-TZVPP[144]) as well as **84** (B3LYP and def2-SVP). Calculations were performed with the Gaussian 03 suite of programs.[145]

DFT calculations on the model complex [{CpFe(CO)$_2$}$_2$(μ,$\eta^{1:1}$-P$_4$)] were executed by Dr. Gábor Balázs (University of Regensburg) and employ the BP86 functional[143b, 146] and def-SVP basis sets.[147] The calculations were performed using the TURBOMOLE program package.[148]

DFT and CCSD(T) (coupled cluster) calculations on compound **82** were carried out by Prof. Dr. Marek Sierka (University of Jena) using the TURBOMOLE program package.[148] DFT calculations employ the B3LYP exchange-correlation functional. All calculations use quadruple zeta valence plus a double set of polarization functions (QZVPP) basis sets.[144] In addition, the CCSD(T) calculations used corresponding auxiliary basis sets.[149] Quasirelativistic pseudopotentials were used for Ag and Au.[150] The topological analysis of the electron density[151] obtained at this level (at experimental geometrical structures) has been performed using the DGrid program.[152] All structure have been optimized at the DFT level. The stationary points to potential energy surfaces were characterized by calculations of vibrational frequencies based on analytical second derivatives of the energy with respect to the nuclear coordinates.[153]

4.2 Synthesis of solutions of yellow arsenic (As_4)

The preparation of solutions of the highly unstable yellow arsenic in toluene was performed according to literature procedures.[114] However, the hot As_4 solutions conatain a considerable amount of grey arsenic and the exact amount of dissolved As_4 is not known. Hence, the solutions were allowed to cool to room temperature in a water bath within 5 minutes and subsequently filtered through a frit plate (G3) to remove grey arsenic. The so obtained solutions show reproducable concentrations of $\beta(As_4) = 1.1\ g\ L^{-1} \leftrightarrow c(As_4) = 3.67 \cdot 10^{-3}\ mol\ L^{-1}$.

$^{75}As\{^1H\}$ NMR (CD_2Cl_2) δ [ppm] = -892 (br s).

4.3 Synthesis of Carbene compounds

4.3.1 [(^{Menthyl}CAAC)$_2$As$_2$] (43)

To a solution of ^{Menthyl}CAAC (**17**) (0.280 g, 0.734 mmol) in toluene (20 ml) is given a freshly prepared solution of As_4 (110 mg, 0.386 mmol) in toluene (125 ml) under the exclusion of light at room temperature. The pale green reaction mixture is stirred for 16 h during which the color changes to bright yellow. The resulting solution shows thermochromic behavior with a color change from yellow to green upon cooling. All volatiles are removed under reduced pressure to yield a bright yellow solid. The solid is taken up in hexane, filtered from grey arsenic and again taken to dryness to remove last traces of toluene. The crude product is taken up in Et_2O (20 ml) and filtered from all insoluble by-products. The bright orange solution is reduced in vacuum and stored at 4 °C to yield **43** as pale yellow crystals suitable for X-ray structure determination.

Analytical data for [(^{Menthyl}CAAC)$_2$As$_2$] (**43**):

Yield 171 mg (0.187 mmol, 51 %).

^1H NMR (C_6D_6) δ [ppm] = 0.80 – 1.40 (multiple signals), 3.15 (sept, $^3J_{HH}$ = 6.0 Hz, ^{i}Pr), 3.25 (sept, $^3J_{HH}$ = 6.3 Hz, ^{i}Pr), 3.64 (sept, $^3J_{HH}$ = 6.7 Hz, ^{i}Pr), 4.12 (sept, $^3J_{HH}$ = 6.8 Hz, ^{i}Pr), 7.16 (mult, H_{arom}).

The ^{1}H NMR spectrum clearly indicates several impurities. This together with the complex natue of the used CAAC does not allow a meaningful assignment of signals. The ^{1}H NMR spectrum is additionally depicted in Figure 62 (Appendix). However, the signals for the ^{i}Pr groups can clearly be identified. Their chemical shift significantly differs from the one of pure ^{Menthyl}CAAC. A signal for the carbene carbon atom in the $^{13}C\{^1H\}$ NMR spectrum of **43** could not be detected.

FD-MS (toluene) *m*/*z* [%] = 912.4 (100) [M^+].

Elemental analysis calcd. for $C_{54}H_{86}As_2N_2$ (913.12 g mol^{-1}) C 71.03, H 9.49, N 3.07; found C 64.12, H 8.80, N 2.34.

4.3.2 [(^{cHex}CAAC)$_3$As$_4$] (44)

To a solution of ^{cHex}CAAC (**19**) (0.716 g, 2.2 mmol) in toluene (20 ml) is given a freshly prepared solution of As_4 (220 mg, 0.734 mmol) in toluene (250 ml) under the exclusion of light. The reaction mixture is stirred for 16 h at room temperature during which the colorless solution turns orange. All volatiles are removed under reduced pressure and the orange residue is taken up in Et_2O (40 ml). The solution is filtered from grey arsenic over diatomaceous earth and concentrated until clouding. Storing at -28 °C for 16 h affords a brownish precipitate that is filtered off. Further concentration to about 2 ml and storing at 4 °C affords **44** as pale yellow crystals suitable for X-ray structure analysis.

Analytical data for [(^{cHex}CAAC)$_3$As$_4$] (**44**):

Yield 200 mg (0.156 mmol, 21 %).

^{1}H NMR (C_6D_6) δ [ppm] = 1.09 (s, 18 H, -$(CH_3)_2$), 1.23 (d, 18 H, $^3J_{HH}$ = 7 Hz, ^{i}Pr), 1.41 (d, 18 H, $^3J_{HH}$ = 7 Hz, ^{i}Pr), 1.00 – 1.90 (m, ^{c}Hex), 1.97 (s, 6H, CH_2), 2.95 (sept., 6H, $^3J_{HH}$ = 7 Hz, ^{i}Pr), 3.34 (m, 6H, ^{c}Hex), 7.04 (s, 3H, H_{arom}), 7.06 (s, 3H, H_{arom}), 7.18 (s, 1H, H_{arom}), 7.19 (s, 1H, H_{arom}), 7.19 (s, 1H, H_{arom}).

^{13}C{^{1}H} NMR (C_6D_6) δ [ppm] = 224.5 (s, $C_{Carbene}$).

Due to major impurities a further assignment of signals in the ^{13}C{^{1}H} NMR spectrum is not possible.

FD-MS (toluene) *m*/*z* [%] = 1275.4 (16) [M^+], 875.7 (40) [{CAAC}$_2$As$_3$]$^+$, 326.5 (100) [CAACH]$^+$.

Elemental analysis calcd. for $C_{69}H_{105}As_4N_3$ (1276.28 g mol^{-1}) C 64.93, H 8.29, N 3.29; found C 70.83, H 9.42, N 3.09.

Elemental analysis indicates ^{cHex}CAAC as a major impurity.

Calcd. For M·(^{cHex}CAAC)$_2$ C 71.69, H 9.15, N 3.63.

4.4 Synthesis of dichromium complexes

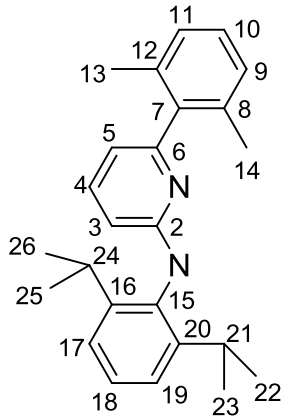

Scheme 10. Labeling scheme for the ligand L = (2,6-diisopropylphenyl)-{6-(2,6-dimethylphenyl)-pyridin-2-yl}-amid).

4.4.1 $[L_2Cr_2(\mu,\eta^{1:1:2:2}\text{-}P_4)]$ (46)

To a solution of $[L_2Cr_2]$ (**45**) (500 mg, 0.61 mmol) in thf (15 ml) is given a solution of P_4 (76 mg, 0.61 mmol) in thf (15 ml). The reaction mixture is stirred for 16 h during which the color changes to green brown. The solvent is removed under reduced pressure and the resulting solid is washed three times with hexane (5ml). Drying in vacuum yields **46** as pure product. Crystals suitable for X-ray structure analysis are obtained upon cooling a solution of **46** in hexane/toluene (1:5) to -28 °C.

Analytical data for $[L_2Cr_2(\mu,\eta^{1:1:2:2}\text{-}P_4)]$ (**46**):

Yield 351 mg (0.37 mmol, 60 %).

^{1}H NMR (C_6D_6) δ[ppm] = 0.64 (d, 6H, *J* = 6.8 Hz, $H^{22,23/25,26}$), 0.78 (d, 6H, *J* = 6.8 Hz, $H^{22,23/25,26}$), 1.10 (s, 6H, $H^{13,14}$), 1.19 (d, 6H, *J* = 6.8 Hz, $H^{22,23/25,26}$), 1.50 (d, 6H, *J* = 6.8 Hz, $H^{22,23/25,/26}$), 1.70 (s, 6H, $H^{13,14}$), 2.48 (sep, 2H, *J* = 6.8 Hz, $H^{21/24}$), 3.99 (sep, 2H, *J* = 6.8 Hz, $H^{21,24}$), 5.74 (d, 2H, *J* = 6.4 Hz, H^3), 6.30 (d, 2H, *J* = 7.5 Hz, $H^{9,11/17,19}$), 6.36 (d, 2H, *J* = 8.8 Hz, H^5), 6.80 (d, 2H, *J* = 7.5 Hz, H^4), 6.70 (d, 4H, *J* = 7.2 Hz, $H^{9,11/17,19}$), 7.02 (d, 2H, *J* = 7.0 Hz, $H^{9,11/17,19}$), 7.19 (t, 2H, *J* = 7.5 Hz, $H^{10/18}$), 7.26 (m, 2H, $H^{10/18}$).

^{13}C{^{1}H} NMR (C_6D_6) δ[ppm] = 18.7 ($C^{13,14}$), 21.6 ($C^{13,14}$), 22.4 ($C^{22,23/25,26}$), 24.8 ($C^{22,23/25,26}$), 25.9 ($C^{22,23/25,26}$), 26.6 ($C^{22,23/25,26}$), 28.4 ($C^{21,24}$), 29.0

($C^{21,24}$), 110.0 (C^{3}), 110.8 (C^{5}), 124.7 ($C^{9,11/17,19}$), 125.8 ($C^{10/18}$), 127.0 ($C^{9,11/17,19}$), 127.0 ($C^{10/18}$), 128.1 ($C^{9,11/17,19}$), 129.1 (C^{4}), 134.8 ($C^{9,11/17,19}$), 135.3 ($C^{8,12}$), 138.3 ($C^{8,12}$), 138.5 (C^{7}), 143.4 (C^{7}), 145.3 ($C^{16,20}$), 146.0 (C^{15}), 156.8 (C^{6}), 172.6 (C^{2}) .

$^{31}P\{^{1}H\}$ NMR (C_6D_6) δ[ppm] = 242.2 - 245.7 (m, 2P), 273.8 - 277.3 (m, 2P).

Elemental analysis calcd. for $C_{50}H_{58}Cr_2N_4P_4$ (942.91 g mol^{-1}) C 63.62, H 6.30, N 5.94; found C 63.00, H 6.32, N 5.78.

4.4.2 $[L_2Cr_2(\mu,\eta^{1:1:2:2}\text{-}As_4)]$ (47)

To a solution of $[L_2Cr_2]$ (**45**) (410 mg, 0.5 mmol) in toluene (20 ml) is given a freshly prepared solution of As_4 (200 mg, 0.66 mmol) in toluene (200 ml). The reaction mixture is stirred for 1 h during which the color changes to green brown. An excess of grey arsenic is removed by filtration over diatomaceous earth. The resulting solution is reduced to about 20 ml under vacuum and stored at -28 °C to yield **47** as a dark green crystalline solid.

Analytical data for $[L_2Cr_2(\mu,\eta^{1:1:2:2}\text{-}As_4)]$ (**47**):

Yield 381 mg (0.34 mmol, 68 %).

^{1}H NMR (C_6D_6) δ[ppm] = 0.73 (d, 6H, *J* = 6.8 Hz, $H^{22,23/25,26}$), 0.80 (d, 6H, *J* = 6.8 Hz, $H^{22,23/25,26}$), 1.05 (s, 6H, $H^{13,14}$), 1.15 (d, 6H, *J* = 6.8 Hz, $H^{22,23/25,26}$), 1.51 (d, 6H, *J* = 6.8 Hz, $H^{22,23/25,/26}$), 1.79 (s, 6H, $H^{13,14}$), 2.74 (sep, 2H, *J* = 6.8 Hz, $H^{21/24}$), 3.99 (sep, 2H, *J* = 6.8 Hz, $H^{21,24}$), 5.77 (d, 2H, *J* = 6.6 Hz, H^{3}), 6.32 (d, 2H, *J* = 7.5 Hz, $H^{9,11/17,19}$), 6.37 (d, 2H, *J* = 8.8 Hz, H^{5}), 6.69 (d, 4H, *J* = 8.2 Hz, $H^{9,11/17,19}$), 6.81 (t, 2H, *J* = 7.5 Hz, H^{4}), 7.02 (d, 2H, *J* = 7.0 Hz, $H^{9,11/17,19}$), 7.18 (t, 2H, *J* = 7.5 Hz, $H^{10/18}$), 7.24 (m, 2H, $H^{10/18}$).

$^{13}C\{^{1}H\}$ NMR (C_6D_6) δ[ppm] = 18.5 ($C^{13,14}$), 22.2 ($C^{13,14}$), 24.5 ($C^{22,23/25,26}$), 26.1 ($C^{22,23/25,26}$), 26.7 (d, $C^{22,23/25,26}$), 28.4 ($C^{21,24}$), 29.0 ($C^{21,24}$), 110.2 (C^{3}), 110.9 (C^{5}), 124.7 ($C^{9,11/17,19}$), 125.8 ($C^{10/18}$), 127.0 ($C^{9,11/17,19}$), 127.1 ($C^{10/18}$), 127.9 ($C^{9,11/17,19}$), 129.2 (C^{4}), 134.6 ($C^{9,11/17,19}$), 135.4 ($C^{8,12}$), 138.6 ($C^{8,12}$), 139.1 (C^{7}), 143.5 (C^{7}), 145.6 ($C^{16,20}$), 146.4 (C^{15}), 157.1 (C^{6}), 172.4 (C^{2}).

Elemental analysis calcd. for $C_{50}H_{58}Cr_2As_4N_4$ (1118.70 g mol^{-1}) C 53.63, H 5.31, N 5.00; found C 53.10, H 5.58, N 4.67.

4.4.3 $[L_2Cr_2(\mu,\eta^{1:1:2:2}\text{-}AsP_3)]$ (48)

To a solution of $[L_2Cr_2]$ (**45**) (100 mg, 0.122 mmol) in thf (5 ml) is given a solution of AsP_3 (20 mg, 0.122 mmol) in thf (5 ml). The reaction mixture is stirred for 16 h during which the color changes to green brown. The solvent is removed under reduced pressure and the resulting solid is washed three times with hexane (5ml). Drying in vacuum yields **48** as pure product. Crystals suitable for X-ray structure analysis are obtained upon cooling a solution of **48** in toluene to -28 °C.

Analytical data for $[L_2Cr_2(\mu,\eta^{1:1:2:2}\text{-}AsP_3)]$ (**48**):

Yield 83 mg (0.084 mmol, 69 %).

^{1}H NMR (C_6D_6) δ[ppm] = 0.63 (d, 3H, J = 6.9 Hz, $H_P^{22/23,25/26}$), 0.71 (d, 3H, J = 6.9 Hz, $H_P^{22/23,25/26}$), 0.76 (d, 3H, J = 6.6 Hz, $H_P^{22/23,25/26}$), 0.80 (d, 3H, J = 6.6 Hz, $H_P^{22/23,25/26}$), 1.08 (s, 6H, $H_{As}^{13/14}$), 1.19 (pseudo t, 6H, J = 7.3 Hz, $H_{As}^{22/23,24/25}$), 1.52 (pseudo, 6H, J = 6.4Hz, $H_{As}^{22/23,25/26}$), 1.67 (s, 3H, $H_P^{13,14}$), 1.74 (s, 3H, $H_P^{13,14}$), 2.48 (sep, 1H, J = 6.9Hz, $H_P^{21,24}$), 2.58 (sep, 1H, J = 6.6Hz, $H_P^{21/24}$), 4.03 (2 sep, 2H, J = 7.3Hz + 6.4 Hz, $H_{As}^{21/24}$), 5.75 (d, 1H, J = 6.6Hz, H_P^3), 5.77 (d, 1H, J = 6.96Hz, H_{As}^3), 6.30 (pseudo t, 2H, J = 6.60 Hz, $H^{9/11,17/19}$), 6.36 (d, 1H, J = 8.8Hz, H_P^5), 6.39 (d, 1H, J = 8.8, H_{As}^5), 6.64 – 6.75 (m, 4H, $H^{9/11,17/19}$), 6.79 (pseudo t, 2H, J = 7.5Hz, H^4), 7.03 (m, 2H, $H^{9/11,17/19}$), 7.19 (t, 2H, J = 7.5Hz, $H^{10/18}$), 7.26 (m, 2H, $H^{10/18}$).

^{13}C{^{1}H} NMR (C_6D_6) δ[ppm] = 18.6 ($C^{13,14}$), 18.7 ($C^{13,14}$), 22.0 ($C^{13,14}$), 22.3 ($C^{13,14}$), 24.7 ($C^{22,23/25,26}$), 24.8 ($C^{22,23/25,26}$), 25.9 ($C^{22,23/25,26}$), 26.0 ($C^{22,23/25,26}$), 26.5 ($C^{22,23/25,26}$), 26.6 ($C^{22,23/25,26}$), 28.4 ($C^{21,24}$), 28.7 ($C^{21,24}$), 29.2 ($C^{21,24}$), 109.9 (C^3), 110.3 (C^3), 110.7 (C^5) 110.9 (C^5), 124.6 ($C^{9,11/17,19}$), 124.7 ($C^{9,11/17,19}$), 125.7 ($C^{10/18}$), 125.9 ($C^{10/18}$), 126.9 ($C^{9,11/17,19}$), 127.0 ($C^{9,11/17,19}$), 127.0 ($C^{10/18}$), 127.2 ($C^{10/18}$), 128.6 ($C^{9,11/17,19}$), 129.0 (C^4), 129.2 (C^4), 134.7 ($C^{9,11/17,19}$), 135.2 ($C^{8,12}$), 135.3 ($C^{8,12}$), 138.3 ($C^{8,12}$), 138.6 (C^7), 138.8 (C^7),

143.4 (C^{7}), 143.5 (C^{7}), 145.4 ($C^{16,20}$), 145.5 ($C^{16,20}$), 145.9 (C^{15}), 146.3 (C^{15}), 156.8 (C^{6}), 157 (C^{6}), 172.6 (C^{2}), 172.7 (C^{2}).

$^{31}P\{^{1}H\}$ NMR (C_6D_6) δ [ppm] = 255.6 (dd, 1P, $^{1}J_{PP}$ = 316Hz, $^{2}J_{PP}$ = 23Hz), 260.6(dd, 1P, $^{1}J_{PP}$ = 274Hz, $^{2}J_{PP}$ = 23Hz), 291.0 (dd, 1P, $^{1}J_{PP}$ = 316Hz, $^{1}J_{PP}$ = 274Hz).

Elemental analysis calcd. for $C_{50}H_{58}AsCr_2N_4P_3$ (986.86 g mol^{-1}) C 60.85, H 5.92, N 5.68; found C 58.88, H 6.36, N 4.80.

4.4.4 [{L_2Cr_2}(μ_3,$\eta^{1:1:1:2:2}$-P_4){$W(CO)_5$}] (49)

To a solution of [L_2Cr_2] (**45**) (204 mg, 0.25 mmol) in thf (10 ml) is given a solution of P_4 (31 mg, 0.25 mmol) in thf (10 ml). The reaction mixture is stirred for 1h at room temperature. To this solution is given a solution of [$W(CO)_5$(thf)] in thf (17.8 ml, 0.028 mol L^{-1}, 0.5 mmol) and the reaction mixture is stirred for 48 h during which the color changes from green to red. The solvent is removed under reduced pressure and the dark residue is taken up in dichloromethane (15 ml). After filtration over diatomaceous earth the solution is reduced in vacuum and kept at -28 °C to yield **49** as dark red crystalline product.

Analytical data for [{L_2Cr_2}(μ_3,$\eta^{1:1:1:2:2}$-P_4){$W(CO)_5$}] (**49**):

Yield 61 mg (0.048 mmol, 19 %).

^{1}H NMR (CD_2Cl_2) δ[ppm] = 0.57 (d, 6H, *J* = 6.7 Hz, $H^{22,23/25,26}$), 0.61 (d, 6H, *J* = 6.7 Hz, $H^{22,23/25,26}$), 0.94 (s, 6H, $H^{13,14}$), 1.06 (d, 6H, *J* = 6.7 Hz, $H^{22,23/25,26}$), 1.48 (d, 6H, *J* = 6.7 Hz, $H^{22,23/25,/26}$), 1.62 (s, 6H, $H^{13,14}$), 2.03 (sep, 2H, *J* = 6.7 Hz, $H^{21/24}$), 3.79 (sep, 2H, *J* = 6.7 Hz, $H^{21,24}$), 6.17 (d, 2H, *J* = 6.7 Hz, H^{3}), 6.35 (d, 2H, *J* = 7.5 Hz, $H^{9,11/17,19}$), 6.50 (d, 2H, *J* = 8.8 Hz, H^{5}), 6.86 (d, 2H, *J* = 7.5 Hz, H^{4}), 6.94 (m, 2H, *J* = 7.2 Hz, $H^{9,11/17,19}$), 7.07 (dd, 2H, *J* = 7.4 Hz, *J* = 6.6 Hz, $H^{9,11/17,19}$), 7.27-7.40 (m, 6H, $H^{9,11/17,19/10/18}$).

$^{13}C\{^{1}H\}$ NMR (CD_2Cl_2) δ[ppm] = 18.7 ($C^{13,14}$), 22.0 ($C^{13,14}$), 22.9 ($C^{22,23/25,26}$), 24.9 ($C^{22,23/25,26}$), 26.0 ($C^{22,23/25,26}$), 26.4 ($C^{22,23/25,26}$), 28.8 ($C^{21,24}$), 29.9 ($C^{21,24}$), 111.8 (C^{3}), 111.9 (C^{5}), 125.0 ($C^{9,11/17,19}$), 126.5 ($C^{10/18}$), 127.5 ($C^{9,11/17,19}$), 127.8 ($C^{10/18}$), 128.3 ($C^{9,11/17,19}$), 129.9 (C^{4}), 136.1 ($C^{9,11/17,19}$), 136.2 ($C^{8,12}$), 137.9 ($C^{8,12}$), 138.4 (C^{7}), 142.9

(C^{7}), 145.7 ($C^{16,20}$), 145.8 (C^{15}), 157.3 (C^{6}), 174.0 (C^{2}) 198.6 (C^{CO}).

$^{31}P\{^{1}H\}$ NMR (CD_2Cl_2, 298K) δ [ppm] = 250.0 (dd, J = 253.8 Hz, J = 283.8 Hz, 2P), 218.4 (br s, 2P).

$^{31}P\{^{1}H\}$ NMR (CD_2Cl_2, 183K) δ [ppm] = 133.1 (t, $^{1}J_{PP}$ = 244.1 Hz, 1P), 251.1 (t, $^{1}J_{PP}$ = 266.1 Hz, 1P), 254.4 (t, $^{1}J_{PP}$ = 262.7 Hz, 1P), 269.0 (t, $^{1}J_{PP}$ = 299.4 Hz, 1P).

Elemental analysis calcd. for $C_{55}H_{58}O_5N_4Cr_2P_4W$ (1266.80 g mol^{-1}) C 52.15, H 4.61, N 4.42; found C 51.68 H 4.63 N 4.28.

4.5 Synthesis of E_4 butterfly complexes (E_4 = P_4, AsP_3, As_4)

4.5.1 [{Cp'''Fe(CO)$_2$}$_2$] (10b) and K[Cp'''Fe(CO)$_2$] (50)

To a suspension of KC_8 (6.75 g, 50 mmol) in toluene (30 ml) is given a solution of [Cp'''Fe(CO)$_2$Br] (17.0 g, 40 mmol) in toluene (200 ml). The resulting brownish purple solution is stirred for four days at room temperature and filtered over diatomaceous earth. The solvent is removed under reduced pressure to yield a mixture of **10b** and **50** as brown solid. The crude product is extracted with several portions of acetonitrile (total of 200 ml) which dissolves mainly the ionic complex **50** and small fractions of **10b**. The resulting purple solid is dried in high vacuum to give pure [{Cp'''Fe(CO)$_2$}$_2$] (**10b**). The acetonitrile fractions are collected and the solvent is removed under reduced pressure. The resulting brownish solid is extracted with hexane until the liquid fractions are colorless. The remaining solid is dried in high vacuum to give pure **50** as orange solid.

Analytical data for [{Cp'''Fe(CO)$_2$}$_2$] (**10b**):

Yield 11.04 g (15.8 mmol, 79 %).

^{1}H NMR (C_6D_6) δ [ppm] = 1.22 (s, 9H, -(C_4H_9)), 1.51 (s, 18H, -(C_4H_9)$_2$), 4.53 (s, 2H, $C_5\underline{H}_2{}^{t}Bu_3$).

IR (toluene) $\tilde{\nu}$ [cm^{-1}] = 1934 (vs), 1764 (s).

Analytical data for K[Cp'''Fe(CO)$_2$] (**50**):

Yield	2.8 g (7.3 mmol, 18 %).
^{1}H NMR (C_6D_6)	δ [ppm] = 1.43 (s, 9H, -(C_4H_9)), 1.59 (s, 18H, -(C_4H_9)$_2$), 4.53 (s, 2H, $C_5\underline{H}_2{}^tBu_3$).
IR (toluene)	$\tilde{\nu}$ [cm^{-1}] = 2001 (s), 1894 (w).

4.5.2 [{Cp'''Fe(CO)$_2$}$_2$(μ,$\eta^{1:1}$-P$_4$)] (9b)

To a solution of P_4 (360 mg, 2.9 mmol) in toluene (100 ml) is given a solution of [{Cp'''Fe(CO)$_2$}$_2$] (2 g, 2.9 mmol) in toluene (150 ml). Upon addition, the color turns immediately bright orange. The resulting reaction mixture is stirred for ten minutes at room temperature and the solvent is removed under reduced pressure. A small amount of hexane (10 ml) is added and the resulting suspension is again taken to dryness in vacuum to remove last traces of toluene. Compound **9b** is isolated as analytically pure, orange solid.

Analytical data for [{Cp'''Fe(CO)$_2$}$_2$(μ,$\eta^{1:1}$-P$_4$)] (**9b**):

Yield	2.20 g (2.68 mmol, 93 %).
^{1}H NMR (C_6D_6)	δ [ppm] = 1.20 (s, 9H, -(C_4H_9)), 1.21 (s, 18H, -(C_4H_9)$_2$), 4.64 (s, 2H, $C_5\underline{H}_2{}^tBu_3$).
^{1}H NMR (CD_2Cl_2)	δ [ppm] = 1.23 (s, 9H, -(C_4H_9)), 1.38 (s, 18H, -(C_4H_9)$_2$), 4.64 (s, 2H, $C_5\underline{H}_2{}^tBu_3$).
^{31}P{^{1}H} NMR (C_6D_6)	δ [ppm] = -81.4 (t, 2P, $^1J_{AM}$ = 187 Hz, P_A), -325.0 (t, 2P, $^1J_{AM}$ = 187 Hz, P_M).
^{31}P{^{1}H} NMR (CD_2Cl_2)	δ [ppm] = -75.2 (t, 2P, $^1J_{AM}$ = 189 Hz, P_A), -322.3 (t, 2P, $^1J_{AM}$ = 189 Hz, P_M).
IR (toluene)	$\tilde{\nu}$ [cm^{-1}] = 2000 (vs), 1950 (vs).

4.5.3 [{Cp'''Fe(CO)$_2$}$_2$(μ,η$^{1:1}$-AsP$_3$)] (51)

To a solution of AsP_3 (54 mg, 0.322 mmol) in toluene (10 ml) is given a solution of [{Cp'''Fe(CO)$_2$}$_2$] (**10b**) (222 mg, 0.322 mmol) in toluene (10 ml). Upon addition the solution turns immediately bright orange. The reaction mixture is stirred for ten minutes and the solvent is removed under reduced pressure. The resulting orange solid is washed once with cold hexane (5 ml) and dried in vacuum to yield pure **51** as a bright orange solid.

Analytical data for [{Cp'''Fe(CO)$_2$}$_2$(μ,η$^{1:1}$-AsP$_3$)] (**51**):

Yield 210 mg (0.244 mmol, 76 %).

^{1}H NMR (C_6D_6) δ[ppm] = 1.16 (s, 9H, -(C_4H_9)^{As}), 1.21 (s, 18H, -(C_4H_9)$_2^P$), 1.22 (s, 9H, -(C_4H_9)^P), 1.22 (s, 18H, -(C_4H_9)$_2^{As}$), 4.60 (s, 2H, $C_5\underline{H}_2{}^t Bu_3^P$), 4.66 (s,1H, $C_5\underline{H}_2{}^t Bu_3^{As}$), 4.67 (s,1H, $C_5\underline{H}_2{}^t Bu_3^{As}$).

^{13}C{^{1}H} NMR (C_6D_6) δ[ppm] = 31.2 (s, -($\underline{C}(CH_3)_3$)^P), 31.2 (s, -($\underline{C}(CH_3)_3$)^{As}), 31.9 (s, -($\underline{C}(CH_3)_3$)$_2^P$), 31.9 (s, -($\underline{C}(CH_3)_3$)$_2^{As}$), 32.7 (s, -(C($\underline{C}H_3$)$_3$)^P), 32.8 (s, -(C($\underline{C}H_3$)$_3$)^{As}), 33.7 (s, -(C($\underline{C}H_3$)$_3$)$_2^P$), 33.7 (s, -(C($\underline{C}H_3$)$_3$)$_2^{As}$), 87.6 (s, $\underline{C}_2H_2C{}^t BuC_2{}^t Bu_2^{As}$), 89.0 (d, $^2J_{CP}$ = 5.5 Hz, $\underline{C}_2H_2C{}^t BuC_2{}^t Bu_2^P$), 107.8 (s, $C_2H_2\underline{C}{}^t BuC_2{}^t Bu_2^{As}$), 108.4 (s, $C_2H_2\underline{C}{}^t BuC_2{}^t Bu_2^P$), 109.6 (s, $C_2H_2C{}^t Bu\underline{C}_2{}^t Bu_2^{As}$), 110.1 (s, $C_2H_2C{}^t Bu\underline{C}_2{}^t Bu_2^P$), 215.8 (s, CO).

^{31}P{^{1}H} NMR (C_6D_6) δ[ppm] = -94.2 (t, 1P, $^1J_{AM}$ = 192 Hz, P_A), -312.0 (d, 2P, $^1J_{AM}$ = 192 Hz, P_M)

FD-MS (toluene) *m*/*z* [%] = 858.1 (100) [M^+], 830.2 (20) [M^+ – CO], 802.1 (10) [M^+ – 2(CO)].

IR (toluene) $\tilde{\nu}$ [cm^{-1}] = 1998 (s), 1990 (sh), 1950 (s), 1940 (sh).

Elemental analysis calcd. for $C_{38}H_{58}AsFe_2O_4P_3$ (858.40 g mol^{-1}) C 53.17, H 6.81; found C 53.52, H 6.80.

4.5.4 [{Cp'''Fe(CO)$_2$}$_2$(μ,η$^{1:1}$-As$_4$)] (52)

To freshly prepared solution of As_4 (220 mg, 0.733 mmol) in toluene (250 ml) at room temperature is given a solution of [{Cp'''Fe(CO)$_2$}$_2$] (**10b**) (506 mg, 0.733 mmol) in toluene (50

ml) under the exclusion of light leading to an immediate color change from dark purple to brownish orange. The reaction mixture is stirred for 10 minutes and the solvent is removed under reduced pressure to give crude **52** together with grey arsenic. The brown residue is taken up in dichloromethane (50 ml) and filtered through diatomaceous earth. The resulting bright orange solution is taken to dryness under reduced pressure to give **52** as an orange solid. Single crystals of **52** were obtained by cooling a concentrated solution of **52** in hexane/toluene (2:1) to -28 °C.

Analytical data for [{Cp'''Fe(CO)$_2$}$_2$(μ,$\eta^{1:1}$-As$_4$)] (**52**):

Yield	556 mg (0.561 mmol, 77 %).
^{1}H NMR (C_6D_6)	δ [ppm] = 1.18 (s, 9H, -(C_4H_9)), 1.23 (s, 18H, -(C_4H_9)$_2$), 4.66 (s, 2H, $C_5\underline{H}_2{}^tBu_3$).
^{13}C{^{1}H} NMR (C_6D_6)	δ [ppm] = 31.2 (s, -($\underline{C}(CH_3)_3$)), 32.0 (s, -($\underline{C}(CH_3)_3$)$_2$), 32.8 (s, -(C($\underline{C}H_3$)$_3$)), 33.8 (s, -(C($\underline{C}H_3$)$_3$)$_2$), 87.8 (s, $\underline{C}_2H_2C^tBuC_2{}^tBu_2$), 107.9 (s, $C_2H_2\underline{C}^tBuC_2{}^tBu_2$), 109.7 (s, $C_2H_2C^tBu\underline{C}_2{}^tBu_2$), 216.7 (s, CO).
FD-MS (toluene)	*m*/*z* [%] = 990.0 (100) [M^+].
IR (CH_2Cl_2)	$\tilde{\nu}$ [cm^{-1}] = 1990 (vs), 1940 (vs).
Elemental analysis	calcd. for $C_{38}H_{58}As_4Fe_2O_4$ (990.24 g mol^{-1}) C 46.09, H 5.90; found C 45.94, H 5.92.

4.5.5 [{Cp*Cr(CO)$_3$}$_2$(μ,$\eta^{1:1}$-P$_4$)] (54)

To a solution of P_4 (124 mg, 1 mmol) in toluene (10 ml) is given a solution of [{Cp*Cr(CO)$_3$}$_2$] (543 mg, 1 mmol) in toluene (10 ml). Upon addition the solution turns immediately bright orange. The reaction mixture is stirred for 10 minutes and the solvent is removed under reduced pressure to give pure **54**. Crystals suitable for X-ray structure analysis were grown from a saturated solution of **54** in toluene upon cooling to -28 °C.

Analytical data for [{Cp*Cr(CO)$_3$}$_2$(μ,$\eta^{1:1}$-P$_4$)] (**54**):

Yield	617 mg (0.925 mmol, 93 %).

^{1}H NMR (CD_2Cl_2) δ [ppm] = 1.83 (s, 15H, C_5Me_5).

^{13}C{^{1}H} NMR (CD_2Cl_2) δ [ppm] = 10.1 (s, $C_5\underline{Me}_5$), 101.9 (s, $\underline{C}_5Me_5$), 238.0 (s, CO), 247.7 (s, CO).

^{31}P{^{1}H} NMR (CD_2Cl_2) δ [ppm] = -95.2 (t, 2P, $^{1}J_{AM}$ = 196 Hz, P_A), -327.4 (t, 2P, $^{1}J_{AM}$ = 196 Hz, P_M).

FD-MS (toluene) *m*/*z* [%] = No peaks with reasonable composition detectable.

IR (KBr) $\tilde{\nu}$ [cm^{-1}] = 1983 (vs), 1967 (vs), 1916 (vs), 1900 (vs).

Elemental analysis calcd. for $C_{26}H_{30}Cr_2O_6P_4$ (666.40 g mol^{-1}) C 46.86, H 4.54; found C 46.72, H 4.65.

4.5.6 [{Cp*Cr(CO)$_3$}$_2$(μ,$\eta^{1:1}$-AsP$_3$)] (55)

To a solution of AsP_3 (31 mg, 0.184 mmol) in toluene (10 ml) is given a solution of [{Cp*Cr(CO)$_3$}$_2$] (100 mg, 0.184 mmol) in toluene (10 ml). Upon addition the solution turns immediately bright orange. The reaction mixture is stirred for 10 minutes and the solvent is removed under reduced pressure to give pure **55**. Crystals suitable for X-ray structure analysis were grown from a saturated solution of **55** in toluene upon cooling to 4 °C.

Analytical data for [{Cp*Cr(CO)$_3$}$_2$(μ,$\eta^{1:1}$-AsP$_3$)] (**55**):

Yield 83 mg (0.116 mmol, 63 %).

^{1}H NMR (C_6D_6) δ [ppm] = 1.43 (s, 15H, $C_5Me_5^{P}$), 1.44 (s, 15H, $C_5Me_5^{As}$).

^{13}C{^{1}H} NMR (C_6D_6) δ [ppm] = 9.6 (s, $C_5\underline{Me}_5$), 9.6 (s, $C_5\underline{Me}_5$), 9.7 (s, $C_5\underline{Me}_5$), 9.7 (s, $C_5\underline{Me}_5$), 100.4 (s, $\underline{C}_5Me_5$), 101.4 (s, $\underline{C}_5Me_5$), 237.8 (s, CO), 238.0 (s, CO), 247.2 (s, CO), 247.6 (s, CO).

^{31}P{^{1}H} NMR (C_6D_6) δ [ppm] = -112.9 (t, 1P, $^{1}J_{AM}$ = 201 Hz, P_A), -312.9 (d, 2P, $^{1}J_{AM}$ = 201 Hz, P_M).

ESI-MS (toluene) *m*/*z* [%] = 710.1 (18) [M^+], 641.1 (35) [M^+ – 3(CO) + O], 625.1 (47) [M^+ -3(CO)].

IR (KBr) $\tilde{\nu}$ [cm^{-1}] = 1980 (vs), 1964 (vs), 1897 (vs, br).

Elemental analysis calcd. for $C_{26}H_{30}AsCr_2O_6P_3$ (710.35 g mol^{-1}) C 43.96, H 4.26; found C 43.89, H 4.52.

4.5.7 [{Cp*Cr(CO)$_3$}$_2$(μ,η$^{1:1}$-As$_4$)] (56)

To a solution of freshly prepared As_4 (220 mg, 0.733 mmol) in toluene (250 ml) at room temperature is given a solution of [{Cp*Cr(CO)$_3$}$_2$] (380 mg, 0.7 mmol) in toluene (20 ml). The reaction mixture is stirred for 30 minutes under the exclusion of light. The resulting bright orange solution is taken to dryness under reduced pressure. The crude product is taken up in dichloromethane and filtered from grey arsenic. After removal of the solvent, **56** is obtained as an orange solid. Cooling of a concentrated solution of **56** in dichloromethane to 4 °C yields single crystals suitable for X-ray structure analysis that contain **56** as well as **64** in a 2:1 ratio.

Analytical data for [{Cp*Cr(CO)$_3$}$_2$(μ,η$^{1:1}$-As$_4$)] (**56**):

Yield 437 mg (0.52 mmol, 75 %).

^{1}H NMR (CD_2Cl_2) δ [ppm] = 1.84 (s, 15H, C_5Me_5).

^{13}C{^{1}H} NMR (CD_2Cl_2) δ [ppm] = 10.2 (s, $C_5\underline{Me}_5$), 101.7 (s, $\underline{C}_5Me_5$), 240.9 (s, CO), 242.1 (s, CO), 248.5 (s, CO).

ESI-MS (CH_2Cl_2) *m*/*z* [%] = 749.0 (50) $[Cp^*_2Cr_2As_5]^+$, 412.2 (35) $[Cp^*CrAs_3]^+$, 300.0 (100) $[As_4^+]$.

IR (CH_2Cl_2) $\tilde{\nu}$ [cm^{-1}] = 1977 (vs), 1965 (vs), 1904 (vs).

IR (KBr) $\tilde{\nu}$ [cm^{-1}] = 1969 (vs), 1956 (vs), 1892 (vs, br).

Elemental analysis calcd. for $C_{26}H_{30}As_4Cr_2O_6$ (842.19 g mol^{-1}) C 37.08, H 3.59; found C 36.15, H 3.48.

4.5.8 [{Cp*Fe(CO)$_2$}{Cp'''Fe(CO)$_2$}] (57)

To a solution of [Cp*Fe(CO)$_2$Br] (1000 mg, 5.2 mmol) in toluene (50 ml) is given a solution of $K^+[Cp'''Fe(CO)_2]^-$ (860 mg, 5.2 mmol) in toluene (50 ml) within 30 minutes. The reaction mixture is stirred for 1 hour during which the color changes from reddish brown to dark purple.

The solvent is removed in vacuum and the dark residue is taken up in hot hexane (200 ml). Filtration and storage at -28 °C yields **57** as dark brown crystals, suitable for X-ray structure analysis.

Analytical data for [{Cp*Fe(CO)$_2$}{Cp'''Fe(CO)$_2$}] (**57**):

Yield	1.16 g (1.95 mmol, 75 %).
^{1}H NMR (C_6D_6)	δ [ppm] = 1.34 (s, 9 H, -C_4H_9), 1.49 (s, 18 H, -(C_4H_9)$_2$), 1.56 (s, 15 H, $C_5(C\underline{H}_3)_5$), 4.40 (s, 2 H, $C_5\underline{H}_2{}^t Bu_3$).
^{13}C{^{1}H} NMR (C_6D_6)	δ [ppm] = 8.2 (s, $C_5(\underline{C}H_3)_5$), 30.2 (s, $C_5H_2(C(\underline{C}H_3)_3)_2(C(CH_3))$), 31.4 (s, $C_5H_2(C(CH_3)_3)_2(C(\underline{C}H_3))$), 32.9 (s, $C_5H_2(\underline{C}(CH_3)_3)_2(C(CH_3))$), 33.2 (s, $C_5H_2(C(CH_3)_3)_2(C(\underline{C}H_3))$), 83.2 (s, $\underline{C}_2H_2C_3{}^t Bu_3$), 98.1 (s, $\underline{C}_5Me_5$), 113.7 (s, $C_2H_2(\underline{C}_2{}^t Bu_2)(C{}^t Bu)$), 118.5 (s, $C_2H_2(C_2{}^t Bu_2)(\underline{C}{}^t Bu)$), 245.5 (s, CO)
IR (KBr)	$\tilde{\nu}$ [cm^{-1}] = 1929 (vs); 1760 (vs).
Elemental analysis	calcd. for $C_{31}H_{44}Fe_2O_4$ (592.37 g mol^{-1}) C 62.85, H 7.49; found C 62.67, H 7.03.

4.5.9 [{Cp*Fe(CO)$_2$}(μ,$\eta^{1:1}$-P$_4$){Cp'''Fe(CO)$_2$}] (58) and [{Cp*Fe(CO)$_2$}$_2$(μ,$\eta^{1:1}$-P$_4$)] (9d)

A solution of [{Cp'''Fe(CO)$_2$}{Cp*Fe(CO)$_2$}] (**57**) (500 mg, 0.844 mmol) and P_4 (105 mg, 0.844 mmol) in toluene (150 ml) is stirred for 5 days at room temperature during which the color changes slightly from dark purple to brownish orange. The solvent is removed under reduced pressure and the residual dark solid is preadsorbed in silica gel. Subsequent column chromatographic workup (hexane, 40 × 2 cm, -40 °C) slowly elutes a purple fraction of unreacted **57**. Elution with hexane/toluene (5:1) gives an orange fraction of **9b** (140 mg). With hexane/toluene (1:4) an orange fraction of **58** (210 mg) is eluted. Finally THF elutes an orange fraction of **9d** (107 mg).

Analytical data for [{Cp*Fe(CO)$_2$}(μ,$\eta^{1:1}$-P$_4$){Cp'''Fe(CO)$_2$}] (**58**):

The product readily symmetrizes in solution to give a 1 : 2 : 1 mixture of the three butterfly complexes **9b**, **58** and **9d**.

Yield 210 mg (0.293 mmol, 35 %).

^{1}H NMR (CD_2Cl_2) δ [ppm] = 1.23 (s, 9H, -(C_4H_9)), 1.24 (s, 18H, -(C_4H_9)$_2$), 1.40 (s, 15H, C_5Me_5), 4.64 (s, 1H, $C_5H_2{}^tBu_3$), 4.65 (s, 1H, $C_5H_2{}^tBu_3$).

^{31}P{^{1}H} NMR (CD_2Cl_2) δ [ppm] = -56.4 (dt, 1P, $^{1}J_{AM}$ = 185 Hz, $^{2}J_{AB}$ = 292 Hz, P_A(Cp*)), -73.7 (dt, 1P, $^{1}J_{BM}$ = 186 Hz, $^{2}J_{AB}$ = 292 Hz, P_B(Cp’’’)), -330.9 (pseudo t, 2P, $^{1}J_{AM}$ = 185 Hz, $^{1}J_{BM}$ = 186 Hz, P_M).

IR (toluene) $\tilde{\nu}$ [cm^{-1}] = 1998 (s), 1987 (sh), 1950 (s), 1931 (s).

Analytical data for and [{Cp*Fe(CO)$_2$}$_2$(μ,$\eta^{1:1}$-P_4)] (**9d**):

Yield 107 mg (0.173 mmol, 20 %).

^{1}H NMR (CD_2Cl_2) δ [ppm] = 1.44 (s, 15H, C_5Me_5).

^{31}P{^{1}H} NMR (CD_2Cl_2) δ [ppm] = -45.1 (t, 2P, $^{1}J_{AM}$ = 184.6 Hz, P_A), -334.9 (t, 2P, $^{1}J_{AM}$ = 184.6 Hz, P_M).

IR (toluene) $\tilde{\nu}$ [cm^{-1}] = 1987 (s), 1931 (s).

4.5.10 [Cp’’’$_2$P$_4$] (60)

To a solution of [{Cp’’’Fe}$_2$(μ-Br)$_2$] (3.518 g, 4.765 mmol) in toluene (100 ml) is given a solution of P_4 (590 mg, 4.765 mmol) in toluene (100 ml). The solution is stirred for 16 h during which the color changes to dark red and a brownish solid forms. The solvent is removed under reduced pressure and the dark residue is preadsorbed on silica gel. Subsequent column chromatographic separation of the solid (hexane, 50 × 4 cm) eluted an almost colorless to pale yellow fraction of **60** followed by a dark red fraction of [{Cp’’’Fe}$_2$(μ,$\eta^{4:4}$-P_4)]. Removal of the solvent of the first fraction gives crude **60** as pale orange syrup like oil. The oil is taken up in Et_2O (10 ml) and the resulting solution is concentrated in vacuum. Colorless crystals of **60** form upon standing at room temperature.

Analytical data for [Cp’’’$_2$P$_4$] (**60**):

Yield 200 mg (0.338 mmol, 14 %).

^{1}H NMR (C_6D_6) δ [ppm] = 1.03 (s, -(C_4H_9)), 1.15 – 1.26 (mult. s, -(C_4H_9)), 1.35 – 1.45 (mult. s, -(C_4H_9)), 1.55 (s, -(C_4H_9)), 5.59 (br s, 2H, $C_5\underline{H}_2{}^t Bu_3$, **C** or **D**), 6.02 (br s, 1.2H, $C_5\underline{H}_2{}^t Bu_3$, **A** and **B**), 6.29 (mult. s, 2H, $C_5\underline{H}_2{}^t Bu_3$, **C** or **D**)

^{13}C{^{1}H} NMR (C_6D_6) δ [ppm] = 30.7 – 37.4 (mult. s, -$\underline{C}(CH_3)_3$), 32.1 – 37.6 (mult. s, -C($\underline{C}H_3)_3$), 131.3 (d, $^{1}J_{CP}$ = 20 Hz, C_P), 131.4 (d, $^{1}J_{CP}$ = 28 Hz, C_P), 136.9 (s), 151.5 (d, $^{1}J_{CP}$ = 27 Hz, C_P), 154.1 (d, $^{1}J_{CP}$ = 27 Hz, C_P), 154.2 (s), 160.2 (d, $^{1}J_{CP}$ = 21 Hz, C_P), 160.8 (s).

^{31}P{^{1}H} NMR (C_6D_6) **A** δ [ppm] = -162.4 (t, 2P, $^{1}J_{AM}$ = $^{1}J_{AN}$ = $^{1}J_{A'M}$ = $^{1}J_{A'N}$ = 181 Hz, $P_AP_{A'}$), -307.3 (dt, 1P, $^{1}J_{AM}$ = $^{1}J_{A'M}$ = 181 Hz, $^{1}J_{MN}$ = 181 Hz, P_M), -366.0 (dt, 1P, $^{1}J_{AN}$ = $^{1}J_{A'N}$ = 181 Hz, $^{1}J_{MN}$ = 181 Hz, P_N).

^{31}P{^{1}H} NMR (C_6D_6) **B** δ [ppm] = -154.9 (t, 2P, $^{1}J_{AM}$ = 181 Hz, P_A), -341.6 (t, 2P, $^{1}J_{AM}$ = 181 Hz, P_M).

^{31}P{^{1}H} NMR (C_6D_6) **C** δ [ppm] = -157.9 (t, 2P, $^{1}J_{AM}$ = 183 Hz, P_A), -334.8 (t, 2P, $^{1}J_{AM}$ = 183 Hz, P_M).

^{31}P{^{1}H} NMR (C_6D_6) **D** δ [ppm] = -154.6 (ddd, 1P, $^{1}J_{AM}$ = 191 Hz, $^{1}J_{AN}$ = 175 Hz, $^{1}J_{AB}$ = 317 Hz, P_A), -162.5 (ddd, 1P, $^{1}J_{BM}$ = 175 Hz, $^{1}J_{BN}$ = 191 Hz, $^{1}J_{AB}$ = 317 Hz, P_B) , -324.8 (ddd, 1P, $^{1}J_{AM}$ = 191 Hz, $^{1}J_{BM}$ = 175 Hz, $^{1}J_{MN}$ = 173 Hz, P_M), -352.1 (ddd, 1P, $^{1}J_{AN}$ = 175 Hz, $^{1}J_{BN}$ = 191 Hz, $^{1}J_{MN}$ = 173 Hz, P_N).

EI-MS (toluene) *m*/*z* [%] = 590.4 (5) [M^+], 533.3 (10) [M^+ - (C_4H_9)], 466.3 (60) [Cp'''$P_4(C_8H_{13})]^+$, 357.1 (20) [Cp'''$P_4]^+$, 301.1 (17) [Cp''$P_4]^+$.

Elemental analysis calcd. for $C_{34}H_{58}P_4$ (590.72 g mol^{-1}) C 69.13, H 9.90; found C 69.19, H 9.68.

4.6 As_8 cuneane complexes

4.6.1 [{Cp'''Fe(CO)$_2$}(μ,η$^{1:2}$-As$_4$){Cp'''Fe(CO)}] (62) and [{Cp'''Fe(CO)$_2$}$_2$(μ$_4$,η$^{1:1:2:2}$-As$_8$){Cp'''Fe(CO)}$_2$] (63)

A solution of [{Cp'''Fe(CO)$_2$}$_2$(μ,η$^{1:1}$-As$_4$)] (**52**) (500 mg, 0.5 mmol) in toluene (60 ml) is irradiated with a high pressure Hg vapor lamp at room temperature for 2 hours. During the irradiation the color of the solution changes from bright orange to dark brown. After removal of the solvent under reduced pressure, the resulting dark solid is taken up in dichloromethane and preadsorbed on silica gel. Subsequent column chromatographic workup (hexane, 25 × 4 cm) elutes a very weak reddish brown fraction that is not collected. Elution with hexane/toluene (10:1) gives a brown fraction of **62** (158 mg) as well as a dark green fraction of **63** (45 mg). Single crystals of **63** are obtained by cooling a saturated solution of **63** in hexane/toluene to -28 °C.

Analytical data for [{Cp'''Fe(CO)$_2$}(μ,η$^{1:2}$-As$_4$){Cp'''Fe(CO)}] (**62**):

Yield 158 mg (0.164 mmol, 32 %).

IR (CH_2Cl_2) $\tilde{\nu}$ [cm^{-1}] = 1988 (vs), 1939 (vs), 1908 (vs).

[{Cp'''Fe(CO)$_2$}$_2$(μ$_4$,η$^{1:1:2:2}$-As$_8$){Cp'''Fe(CO)}$_2$] (**63**):

^{1}H NMR (C_6D_6) δ [ppm] = 1.27 (s, 9H, -(C_4H_9)), 1.35 (s, 9H, -(C_4H_9)), 1.40 (s, 18H, -(C_4H_9)$_2$), 1.66 (s, 9H, -(C_4H_9)), 1.87 (s, 9H, -(C_4H_9)), 4.51 (d, 1H, $^4J_{HH}$ = 1.8 Hz, $C_5\underline{H}_2{}^t Bu_3$), 4.94 (s, 1H, $^4J_{HH}$ = 1.8 Hz, $C_5\underline{H}_2{}^t Bu_3$), 5.00 – 6.00 (br s, 2H, $C_5\underline{H}_2{}^t Bu_3$).

^{13}C{^{1}H} NMR (C_6D_6) δ [ppm] = 31.6 (s, -($\underline{C}(CH_3)_3$)), 32.2 (s, -($\underline{C}(CH_3)_3$)), 32.8 (s, -($\underline{C}(CH_3)_3$)), 33.0 (s, -($\underline{C}(CH_3)_3$)), 33.4 (s, -($\underline{C}(CH_3)_3$)), 33.5 (s, -(C($\underline{C}H_3)_3$)$_2$), 33.6 (s, -(C($\underline{C}H_3)_3$)$_2$), 33.6 (s, -(C($\underline{C}H_3)_3$)$_2$), 33.7 (s, -(C($\underline{C}H_3)_3$)$_2$), 34.1 (s, -(C($\underline{C}H_3)_3$)$_2$), 34.3 (s, -(C($\underline{C}H_3)_3$)$_2$), 73.1 (s, $\underline{C}_2H_2C_3{}^t Bu_3$), 83.7 (s, $\underline{C}_2H_2C_3{}^t Bu_3$), 89.4 (s, $\underline{C}_2H_2C_3{}^t Bu_3$), 110.2 (s, $C_2H_2\underline{C}_3{}^t Bu_3$), 112.3 (s, $C_2H_2\underline{C}_3{}^t Bu_3$), 116.8 (s, $C_2H_2\underline{C}_3{}^t Bu_3$), 213.7 (s, CO), 217.8 (s, CO), 223.5 (s, CO).

FD-MS (toluene) *m*/*z* [%] = 1924.5 (100) [M$^+$].

IR (CH_2Cl_2) $\tilde{\nu}$ [cm^{-1}] = 1997 (vs), 1954 (vs), 1885 (vs).

IR (KBr) $\tilde{\nu}$ [cm^{-1}] = 1999 (vs), 1953 (vs), 1897 (vs).

4.6.2 $[\{Cp^*Cr(CO)_3\}_4(\mu_4,\eta^{1:1:1:1}\text{-}As_8)]$ (64)

A solution of $[\{Cp^*Cr(CO)_3\}_2(\mu,\eta^{1:1}\text{-}As_4)]$ (**56**) (100 mg, 0.119 mmol) in THF is stirred for 5 days at room temperature during which the color changes from bright orange to brownish red. The solution is concentrated under reduced pressure and stored at 4 °C to **64** as dark red crystals suitable for X-ray structure analysis.

Analytical data for $[\{Cp^*Cr(CO)_3\}_4(\mu_4,\eta^{1:1:1:1}\text{-}As_8)]$ (**64**):

Yield 32 mg (0.019 mmol, 32 %).

^{1}H NMR (CD_2Cl_2) δ [ppm] = 1.84 (s, 15H, C_5Me_5).

^{13}C{^{1}H} NMR (CD_2Cl_2) δ [ppm] = 10.2 (s, $C_5\underline{Me}_5$), 101.7 (s, $\underline{C}_5Me_5$), 240.9 (s, CO), 242.1 (s, CO), 248.5 (s, CO).

IR (KBr) $\tilde{\nu}$ [cm^{-1}] = 1973 (vs, br), 1902 (vs, br).

IR (CH_2Cl_2) $\tilde{\nu}$ [cm^{-1}] = 1978 (s), 1966 (s), 1905 (vs, br).

4.7 E_n butterfly complexes ($E_4 = P_4$, AsP_3, As_4) as chelating ligands

4.7.1 $[\{\{Cp'''Fe(CO)_2\}_2(\mu_3,\eta^{1:1:1:1}\text{-}P_4)\}_2Cu]^+[BF_4]^-$ (65)

To a solution of $[Cu(MeCN)_4]^+[BF_4]^-$ (20 mg, 0.061 mmol) in dichloromethane (5 ml) is given a solution of $[\{Cp'''Fe(CO)_2\}_2(\mu,\eta^{1:1}\text{-}P_4)]$ (**9b**) (100 mg, 0.123 mmol) in dichloromethane (5 ml). Upon addition the color of the reaction mixture turns dark purple. The reaction mixture is stirred for 16 hours at room temperature and the solvent is removed under reduced pressure. The resulting dark solid is washed with hexane (5 ml) and dried in vacuum. The crude product is taken up in THF (4 ml) and layered with hexane (4 ml) to yield **65** as dark red crystals, suitable for X-ray structure determination.

Analytical data for $[\{\{Cp'''Fe(CO)_2\}_2(\mu_3,\eta^{1:1:1:1}\text{-}P_4)\}_2Cu]^+[BF_4]^-$ (**65**):

Yield 60 mg (0.033 mmol, 54 %).

^{1}H NMR (CD_2Cl_2) δ [ppm] = 1.42 (s, 9H, -(C_4H_9)), 1.44 (s, 18H, -(C_4H_9)$_2$), 4.82 (s, 2H, $C_5\underline{H}_2{}^tBu_3$).

$^{13}C\{^1H\}$ NMR (CD_2Cl_2) δ[ppm] = 31.8 (s, -(<u>C</u>(CH_3)$_3$)), 32.8 (s, -(<u>C</u>(CH_3)$_3$)$_2$), 33.2 (s, -(C(<u>C</u>H_3)$_3$)), 34.0 (s, -(C(<u>C</u>H_3)$_3$)$_2$), 81.9 (s, <u>C</u>$_2H_2C^tBuC_2{}^tBu_2$), 88.5 (s, <u>C</u>$_2H_2C^tBuC_2{}^tBu_2$), 109.8 (s, C_2H_2<u>C</u>$^tBuC_2{}^tBu_2$), 111.8 (s, $C_2H_2C^tBu$<u>C</u>$_2{}^tBu_2$), 214.1 (s, CO).

$^{31}P\{^1H\}$ NMR (CD_2Cl_2) δ[ppm] = -81.1 (t, 2P, $^1J_{AM}$ = 182 Hz, P_A), -282.0 (t, 2P, $^1J_{AM}$ = 182 Hz, P_M).

ES-MS (CH_2Cl_2) *m/z* [%] = 1131.4 (100) [{Cp'''Fe(CO)$_2$}$_2$(P_4){(CO)FeCp'''}]$^+$, 1103.6 (69) [{Cp'''Fe(CO)$_2$}$_2$(P_4){FeCp'''}]$^+$.

IR (KBr) $\tilde{\nu}$ [cm^{-1}] = 2008 (vs, br), 1960 (vs, br), 1930 (s, sh).

Elemental analysis calcd. for $C_{76}H_{116}BCuF_4Fe_4O_8P_8$ (1779.25 g mol^{-1}) C 51.30, H 6.57; found C 49.70, H 6.55.

4.7.2 [{{Cp*Cr(CO)$_3$}$_2$(μ_3,$\eta^{1:1:1:1}$-P_4)}$_2$Cu]$^+$[BF_4]$^-$ (66)

To a solution of [Cu(MeCN)$_4$]$^+$[BF_4]$^-$ (18 mg, 0.057 mmol) in dichloromethane (5 ml) is given a solution of [{Cp*Cr(CO)$_3$}$_2$(μ,$\eta^{1:1}$-P_4)] (**54**) (75 mg, 0.114 mmol) in dichloromethane (5 ml). Upon addition the color of the reaction mixture turns dark red. The reaction mixture is stirred for 1 hour at room temperature and the solvent is removed under reduced pressure. The resulting dark solid is washed with hexane (5 ml) and dried in vacuum. The crude product is taken up in a mixture of THF and dichloromethane (3 + 3 ml) and layered with hexane (6 ml) to yield **66** as dark red crystals, suitable for X-ray structure determination.

Analytical data for [{{Cp*Cr(CO)$_3$}$_2$(μ_3,$\eta^{1:1:1:1}$-P_4)}$_2$Cu]$^+$[BF_4]$^-$ (**66**):

Yield 25 mg (0.017 mmol, 33 %).

^1H NMR (CD_2Cl_2) δ[ppm] = 1.94 (s, 15H, C_5<u>Me</u>$_5$).

$^{13}C\{^1H\}$ NMR (CD_2Cl_2) δ[ppm] = 10.7 (s, C_5<u>Me</u>$_5$), 103.5 (s, <u>C</u>$_5Me_5$), 238.5 (s, CO), 245.0 (s, CO).

$^{31}P\{^1H\}$ NMR (CD_2Cl_2) δ[ppm] = -89.1(t, 2P, $^1J_{AM}$ = 191 Hz, P_A), -284.4 (t, 2P, $^1J_{AM}$ = 191 Hz, P_M).

ES-MS (CH_2Cl_2) *m/z* [%] = No peaks with reasonable composition detectable.

IR (KBr) $\tilde{\nu}$ [cm^{-1}] = 1990 (vs), 1932 (vs, sh), 1913 (vs).

4.7.3 [{Cp'''Fe(CO)$_2$}$_2$(μ_3,$\eta^{1:1:2}$-P$_4$){Cu(MeCN)}]$^+$[BF$_4$]$^-$ (67)

To a solution of [Cu(MeCN$_4$)]$^+$[BF$_4$]$^-$ (40 mg, 0.123 mmol) in dichloromethane (3 ml) is given a solution of [{Cp'''Fe(CO)$_2$}$_2$(μ,$\eta^{1:1}$-P$_4$)] (**9b**) (100 mg, 0.123 mmol) in dichloromethane (3 ml). Upon addition the color of the reaction mixture turns red. The reaction mixture is stirred for 5 minutes at room temperature and the solvent is removed under reduced pressure. The resulting red solid is washed with hexane (5 ml) and dried in vacuum. The crude product is taken up in dichloromethane (3 ml) and layered with hexane (4 ml) to yield **67** as reddish orange crystals suitable for X-ray structure determination.

Analytical data for [{Cp'''Fe(CO)$_2$}$_2$(μ_3,$\eta^{1:1:2}$-P$_4$){Cu(MeCN)}]$^+$[BF$_4$]$^-$ (**67**):

Yield 74 mg (0.073 mmol, 59 %).

^{1}H NMR (CD_2Cl_2) δ [ppm] = 1.36 (s, 18H, -(C$_4$H$_9$)), 1.41 (s, 36 H, -(C$_4$H$_9$)$_2$), 2.36 (s, 3H, NCCH$_3$), 4.85 (s, 4H, C$_5$H$_2$^{t}Bu$_3$).

^{13}C{^{1}H} NMR (CD_2Cl_2) δ [ppm] = 2.6 (s, H$_3$CCN), 31.2 (s, -(C(CH$_3$)$_3$)), 32.0 (s, -(C(CH$_3$)$_3$)), 33.3 (s, -(C(CH$_3$)$_3$)$_3$), 33.4 (s, -(C(CH$_3$)$_3$)$_3$), 33.8 (s, -(C(CH$_3$)$_3$)$_3$), 33.9 (s, -(C(CH$_3$)$_3$)$_3$), 91.0 (s, C$_2$H$_2$C^{t}BuC$_2$^{t}Bu$_2$), 109.9 (s, C$_2$H$_2$C^{t}BuC$_2$^{t}Bu$_2$), 111.8 (s, C$_2$H$_2$C^{t}BuC$_2$^{t}Bu$_2$), 120.0 (s, MeCN), 203.7 (s, CO).

^{31}P{^{1}H} NMR (CD_2Cl_2) δ [ppm] = -73.2 (t, 2P, $^1J_{AM}$ = 181 Hz, P$_A$), -313.7 (t, 2P, $^1J_{AM}$ = 181 Hz, P$_M$).

ES-MS (CH_2Cl_2) *m*/*z* [%] = 1103.6 (100) [{Cp'''Fe(CO)$_2$}$_2$(P$_4$){FeCp'''}]$^+$.

IR (KBr) $\tilde{\nu}$ [cm^{-1}] = 2286 (w, CN), 2009 (vs), 2000 (vs), 1962 (vs), 1956 (vs).

Elemental analysis calcd. for $C_{40}H_{61}BCuF_4Fe_2NO_4P_4$ (1005.85 g mol^{-1}) C 47.76, H 6.11, N 1.39; found C 47.60, H 6.09, N 1.15.

4.7.4 $[\{\{Cp'''Fe(CO)_2\}_2(\mu_3,\eta^{1:1:1:1}\text{-}P_4)\}_2Ag]^+[PF_6]^-$ (68)

To a solution of $Ag^+PF_6^-$ (16 mg, 0.061 mmol) in dichloromethane (5 ml) is given a solution of $[\{Cp'''Fe(CO)_2\}_2(\mu,\eta^{1:1}\text{-}P_4)]$ (**9b**) (100 mg, 0.123 mmol) in dichloromethane (5 ml). The reaction mixture is stirred for 16 hours at room temperature and the solvent is removed under reduced pressure. The resulting solid is washed with hexane (5 ml) and dried in vacuum. The crude product is taken up in THF (4 ml) and layered with hexane (4 ml) to yield **68** as orange crystals, suitable for X-ray structure determination.

Analytical data for $[\{\{Cp'''Fe(CO)_2\}_2(\mu_3,\eta^{1:1:1:1}\text{-}P_4)\}_2Ag]^+[PF_6]^-$ (**68**):

Yield 38 mg (0.020 mmol, 33 %).

^{1}H NMR (CD_2Cl_2) δ [ppm] = 1.41 (s, 9H, -(C_4H_9)), 1.44 (s, 18H, -(C_4H_9)$_2$), 4.81 (s, 2H, $C_5\underline{H}_2{}^tBu_3$).

^{13}C{^{1}H} NMR (CD_2Cl_2) δ [ppm] = 32.0 (s, -($\underline{C}(CH_3)_3$)), 32.6 (s, -($\underline{C}(CH_3)_3$)$_2$), 33.4 (s, -(C($\underline{C}H_3$)$_3$)), 34.1 (s, -(C($\underline{C}H_3$)$_3$)$_2$), 88.7 (s, $\underline{C}_2H_2C^tBuC_2{}^tBu_2$), 109.6 (s, $C_2H_2\underline{C}^tBuC_2{}^tBu_2$), 111.7 (s, $C_2H_2C^tBu\underline{C}_2{}^tBu_2$), 213.9 (s, CO).

^{31}P{^{1}H} NMR (CD_2Cl_2) δ [ppm] = -63.8 (dt, 2P, $^1J_{AM}$ = 191 Hz, $^1J_{P^{109}Ag}$ = 158 Hz, P_A), -63.8 (dt, 2P, $^1J_{AM}$ = 191 Hz, $^1J_{P^{107}Ag}$ = 138 Hz, P_A), -143.9 (sept, 1P, $^1J_{PF}$ = 710 Hz, PF_6), -305.0 (t, 4P, $^1J_{AM}$ = 191 Hz, P_M).

ES-MS (CH_2Cl_2) *m*/*z* [%] = 1736.2 (100) [M^+], 1709.0 (10) [M^+ - CO], 1679.0 (5) [M^+ - 2CO], 1651.2 (1) [M^+ - 3CO].

IR (KBr) $\tilde{\nu}$ [cm^{-1}] = 2006 (vs), 1961 (vs).

Elemental analysis calcd. for $C_{76}H_{116}AgF_6Fe_4O_8P_9$ (1881.73 g mol^{-1}) C 48.51, H 6.21; found C 48.91, H 6.54.

4.7.5 $[\{\{Cp^*Cr(CO)_3\}_2(\mu_3,\eta^{1:1:1:1}\text{-}P_4)\}_2Ag]^+[PF_6]^-$ (69)

To a solution of $AgPF_6$ (10 mg, 0.038 mmol) in dichloromethane (5 ml) is given a solution of $[\{Cp^*Cr(CO)_3\}_2(\mu,\eta^{1:1}\text{-}P_4)]$ (**54**) (50 mg, 0.076 mmol) in dichloromethane (5 ml). The reaction mixture is stirred for 16 hours at room temperature and the solvent is removed under reduced pressure. The resulting dark solid is washed with hexane (5 ml) and dried in vacuum. The crude

product is taken up in THF (3 ml) and layered with hexane (6 ml) to yield **69** as orange crystals, suitable for X-ray structure determination.

Analytical data for $[\{\{Cp^*Cr(CO)_3\}_2(\mu_3,\eta^{1:1:1:1}\text{-}P_4)\}_2Ag]^+[PF_6]^-$ (**69**):

Yield 18 mg (0.011 mmol, 30 %).

^{1}H NMR (CD_2Cl_2) δ [ppm] = 1.91 (s, 15H, $C_5\underline{Me}_5$).

^{13}C{^{1}H} NMR (CD_2Cl_2) δ [ppm] = 10.5 (s, $C_5\underline{Me}_5$), 103.1 (s, $\underline{C}_5Me_5$), 237.8 (s, CO), 244.8 (s, CO).

^{31}P{^{1}H} NMR (CD_2Cl_2) δ [ppm] = -68.6 (dt, 2P, $^1J_{AM}$ = 200 Hz, $^1J_{P^{109}Ag}$ = 144 Hz, P_A), -68.6 (dt, 2P, $^1J_{AM}$ = 200 Hz, $^1J_{P^{107}Ag}$ = 125 Hz, P_A), -143.5 (sept, 1P, $^1J_{PF}$ = 710 Hz, PF_6), -310.3 (t, 4P, $^1J_{AM}$ = 200 Hz, P_M).

ES-MS (CH_2Cl_2) m/z [%] = 1441.2 (1.8) [M^+].

IR (KBr) $\tilde{\nu}$ [cm^{-1}] = 1998 (vs), 1988 (vs), 1935 (s, sh), 1918 (vs).

Elemental analysis calcd. for $C_{52}H_{60}AgCr_4F_6O_{12}P_9$ (1585.63 g mol^{-1}) C 39.39, H 3.81; found C 40.47, H 4.05.

4.7.6 $[\{Cp'''Fe(CO)_2\}_2(\mu_3,\eta^{1:1:1:1}\text{-}P_4)\{Au(PPh_3)\}]^+[PF_6]^-$ (70)

To a solution of $[(Ph_3P)Au(tht)]^+PF_6^-$ (43 mg, 0.061 mmol) in THF (5 ml) is given a solution of $[\{Cp'''Fe(CO)_2\}_2(\mu,\eta^{1:1}\text{-}P_4)]$ (**9b**) (50 mg, 0.061 mmol) in THF (5 ml) leading to a bright red colored solution. The reaction mixture is stirred for one hour at room temperature and the solution is reduced to about 3 ml in vacuum. Filtration via canula and layering with hexane (4 ml) yields **70** as orange crystals, suitable for X-ray structure determination.

Analytical data for $[\{Cp'''Fe(CO)_2\}_2(\mu_3,\eta^{1:1:1:1}\text{-}P_4)\{Au(PPh_3)\}]^+[PF_6]^-$ (**70**):

Yield 42 mg (0.029 mmol, 48 %).

^{1}H NMR (CD_2Cl_2) δ [ppm] = 1.21 (s, 18H, -(C_4H_9)), 1.31 (s, 36H, -(C_4H_9)$_2$), 4.67 (s, 4H, $C_5\underline{H}_2{}^tBu_3$), 7.55 – 7.65 (m, 15H, $P\underline{Ph}_3$).

^{13}C{^{1}H} NMR (CD_2Cl_2) δ [ppm] = 31.7 (s, -($\underline{C}(CH_3)_3$)), 31.9 (s, -($\underline{C}(CH_3)_3$)$_2$), 33.2 (s, -(C($\underline{C}H_3$)$_3$)), 33.7 (s, -(C($\underline{C}H_3$)$_3$)$_2$), 91.0 (s, $\underline{C}_2H_2C^tBuC_2{}^tBu_2$),

109.9 (s, $C_2H_2\underline{C}^tBuC_2{}^tBu_2$), 111.9 (s, $C_2H_2C^tBu\underline{C}_2{}^tBu_2$), 130.1 (br, $P\underline{Ph}_3$), 134.4 (br, $P\underline{Ph}_3$).

$^{31}P\{^1H\}$ NMR (CD_2Cl_2) δ[ppm] = 42.5 (t, 1P, $^2J_{AM}$ = 111 Hz, Au-P_APh3), -22.9 (dt, 2P, $^1J_{MX}$ = 196 Hz, $^2J_{AM}$ = 111 Hz, P_M), -143.5 (sept, 1P, $^1J_{PF}$ = 710 Hz, PF_6), -299.2 (t, 2P, $^1J_{MX}$ = 196 Hz, P_X).

ES-MS (CH_2Cl_2) *m/z* [%] = 1245.8 (5) [M_2^{2+}], 721.2 (100) [$(PPh_3)_2Au^+$].

IR (KBr) $\tilde{\nu}$ [cm^{-1}] = 2030 (s, sh), 2008 (vs), 1966 (vs), 1944 (s, sh).

Elemental analysis calcd. for $C_{55}H_{73}AuF_6Fe_2O_4P_6$ (1418.67 g mol^{-1}) C 47.41, H 5.19; found C 45.62, H 4.93

4.7.7 [{Cp*Cr(CO)$_3$}$_2$(μ_3,$\eta^{1:1:1:1}$-P$_4$){Au(PPh$_3$)}]$^+$[PF$_6$]$^-$ (71)

To a solution of $[(PPh_3)Au(tht)]^+[PF_6]^-$ (42 mg, 0.060 mmol) in dichloromethane (5 ml) is given a solution of [{Cp*Cr(CO)$_3$}$_2$(μ,$\eta^{1:1}$-P$_4$)] (**54**) (40 mg, 0.060 mmol) in dichloromethane (5 ml). Upon addition the color of the solution turns bright red. The reaction mixture is stirred for 16 hours at room temperature and the solvent is removed under reduced pressure. The resulting dark solid is washed with hexane (5 ml) and dried in vacuum. The crude product is taken up in THF and dichloromethane (3 + 3 ml) and layered with hexane (6 ml) to yield **71** as orange crystals, suitable for X-ray structure determination.

Analytical data for [{Cp*Cr(CO)$_3$}$_2$(μ_3,$\eta^{1:1:1:1}$-P$_4$){Au(PPh$_3$)}]$^+$[PF$_6$]$^-$ (**71**):

Yield 10 mg (0.008 mmol, 13 %).

^1H NMR (CD_2Cl_2) δ[ppm] = 1.75 (s, 15H, $C_5\underline{Me}_5$), 7.46 – 7.66 (m, 15H, $P\underline{Ph}_3$).

$^{13}C\{^1H\}$ NMR (CD_2Cl_2) δ[ppm] = 10.0 (s, $C_5\underline{Me}_5$), 103.7 (s, $\underline{C}_5Me_5$), 129.9 (s, $P\underline{Ph}_3$), 130.0 (s, $P\underline{Ph}_3$), 132.55 (s, $P\underline{Ph}_3$), 134.1 (s, $P\underline{Ph}_3$), 134.2 (s, $P\underline{Ph}_3$), 236.9 (s, CO), 242.4 (s, CO), 244.4 (s, CO).

$^{31}P\{^1H\}$ NMR (CD_2Cl_2) δ[ppm] = 44.0 (t, 1P, $^2J_{AM}$ = 103 Hz, Au-P_APh3), -16.8 (dt, 2P, $^1J_{MX}$ = 207 Hz, $^2J_{AM}$ = 103 Hz, P_M), -143.5 (sept, 1P, $^1J_{PF}$ = 710 Hz, PF_6), -302.6 (t, 2P, $^1J_{MX}$ = 206 Hz, P_X).

ES-MS (CH_2Cl_2) *m/z* [%] = 1125.3 (8.5) [M^+], 721.3 (100) [$(PPh_3)_2Au]^+$.

IR (KBr) $\tilde{\nu}$ [cm^{-1}] = 2004 (vs), 1991 (vs, sh), 1948 (s, sh), 1932 (vs, br), 1916 (s, sh).

Elemental analysis calcd. for $C_{44}H_{45}AuCr_2F_6O_6P_6$ (1270.62 g mol^{-1}) C 41.59, H 3.57; found C 41.21, H 3.75.

4.7.8 [{Cp'''Fe(CO)$_2$}$_2$(μ_3,$\eta^{1:1:1:1}$-P$_4$)FeBr$_2$] (72)

To a suspension of $FeBr_2$·dme (38 mg, 0.123 mmol) in dichloromethane (5ml) is given a solution of [{Cp'''Fe(CO)$_2$}$_2$(μ,$\eta^{1:1}$-P$_4$)] (**9b**) (100 mg, 0.123 mmol) in dichloromethane (5ml). The reaction mixture is stirred for 10 minutes resulting in a dark red colored solution. The solution is filtered via canula and concentrated in vacuum (2 ml). Storing the solution at -28 °C yields **72** as a dark red crystalline solid.

Analytical data for [{Cp'''Fe(CO)$_2$}$_2$(μ_3,$\eta^{1:1:1:1}$-P$_4$)FeBr$_2$] (**72**):

Yield 60 mg (0.058 mmol, 52 %).

^{1}H NMR (CD_2Cl_2) δ [ppm] = -3.44 (s br, 9H, -(C_4H_9)), -2.18 (s br, 18H, -(C_4H_9)$_2$).

Due to the paramagnetic character of the sample no ^{13}C or ^{31}P NMR spectra could be obtained.

Evans method μ_{eff} [μ_B] = 6.13.

Spin N = 5.2.

FD-MS (toluene) *m*/*z* [%] = 1283.3 (5) [{Cp'''Fe(CO)$_2$}$_3$P$_8$]$^+$, 1253.4 (10) [{Cp'''Fe(CO)$_2$}$_3$P$_8$ – CO – 2H]$^+$, 733.3 (100) [{Cp'''Fe}$_2$P$_5$]$^+$.

IR (KBr) $\tilde{\nu}$ [cm^{-1}] = 2029 (vs), 1983 (vs).

Elemental analysis calcd. for $C_{38}H_{58}Br_2Fe_3O_4P_4$·$(CH_2Cl_2)_{0.5}$ (1072.57 g mol^{-1}) C 43.11, H 5.54; found C 43.12, H 5.65.

4.7.9 $[\{\{Cp'''Fe(CO)_2\}_2(\mu_3,\eta^{1:1:1:1}\text{-}AsP_3)\}_2Cu]^+[BF_4]^-$ (73)

To a solution of $[Cu(MeCN)_4]^+[BF_4]^-$ (19 mg, 0.058 mmol) in dichloromethane (5 ml) is given a solution of $[\{Cp'''Fe(CO)_2\}_2(\mu,\eta^{1:1}\text{-}AsP_3)]$ (**51**) (100 mg, 0.116 mmol) in dichloromethane (5 ml). Upon addition the color of the reaction mixture turns dark purple. The reaction mixture is stirred for 16 hours at room temperature filtrated via canula and the solvent is removed under reduced pressure. The resulting dark solid is washed with hexane (5 ml) and dried in vacuum to afford **73** as dark red solid.

Analytical data for $[\{\{Cp'''Fe(CO)_2\}_2(\mu_3,\eta^{1:1:1:1}\text{-}AsP_3)\}_2Cu]^+[BF_4]^-$ (**73**):

Yield 59 mg (0.033 mmol, 55 %).

^{1}H NMR (CD_2Cl_2) δ[ppm] = 1.38 – 1.46 (mult. s, 54H, $C_5H_2{}^t\underline{Bu}_3$), 4.80 (s, 2H, $C_5\underline{H}_2{}^tBu_3$), 4.84 (br s, 2H, $C_5\underline{H}_2{}^tBu_3$).

^{13}C{^{1}H} NMR (CD_2Cl_2) δ[ppm] = 31.8 (s, -($\underline{C}(CH_3)_3$)), 31.8 (s, -($\underline{C}(CH_3)_3)_2$), 32.7 (s, -($\underline{C}(CH_3)_3)_2$), 32.8 (s, -($\underline{C}(CH_3)_3)_2$), 33.1 (s, -(C($\underline{C}H_3)_3$)), 33.3 (s, -(C($\underline{C}H_3)_3)_2$), 33.3 (s, -(C($\underline{C}H_3)_3)_2$), 33.7 (s, -(C($\underline{C}H_3)_3)_2$), 33.8 (s, -(C($\underline{C}H_3)_3)_2$), 33.9 (s, -(C($\underline{C}H_3)_3)_2$), 34.1 (s, -(C($\underline{C}H_3)_3)_2$), 87.4 (s, $\underline{C}_2H_2C^tBuC_2{}^tBu_2$), 88.7 (s, $\underline{C}_2H_2C^tBuC_2{}^tBu_2$), 109.1 (s, $C_2H_2\underline{C}^tBuC_2{}^tBu_2$), 109.9 (s, $C_2H_2\underline{C}^tBuC_2{}^tBu_2$), 111.1 (s, $C_2H_2C^tBu\underline{C}_2{}^tBu_2$), 111.2 (s, $C_2H_2C^tBu\underline{C}_2{}^tBu_2$), 111.8 (s, $C_2H_2C^tBu\underline{C}_2{}^tBu_2$), 112.2 (s, $C_2H_2C^tBu\underline{C}_2{}^tBu_2$), 213.7 (s, CO), 214.2 (s, CO), 214.4 (s, CO).

^{31}P{^{1}H} NMR (CD_2Cl_2) δ[ppm] = -96.9 (ddd, 1P, $^1J_{A'M'}$ = 193 Hz, $^1J_{A'N'}$ = 187 Hz, $^2J_{AA'}$ = 53 Hz, $P_{A'}$), -97.0 (ddd, 1P, $^1J_{AM}$ = 192 Hz, $^1J_{AN}$ = 187 Hz, $^2J_{AA'}$ = 53 Hz, P_A), -272.9 (dd, 1P, $^1J_{AM}$ = 192 Hz, $^1J_{MN}$ = 171 Hz, P_M), -272.9 (dd, 1P, $^1J_{A'M'}$ = 193 Hz, $^1J_{M'N'}$ = 175 Hz, $P_{M'}$), -273.7 (dd, 1P, $^1J_{AN}$ = 187 Hz, $^1J_{MN}$ = 171 Hz, P_N), -273.7 (dd, 1P, $^1J_{A'N'}$ = 187 Hz, $^1J_{M'N'}$ = 175 Hz, $P_{N'}$).

ES-MS (CH_2Cl_2) *m/z* [%] = 1780.0 (25) [M^+], 1724.0 (10) [M^+ - 2(CO)], 1175.5 (100) $[\{Cp'''Fe(CO)_2\}_2AsP_3\{Cp'''Fe(CO)\}]^+$.

IR (KBr) $\tilde{\nu}$ [cm^{-1}] = 2008 (vs), 1993 (vs), 1959 (vs).

Elemental analysis calcd. for $C_{76}H_{116}As_2BCuF_4Fe_4O_8P_6$ (1867.15 g mol^{-1}) C 48.89, H 6.26; found C 47.76, H 6.19.

4.7.10 [{{Cp*Cr(CO)$_3$}$_2$(μ_3,$\eta^{1:1:1:1}$-AsP$_3$)}$_2$Cu]$^+$[BF$_4$]$^-$ (74)

To a solution of $[Cu(MeCN)_4]^+[BF_4]^-$ (17 mg, 0.053 mmol) in dichloromethane (5 ml) is given a solution of [{Cp*Cr(CO)$_3$}$_2$(μ,$\eta^{1:1}$-AsP$_3$)] (**55**) (75 mg, 0.105 mmol) in dichloromethane (5 ml). Upon addition the color of the reaction mixture turns bright red. The reaction mixture is stirred for 16 hours at room temperature and the solvent is removed under reduced pressure. The resulting solid is washed with hexane (5 ml) and dried in vacuum. The crude product is taken up in THF (5 ml) and layered with hexane (6 ml) to yield **74** as reddish orange crystals, suitable for X-ray structure determination.

Analytical data for [{{Cp*Cr(CO)$_3$}$_2$(μ_3,$\eta^{1:1:1:1}$-AsP$_3$)}$_2$Cu]$^+$[BF$_4$]$^-$ (**74**):

Yield 10 mg (0.006 mmol, 11 %).

^{1}H NMR (CD_2Cl_2) δ [ppm] = 1.94 (s, 15H, $C_5Me_5^P$), 1.95 (s, 15H, $C_5Me_5^{As}$).

^{13}C{^{1}H} NMR (CD_2Cl_2) δ [ppm] = 10.8 (s, $C_5\underline{Me}_5$), 102.7 (s, $\underline{C}_5Me_5$), 103.8 ($\underline{C}_5Me_5$).

^{31}P{^{1}H} NMR (CD_2Cl_2) δ [ppm] = -104.9 (ddd, 1P, $^1J_{AM}$ = 197 Hz, $^1J_{AN}$ = 199 Hz, $^2J_{AA'}$ = 61 Hz, P_A), -105.0 (ddd, 1P, $^1J_{A'M'}$ = 196 Hz, $^1J_{A'N'}$ = 199 Hz, $^2J_{AA'}$ = 61 Hz, $P_{A'}$), -273.0 (dd, 1P, $^1J_{AM}$ = 197 Hz, $^1J_{MN}$ = 173 Hz, P_M), -273.0 (dd, 1P, $^1J_{A'M'}$ = 196 Hz, $^1J_{M'N'}$ = 173 Hz, $P_{M'}$), -277.6 (dd, 1P, $^1J_{AN}$ = 199 Hz, $^1J_{MN}$ = 173 Hz, P_N), -277.6 (dd, 1P, $^1J_{A'N'}$ = 199 Hz, $^1J_{M'N'}$ = 173 Hz, $P_{N'}$).

ES-MS (CH_2Cl_2) *m*/*z* [%] = 1003.1 (100) $[Cp^*_4Cr_4AsP_3(CO)_3 + 3H]^+$.

IR (KBr) $\tilde{\nu}$ [cm^{-1}] = 1996 (vs), 1979 (vs), 1910 (vs, br).

Elemental analysis calcd. for $C_{52}H_{60}As_2BCr_4CuF_4O_{12}P_6$ (1571.05 g mol^{-1}) C 39.75, H 3.85; found C 39.59, H 4.07.

4.7.11 $[\{\{Cp'''Fe(CO)_2\}_2(\mu_3,\eta^{1:1:1:1}\text{-}AsP_3)\}_2Ag]^+[PF_6]^-$ (75)

To a solution of $Ag^+PF_6^-$ (11 mg, 0.044 mmol) in dichloromethane (5 ml) is given a solution of $[\{Cp'''Fe(CO)_2\}_2(\mu,\eta^{1:1}\text{-}AsP_3)]$ (**51**) (75 mg, 0.087 mmol) in dichloromethane (5 ml). The reaction mixture is stirred for 16 hours at room temperature and the solvent is removed under reduced pressure. The resulting solid is washed with hexane (5 ml) and dried in vacuum. The crude product is taken up in THF (4 ml) and layered with hexane (4 ml) to yield **75** as orange crystals, suitable for X-ray structure determination.

Analytical data for $[\{\{Cp'''Fe(CO)_2\}_2(\mu_3,\eta^{1:1:1:1}\text{-}AsP_3)\}_2Ag]^+(PF_6)^-$ (**75**):

Yield 11 mg (0.006 mmol, 14 %).

^{1}H NMR (CD_2Cl_2) δ [ppm] = 1.39 (s, 9H, -(C_4H_9)), 1.41 (s, 9H, -(C_4H_9)), 1.43 (s, 18H, -(C_4H_9)$_2$), 1.44 (s, 18H, -(C_4H_9)$_2$), 4.78 (s, 2H, $C_5\underline{H}_2{}^tBu_3$), 4.81 (br s, 2H, $C_5\underline{H}_2{}^tBu_3$).

^{13}C{^{1}H} NMR (CD_2Cl_2) δ [ppm] = 32.0 (s, -($\underline{C}(CH_3)_3$)), 32.6 (s, -($\underline{C}(CH_3)_3$)$_2$), 33.3 (s, -(C($\underline{C}H_3$)$_3$)), 34.0 (s, -(C($\underline{C}H_3$)$_3$)$_2$), 87.6 (s, $\underline{C}_2H_2C^tBuC_2{}^tBu_2$), 89.3 (s, $\underline{C}_2H_2C^tBuC_2{}^tBu_2$), 109.0 (s, $C_2H_2\underline{C}^tBuC_2{}^tBu_2$), 109.7 (s, $C_2H_2C^tBu\underline{C}_2{}^tBu_2$), 111.1 (s, $C_2H_2C^tBu\underline{C}_2{}^tBu_2$), 213.5 (s, CO), 214.1 (s, CO).

^{31}P{^{1}H} NMR (CD_2Cl_2) δ [ppm] = -85.3 (br dt, 2P, $^1J_{AM}$ = 200 Hz, $^1J_{PAg}$ = 305 Hz, P_A), -143.9 (sept, 1P, $^1J_{PF}$ = 710 Hz, PF_6^-), -293.9 (d, 2P, $^1J_{AM}$ = 200 Hz, P_M), -294.1 (d, 2P, $^1J_{AM}$ = 200 Hz, P_M).

ES-MS (CH_2Cl_2) *m*/*z* [%] = 1768.7 (4) [M^+ - 2CO], 1747.4 (75) $[\{Cp'''Fe(CO)_2\}_2AsP_3\{Cp'''Fe\}]^+$, 831.2 (100) $[\{Cp'''Fe(CO)_2\}AsP_3\{Cp'''Fe(CO)\}]^+$.

IR (KBr) $\tilde{\nu}$ [cm^{-1}] = 2009 (vs), 1993 (vs), 1959 (vs, br).

Elemental analysis calcd. for $C_{76}H_{116}AgAs_2F_6Fe_4O_8P_7$ (1969.63 g mol^{-1}) C 46.34, H 5.94; found C 44.24, H 5.82.

4.7.12 [{{Cp*Cr(CO)$_3$}$_2$(μ_3,$\eta^{1:1:1:1}$-AsP$_3$)}$_2$Ag]$^+$[PF$_6$]$^-$ (76)

To a solution of $AgPF_6$ (8 mg, 0.030 mmol) in dichloromethane (5 ml) is given a solution of [{Cp*Cr(CO)$_3$}$_2$(μ,$\eta^{1:1}$-AsP$_3$)] (**55**) (40 mg, 0.056 mmol) in dichloromethane (5 ml). The reaction mixture is stirred for 16 hours at room temperature and the solvent is removed under reduced pressure. The resulting solid is washed with hexane (5 ml) and dried in vacuum. The crude product is taken up in THF (5 ml) and layered with hexane (6 ml) to yield **76** as orange crystals, suitable for X-ray structure determination.

Analytical data for [{{Cp*Cr(CO)$_3$}$_2$(μ_3,$\eta^{1:1:1:1}$-AsP$_3$)}$_2$Ag]$^+$[PF$_6$]$^-$ (**76**):

Yield 15 mg (0.009 mmol, 32 %).

^{1}H NMR (CD_2Cl_2) δ [ppm] = 1.91 (s, 15H, $C_5Me_5^P$), 1.92 (s, 15H, $C_5Me_5^{As}$).

^{13}C{^{1}H} NMR (CD_2Cl_2) δ [ppm] = 10.5 (s, $C_5\underline{Me}_5$), 10.6 (s, $C_5\underline{Me}_5$) 102.5 (s, $\underline{C}_5Me_5$), 103.4 ($\underline{C}_5Me_5$), 238.0 (s, CO), 244.7 (s, CO).

^{31}P{^{1}H} NMR (CD_2Cl_2) δ [ppm] = -92.7 (dddd, 1P, $^1J_{AM}$ = 212 Hz, $^1J_{AN}$ = 208 Hz, $^1J_{PAg107}$ = 273 Hz, $^2J_{AA'}$ = 34 Hz, P_A), -92.7 (ddd, 1P, $^1J_{AM}$ = 212 Hz, $^1J_{AN}$ = 208 Hz, $^1J_{PAg109}$ = 310 Hz, $^2J_{AA'}$ = 34 Hz, P_A), -92.7 (ddd, 1P, $^1J_{A'M'}$ = 214 Hz, $^1J_{A'N'}$ = 209 Hz, $^1J_{PAg107}$ = 267 Hz, $^2J_{AA'}$ = 34 Hz, $P_{A'}$), -92.7 (ddd, 1P, $^1J_{A'M'}$ = 214 Hz, $^1J_{A'N'}$ = 209 Hz, $^1J_{PAg109}$ = 305 Hz, $^2J_{AA'}$ = 34 Hz, $P_{A'}$), -295.9 (dd, 1P, $^1J_{AM}$ = 212 Hz, $^1J_{MN}$ = 167 Hz, P_M), -295.9 (dd, 1P, $^1J_{A'M'}$ = 214 Hz, $^1J_{M'N'}$ = 167 Hz, $P_{M'}$), -300.4 (dd, 1P, $^1J_{AN}$ = 208 Hz, $^1J_{MN}$ = 167 Hz, P_N), -300.4 (dd, 1P, $^1J_{A'N'}$ = 209 Hz, $^1J_{M'N'}$ = 167 Hz, $P_{N'}$).

ES-MS (CH_2Cl_2) m/z [%] = 1528.4 (100) [M^+].

IR (KBr) $\tilde{\nu}$ [cm^{-1}] = 1998 (vs), 1979 (vs), 1916 (vs, br).

Elemental analysis calcd. for $C_{52}H_{60}AgAs_2Cr_4F_6O_{12}P_7$ 1673.53 g mol^{-1}) C 37.32, H 3.61; found C 35.70, H 3.72.

4.7.13 $[\{Cp'''Fe(CO)_2\}_2(\mu_3,\eta^{1:1:1:1}\text{-}AsP_3)\{Au(PPh_3)\}]^+[PF_6]^-$ (77)

To a solution of $[(PPh_3)Au(tht)]^+[PF_6]^-$ (57 mg, 0.082 mmol) in dichloromethane (5 ml) is given a solution of $[\{Cp'''Fe(CO)_2\}_2(\mu,\eta^{1:1}\text{-}AsP_3)]$ (**51**) (70 mg, 0.082 mmol) in dichloromethane (5 ml). Upon addition the color of the reaction mixture turns red. The reaction mixture is stirred for 16 hours at room temperature filtrated via canula and the solvent is removed under reduced pressure. The resulting dark solid is washed with hexane (5 ml) and dried in vacuum to give **77** as red solid.

Analytical data for $[\{Cp'''Fe(CO)_2\}_2(\mu_3,\eta^{1:1:1:1}\text{-}AsP_3)\{Au(PPh_3)\}]^+[PF_6]^-$ (**77**):

Yield 74 mg (0.051 mmol, 61 %).

^{1}H NMR (CD_2Cl_2) δ[ppm] = 1.14 (s, 9H, -$(C_4H_9)^{As}$), 1.30 (s, 18H, -$(C_4H_9)_2{}^{P}$), 1.32 (s, 9H, -$(C_4H_9)^{P}$), 1.35 (s, 18H, -$(C_4H_9)_2{}^{As}$), 4.61 (s, 2H, $C_5\underline{H}_2{}^t Bu_3{}^{P}$), 4.78 (s,1H, $C_5\underline{H}_2{}^t Bu_3{}^{As}$), 4.79 (s,1H, $C_5\underline{H}_2{}^t Bu_3{}^{As}$), 7.44 – 7.67 (m, 15 H PPh_3).

^{13}C{^{1}H} NMR (CD_2Cl_2) δ[ppm] = 31.4 (s, -$(\underline{C}(CH_3)_3)^{P}$), 31.8 (s, -$(\underline{C}(CH_3)_3)^{As}$), 31.9 (s, -$(\underline{C}(CH_3)_3)_2{}^{P}$), 32.0 (s, -$(\underline{C}(CH_3)_3)_2{}^{As}$), 33.1 (s, -$(C(\underline{C}H_3)_3)^{P}$), 33.1 (s, -$(C(\underline{C}H_3)_3)^{As}$), 33.7 (s, -$(C(\underline{C}H_3)_3)_2{}^{P}$), 33.7 (s, -$(C(\underline{C}H_3)_3)_2{}^{As}$), 88.3(s, $\underline{C}_2H_2C^tBuC_2{}^tBu_2{}^{As}$), 91.9 (s, $\underline{C}_2H_2C^tBuC_2{}^tBu_2{}^{P}$), 109.0 (s, $C_2H_2\underline{C}^tBuC_2{}^tBu_2{}^{As}$), 110.3 (s, $C_2H_2\underline{C}^tBuC_2{}^tBu_2{}^{P}$), 111.0 (s, $C_2H_2C^tBu\underline{C}_2{}^tBu_2{}^{As}$), 112.1 (s, $C_2H_2C^tBu\underline{C}_2{}^tBu_2{}^{P}$), 212.4 (s, CO), 212.5 (s, CO), 214.1 (s, CO).

^{31}P{^{1}H} NMR (CD_2Cl_2) δ[ppm] = 41.2 (d, 1P, $^2J_{AM}$ = 248 Hz, Au-P_APh_3), -49.6 (dt, 1P, $^2J_{AM}$ = 248 Hz, $^1J_{MX}$ = 213 Hz, P_M), -143.8 (sept, 1P, $^1J_{PF}$ = 710 Hz, PF_6^-), -287.3 (d, 2P, $^1J_{MX}$ = 213 Hz, P_X).

ES-MS (CH_2Cl_2) *m/z* [%] = 1317.6 (100) [M^+], 944.4 (10) $[\{(Cp'''Fe(CO)_2)_2AsP_3\}_2Au - CO]^{2+}$, 721.2 (80) $[(PPh_3)_2Au]^+$.

IR (KBr) $\tilde{\nu}$ [cm^{-1}] = 2018 (vs), 1990 (vs), 1973 (vs, sh), 1947 (vs).

Elemental analysis calcd. for $C_{56}H_{73}AsAuF_6Fe_2O_4P_5$ (1462.61 g mol^{-1}) C 45.99, H 5.03; found C 45.40, H 5.02

4.7.14 $[\{Cp^*Cr(CO)_3\}_2(\mu_3,\eta^{1:1:1:1}\text{-}AsP_3)\{Au(PPh_3)\}]^+[PF_6]^-$ (78)

To a solution of $[(PPh_3)Au(tht)]^+[PF_6]^-$ (73 mg, 0.105 mmol) in dichloromethane (5 ml) is given a solution of $[\{Cp^*Cr(CO)_3\}_2(\mu,\eta^{1:1}\text{-}AsP_3)]$ (**55**) (75 mg, 0.105 mmol) in dichloromethane (5 ml). Upon addition the color of the solution turns bright red. The reaction mixture is stirred for 16 hours at room temperature and the solvent is removed under reduced pressure. The resulting dark solid is washed with hexane (5 ml) and dried in vacuum. The crude product is taken up in THF and dichloromethane (5 + 5 ml) and layered with hexane (10 ml) to yield **78** as orange crystals, suitable for X-ray structure determination.

Analytical data for $[\{Cp^*Cr(CO)_3\}_2(\mu_3,\eta^{1:1:1:1}\text{-}AsP_3)\{Au(PPh_3)\}]^+[PF_6]^-$ (**78**):

Yield 75 mg (0.057 mmol, 54 %).

^{1}H NMR (CD_2Cl_2) δ[ppm] = 1.68 (s, 15H, $C_5Me_5^P$), 1.88 (s, 15H, $C_5Me_5^{As}$), 7.48 – 7.67 (m, 15H, Au-PPh_3).

^{13}C{^{1}H} NMR (CD_2Cl_2) δ[ppm] = 10.1 (s, $C_5\underline{Me}_5$), 10.3 (s, $C_5\underline{Me}_5$), 10.3 (s, $C_5\underline{Me}_5$), 102.4 (s, $\underline{C}_5Me_5$), 104.4 (s, $\underline{C}_5Me_5$), 130.1 (s, PPh_3), 130.2 (s, PPh_3), 132.8 (s, PPh_3), 134.3 (s, PPh_3), 134.4 (s, PPh_3).

^{31}P{^{1}H} NMR (CD_2Cl_2) δ[ppm] = 43.1 (br s, 1P, Au-$\underline{P}_APh_3$), -47.4 (br t, 1P, $^1J_{MX}$ = 222 Hz, P_M), -143.9 (sept, 1P, $^1J_{PF}$ = 710 Hz, PF_6^-), -290.0 (d, 2P, $^1J_{MX}$ = 222 Hz, P_X).

^{31}P{^{1}H} NMR (193 K) δ[ppm] = 41.9 (d, 1P, $^2J_{AM}$ = 241 Hz, Au-$\underline{P}_APh_3$), -45.8 (dt, 1P, $^1J_{MX}$ = 229 Hz, $^2J_{AM}$ = 235 Hz, P_M), -143.9 (sept, 1P, $^1J_{PF}$ = 710 Hz, PF_6^-), -291.5 (d, 2P, $^1J_{MX}$ = 224 Hz, P_X).

ES-MS (CH_2Cl_2) *m*/*z* [%] = 1169.3 (0.5) [M^+], 983.3 (4) $[(PPh_3)_3Au]^+$, 721.2 (100) $[(PPh_3)_2Au]^+$.

IR (KBr) $\tilde{\nu}$ [cm^{-1}] = 2009 (vs), 1980 (vs), 1946 (vs, sh), 1933 (vs), 1904 (vs, sh).

Elemental analysis calcd. for $C_{44}H_{45}AsAuCr_2F_6O_6P_5$ (1314.56 g mol^{-1}) C 40.20, H 3.45; found C 39.96, H 3.50.

4.7.15 $[\{\{Cp'''Fe(CO)_2\}_2(\mu_3,\eta^{1:1:1:1}\text{-}As_4)\}_2Cu]^+[BF_4]^-$ (79)

To a solution of $[Cu(MeCN)_4]^+[BF_4]^-$ (16 mg, 0.05 mmol) in dichloromethane (5 ml) is given a solution of $[\{Cp'''Fe(CO)_2\}_2(\mu,\eta^{1:1}\text{-}As_4)]$ (**52**) (100 mg, 0.101 mmol) in dichloromethane (5 ml). Upon addition the color of the solution changes to dark red. The reaction mixture is stirred for 16 hours at room temperature and the solvent is removed under reduced pressure. The resulting solid is washed with hexane (5 ml) and dried in vacuum. The crude product is taken up in THF (3 ml) and layered with hexane (6 ml) to yield **79** as dark purple crystals, suitable for X-ray structure determination.

Analytical data for $[\{\{Cp'''Fe(CO)_2\}_2(\mu_3,\eta^{1:1:1:1}\text{-}As_4)\}_2Cu]^+[BF_4]^-$ (**79**):

Yield 57 mg (0.026 mmol, 52 %).

^{1}H NMR (CD_2Cl_2) δ [ppm] = 1.42 (s, 9H, -(C_4H_9)), 1.44 (s, 18H, -(C_4H_9)$_2$), 4.83 (s, 2H, $C_5\underline{H}_2{}^tBu_3$).

^{13}C{^{1}H} NMR (CD_2Cl_2) δ [ppm] = 31.8 (s, -($\underline{C}(CH_3)_3$)), 33.0 (s, -($\underline{C}(CH_3)_3$)$_2$), 33.4 (s, -($C(\underline{C}H_3)_3$)), 34.1 (s, -($C(\underline{C}H_3)_3$)$_2$), 87.3 (s, $\underline{C}_2H_2C^tBuC_2{}^tBu_2$), 109.3 (s, $C_2H_2\underline{C}^tBuC_2{}^tBu_2$), 111.2 (s, $C_2H_2C^tBu\underline{C}_2{}^tBu_2$), 214.6 (s, CO).

ES-MS (CH_2Cl_2) *m*/*z* [%] = 1961.2 (0.5) [M – 3 CO]$^+$, 1614.0 (5) $[(Cp'''Fe)_3As_8Cu(CO)_3]^+$, 1586.1 (5) $[(Cp'''Fe)_3As_8Cu(CO)_2]^+$, 1417.3 (4) $[(Cp'''Fe)_2As_7Cu(CO)_9]^+$, 1279.4 (7) $[\{Cp'''Fe(CO)_2\}_2As_4\{Cp'''Fe\}]^+$, 953.0 (100) $[\{Cp'''Fe\}_2As_5]^+$, 906.1 (10) $[\{Cp'''Fe(CO)_2\}_2As_4 - (CO)]^+$.

IR (KBr) $\tilde{\nu}$ [cm^{-1}] = 1991 (vs), 1953 (vs).

Elemental analysis calcd. for $C_{76}H_{116}As_8BCuF_4Fe_4O_8$ (2130.83 g mol^{-1}) C 42.84, H 5.49; found C 42.39, H 5.52.

4.7.16 $[\{\{Cp'''Fe(CO)_2\}_2(\mu_3,\eta^{1:1:1:1}\text{-}As_4)\}_2Ag]^+[PF_6]^-$ (80)

To a solution of $Ag^+PF_6^-$ (13 mg, 0.05 mmol) in dichloromethane (5 ml) is given a solution of $[\{Cp'''Fe(CO)_2\}_2(\mu,\eta^{1:1}\text{-}As_4)]$ (**52**) (100 mg, 0.101 mmol) in dichloromethane (5 ml). The reaction mixture is stirred for 16 hours at room temperature and the solvent is removed under reduced pressure. The resulting solid is washed with hexane (5 ml) and dried in vacuum. The

crude product is taken up in THF (3 ml) and layered with hexane (6 ml) to yield **80** as orange crystals, suitable for X-ray structure determination.

Analytical data for $[\{\{Cp'''Fe(CO)_2\}_2(\mu_3,\eta^{1:1:1:1}\text{-}As_4)\}_2Ag]^+[PF_6]^-$ (**80**):

Yield 97 mg (0.043 mmol, 86 %).

^{1}H NMR (CD_2Cl_2) δ[ppm] = 1.39 (s, 9H, -(C_4H_9)), 1.43 (s, 18H, -(C_4H_9)$_2$), 4.81 (s, 2H, $C_5\underline{H}_2{}^tBu_3$).

^{13}C{^{1}H} NMR (CD_2Cl_2) δ[ppm] = 32.0 (s, -($\underline{C}(CH_3)_3$)), 32.8 (s, -($\underline{C}(CH_3)_3$)$_2$), 33.4 (s, -(C($\underline{C}H_3$)$_3$)), 34.1 (s, -(C($\underline{C}H_3$)$_3$)$_2$), 87.7 (s, $\underline{C}_2H_2C^tBuC_2{}^tBu_2$), 109.2 (s, $C_2H_2\underline{C}^tBuC_2{}^tBu_2$), 111.1 (s, $C_2H_2C^tBu\underline{C}_2{}^tBu_2$), 214.5 (s, CO).

ES-MS (CH_2Cl_2) *m/z* [%] = 1943.7 (1.8) $[(Cp'''Fe)_4As_8Ag_2 - C_2H_4]^{2+}$, 1849.7 (1) $[(Cp'''Fe)_3As_8Ag_2(CO)_6]^+$, 1307.5 (30) $[\{Cp'''Fe(CO)_2\}_2As_4\{Cp'''Fe(CO)\}]^+$, 1279.4 (100) $[\{Cp'''Fe(CO)_2\}_2As_4\{Cp'''Fe\}]^+$, 1251.5 (40) $[\{Cp'''Fe(CO)_2\}_2As_4 - CO]^+$, 953.1 (40) $[(Cp'''Fe)_2As_5]^+$.

IR (KBr) $\tilde{\nu}$ [cm^{-1}] = 1998 (vs), 1954 (vs).

Elemental analysis calcd. for $C_{76}H_{116}AgAs_8F_6Fe_4O_8P\cdot(C_4H_8O)_2$ (2377.53 g mol^{-1}) C 42.43, H 5.60; found C 42.15, H 5.59.

4.7.17 $[\{\{Cp^*Cr(CO)_3\}_2(\mu_3,\eta^{1:1:1:1}\text{-}As_4)\}_2Ag]^+[PF_6]^-$ (81)

To a solution of $AgPF_6$ (15 mg, 0.060 mmol) in dichloromethane (5 ml) is given a solution of $[\{Cp^*Cr(CO)_3\}_2(\mu,\eta^{1:1}\text{-}As_4)]$ (**56**) (100 mg, 0.119 mmol) in dichloromethane (5 ml). The reaction mixture is stirred for 16 hours at room temperature and the solvent is removed under reduced pressure. The resulting solid is washed with hexane (5 ml) and dried in vacuum. The crude product is taken up in THF and dichloromethane (3 + 2 ml) and layered with hexane (6 ml) to yield **81** as orange crystals, suitable for X-ray structure determination.

Analytical data for $[\{\{Cp^*Cr(CO)_3\}_2(\mu_3,\eta^{1:1:1:1}\text{-}As_4)\}_2Ag]^+(PF_6)^-$ (**81**):

Yield 45 mg (0.023 mmol, 38 %).

^{1}H NMR (CD_2Cl_2) δ[ppm] = 1.91 (s, 15H, $C_5\underline{Me}_5$).

$^{13}C\{^1H\}$ NMR (CD_2Cl_2) δ [ppm] = 10.7 (s, $C_5\underline{Me}_5$), 102.7 (s, $\underline{C}_5Me_5$), 238.8 (s, CO), 244.8 (s, CO).

$^{31}P\{^1H\}$ NMR (CD_2Cl_2) δ [ppm] = -143.7 (sept, 1P, $^1J_{PF}$ = 710 Hz, PF_6).

ES-MS (CH_2Cl_2) *m/z* [%] = 1793.1 (15) [M^+], 1418.8 (30) [$(Cp^*Cr)_4As_8Ag - C_3H_2]^+$.

IR (KBr) $\tilde{\nu}$ [cm^{-1}] = 1982 (vs, br), 1906 (vs, br).

Elemental analysis calcd. for $C_{52}H_{60}AgAs_8Cr_4F_6O_{12}P$ (1937.22 g mol^{-1}) C 32.24, H 3.12; found C 32.05, H 3.11.

4.8 Complexes of yellow arsenic

4.8.1 $[Ag(\eta^2\text{-}As_4)_2]^+[pftb]^-$ (82)

To a solution of $[Ag(CH_2Cl_2)]^+[pftb]^-$ (0.350 g, 0.3 mmol) in dichloromethane (10 ml) is given a freshly prepared solution of As_4 in toluene (250 ml, 3.6 mmol/l, 270 mg, 0.9 mmol) at room temperature. Under the exclusion of light the reaction mixture is stirred for 30 min. The reaction mixture can then be exposed to light and the solvent is removed in vacuum to give crude **82** together with grey arsenic. Dichloromethane (20 ml) is added and the yellowish solution is filtered through a plug of cellite. Again, all volatiles are removed in vacuum. This procedure is repeated until no grey arsenic is formed during the removal of the solvent. The resulting colorless powder is washed 3 times with hexane (20 ml) and dried in vacuum. Colorless crystals of **82** suitable for X-ray structure analysis are grown from a saturated dichloromethane solution upon cooling to -28 °C or by slow diffusion of hexane (20 ml) into a saturated solution of **82** in dichloromethane (1 ml) at -28 °C.

Analytical data for $[Ag(\eta^2\text{-}As_4)_2]^+[pftb]^-$ (**82**)

Yield 452 mg (0.270 mmol, 90 %).

$^{13}C\{^1H\}$ NMR (CD_2Cl_2) δ [ppm] = 121.6 (q, $^1J_{CF}$ = 294 Hz, $C(\underline{C}F_3)_3$).

$^{19}F\{^1H\}$ NMR (CD_2Cl_2) δ [ppm] = -75.6 (s, $C(C\underline{F}_3)_3$).

^{27}Al{^{1}H} NMR (CD_2Cl_2) δ [ppm] = 33.6 (s, $Al(OR)_4$).

Cation **ESI-MS** (CH_2Cl_2) *m*/*z* [%] = 706.3 (25)$[Ag(As_4)_2]^+$, 406.4 (100) $[Ag(As_4)]^+$.

Anion **ESI-MS** (CH_2Cl_2) *m*/*z* [%] = 967.1 (100) $[Al\{OC(CF_3)_3\}_4]^-$.

Raman: $\tilde{\nu}$ [cm^{-1}] = 210, 265, 343.

Elemental analysis calcd. for $C_{16}AgAlAs_8F_{36}O_4$ (1674.33 g mol^{-1}) C 11.48, H 0.0; found C 12.37, H 0.10.

4.8.2 $[(PPh_3)Au(\eta^2\text{-}As_4)]^+[pftb]^-$ (83)

To a solution of $[Ag(\eta^2\text{-}As_4)_2]^+[pftb]^-$ (**82**) (150 mg, 0.0896 mmol) in dichloromethane (5 ml) is added a solution of $[(PPh_3)AuCl]$ (44 mg, 0.0896 mmol) at room temperature. Upon the addition a beige colored precipitate of AgCl is formed. Under the exclusion of light, the reaction mixture is stirred for 15 min and the solvent is removed in vacuo. The resulting dark solid is taken up in dichloromethane (5ml) and filtered through a plug of cellite. After removal of the solvent **83** is obtained as an air- and moisture sensitive yellowish powder. Colorless crystals suitable for X-ray crystallography are grown by slow diffusion of hexane (10 ml) into a solution of **83** in dichloromethane (2ml) at -28 °C.

Analytical data for $[(PPh_3)Au(\eta^2\text{-}As_4)]^+[pftb]^-$ (**83**):

Yield 109 mg (0.063 mmol, 70 %).

^{1}H NMR (CD_2Cl_2) δ [ppm] = 7.58 (m, 15 H, $P(C_6\underline{H}_5)_3$).

^{13}C{^{1}H} NMR (CD_2Cl_2) δ [ppm] = 121.6 (q, $C(\underline{C}F_3)_3$, $^{1}J_{CF}$ = 293 Hz), 127.5 (m, C_4 PC_6H_5), 130.3 (m, C_3 PC_6H_5), 133.3 (dm, $C_1PC_6H_5$, $^{1}J_{PC}$ = 15 Hz), 134.5 (m, C_2 PC_6H_5).

^{19}F{^{1}H} NMR (CD_2Cl_2) δ [ppm] = -75.6 (s, $C(C\underline{F}_3)_3$).

^{31}P{^{1}H} NMR (CD_2Cl_2) δ [ppm] = 45.6 (s,1P, $\underline{P}Ph_3$).

Cation **ESI-MS** (CH_2Cl_2) *m*/*z* [%] = 721.2 (100) $[(PPh_3)_2Au]^+$.

Anion **ESI-MS** (CH_2Cl_2) *m*/*z* [%] = 967.1 (100) $[Al\{OC(CF_3)_3\}_4]^-$.

Elemental analysis calcd. for $C_{34}H_{15}AlAs_4AuF_{36}O_4P$ (1726.03 g mol^{-1}) C 23.66, H 0.88; found C 24.03, H 0.93.

4.8.3 [Cp*Ru(dppe)(η^1-As_4)]$^+$[pftb]$^-$ (84)

To a solution of [Cp*Ru(dppe)Cl] (60 mg, 0.0895 mmol) in dichloromethane (5ml) at -30 °C is given a solution of [Ag(η^2-As_4)$_2$]$^+$[pftb]$^-$ (**82**) (150 mg, 0.0895 mmol) in dichloromethane (5 ml) within 10 minutes under the exclusion of light. The reaction mixture is stirred for 15 minutes during which the color changes from bright orange to dark red and a pale precipitate is formed. The solvent is removed in vacuo and the resulting dark red solid is taken up in dichloromethane (2 ml). The solution is filtered via canula, layered under hexane (10 ml) and stored at -30 °C for 24 h. Compound **84** is obtained as orange crystals, suitable for X-ray structure analysis**.**

Analytical data for [Cp*Ru(dppe)(η^1-As_4)]$^+$[pftb]$^-$ (**84**):

Yield 107 mg (0.056 mmol, 63 %).

^{1}H NMR (CD_2Cl_2) δ [ppm] = 1.52 (t, $^4J_{HP}$ = 1.65 Hz, 15 H, C_5Me_5), 2.35 – 2.75 (m, 4H, $(CH_2)_2$), 7.22 – 7.58 (m, 20 H, $(C_6H_5)_4$).

^{13}C{^{1}H} NMR (CD_2Cl_2) δ [ppm]: 10.4 (s, $C_5\underline{Me}_5$), 28.6 (d, $^1J_{CP}$ = 24 Hz, $(CH_2)_2$), 28.8 (d, *J*(C, P) = 22 Hz, $(CH_2)_2$), 94.5 (s, $\underline{C}_5Me_5$), 121.7 (q, $^1J_{CF}$ = 292.3 Hz, -C($\underline{C}F_3$)$_3$), 129.3 (mult. s, $C_3C_4C_5$), 129.7 (mult. s, C_2C_6), 131.4 (d, $^1J_{CP}$= 9 Hz, C_1C_1'), 132.3 (mult. s, C_3'C_4'C_5'), 132.7 (mult. s, C_2'C_6').

^{19}F{^{1}H} NMR (CD_2Cl_2) δ [ppm] = -75.58 (s, -C($C\underline{F}_3$)).

^{31}P{^{1}H} NMR (CD_2Cl_2) δ [ppm] = 69.88 (s, dppe).

Cation **ESI-MS** (CH_2Cl_2) *m*/*z* [%] = 635.1 (100) [Cp*Ru(dppe)]$^+$.

Anion **ESI-MS** (CH_2Cl_2) *m*/*z* [%] = 967.0 (100) [Al{OC($C\underline{F}_3$)$_3$}$_4$]$^-$.

Elemental analysis calcd. for $C_{52}H_{39}AlAs_4F_{36}O_4P_2Ru$ (1901.49 g mol^{-1}) C 32.85, H 2.07; found: C32.69, H 2.07.

4.8.4 [{Cp*Ru(dppe)}(μ,η$^{1:3}$-As$_4$){CpRu(PPh$_3$)}]$^{2+}$[pftb]$^-_2$ (85)

To a solution of [CpRu(PPh$_3$)$_2$Cl] (50 mg, 0.0263 mmol) in dichloromethane (5ml) is given a solution of Tl[pftb] (31 mg, 0.0263 mmol) in dichloromethane (5ml). The solution is stirred for 10 minutes during which a pale precipitate forms. The solution is filtered via canula and given to a solution of **84** (50 mg, 0.0263 mmol) in dichloromethane (5 ml). The reaction mixture is stirred for 10 min during which the color changes from dark red to brown. The solution is reduced to about 2 ml under reduced pressure, filtered via canula and carefully layered under hexane (10 ml). Storing at -30 °C for 24 h affords **85** as dark brown crystals suitable for X-ray structure analysis.

Analytical data for [{Cp*Ru(dppe)}(μ$_2$,η$^{1:3}$-As$_4$){CpRu(PPh$_3$)}]$^{2+}$[pftb]$^-_2$ (**85**):

Yield	50 mg (0.015 mmol, 57 %).
^{1}H NMR (CD_2Cl_2)	δ [ppm] = 1.39 (s, 15 H, C_5Me_5), 2.45 – 2.95 (m, 4H, $(CH_2)_2$), 4.72 (s, 5H, C_5H_5), 7.85 – 7.80 (m, 35 H, dppe/PPh_3).
^{13}C{^{1}H} NMR (CD_2Cl_2)	δ [ppm]: 10.38 (s, $C_5\underline{Me}_5$), 29.4 (t, $^1J_{CP}$ = 24 Hz, $(CH_2)_2$), 29.7 (t, $^1J_{CP}$ = 22 Hz, $(CH_2)_2$), 85.6 (s, C_5H_5), 88.5 (s, C_5H_5), 88.7 (s, C_5H_5), 89.9 (s, C_5H_5), 98.9 (s, $\underline{C}_5Me_5$), 121.68 (q, $^1J_{CP}$ = 292.5 Hz, -C($\underline{C}F_3)_3$), 128.42 – 135.20 (mult. s, -(C_6H_5)).
^{19}F{^{1}H} NMR (CD_2Cl_2)	δ [ppm] = -75.53 (s, -C($C\underline{F}_3$)).
^{31}P{^{1}H} NMR (CD_2Cl_2)	δ [ppm] = 12.35 (br s,1 P, PPh_3), 32.91 (s, 1 P, Ru-(PPh_3)), 72.57 (s, 2 P, dppe).
Cation **ESI-MS** (CH_2Cl_2)	*m*/*z* [%] = 1450.4 (3) $[M\cdot(EtCO_2Me)]^+$, 710.1 (12) $[M\cdot(Me_2CO)]^{2+}$.
Anion **ESI-MS** (CH_2Cl_2)	*m*/*z* [%] = 967.0 (100) $[Al\{OC(C\underline{F}_3)_3\}_4]^-$.
Elemental analysis	calcd. for $C_{91}H_{59}Al_2As_4F_{72}O_8P_3Ru_2$ (3297.03 g mol^{-1}) C 33.15, H 1.80; found: C36.49, H 2.32.
	calcd. for $C_{91}H_{59}Al_2As_4F_{72}O_8P_3Ru_2\cdot(C_6H_{14})_3$ (3555.56 g mol^{-1}) C 36.82, H 2.86.

4.8.5 Release of As_4 from $[Ag(\eta^2\text{-}As_4)_2]^+[pftb]^-$ (82)

To a solution of **82** (100 mg, 0.0595 mmol) in CH_2Cl_2, THF or toluene (5 ml) is added a solution of LiCl (2.5 mg, 0.0595 mmol) in THF (1 ml) under the exclusion of light within 5 minutes. After stirring the reaction mixture for 15 min, the brownish precipitate is allowed to settle and the pale yellow solution is filtered via canula.

In order to determine the amount of released As_4, the solvent is removed and the resulting yellow solid exposed to daylight for at least 12 h. The resulting grey solid is washed several times with THF to remove last traces of Li(pftb) and dried in vacuum.

Yield 27 mg (0.09 mmol, 75 %).

$^{75}As\{^1H\}$ NMR (CD_2Cl_2) δ [ppm] = -908 (br s).

4.8.6 $As_4@[\{Cp^*Fe(\eta^5\text{-}P_5)\}_{10}Cu_{30}I_{30}(MeCN)_6]\cdot 2MeCN$ (86)

To solid $[Cp^*Fe(\eta^5\text{-}P_5)]$ (**35a**) (52 mg, 0.15 mmol) is given a solution of freshly released As_4 (27 mg, 0.09 mmol) in a 1:2:5 mixture of THF/dicholoromethane/toluene (8 ml). The solution is filtered via canula and layered with a solution of CuI (60 mg, 0.32 mmol) in acetonitrile (5 ml). After three weeks of slow diffusion small, red, elongated prisms of **86** together with an orange precipitate and large crystals of other crystalline phases are formed. The mother liquid and most of the precipitate are decanted away. The crystals are slurried in hexane and the crystals of the polymeric by products are allowd to settle. The suspension is decanted in a separate Schlenk tube and taken to dryness under reduced pressure. The so obtained (micro)crystalline residue manily consists of unknown microcrystalline material, small crystals of polymeric by products as well as the desired product **86** that could not be further purified.

Analytical data for $As_4@[\{Cp^*Fe(\eta^5\text{-}P_5)\}_{10}Cu_{30}I_{30}(MeCN)_6]\cdot 2MeCN$ (**86**):

Yield $\approx$ 1 mg with major impurities.

4.8.7 $\{Z_4As_4\}@[\{Cp^*Fe(\eta^5\text{-}P_5\}_{12}Cu_{51}I_{56}(MeCN)_3]^-Z^+$ (87)

To solid [Cp*Fe(η^5-P_5)] (**35a**) (52 mg, 0.15 mmol) is given a solution of freshly released As_4 (27 mg, 0.09 mmol) together with LiCl (2.5 mg, 0.06 mmol) in a 1:2:5 mixture of THF/dicholoromethane/toluene (8 ml). The solution is filtered via canula and layered with a solution of CuI (60 mg, 0.32 mmol) in acetonitrile (5 ml). After three weeks of slow diffusion small, reddish brown tetrahedral shaped crystals of **87** together with an orange precipitate, small crystals of **86** and large crystals of known polymeric compounds are formed. The mother liquid and most of the precipitate are decanted away. The crystals are washed six times with THF (6 × 5 ml). Finally, the product crystals as well as small microcrystalline material are slurried in THF and decanted from larger polymer crystals. The solvent is removed under reduced pressure and the crystals are dried in high vacuum. The residue contains crystals of **87** and **86** together with several microcrystalline impurities of unknown origin.

Analytical data for $\{Z_4As_4\}@[\{Cp^*Fe(\eta^5\text{-}P_5\}_{12}Cu_{51}I_{56}(MeCN)_3]^-Z^+$ (**87**):

Yield ≈ 1 mg with major impurities.

^{7}Li{^{1}H} NMR (pyridine-d_5) δ [ppm] = 4.23.

5. Crystallographic Section

5.1 General remarks

Single crystal X-ray diffraction analyses of the reported compounds were generally performed by the author. Exceptions are compounds **54**, **86** and **87** whose X-ray structure analyses were performed by Dr. Alexander V. Virovets and Dr. Eugenia Peresypkina as well as compound **52** which X-ray diffraction analyisis was performed by Dr. Manfred Zabel. Cyrstallographic data for compounds **46** and **47** were acquired by Dr. Germund Glatz (University of Bayreuth).

Except for compounds **46** and **47**, the crystallographic data was acquired either at an Agilent Technologies (formerly Oxford diffraction) Gemini R Ultra diffractometer using Mo or Cu radiation from sealed tubes and a ruby CCD detector or at an Agilent SuperNova device using a microfocus Cu source with an Atlas CCD detecter. The Gemini device was equipped with an Oxford diffraction Cryojet cooler and the SuperNova diffractometer with a Cryostream600 cooling system.

Figures of the molecular structures generated from crystallographic data were prepared with the programs DIAMOND 3.0[154] and SCHAKAL-99.[155]

Complete structural data for the reported structures is attached electronically as CD. The disc contains one file for every compound in .cif format (*Crystallographic-Information-File*) as well the corresponding checkCif file in PDF format together with .hkl, .ins, .res and .lst files.

5.2 General procedures

5.2.1 Sample handling

Most of the processed crystal samples were air and moisture senisitive. Hence, they were handled in mineral oil (Sigma Aldrich, CAS 8042-47-5) or perfluorinated oil (Fomblin, Sigma Aldrich, CAS 69991-67-9). Temperature sensitive samples were handled in a cooled stream of nitrogen in perfluorinated polyether (Galden, Solvay Solexis S.p.A). Appropriate crystals were taken to a CryoLoop (Hampton research) on a goniometer head which was directly attached to the goniometer. Thus, the crystal is brought into the cold nitrogen stream of the cooling system which freezes the surrounding oil and fixes the position of the crystal.

5.2.2 Data processing

Integration and data reduction of the measured data was performed using the CrysAlisPro software package.[156] Either semi-empirical multi-scan absorption correction from equivalents or analytical absorption correction from crystal faces was applied after the absorption coefficient was determined from the final structure model.

5.2.3 Structure solution and refinement

Structure solution was carried out using direct methods (SHELXS-97[157] or SIR-92[158]) or by charge flipping methods (SUPERFLIP[159]). Least-squares refinement on F_0^2 was performed using SHELXL-97.[157] All programs were implemented in WinGX and SXGraph was used for structure representation during the refinement process.[160] In some cases several restraints and constraints had to be used: EADP (equal anistropic displacement parameters (ADP)), EXYZ (equal location parameters), DELU (similar ADP towards bond direction), ISOR (more isotropic ADP), SADI (similar atomic distance), SIMU (similar ADP).

5.3 Crystallographic data for the reported structures

5.3.1 [(^{Menthyl}CAAC)$_2$As$_2$] (43)

Compound **43** cyrstallizes as pale yellow plates from saturated Et_2O solutions upon cooling.

Empirical formula	$C_{54}H_{86}As_2N_2$	
Formula weight M/g·mol^{-1}	913.09	
Device type	Oxford Diffraction Gemini Ultra R	
Crystal color and shape	Pale yellow plate	
Crystal size	0.58 × 0.30 × 0.04	
Temperature T/K	123(1)	
Radiation (λ/Å)	Cu (1.54178)	
Crystal system	Monoclinic	
Space group	$P2_1$	
Unit cell dimensions	a = 10.0932(1) Å	α = 90 °
	b = 21.7023(3) Å	β = 110.470(2) °
	c = 12.2533(2) Å	γ = 90 °
Volume V/Å^3	2514.55(7)	
Formula units Z	2	
Absorption correction type	Multi-Scan	
Absorption coefficient μ/mm^{-1}	1.896	
Density (calculated) ρ_{calc}/g·cm^{-3}	1.206	
F(000)	980	
Theta range θ/°	3.8474 ≤ θ ≤ 66.6383	
Index ranges	-11 < h < 11, -25 < k < 25, -14 < l < 11	
Reflections collected	13138	
Independent reflections [$I > 2\sigma(I)$]	6975 (R_{int} = 0.0295)	
Completeness to full theta	0.980	
Transmission T_{min} / T_{max}	0.408 / 1.0	
Data / parameters / restraints	7068 / 541 / 1	
Flack parameter x	-0.02(1)	
Goodness-of-fit on F^2 S	1.028	
Final R-values [$I > 2\sigma$(I)]	R_1 = 0.0271, wR_2 = 0.0685	
Final R-values (all data)	R_1 = 0.0276, wR_2 = 0.0689	
Largest difference hole and peak $\Delta\rho$/e·Å^{-3}	-0.274, 0.413	

5.3.2 [(^{cHex}CAAC)$_3$As$_4$] (44)

Compound **44** crystallizes as yellowish blocks from saturated Et_2O solutions upon cooling.

Empirical formula	$C_{69}H_{105}As_4N_3 \cdot (C_4H_{10}O)_2$	
Formula weight M/g·mol^{-1}	1424.49	
Device type	Oxford Diffraction Gemini Ultra R	
Crystal color and shape	Pale yellow block	
Crystal size	0.42 × 0.32 × 0.21	
Temperature T/K	123(1)	
Radiation (λ/Å)	Cu (1.54178)	
Crystal system	Triclinic	
Space group	$P\bar{1}$	
Unit cell dimensions	a = 13.9899(3) Å	α = 84.941(2) °
	b = 15.6001(4) Å	β = 77.407(2) °
	c = 17.8266(4) Å	γ = 83.687(2) °
Volume V/Å^3	3765.7(2)	
Formula units Z	2	
Absorption correction type	Analytical	
Absorption coefficient μ/mm^{-1}	2.405	
Density (calculated) ρ_{calc}/g·cm^{-3}	1.259	
F(000)	1512	
Theta range θ/°	$3.2484 \leq \theta \leq 70.5626$	
Index ranges	$-11 < h < 17$, $-17 < k < 18$, $-20 < l < 21$	
Reflections collected	27414	
Independent reflections [$I > 2\sigma(I)$]	13133 (R_{int} = 0.0228)	
Completeness to full theta	0.966	
Transmission T_{min} / T_{max}	0.486 / 0.682	
Data / parameters / restraints	13981 / 795 / 0	
Goodness-of-fit on F^2 S	0.950	
Final R-values [$I > 2\sigma$(I)]	R_1 = 0.0257, wR_2 = 0.0654	
Final R-values (all data)	R_1 = 0.0279, wR_2 = 0.0671	
Largest difference hole and peak $\Delta\rho$/e·Å^{-3}	-0.272, 0.356	

5.3.3 $[L_2Cr_2(\mu,\eta^{1:1:2:2}\text{-}P_4)]$ (46)

Compound **46** cyrstallizes as green needles from THF solutions upon cooling.

Empirical formula	$C_{50}H_{58}Cr_2N_4P_4$	
Formula weight M/g·mol^{-1}	942.88	
Device type	STOE – IPDSII	
Crystal color and shape	Green needle	
Crystal size	0.25 × 0.11 × 0.10	
Temperature T/K	133(2)	
Radiation (λ/Å)	Mo (0.71069)	
Crystal system	Triclinic	
Space group	$P\bar{1}$	
Unit cell dimensions	a = 10.5080(7) Å	α = 99.888(5) °
	b = 12.9430(8) Å	β = 102.371(5) °
	c = 18.425(1) Å	γ = 107.107(5) °
Volume V/Å^3	2264.2(3)	
Formula units Z	2	
Absorption correction type		
Absorption coefficient μ/mm^{-1}	0.662	
Density (calculated) ρ_{calc}/g·cm^{-3}	1.383	
F(000)	988	
Theta range θ/°	$1.70 \leq \theta \leq 25.69$	
Index ranges	$-12 < h < 12$, $-15 < k < 15$, $-22 < l < 22$	
Reflections collected	28048	
Independent reflections [$I > 2\sigma(I)$]	5923 (R_{int} = 0.0853)	
Completeness to full theta	0.965	
Transmission T_{min} / T_{max}		
Data / parameters / restraints	8323 / 545 / 0	
Goodness-of-fit on F^2 S	0.996	
Final R-values [$I > 2\sigma$(I)]	R_1 = 0.0522, wR_2 = 0.1108	
Final R-values (all data)	R_1 = 0.0828, wR_2 = 0.1209	
Largest difference hole and peak $\Delta\rho$/e·Å^{-3}		

5.3.4 $L_2Cr_2(\mu,\eta^{1:1:2:2}\text{-}As_4)]$ (47)

Compound **47** cyrstallizes as green prisms from saturated THF solutions upon cooling.

Empirical formula	$C_{50}H_{58}As_4Cr_2N_4$	
Formula weight M/g·mol^{-1}	1118.68	
Device type	STOE – IPDSII	
Crystal color and shape	Green prism	
Crystal size	0.23 × 0.15 × 0.08	
Temperature T/K	133(2)	
Radiation (λ/Å)	Mo (0.71069)	
Crystal system	Triclinic	
Space group	$P\bar{1}$	
Unit cell dimensions	a = 10.6180(8) Å	α = 99.679(6) °
	b = 13.072(1) Å	β = 101.975(6) °
	c = 18.381(1) Å	γ = 107.600(6) °
Volume V/Å^3	2304.8(3)	
Formula units Z	2	
Absorption correction type	Numerical	
Absorption coefficient μ/mm^{-1}	3.361	
Density (calculated) ρ_{calc}/g·cm^{-3}	1.612	
F(000)	1132	
Theta range θ/°	$1.69 \leq \theta \leq 25.68$	
Index ranges	$-12 < h < 12$, $-15 < k < 15$, $0 < l < 22$	
Reflections collected		
Independent reflections [$I > 2\sigma(I)$]	8681 (R_{int} = 0.0000)	
Completeness to full theta	0.992	
Transmission T_{min} / T_{max}	0.5501 / 0.7626	
Data / parameters / restraints	8681 / 545 / 0	
Goodness-of-fit on F^2 S	0.770	
Final R-values [$I > 2\sigma$(I)]	R_1 = 0.0537, wR_2 = 0.1253	
Final R-values (all data)	R_1 = 0.0992, wR_2 = 0.1403	
Largest difference hole and peak $\Delta\rho$/e·Å^{-3}		

5.3.5 $[L_2Cr_2(\mu,\eta^{1:1:2:2}\text{-}AsP_3)]$ (48)

Compound **48** crystallizes as greenish brown plates from saturated THF solutions upon cooling. Location parameters of the mixed occupied positions P2/As2 and P4/As4 were refined freely. Their displacement parameters were constrained to be the same (EADP).

Empirical formula	$C_{50}H_{58}AsCr_2N_4P_3$	
Formula weight M/g·mol^{-1}	986.83	
Device type	Oxford Diffraction Supernova (Atlas)	
Crystal color and shape	Greenish brown plate	
Crystal size	0.06 × 0.06 × 0.03	
Temperature T/K	123(1)	
Radiation (λ/Å)	Cu (1.54178)	
Crystal system	Triclinic	
Space group	$P\bar{1}$	
Unit cell dimensions	a = 10.5357(3) Å	α = 99.914(3) °
	b = 12.9883(5) Å	β = 102.281(3) °
	c = 18.4212(6) Å	γ = 107.188(3) °
Volume V/Å^3	2277.3(2)	
Formula units Z	2	
Absorption correction type	Analytical	
Absorption coefficient μ/mm^{-1}	6.038	
Density (calculated) ρ_{calc}/g·cm^{-3}	1.439	
F(000)	1024	
Theta range θ/°	$3.6771 \leq \theta \leq 71.1969$	
Index ranges	$-12 < h < 12$, $-15 < k < 13$, $-22 < l < 19$	
Reflections collected	14028	
Independent reflections [$I > 2\sigma(I)$]	7499 (R_{int} = 0.0220)	
Completeness to full theta	0.952	
Transmission T_{min} / T_{max}	0.740 / 0.849	
Data / parameters / restraints	8431 / 559 / 0	
Goodness-of-fit on F^2 S	1.027	
Final R-values [$I > 2\sigma$(I)]	R_1 = 0.0351, wR_2 = 0.0844	
Final R-values (all data)	R_1 = 0.0411, wR_2 = 0.0875	
Largest difference hole and peak $\Delta\rho$/e·Å^{-3}	-0.564, 0.064	

5.3.6 [{L_2Cr_2}(μ_3,$\eta^{1:1:1:2:2}$-P_4){$W(CO)_5$}] (49)

Compound **49** crystallizes as red blocks from saturated CH_2Cl_2 solutions upon cooling. The asymmetric unit contains one molecule of **49** together with two molecules of CH_2Cl_2 of which one is disordered over two positions.

Empirical formula	$C_{55}H_{58}Cr_2N_4O_5P_4W \cdot CH_2Cl_2 \cdot CCl_2$	
Formula weight M/g·mol^{-1}	1399.16	
Device type	Oxford Diffraction Gemini Ultra R	
Crystal color and shape	Dark red block	
Crystal size	0.20 × 0.14 × 0.04	
Temperature T/K	123(2)	
Radiation (λ/Å)	Cu (1.54178)	
Crystal system	Triclinic	
Space group	$P\bar{1}$	
Unit cell dimensions	a = 12.6981(2) Å	α = 98.778(2) °
	b = 13.1405(3) Å	β = 96.873(3) °
	c = 20.6253(5) Å	γ = 115.476(2) °
Volume V/Å^3	3003.5(1)	
Formula units Z	2	
Absorption correction type	Multi-scan	
Absorption coefficient μ/mm^{-1}	2.555	
Density (calculated) ρ_{calc}/g·cm^{-3}	1.547	
F(000)	1406	
Theta range θ/°	2.7420 ≤ θ ≤ 32.5383	
Index ranges	-16 < h < 18, -18 < k < 18, -20 < l < 29	
Reflections collected	35916	
Independent reflections [$I > 2\sigma(I)$]	14085 (R_{int} = 0.0301)	
Completeness to full theta	0.999	
Transmission T_{min} / T_{max}	0.80957 / 1.0	
Data / parameters / restraints	18339 / 714 / 0	
Goodness-of-fit on F^2 S	0.951	
Final R-values [$I > 2\sigma$(I)]	R_1 = 0.0342, wR_2 = 0.0744	
Final R-values (all data)	R_1 = 0.0489, wR_2 = 0.0766	
Largest difference hole and peak $\Delta\rho$/e·Å^{-3}	-2.243, 2.765	

5.3.7 [{Cp'''Fe(CO)$_2$}$_2$(μ,$\eta^{1:1}$-As$_4$)] (52)

Compound **52** crystallizes as orange plates from hexane/toluene (2:1) solutions upon cooling. The examined crystal was a twin which was taken into account by the Crysalis Software. Only the reflections for the major component were used for structure solution and refinement.

Empirical formula	$C_{38}H_{58}As_4Fe_2O_4$	
Formula weight M/g·mol^{-1}	990.22	
Device type	Oxford Diffraction Gemini Ultra R	
Crystal color and shape	Orange platelet	
Crystal size	0.09 × 0.04 × 0.01	
Temperature T/K	123(1)	
Radiation (λ/Å)	Cu (1.54178)	
Crystal system	Monoclinic	
Space group	$P2_1/c$	
Unit cell dimensions	a = 15.095(2) Å	α = 90 °
	b = 19.717(1) Å	β = 117.622(9) °
	c = 15.431(1) Å	γ = 90 °
Volume V/Å^3	4069.2(7)	
Formula units Z	4	
Absorption correction type	Analytical	
Absorption coefficient μ/mm^{-1}	9.617	
Density (calculated) ρ_{calc}/g·cm^{-3}	1.616	
F(000)	2008	
Theta range θ/°	$3.2233 \leq \theta \leq 68.2272$	
Index ranges	$-16 < h < 15$, $-12 < k < 21$, $-15 < l < 17$	
Reflections collected	11313	
Independent reflections [$I > 2\sigma(I)$]	3248 (R_{int} = 0.0942)	
Completeness to full theta	0.962	
Transmission T_{min} / T_{max}	0.480 / 0.937	
Data / parameters / restraints	5625 / 415 / 0	
Goodness-of-fit on F^2 S	1.034	
Final R-values [$I > 2\sigma$(I)]	R_1 = 0.0779, wR_2 = 0.2055	
Final R-values (all data)	R_1 = 0.1328, wR_2 = 0.2321	
Largest difference hole and peak $\Delta\rho$/e·Å^{-3}	-1.109, 0.192	

5.3.8 [{Cp*Cr(CO)$_3$}$_2$(μ,$\eta^{1:1}$-P$_4$)] (54)

Compound **54** crystallizes as orange blocks from a saturated toluene solution upon cooling. The compound is X-ray sensitive and the examined crystals decomposed upon measurement. Hence three crystals were measured and the data was combined with the aid of the Xprep software. For more detailed information please see the corresponding .cif file.

Empirical formula	$C_{26}H_{30}Cr_2O_6P_4$	
Formula weight M/g·mol^{-1}	666.38	
Device type	Oxford Diffraction Supernova (Atlas)	
Crystal color and shape	Orange block	
Crystal size		
Temperature T/K	123(1)	
Radiation (λ/Å)	Cu (1.54178)	
Crystal system	Monoclinic	
Space group	$P2_1/c$	
Unit cell dimensions	a = 9.1637(9) Å	α = 90 °
	b = 17.935(2) Å	β = 94.188(8) °
	c = 18.295(2) Å	γ = 90 °
Volume V/Å^3	2998.7(5)	
Formula units Z	4	
Absorption correction type	Analytical	
Absorption coefficient μ/mm^{-1}	8.310	
Density (calculated) ρ_{calc}/g·cm^{-3}	1.476	
F(000)	1368	
Theta range θ/°	$4.84 \leq \theta \leq 73.19$	
Index ranges	$-11 < h < 11$, $-19 < k < 21$, $-22 < l < 20$	
Reflections collected	16573	
Independent reflections [$I > 2\sigma(I)$]	2933 (R_{int} = 0.0921)	
Completeness to full theta	0.913	
Transmission T_{min} / T_{max}		
Data / parameters / restraints	5498 / 353 / 0	
Goodness-of-fit on F^2 S	0.963	
Final R-values [$I > 2\sigma$(I)]	R_1 = 0.0671, wR_2 = 0.1609	
Final R-values (all data)	R_1 = 0.1291, wR_2 = 0.1871	
Largest difference hole and peak $\Delta\rho$/e·Å^{-3}	-0.378, 1.417	

5.3.9 [{Cp*Cr(CO)$_3$}$_2$(μ,$\eta^{1:1}$-AsP$_3$)] (55)

Compound **55** crystallizes as orange plates from saturated toluene solutions upon cooling. The asymmetric unit conatins one molecule of **55**. Location- and displacement parameters of the mixed occupied atoms P1/As1 and P2/As2 were constrained to be the same (EADP, EXYZ)

Empirical formula	$C_{26}H_{30}AsCr_2O_6P_3$	
Formula weight M/g·mol^{-1}	710.33	
Device type	Oxford Diffraction Gemini Ultra R	
Crystal color and shape	Orange plate	
Crystal size	0.39 × 0.21 × 0.09	
Temperature T/K	123(1)	
Radiation (λ/Å)	Cu (1.54178)	
Crystal system	Monoclinic	
Space group	$C2/c$	
Unit cell dimensions	a = 28.7971(5) Å	α = 90 °
	b = 8.8766(1) Å	β = 108.170(2) °
	c = 12.1826(2) Å	γ = 90 °
Volume V/Å^3	2958.84(9)	
Formula units Z	4	
Absorption correction type	Analytical	
Absorption coefficient μ/mm^{-1}	9.154	
Density (calculated) ρ_{calc}/g·cm^{-3}	1.595	
F(000)	1440	
Theta range θ/°	3.2277 ≤ θ ≤ 70.5398	
Index ranges	-35 < h < 34, -7 < k < 10, -14 < l < 13	
Reflections collected	4689	
Independent reflections [$I > 2\sigma(I)$]	2598 (R_{int} = 0.0190)	
Completeness to full theta	0.957	
Transmission T_{min} / T_{max}	0.243 / 0.518	
Data / parameters / restraints	2718 / 186 / 0	
Goodness-of-fit on F^2 S	1.049	
Final R-values [$I > 2\sigma$(I)]	R_1 = 0.0263, wR_2 = 0.0678	
Final R-values (all data)	R_1 = 0.0275, wR_2 = 0.0686	
Largest difference hole and peak $\Delta\rho$/e·Å^{-3}	-0.395, 0.365	

5.3.10 [{Cp*Cr(CO)$_3$}$_2$(μ,$\eta^{1:1}$-As$_4$)] (56)

Compound **56** cocrystallizes together with compound **64** as red plates from a saturated toluene solution upon cooling. The asymmetric unit contains two molecules of **56** and one molecule of **64**.

Empirical formula	$C_{104}H_{120}As_{16}Cr_8O_{24}$	
Formula weight M/g·mol^{-1}	3368.72	
Device type	Oxford Diffraction Gemini Ultra R	
Crystal color and shape	Red plate	
Crystal size	0.28 × 0.25 × 0.89	
Temperature T/K	123(1)	
Radiation (λ/Å)	Cu (1.54178)	
Crystal system	Monoclinic	
Space group	*Pn*	
Unit cell dimensions	a = 13.8219(1) Å	α = 90 °
	b = 25.0085(2) Å	β = 98.335(1) °
	c = 17.6806(1) Å	γ = 90 °
Volume V/Å^3	6047.01(8)	
Formula units Z	2	
Absorption correction type	Analytical	
Absorption coefficient μ/mm^{-1}	11.105	
Density (calculated) ρ_{calc}/g·cm^{-3}	1.850	
F(000)	3312	
Theta range θ/°	3.0803 ≤ θ ≤ 66.4795	
Index ranges	-12 < h < 16, -23 < k < 28, -21 < l < 21	
Reflections collected	58336	
Independent reflections [$I > 2\sigma(I)$]	18152(R_{int} = 0.0389)	
Completeness to full theta	0.993	
Transmission T_{min} / T_{max}	0.153 / 0.527	
Data / parameters / restraints	18753 / 1441 / 2	
Flack parameter x	0.059(4)	
Goodness-of-fit on F^2 S	1.053	
Final R-values [$I > 2\sigma$(I)]	R_1 = 0.0384, wR_2 = 0.0988	
Final R-values (all data)	R_1 = 0.0398, wR_2 = 0.0999	
Largest difference hole and peak $\Delta\rho$/e·Å^{-3}	-1.237, 1.637	

5.3.11 [{Cp*Fe(CO)$_2$}{Cp'''Fe(CO)$_2$}] (57)

Compound **57** crystallizes as red/green/brown pleochromic plates from hot hexane solutions upon cooling.

Empirical formula	$C_{31}H_{44}Fe_2O_4$	
Formula weight M/g·mol^{-1}	592.36	
Device type	Oxford Diffraction Gemini R Ultra	
Crystal color and shape	pleochromic brown/green/purple plate	
Crystal size	0.16 × 0.16 × 0.03	
Temperature T/K	123(1)	
Radiation (λ/Å)	Cu (1.54178)	
Crystal system	triclinic	
Space group	$P\bar{1}$	
Unit cell dimensions	a = 8.6488(4) Å	α = 101.366(4) °
	b = 11.3085(7) Å	β = 91.192(3) °
	c = 15.9117(6) Å	γ = 109.331(5) °
Volume V/Å^3	1433.4(1)	
Formula units Z	2	
Absorption correction type	analytical	
Absorption coefficient μ/mm^{-1}	8.376	
Density (calculated) ρ_{calc}/g·cm^{-3}	1.372	
F(000)	628	
Theta range θ/°	$4.2339 \leq \theta \leq 66.6433$	
Index ranges	$-10 < h < 8$, $-13 < k < 13$, $-18 < l < 14$	
Reflections collected	10634	
Independent reflections [$I > 2\sigma(I)$]	4208 (R_{int} = 0.0320)	
Completeness to full theta	0.981	
Transmission T_{min} / T_{max}	0.575 / 0.888	
Data / parameters / restraints	4986 / 348 / 0	
Goodness-of-fit on F^2 S	0.963	
Final R-values [$I > 2\sigma$(I)]	R_1 = 0.0295, wR_2 = 0.0694	
Final R-values (all data)	R_1 = 0.0356, wR_2 = 0.0708	
Largest difference hole and peak $\Delta\rho$/e·Å^{-3}	-0.366, 0.365	

5.3.12 [Cp'''$_2$P$_4$] (60)

Compound **60** crystallizes as colorless plates from saturated Et_2O solutions at room temperature. The assymmetric unit contains two molecules of isomer **60-C** and one molecule of **60-D** which is disordered over two positions. Additionally the crystal was twinned by inversion.

Empirical formula	$C_{34}H_{58}P_4$	
Formula weight M/g·mol^{-1}	590.68	
Device type	Oxford Diffraction Supernova (Atlas)	
Crystal color and shape	Colorless plate	
Crystal size	0.25 × 0.19 × 0.04	
Temperature T/K	123(1)	
Radiation (λ/Å)	Cu (1.54178)	
Crystal system	Monoclinic	
Space group	*Cc*	
Unit cell dimensions	a = 36.6533(3) Å	α = 90 °
	b = 10.3079(1) Å	β = 96.283(1) °
	c = 28.2745(2) Å	γ = 90 °
Volume V/Å^3	10618.5(2)	
Formula units Z	12	
Absorption correction type	Analytical	
Absorption coefficient μ/mm^{-1}	2.104	
Density (calculated) ρ_{calc}/g·cm^{-3}	1.109	
F(000)	3864	
Theta range θ/°	$3.0293 \leq \theta \leq 70.7602$	
Index ranges	$-44 < h < 44$, $-12 < k < 12$, $-34 < l < 24$	
Reflections collected	55596	
Independent reflections [$I > 2\sigma(I)$]	14553 (R_{int} = 0.0362)	
Completeness to full theta	0.984	
Transmission T_{min} / T_{max}	0.558 / 0.900	
Data / parameters / restraints	16897 / 1208 / 18	
Goodness-of-fit on F^2 S	1.029	
Final R-values [$I > 2\sigma$(I)]	R_1 = 0.0421, wR_2 = 0.1087	
Final R-values (all data)	R_1 = 0.0505, wR_2 = 0.1168	
Largest difference hole and peak $\Delta\rho$/e·Å^{-3}	-0.558, 0.522	

5.3.13 [{Cp'''Fe(CO)$_2$}$_2$(μ_4,$\eta^{1:1:2:2}$-As$_8$){Cp'''Fe(CO)}$_2$] (63)

Compound **63** crystallizes as dark green plates from hexane/toluene (2:1) solutions upon cooling. The asymmetric unit contains two molecules of **63** together with two heavily disordered molecules of toluene which were treated with PLATON/SQUEEZE.

Empirical formula	$C_{74}H_{116}As_8Fe_4O_6 \cdot (C_7H_8)_2$	
Formula weight M/g·mol^{-1}	2108.70	
Device type	Oxford Diffraction Gemini Ultra R	
Crystal color and shape	Dark green plate	
Crystal size	0.36 × 0.17 × 0.08	
Temperature T/K	123(1)	
Radiation (λ/Å)	Cu (1.54178)	
Crystal system	Triclinic	
Space group	$P\bar{1}$	
Unit cell dimensions	a = 13.9248(3) Å	α = 92.087(2) °
	b = 17.5949(4) Å	β = 96.720(2) °
	c = 19.0310(3) Å	γ = 93.998(2) °
Volume V/Å^3	4614.7(2)	
Formula units Z	2	
Absorption correction type	Analytical	
Absorption coefficient μ/mm^{-1}	8.501	
Density (calculated) ρ_{calc}/g·cm^{-3}	1.518	
F(000)	2152	
Theta range θ/°	3.2019 ≤ θ ≤ 66.6174	
Index ranges	-16 < h < 16, -20 < k < 20, -18 < l < 22	
Reflections collected	66321	
Independent reflections [$I > 2\sigma(I)$]	14750 (R_{int} = 0.0576)	
Completeness to full theta	0.994	
Transmission T_{min} / T_{max}	0.169 / 0.548	
Data / parameters / restraints	16266 / 933 / 40	
Goodness-of-fit on F^2 S	1.014	
Final R-values [$I > 2\sigma$(I)]	R_1 = 0.0360, wR_2 = 0.0896	
Final R-values (all data)	R_1 = 0.0399, wR_2 = 0.0922	
Largest difference hole and peak $\Delta\rho$/e·Å^{-3}	-0.969, 0.858	

5.3.14 [{Cp*Cr(CO)$_3$}$_4$(μ_4,$\eta^{1:1:1:1}$-As$_8$)] (64)

Compound **64** crystallizes as red blocks from THF solutions upon cooling. The examined crystal was merohedrally twinned. The asymmetric unit contains two molecules of **64** together with at least one molecule of THF. Several other THF molecules were heavily disordered but could not be refined reasonably.

Empirical formula	$C_{104}H_{120}As_{16}Cr_8O_{24}\cdot(C_4H_8O)$	
Formula weight M/g·mol^{-1}	3440.83	
Device type	Oxford Diffraction Gemini Ultra R	
Crystal color and shape	Red block	
Crystal size	0.46 × 0.28 × 0.09	
Temperature T/K	123(1)	
Radiation (λ/Å)	Mo (0.71069)	
Crystal system	Tetragonal	
Space group	$I4_1/a$	
Unit cell dimensions	a = 43.6510(5) Å	α = 90 °
	b = 43.6510(5) Å	β = 90 °
	c = 28.5230(4) Å	γ = 90 °
Volume V/Å^3	54348(1)	
Formula units Z	16	
Absorption correction type	Analytical	
Absorption coefficient μ/mm^{-1}	4.542	
Density (calculated) ρ_{calc}/g·cm^{-3}	1.682	
F(000)	27136	
Theta range θ/°	$2.8729 \leq \theta \leq 28.6954$	
Index ranges	$-58 < h < 57$, $-59 < k < 59$, $-36 < l < 38$	
Reflections collected	286137	
Independent reflections [$I > 2\sigma(I)$]	29243 (R_{int} = 0.0553)	
Completeness to full theta	0.949	
Transmission T_{min} / T_{max}	0.226 / 0.715	
Data / parameters / restraints	33539 / 1390 / 12	
Goodness-of-fit on F^2 S	1.069	
Final R-values [$I > 2\sigma$(I)]	R_1 = 0.0407, wR_2 = 0.1226	
Final R-values (all data)	R_1 = 0.0523, wR_2 = 0.1292	
Largest difference hole and peak $\Delta\rho$/e·Å^{-3}	-0.603, 1.561	

5.3.15 $[\{\{Cp'''Fe(CO)_2\}_2(\mu_3,\eta^{1:1:1:1}\text{-}P_4)\}_2Cu]^+[BF_4]^-$ (65)

Compound **65** crystallizes as red plates from hexane/THF mixtures. The asymmetric unit contains one molecule of **65** together with two molecules of THF. One of the THF molecules as well as two of the ^{tert}butyl groups are disordered over two positions which were refined using EADP (THF) as well as SADI (^{tert}butyl) restraints.

Empirical formula	$C_{76}H_{116}BCuF_4Fe_4O_8P_8\cdot(C_4H_8O)_2$	
Formula weight M/g·mol^{-1}	1923.42	
Device type	Oxford Diffraction Supernova (Atlas)	
Crystal color and shape	Red plate	
Crystal size	0.15 × 0.12 × 0.03	
Temperature T/K	123(1)	
Radiation (λ/Å)	Cu (1.54178)	
Crystal system	Triclinic	
Space group	$P\bar{1}$	
Unit cell dimensions	a = 13.9316(4) Å	α = 84.487(2) °
	b = 14.1024(3) Å	β = 83.531(2) °
	c = 25.1954(6) Å	γ = 75.126(2) °
Volume V/Å^3	4742.2(2)	
Formula units Z	2	
Absorption correction type	Analytical	
Absorption coefficient μ/mm^{-1}	6.799	
Density (calculated) ρ_{calc}/g·cm^{-3}	1.347	
F(000)	2020	
Theta range θ/°	$3.2477 \leq \theta \leq 76.4685$	
Index ranges	$-17 < h < 17$, $-17 < k < 16$, $-31 < l < 21$	
Reflections collected	38256	
Independent reflections [$I > 2\sigma(I)$]	16723 (R_{int} = 0.0362)	
Completeness to full theta	0.963	
Transmission T_{min} / T_{max}	0.544 / 0.813	
Data / parameters / restraints	19224 / 1103 / 120	
Goodness-of-fit on F^2 S	1.027	
Final R-values [$I > 2\sigma$(I)]	R_1 = 0.0454, wR_2 = 0.1162	
Final R-values (all data)	R_1 = 0.0531, wR_2 = 0.1228	
Largest difference hole and peak $\Delta\rho$/e·Å^{-3}	-0.549, 1.665	

5.3.16 $[\{\{Cp^*Cr(CO)_3\}_2(\mu_3,\eta^{1:1:1:1}\text{-}P_4)\}_2Cu]^+[BF_4]^-$ (66)

Compound **66** crystallizes as red blocks from THF/hexane mixtures. The asymmetric unit contains one molecule of **66**. Two of the carbonyl ligands as well as one Cp* unit were disordered over two positions.

Empirical formula	$C_{52}H_{60}BCr_4CuF_4O_{12}P_8$	
Formula weight M/g·mol^{-1}	1483.12	
Device type	Oxford Diffraction Gemini R Ultra	
Crystal color and shape	Red block	
Crystal size	0.37 × 0.25 × 0.16	
Temperature T/K	123(1)	
Radiation (λ/Å)	Cu (1.54178)	
Crystal system	Triclinic	
Space group	$P\bar{1}$	
Unit cell dimensions	a = 13.1410(2) Å	α = 77.708(1) °
	b = 14.8142(2) Å	β = 89.093(1) °
	c = 17.8398(2) Å	γ = 67.999(1) °
Volume V/Å^3	3138.37(8)	
Formula units Z	2	
Absorption correction type	Analytical	
Absorption coefficient μ/mm^{-1}	8.419	
Density (calculated) ρ_{calc}/g·cm^{-3}	1.569	
F(000)	1508	
Theta range θ/°	$3.6338 \leq \theta \leq 66.5017$	
Index ranges	$-15 < h < 10$, $-17 < k < 17$, $-20 < l < 20$	
Reflections collected	20006	
Independent reflections [$I > 2\sigma(I)$]	10355 (R_{int} = 0.0206)	
Completeness to full theta	0.966	
Transmission T_{min} / T_{max}	0.191 / 0.380	
Data / parameters / restraints	10741 / 875 / 0	
Goodness-of-fit on F^2 S	1.022	
Final R-values [$I > 2\sigma$(I)]	R_1 = 0.0283, wR_2 = 0.0733	
Final R-values (all data)	R_1 = 0.0293, wR_2 = 0.0740	
Largest difference hole and peak $\Delta\rho$/e·Å^{-3}	-0.506, 0.513	

5.3.17 [{Cp'''Fe(CO)$_2$}$_2$(μ_3,$\eta^{1:1:2}$-P$_4$){Cu(MeCN)}]$^+$[BF$_4$]$^-$ (67)

Compound **67** crystallizes as orange bars from THF/hexane solutions. The asymmetric unit contains one molecule of **67**.

Empirical formula	$C_{40}H_{61}BCuF_4Fe_2NO_4P_4$	
Formula weight M/g·mol^{-1}	1005.84	
Device type	Oxford Diffraction Supernova (Atlas)	
Crystal color and shape	Orange bar	
Crystal size	0.27 × 0.11 × 0.07	
Temperature T/K	123(1)	
Radiation (λ/Å)	Cu (1.54178)	
Crystal system	Monoclinic	
Space group	$P2_1/c$	
Unit cell dimensions	a = 18.1996(2) Å	α = 90 °
	b = 14.3953(1) Å	β = 100.487(1) °
	c = 18.3849(1) Å	γ = 90 °
Volume V/Å^3	4736.18(7)	
Formula units Z	4	
Absorption correction type	Analytical	
Absorption coefficient μ/mm^{-1}	7.098	
Density (calculated) ρ_{calc}/g·cm^{-3}	1.411	
F(000)	2088	
Theta range θ/°	$3.7755 \leq \theta \leq 74.0625$	
Index ranges	$-22 < h < 16$, $-17 < k < 16$, $-22 < l < 21$	
Reflections collected	16021	
Independent reflections [$I > 2\sigma(I)$]	8445 (R_{int} = 0.0339)	
Completeness to full theta	0.952	
Transmission T_{min} / T_{max}	0.378 / 0.712	
Data / parameters / restraints	9191 / 533 / 0	
Goodness-of-fit on F^2 S	1.020	
Final R-values [$I > 2\sigma$(I)]	R_1 = 0.0389, wR_2 = 0.1014	
Final R-values (all data)	R_1 = 0.0425, wR_2 = 0.1053	
Largest difference hole and peak $\Delta\rho$/e·Å^{-3}	-0.572, 0.577	

5.3.18 $[\{\{Cp'''Fe(CO)_2\}_2(\mu_3,\eta^{1:1:1:1}\text{-}P_4)\}_2Ag]^+[PF_6]^-$ (68)

Compound **68** crystallizes as orange plates from THF/hexane mixtures. The asymmetric unit contains two molecules of **68** together with seven molecules of THF. The crystals were twinned by inversion.

Empirical formula	$C_{152}H_{232}Ag_2F_{12}Fe_8O_{16}P_{18}\cdot(C_4H_8O)_7$	
Formula weight M/g·mol^{-1}	4268.12	
Device type	Oxford Diffraction Gemini Ultra R	
Crystal color and shape	Orange plate	
Crystal size	0.51 × 0.19 × 0.05	
Temperature T/K	123(1)	
Radiation (λ/Å)	Cu (1.54178)	
Crystal system	Monoclinic	
Space group	*Cc*	
Unit cell dimensions	a = 17.9166(1) Å	α = 90 °
	b = 37.5514(2) Å	β = 116.765(1) °
	c = 17.3427(1) Å	γ = 90 °
Volume V/Å^3	10418.0(1)	
Formula units Z	2	
Absorption correction type	Analytical	
Absorption coefficient μ/mm^{-1}	7.671	
Density (calculated) ρ_{calc}/g·cm^{-3}	1.361	
F(000)	4464	
Theta range θ/°	$3.1693 \leq \theta \leq 66.4730$	
Index ranges	$-21 < h < 19$, $-43 < k < 44$, $-11 < l < 20$	
Reflections collected	40334	
Independent reflections [$I > 2\sigma(I)$]	13041 (R_{int} = 0.0422)	
Completeness to full theta	0.991	
Transmission T_{min} / T_{max}	0.178 / 0.691	
Data / parameters / restraints	13176 / 1163 / 2	
Goodness-of-fit on F^2 S	1.036	
Final R-values [$I > 2\sigma$(I)]	R_1 = 0.0343, wR_2 = 0.0914	
Final R-values (all data)	R_1 = 0.0345, wR_2 = 0.0917	
Largest difference hole and peak $\Delta\rho$/e·Å^{-3}	-0.436, 0.811	

5.3.19 $[\{\{Cp^*Cr(CO)_3\}_2(\mu_3,\eta^{1:1:1:1}\text{-}P_4)\}_2Ag]^+[PF_6]^-$ (69)

Compound **69** crystallizes as orange plates from THF/hexane mixtures. The asymmetric unit contains one quarter of a molecule **69**. The PF_6 counterion was refined using several SADI restraints. Additionally a severely disordered THF molecule was treated with PLATON/SQUEEZE.

Empirical formula	$C_{52}H_{60}AgCr_4F_6O_{12}P_9\cdot(C_4H_8O)$	
Formula weight M/g·mol^{-1}	1657.70	
Device type	Oxford Diffraction Gemini R Ultra	
Crystal color and shape	Orange plate	
Crystal size	0.30 × 0.15 × 0.10	
Temperature T/K	123(1)	
Radiation (λ/Å)	Cu (1.54178)	
Crystal system	Tetragonal	
Space group	$P4/n$	
Unit cell dimensions	a = 17.3327(1) Å	α = 90 °
	b = 17.3327(1) Å	β = 90 °
	c = 11.4808(2) Å	γ = 90 °
Volume V/Å^3	3449.09(7)	
Formula units Z	2	
Absorption correction type	Analytical	
Absorption coefficient μ/mm^{-1}	9.877	
Density (calculated) ρ_{calc}/g·cm^{-3}	1.596	
F(000)	1680	
Theta range θ/°	$3.6034 \leq \theta \leq 70.7178$	
Index ranges	$-14 < h < 14$, $0 < k < 21$, $0 < l < 14$	
Reflections collected	3299	
Independent reflections [$I > 2\sigma(I)$]	3123 (R_{int} = 0.0438)	
Completeness to full theta	0.989	
Transmission T_{min} / T_{max}	0.157 / 0.460	
Data / parameters / restraints	3299 / 197 / 5	
Goodness-of-fit on F^2 S	1.062	
Final R-values [$I > 2\sigma$(I)]	R_1 = 0.0377, wR_2 = 0.1036	
Final R-values (all data)	R_1 = 0.0396, wR_2 = 0.1054	
Largest difference hole and peak $\Delta\rho$/e·Å^{-3}	-0.638, 1.044	

5.3.20 [{Cp'''Fe(CO)$_2$}$_2$(μ_3,$\eta^{1:1:1:1}$-P$_4$){Au(PPh$_3$)}]$^+$[PF$_6$]$^-$ (70)

Compound **70** crystallizes as orange plates from THF/hexane mixtures. The crystals were heavily intergrown. The asymmetric unit conatins one molecule of **70**. The largest single crystal that could be found showed a diffraction limit of 1.0 Å.

Empirical formula	$C_{56}H_{73}AuF_6Fe_2O_4P_6$	
Formula weight M/g·mol^{-1}	1418.64	
Device type	Oxford Diffraction Gemini Ultra R	
Crystal color and shape	Orange plate	
Crystal size	0.22 × 0.07 × 0.01	
Temperature T/K	123(1)	
Radiation (λ/Å)	Cu (1.54178)	
Crystal system	Monoclinic	
Space group	$P2_1/n$	
Unit cell dimensions	a = 9.9443(7) Å	α = 90 °
	b = 31.748(2) Å	β = 99.739(7) °
	c = 19.084(1) Å	γ = 90 °
Volume V/Å^3	5938.2(7)	
Formula units Z	4	
Absorption correction type	Analytical	
Absorption coefficient μ/mm^{-1}	10.472	
Density (calculated) ρ_{calc}/g·cm^{-3}	1.587	
F(000)	2864	
Theta range θ/°	3.5402 ≤ θ ≤ 51.5088	
Index ranges	-9 < h < 9, -32 < k < 24, -19 < l < 9	
Reflections collected	11651	
Independent reflections [$I > 2\sigma(I)$]	4460 (R_{int} = 0.0546)	
Completeness to full theta	0.952	
Transmission T_{min} / T_{max}	0.403 / 0.877	
Data / parameters / restraints	6205 / 694 / 0	
Goodness-of-fit on F^2 S	0.972	
Final R-values [$I > 2\sigma$(I)]	R_1 = 0.0480, wR_2 = 0.0899	
Final R-values (all data)	R_1 = 0.0824, wR_2 = 0.1037	
Largest difference hole and peak $\Delta\rho$/e·Å^{-3}	-0.846, 1.436	

5.3.21 $[\{Cp^*Cr(CO)_3\}_2(\mu_3,\eta^{1:1:1:1}\text{-}P_4)\{Au(PPh_3)\}]^+[PF_6]^-$ (71)

Compound **71** crystallizes as orange bars from THF/hexane mixtures. The asymmetric unit contains one molecule of **71** together with one or two heavily disordered THF molecules that were treated with PLATON/SQUEEZE. As the crystals decomposed during measurement only a complete data set up to 1.46 Å could be obtained.

Empirical formula	$C_{44}H_{45}AuCr_2F_6O_6P_6$	
Formula weight M/g·mol^{-1}	1270.59	
Device type	Oxford Diffraction Supernova (Atlas)	
Crystal color and shape	Orange bar	
Crystal size	0.11 × 0.02 × 0.01	
Temperature T/K	123(1)	
Radiation (λ/Å)	Cu (1.54178)	
Crystal system	Orthorhombic	
Space group	*Pccn*	
Unit cell dimensions	a = 17.1566(9) Å	α = 90 °
	b = 41.664(3) Å	β = 90 °
	c = 14.3013(8) Å	γ = 90 °
Volume V/Å^3	10223(1)	
Formula units Z	8	
Absorption correction type	Analytical	
Absorption coefficient μ/mm^{-1}	11.079	
Density (calculated) ρ_{calc}/g·cm^{-3}	1.651	
F(000)	5024	
Theta range θ/°	$3.0835 \leq \theta \leq 31.9538$	
Index ranges	$0 < h < 11$, $0 < k < 28$, $0 < l < 9$	
Reflections collected	1727	
Independent reflections [$I > 2\sigma(I)$]	1315 (R_{int} = 0.0000)	
Completeness to full theta	0.993	
Transmission T_{min} / T_{max}	0.625 / 0.942	
Data / parameters / restraints	1727 / 361 / 0	
Goodness-of-fit on F^2 S	1.122	
Final R-values [$I > 2\sigma$(I)]	R_1 = 0.1001, wR_2 = 0.2656	
Final R-values (all data)	R_1 = 0.1144, wR_2 = 0.2839	
Largest difference hole and peak $\Delta\rho$/e·Å^{-3}	-0.907, 1.798	

5.3.22 [{Cp'''Fe(CO)$_2$}$_2$(μ_3,$\eta^{1:1:1:1}$-P$_4$)FeBr$_2$] (72)

Compound **72** crystallizes as red plates from CH_2Cl_2 solutions upon cooling. The asymmetric unit contains one molecule of **72**.

Empirical formula	$C_{40}H_{62}Br_2Cl_4Fe_3O_4P_4$	
Formula weight M/g·mol^{-1}	1199.93	
Device type	Oxford Diffraction Supernova (Atlas)	
Crystal color and shape	Red plate	
Crystal size	0.24 × 0.09 × 0.02	
Temperature T/K	123(1)	
Radiation (λ/Å)	Cu (1.54178)	
Crystal system	Monoclinic	
Space group	$P2_1/c$	
Unit cell dimensions	a = 21.2045(2) Å	α = 90 °
	b = 13.3322(1) Å	β = 114.893(1) °
	c = 19.7875(2) Å	γ = 90 °
Volume V/Å^3	5074.27(9)	
Formula units Z	4	
Absorption correction type	Analytical	
Absorption coefficient μ/mm^{-1}	12.056	
Density (calculated) ρ_{calc}/g·cm^{-3}	1.571	
F(000)	2440	
Theta range θ/°	3.3122 ≤ θ ≤ 70.6848	
Index ranges	-25 < h < 25, -16 < k < 15, -23 < l < 22	
Reflections collected	27122	
Independent reflections [$I > 2\sigma(I)$]	8757 (R_{int} = 0.0268)	
Completeness to full theta	0.973	
Transmission T_{min} / T_{max}	0.298 / 0.767	
Data / parameters / restraints	9502 / 532 / 0	
Goodness-of-fit on F^2 S	1.033	
Final R-values [$I > 2\sigma$(I)]	R_1 = 0.0303, wR_2 = 0.0731	
Final R-values (all data)	R_1 = 0.0339, wR_2 = 0.0756	
Largest difference hole and peak $\Delta\rho$/e·Å^{-3}	-1.593, 1.428	

5.3.23 $[\{\{Cp^*Cr(CO)_3\}_2(\mu_3,\eta^{1:1:1:1}\text{-}AsP_3)\}_2Cu]^+[BF_4]^-$ (74)

Compound **74** crystallizes as orange platelets from THF/hexane solutions. Due to crystal decomposition no complete data set could be obtained. Location- and displacement parameters of the mixed occupied atom sites were constrained to be the same (EADP, EXYZ). The copper atom is disordered over 4 positions with occupancy factors correlating with the P/As occupancy.

Empirical formula	$C_{52}H_{60}As_2BCr_4CuF_4O_{12}P_6$	
Formula weight M/g·mol^{-1}	1571.02	
Device type	Oxford Diffraction Supernova (Atlas)	
Crystal color and shape	Orange platelet	
Crystal size	0.17 × 0.05 × 0.04	
Temperature T/K	123(1)	
Radiation (λ/Å)	Cu (1.54178)	
Crystal system	Triclinic	
Space group	$P\bar{1}$	
Unit cell dimensions	a = 13.2216(7) Å	α = 77.134(5) °
	b = 14.8761(9) Å	β = 89.005(5) °
	c = 17.984(1) Å	γ = 67.863(6) °
Volume V/Å^3	3185.5(4)	
Formula units Z	2	
Absorption correction type	Analytical	
Absorption coefficient μ/mm^{-1}	8.974	
Density (calculated) ρ_{calc}/g·cm^{-3}	1.637	
F(000)	1580	
Theta range θ/°	$3.2956 \leq \theta \leq 73.6116$	
Index ranges	$-14 < h < 14$, $-16 < k < 18$, $-21 < l < 14$	
Reflections collected	14069	
Independent reflections [$I > 2\sigma(I)$]	6595 (R_{int} = 0.0540)	
Completeness to full theta	0.754	
Transmission T_{min} / T_{max}	0.593 / 0.815	
Data / parameters / restraints	9741 / 788 / 0	
Goodness-of-fit on F^2 S	1.017	
Final R-values [$I > 2\sigma$(I)]	R_1 = 0.0641, wR_2 = 0.1644	
Final R-values (all data)	R_1 = 0.0930, wR_2 = 0.1922	
Largest difference hole and peak $\Delta\rho$/e·Å^{-3}	-0.956, 0.768	

5.3.24 $[\{\{Cp'''Fe(CO)_2\}_2(\mu_3,\eta^{1:1:1:1}\text{-}AsP_3)\}_2Ag]^+[PF_6]^-$ (75)

Compound **75** crystallizes as orange plates from THF/hexane solutions. The examined crystal was twinned by inversion. Location- and displacement parameters of the mixed occupied atom sites were constrained to be the same (EADP, EXYZ). The silver atom is disordered over 4 positions with occupancy factors correlating with the P/As occupancy.

Empirical formula	$C_{76}H_{116}AgAs_2F_6Fe_4O_8P_7\cdot(C_4H_8O)_4$	
Formula weight M/g·mol^{-1}	2258.00	
Device type	Oxford Diffraction Supernova (Atlas)	
Crystal color and shape	Orange plate	
Crystal size	0.20 × 0.06 × 0.03	
Temperature T/K	123(1)	
Radiation (λ/Å)	Cu (1.54178)	
Crystal system	Monoclinic	
Space group	*Cc*	
Unit cell dimensions	a = 18.0419(5) Å	α = 90 °
	b = 37.4538(6) Å	β = 116.777(4) °
	c = 17.4301(6) Å	γ = 90 °
Volume V/Å^3	10515.2(6)	
Formula units Z	4	
Absorption correction type	Analytical	
Absorption coefficient μ/mm^{-1}	8.024	
Density (calculated) ρ_{calc}/g·cm^{-3}	1.426	
F(000)	4688	
Theta range θ/°	$2.9840 \leq \theta \leq 72.7647$	
Index ranges	$-21 < h < 22$, $-45 < k < 45$, $-20 < l < 18$	
Reflections collected	34099	
Independent reflections [$I > 2\sigma(I)$]	15461 (R_{int} = 0.0356)	
Completeness to full theta	0.970	
Transmission T_{min} / T_{max}	0.308 / 0.697	
Data / parameters / restraints	15761 / 1229 / 2	
Goodness-of-fit on F^2 S	1.022	
Final R-values [$I > 2\sigma$(I)]	R_1 = 0.0439, wR_2 = 0.1172	
Final R-values (all data)	R_1 = 0.0447, wR_2 = 0.1183	
Largest difference hole and peak $\Delta\rho$/e·Å^{-3}	-0.600, 1.255	

5.3.25 $[\{\{Cp^*Cr(CO)_3\}_2(\mu_3,\eta^{1:1:1}\text{-}AsP_3)\}_2Ag]^+[PF_6]^-$ (76)

Compound **76** crystallizes as orange blocks from THF/hexane solutions. The asymmetric unit contains one molecule of **76** together with 1.5 molecule of THF of which the half occupied one is disordered over two positions. The refinement of occupancy and disorder of the silver atom as well as mixed occupied P/As positions was performed as described in 5.3.24.

Empirical formula	$C_{52}H_{60}AgAs_2Cr_4F_6O_{12}P_7\cdot(C_4H_8O)_{1.5}$	
Formula weight M/g·mol^{-1}	1781.66	
Device type	Oxford Diffraction Gemini Ultra R	
Crystal color and shape	Orange block	
Crystal size	0.49 × 0.42 × 0.15	
Temperature T/K	123(1)	
Radiation (λ/Å)	Cu (1.54178)	
Crystal system	Triclinic	
Space group	$P\bar{1}$	
Unit cell dimensions	a = 13.8850(5) Å	α = 78.997(3) °
	b = 15.7388(6) Å	β = 85.771(3) °
	c = 17.0669(3) Å	γ = 80.541(3) °
Volume V/Å^3	3521.7(2)	
Formula units Z	2	
Absorption correction type	Analytical	
Absorption coefficient μ/mm^{-1}	10.307	
Density (calculated) ρ_{calc}/g·cm^{-3}	1.680	
F(000)	1792	
Theta range θ/°	$3.3062 \leq \theta \leq 66.6612$	
Index ranges	$-15 < h < 16$, $-18 < k < 17$, $-20 < l < 15$	
Reflections collected	22206	
Independent reflections [$I > 2\sigma(I)$]	11173 (R_{int} = 0.0704)	
Completeness to full theta	0.966	
Transmission T_{min} / T_{max}	0.044 / 0.323	
Data / parameters / restraints	12056 / 858 / 0	
Goodness-of-fit on F^2 S	1.028	
Final R-values [$I > 2\sigma$(I)]	R_1 = 0.0846, wR_2 = 0.2312	
Final R-values (all data)	R_1 = 0.0876, wR_2 = 0.2368	
Largest difference hole and peak $\Delta\rho$/e·Å^{-3}	-0.995, 1.929	

5.3.26 $[\{Cp^*Cr(CO)_3\}_2(\mu_3,\eta^{1:1:1:1}\text{-}AsP_3)\{Au(PPh_3)\}]^+[PF_6]^-$ (78)

Compound **78** crystallizes as orange wedges from THF/hexane solutions. The asymmetric unit contains one molecule of **78**. The PF_6^- counterion is disordered over two positions. The displacement parameters of the F atoms were constrained (EADP).

Empirical formula	$C_{44}H_{45}AsAuCr_2F_6O_6P_5$	
Formula weight M/g·mol^{-1}	1314.54	
Device type	Oxford Diffraction Gemini Ultra R	
Crystal color and shape	Orange wedge	
Crystal size	0.20 × 0.10 × 0.07	
Temperature T/K	123(1)	
Radiation (λ/Å)	Cu (1.54178)	
Crystal system	Monoclinic	
Space group	$C2/c$	
Unit cell dimensions	a = 37.2281(6) Å	α = 90 °
	b = 17.5167(2) Å	β = 92.795(1) °
	c = 14.8502(2) Å	γ = 90 °
Volume V/Å^3	9672.5(2)	
Formula units Z	8	
Absorption correction type	Analytical	
Absorption coefficient μ/mm^{-1}	12.157	
Density (calculated) ρ_{calc}/g·cm^{-3}	1.805	
F(000)	5168	
Theta range θ/°	$3.7150 \leq \theta \leq 66.4815$	
Index ranges	$-43 < h < 40$, $-20 < k < 20$, $-17 < l < 16$	
Reflections collected	24041	
Independent reflections [$I > 2\sigma(I)$]	7914 (R_{int} = 0.0412)	
Completeness to full theta	0.985	
Transmission T_{min} / T_{max}	0.297 / 0.588	
Data / parameters / restraints	8446 / 585 / 31	
Goodness-of-fit on F^2 S	1.029	
Final R-values [$I > 2\sigma$(I)]	R_1 = 0.0420, wR_2 = 0.1117	
Final R-values (all data)	R_1 = 0.0477, wR_2 = 0.1141	
Largest difference hole and peak $\Delta\rho$/e·Å^{-3}	-1.603, 1.690	

5.3.27 [{{Cp'''Fe(CO)$_2$}$_2$(μ_3,$\eta^{1:1:1:1}$-As$_4$)}$_2$Cu]$^+$[BF$_4$]$^-$ (79)

Compound **79** crystallizes as dark purple plates from THF/hexane solutions. The asymmetric unit contains one molecule of **79** together with two molecules of THF which were treated with PLATON/SQUEEZE.

Empirical formula	$C_{76}H_{116}As_8BCuF_4Fe_4O_8P\cdot(C_4H_8O)_2$	
Formula weight M/g·mol^{-1}	2275.02	
Device type	Oxford Diffraction Supernova (Atlas)	
Crystal color and shape	Dark purple plate	
Crystal size	0.16 × 0.15 × 0.03	
Temperature T/K	123(1)	
Radiation (λ/Å)	Cu (1.54178)	
Crystal system	Triclinic	
Space group	$P\bar{1}$	
Unit cell dimensions	a = 13.8977(3) Å	α = 85.113(2) °
	b = 14.3511(3) Å	β = 85.305(2) °
	c = 24.9269(5) Å	γ = 76.006(2) °
Volume V/Å^3	4796.9(2)	
Formula units Z	2	
Absorption correction type	Analytical	
Absorption coefficient μ/mm^{-1}	8.510	
Density (calculated) ρ_{calc}/g·cm^{-3}	1.575	
F(000)	2228	
Theta range θ/°	3.1783 ≤ θ ≤ 73.5322	
Index ranges	-17 < h < 17, -17 < k < 16, -30 < l < 30	
Reflections collected	67332	
Independent reflections [$I > 2\sigma(I)$]	17617 (R_{int} = 0.0368)	
Completeness to full theta	0.980	
Transmission T_{min} / T_{max}	0.356 / 0.771	
Data / parameters / restraints	18998 / 1000 / 4	
Goodness-of-fit on F^2 S	1.053	
Final R-values [$I > 2\sigma$(I)]	R_1 = 0.0298, wR_2 = 0.0790	
Final R-values (all data)	R_1 = 0.0322, wR_2 = 0.0809	
Largest difference hole and peak $\Delta\rho$/e·Å^{-3}	-0.665, 0.659	

5.3.28 $[\{\{Cp'''Fe(CO)_2\}_2(\mu_3,\eta^{1:1:1:1}\text{-}As_4)\}_2Ag]^+[PF_6]^-$ (80)

Compound **80** crystallizes as red bars from THF/hexane solutions. The asymmetric unit contains one molecule of **80** together with four molecules of THF. One of the coordinating As_4-butterfly complexes is disordered over two positions.

Empirical formula	$C_{76}H_{116}AgAs_8F_6Fe_4O_8P\cdot(C_4H_8O)_4$	
Formula weight M/g·mol^{-1}	2519.69	
Device type	Oxford Diffraction Supernova (Atlas)	
Crystal color and shape	Red bar	
Crystal size	0.20 × 0.07 × 0.04	
Temperature T/K	123(1)	
Radiation (λ/Å)	Cu (1.54178)	
Crystal system	Triclinic	
Space group	$P\bar{1}$	
Unit cell dimensions	a = 17.5747(5) Å	α = 63.743(2) °
	b = 18.2923(4) Å	β = 78.378(2) °
	c = 20.6709(4) Å	γ = 62.931(2) °
Volume V/Å^3	5306.8(3)	
Formula units Z	2	
Absorption correction type	Analytical	
Absorption coefficient μ/mm^{-1}	9.173	
Density (calculated) ρ_{calc}/g·cm^{-3}	1.577	
F(000)	2556	
Theta range θ/°	2.9610 ≤ θ ≤ 74.0820	
Index ranges	-20 < h < 21, -22 < k < 22, -24 < l < 25	
Reflections collected	47818	
Independent reflections [$I > 2\sigma(I)$]	18331 (R_{int} = 0.0394)	
Completeness to full theta	0.963	
Transmission T_{min} / T_{max}	0.302 / 0.729	
Data / parameters / restraints	20824 / 1602 / 18	
Goodness-of-fit on F^2 S	1.072	
Final R-values [$I > 2\sigma$(I)]	R_1 = 0.0510, wR_2 = 0.1371	
Final R-values (all data)	R_1 = 0.0579, wR_2 = 0.1315	
Largest difference hole and peak $\Delta\rho$/e·Å^{-3}	-0.878, 1.051	

5.3.29 $[\{\{Cp^*Cr(CO)_3\}_2(\mu_3,\eta^{1:1:1:1}\text{-}As_4)\}_2Ag]^+[PF_6]^-$ (81)

Compound **81** crystallizes as red blocks from THF/hexane solutions. The asymmetric unit contains one molecule of **81**. The PF_6^- counterion was disordered over two positions which was refined using several SADI and EADP restraints and constraints.

Empirical formula	$C_{52}H_{60}AgAs_8Cr_4F_6O_{12}P$	
Formula weight M/g·mol^{-1}	1937.20	
Device type	Oxford Diffraction Gemini R Ultra	
Crystal color and shape	Red block	
Crystal size	0.41 × 0.30 × 0.16	
Temperature T/K	123(1)	
Radiation (λ/Å)	Cu (1.54178)	
Crystal system	Triclinic	
Space group	$P\bar{1}$	
Unit cell dimensions	a = 13.4565(6) Å	α = 75.556(5) °
	b = 14.9172(8) Å	β = 89.186(4) °
	c = 18.460(1) Å	γ = 69.014(3) °
Volume V/Å^3	3338.7(3)	
Formula units Z	2	
Absorption correction type	Analytical	
Absorption coefficient μ/mm^{-1}	12.756	
Density (calculated) ρ_{calc}/g·cm^{-3}	1.927	
F(000)	1888	
Theta range θ/°	$3.2850 \leq \theta \leq 70.8605$	
Index ranges	$-16 < h < 14$, $-18 < k < 18$, $-22 < l < 15$	
Reflections collected	26042	
Independent reflections [$I > 2\sigma(I)$]	11186 (R_{int} = 0.0925)	
Completeness to full theta	0.955	
Transmission T_{min} / T_{max}	0.064 / 0.313	
Data / parameters / restraints	12335 / 790 / 34	
Goodness-of-fit on F^2 S	1.063	
Final R-values [$I > 2\sigma$(I)]	R_1 = 0.0910, wR_2 = 0.2455	
Final R-values (all data)	R_1 = 0.0952, wR_2 = 0.2557	
Largest difference hole and peak $\Delta\rho$/e·Å^{-3}	-1.963, 3.387	

5.3.30 $[Ag(\eta^2\text{-}As_4)_2]^+[pftb]^-$ (82)

Compound **82** crystallizes as colorless blocks from CH_2Cl_2 solutions upon cooling to -78 °C. The asymmetric unit contains one molecule of **82**. One of the four $C(CF_3)_3$ groups is disordered over two positions. Several ISOR, SADI and DELU restraints were applied for the refinement.

Empirical formula	$C_{16}AgAlAs_8F_{36}O_4$	
Formula weight M/g·mol^{-1}	1674.37	
Device type	Oxford Diffraction Supernova (Atlas)	
Crystal color and shape	Colorless block	
Crystal size	0.15 × 0.04 × 0.03	
Temperature T/K	123(1)	
Radiation (λ/Å)	Cu (1.54178)	
Crystal system	Monoclinic	
Space group	$P2_1/c$	
Unit cell dimensions	a = 10.3125(5) Å	α = 90 °
	b = 18.9558(6) Å	β = 99.739(3) °
	c = 20.6898(6) Å	γ = 90 °
Volume V/Å^3	3986.2(3)	
Formula units Z	4	
Absorption correction type	Analytical	
Absorption coefficient μ/mm^{-1}	13.579	
Density (calculated) ρ_{calc}/g·cm^{-3}	2.790	
F(000)	3104	
Theta range θ/°	$3.1804 \leq \theta \leq 62.3016$	
Index ranges	$-11 < h < 11$, $-20 < k < 20$, $-22 < l < 22$	
Reflections collected	40921	
Independent reflections [$I > 2\sigma(I)$]	3747 (R_{int} = 0.0936)	
Completeness to full theta	0.967	
Transmission T_{min} / T_{max}	0.404 / 0.772	
Data / parameters / restraints	5546 / 703 / 121	
Goodness-of-fit on F^2 S	1.037	
Final R-values [$I > 2\sigma$(I)]	R_1 = 0.0577, wR_2 = 0.1327	
Final R-values (all data)	R_1 = 0.0976, wR_2 = 0.1552	
Largest difference hole and peak $\Delta\rho$/e·Å^{-3}	-1.037, 0.932	

5.3.31 $[(PPh_3)Au(\eta^2\text{-}As_4)]^+[pftb]^-$ (83)

Compound **83** crystallizes as colorless bars from CH_2Cl_2/hexane solutions at -28 °C. The asymmetric unit contains two molecules of **83**.

Empirical formula	$C_{34}H_{15}AlAs_4AuF_{36}O_4P$	
Formula weight M/g·mol^{-1}	1726.06	
Device type	Oxford Diffraction Supernova (Atlas)	
Crystal color and shape	Colorless bar	
Crystal size	0.23 × 0.06 × 0.04	
Temperature T/K	123(1)	
Radiation (λ/Å)	Cu (1.54178)	
Crystal system	Triclinic	
Space group	$P\bar{1}$	
Unit cell dimensions	a = 11.7548(3) Å	α = 83.675(2) °
	b = 16.4915(3) Å	β = 81.207(2) °
	c = 27.0668(5) Å	γ = 71.462(2) °
Volume V/Å^3	4905.7(2)	
Formula units Z	4	
Absorption correction type	Analytical	
Absorption coefficient μ/mm^{-1}	10.793	
Density (calculated) ρ_{calc}/g·cm^{-3}	2.337	
F(000)	3256	
Theta range θ/°	$3.1830 \leq \theta \leq 75.3183$	
Index ranges	$-14 < h < 13$, $-20 < k < 20$, $-33 < l < 33$	
Reflections collected	98916	
Independent reflections [$I > 2\sigma(I)$]	17899 (R_{int} = 0.0483)	
Completeness to full theta	0.984	
Transmission T_{min} / T_{max}	0.333 / 0.669	
Data / parameters / restraints	20017 / 1459 / 0	
Goodness-of-fit on F^2 S	1.035	
Final R-values [$I > 2\sigma$(I)]	R_1 = 0.0371, wR_2 = 0.0960	
Final R-values (all data)	R_1 = 0.0419, wR_2 = 0.1001	
Largest difference hole and peak $\Delta\rho$/e·Å^{-3}	-1.794, 2.662	

5.3.32 [Cp*Ru(dppe)(η^1-As$_4$)]$^+$[pftb]$^-$ (84)

Compound **84** crystallizes as orange blocks from CH_2Cl_2/hexane solutions at -28 °C. The asymmetric unit contains one molecule of **84** together with half a molecule of CH_2Cl_2. The $[pftb]^-$ counterion was refined using several SADI, ISOR and DELU restraints.

Empirical formula	$C_{52}H_{39}AlAs_4F_{36}O_4P_2Ru\cdot(CH_2Cl_2)_{0.5}$	
Formula weight M/g·mol^{-1}	1943.96	
Device type	Oxford Diffraction Supernova (Atlas)	
Crystal color and shape	Orange block	
Crystal size	0.27 × 0.19 × 0.10	
Temperature T/K	123(1)	
Radiation (λ/Å)	Cu (1.54178)	
Crystal system	Triclinic	
Space group	$P\bar{1}$	
Unit cell dimensions	a = 15.3443(2) Å	α = 115.302(1) °
	b = 15.8555(2) Å	β = 103.457(1) °
	c = 17.7174(2) Å	γ = 101.339(1) °
Volume V/Å^3	3568.65(9)	
Formula units Z	2	
Absorption correction type	Analytical	
Absorption coefficient μ/mm^{-1}	5.984	
Density (calculated) ρ_{calc}/g·cm^{-3}	1.809	
F(000)	1894	
Theta range θ/°	$2.9514 \leq \theta \leq 76.4839$	
Index ranges	$-19 < h < 19$, $-20 < k < 19$, $-21 < l < 22$	
Reflections collected	112013	
Independent reflections [$I > 2\sigma(I)$]	14038 (R_{int} = 0.0761)	
Completeness to full theta	0.975	
Transmission T_{min} / T_{max}	0.383 / 0.636	
Data / parameters / restraints	14635 / 960 / 118	
Goodness-of-fit on F^2 S	1.039	
Final R-values [$I > 2\sigma$(I)]	R_1 = 0.0727, wR_2 = 0.2153	
Final R-values (all data)	R_1 = 0.0742, wR_2 = 0.2172	
Largest difference hole and peak $\Delta\rho$/e·Å^{-3}	-1.392, 2.862	

5.3.33 [{Cp*Ru(dppe)}(μ,η$^{1:3}$-As$_4$){CpRu(PPh$_3$)}]$^{2+}$[pftb]$^-_2$ (85)

Compound **85** crystallizes as brown bars from CH_2Cl_2/hexane solutions at -28 °C. The asymmetric unit contains one molecule of **85** together with three heavily disorderd hexane and CH_2Cl_2 molecules that were treated with PLATON/SQUEEZE.

Empirical formula	$C_{91}H_{59}Al_2As_4F_{72}O_8P_3Ru_2$	
Formula weight M/g·mol^{-1}	3297.08	
Device type	Oxford Diffraction Supernova (Atlas)	
Crystal color and shape	Brown bar	
Crystal size	0.34 × 0.17 × 0.06	
Temperature T/K	123(1)	
Radiation (λ/Å)	Cu (1.54178)	
Crystal system	Triclinic	
Space group	$P\bar{1}$	
Unit cell dimensions	a = 15.0875(4) Å	α = 87.700(2) °
	b = 16.3946(5) Å	β = 82.608(2) °
	c = 27.6665(6) Å	γ = 68.657(3) °
Volume V/Å^3	6320.9(3)	
Formula units Z	2	
Absorption correction type	Analytical	
Absorption coefficient μ/mm^{-1}	5.023	
Density (calculated) ρ_{calc}/g·cm^{-3}	1.732	
F(000)	3216	
Theta range θ/°	3.1660 ≤ θ ≤ 70.6439	
Index ranges	-18 < h < 18, -18 < k < 19, 0 < l < 33	
Reflections collected	23348	
Independent reflections [$I > 2\sigma(I)$]	18968 (R_{int} = 0.0609)	
Completeness to full theta	0.960	
Transmission T_{min} / T_{max}	0.406 / 0.778	
Data / parameters / restraints	23.348 / 1671 / 247	
Goodness-of-fit on F^2 S	1.096	
Final R-values [$I > 2\sigma$(I)]	R_1 = 0.0950, wR_2 = 0.2736	
Final R-values (all data)	R_1 = 0.1055, wR_2 = 0.2858	
Largest difference hole and peak $\Delta\rho$/e·Å^{-3}	-1.443, 1.950	

5.3.34 $As_4@[\{Cp^*Fe(\eta^5\text{-}P_5)\}_{10}Cu_{30}I_{30}(MeCN)_6]$ (86)

Compound **86** crystallizes as red laths from toluene/CH_2Cl_2/THF/MeCN mixtures. The asymmetric unit contains half a molecule of **86**.

Empirical formula	$C_{111.20}H_{166.80}Cu_{29.60}Fe_{10}I_{29.60}N_{5.60}P_{50}\cdot As_4\cdot(CH_3CN)_{4.6}$	
Formula weight M/g·mol^{-1}	9814.65	
Device type	Oxford Diffraction Supernova (Atlas)	
Crystal color and shape	Red lath	
Crystal size	0.12 × 0.04 × 0.03	
Temperature T/K	123(1)	
Radiation (λ/Å)	Cu (1.54178)	
Crystal system	Monoclinic	
Space group	$P2_1/n$	
Unit cell dimensions	a = 19.8517(9) Å	α = 90 °
	b = 26.727(1) Å	β = 105.328(4) °
	c = 28.7040(9) Å	γ = 90 °
Volume V/Å^3	14688(1)	
Formula units Z	2	
Absorption correction type	analytical	
Absorption coefficient μ/mm^{-1}	33.803	
Density (calculated) ρ_{calc}/g·cm^{-3}	2.219	
F(000)	9087	
Theta range θ/°	$3.4071 \leq \theta \leq 70.5429$	
Index ranges	$-19 < h < 22$, $-29 < k < 26$, $-31 < l < 31$	
Reflections collected	42478	
Independent reflections [$I > 2\sigma(I)$]	12004 (R_{int} = 0.1018)	
Completeness to full theta	0.997	
Transmission T_{min} / T_{max}	0.124 / 0.445	
Data / parameters / restraints	21045 / 1222 / 37	
Goodness-of-fit on F^2 S	1.000	
Final R-values [$I > 2\sigma$(I)]	R_1 = 0.0828, wR_2 = 0.2147	
Final R-values (all data)	R_1 = 0.1472, wR_2 = 0.2612	
Largest difference hole and peak $\Delta\rho$/e·Å^{-3}	-1.767, 3.925	

5.3.35 $\{Z_4As_4\}@[\{Cp^*Fe(\eta^5\text{-}P_5\}_{12}Cu_{51}I_{56}(MeCN)_3]^-Z^+$ (87)

Compound **87** crystallizes as reddish brown tetrahedra from toluene/CH_2Cl_2/THF/MeCN mixtures. The asymmetric unit contains one third of a molecule **87**. Due to the unclear nature of atom Z only preliminary crystallographic data is given

Empirical formula	$C_{120}H_{180}Cu_{51}Fe_{12}I_{56}P_{60}Z_5 \cdot As_4 \cdot (CH_3CN)_{1.5}$	
Device type	Oxford Diffraction Supernova (Atlas)	
Crystal color and shape	Reddish brown tetrahedron	
Temperature *T*/K	123(1)	
Radiation (λ/Å)	Cu (1.54178)	
Crystal system	cubic	
Space group	$P2_13$	
Unit cell dimensions	a = 34.8665 Å	α = 90 °
	b = 34.8665 Å	β = 90 °
	c = 34.8665 Å	γ = 90 °
Volume *V*/Å^3	42386	
Formula units *Z*	4	

6. Conclusions

6.1 Selective activation of the E_4 tetrahedron ($E_4 = P_4$, AsP_3, As_4)

In the first part of this thesis, the activation of white phosphorus, yellow arsenic and the interpnictide molecule AsP_3 is investigated. The reaction of the E_4 tetrahedron with suitable main group and transition metal compounds leads to the selective cleavage of one, two, three or four E–E bonds (c.f. Scheme 2). In case of As_4 and AsP_3 this affords several novel compounds with unprecedented structural motifs.

The reaction of the cyclic (alkyl)-(amino)carbene [^{Menthyl}CAAC] (**17**), bearing a menthyl substituent, leads to the cleavage of four bonds of the As_4 tetrahedron to afford [{^{Menthyl}CAAC}$_2$As$_2$] (**43**) (Scheme 11). The As_2 unit in **43** is stabilized by two carbene moieties in an end-on bonding mode. The formation of an As_2 unit from the reaction of As_4 with **17** is contrary to the reaction of the carbene with P_4 which leads to a carbene stabilized P_4 chain.[44] This different reaction behavior is rationalized by theoretical calculations that clearly show a thermodynamically stable P_4 but a labile As_4 chain. In case of the *cyclo*-hexyl substituted CAAC **19**, the reaction with As_4 leads to the cleavage of only three As–As bonds. The resulting product is [{^{cHex}CAAC}$_3$As$_4$] (**44**) which exhibits a unique *iso*-tetraarsane framework (Scheme 11) and is similar to the reaction product of **19** with white phosphorus.

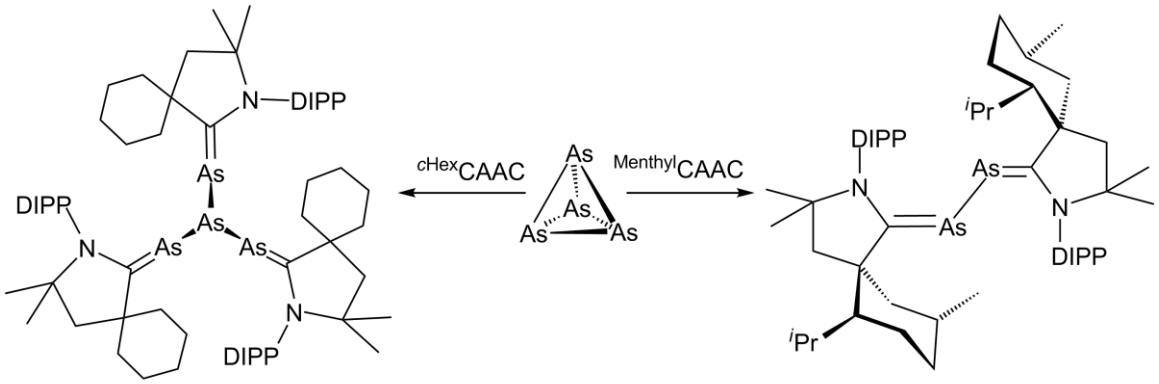

44 **43**

Scheme 11. Degradation of the As_4 tetrahedron induced by cyclic (alkyl)-(amino)carbenes.

The selective cleavage of two bonds of the E_4 tetrahedron ($E_4 = P_4$, As_4, AsP_3) is achieved quantitatively by the reaction with the dichromium complex [L_2Cr_2] (**45**) (L = (2,6-diisopropylphenyl)-{6-(2,6-dimethylphenyl)-pyridin-2-yl}-amid) that exhibits a Cr–Cr quintuple bond. The unique complexes [$L_2Cr_2(\mu,\eta^{1:1:2:2}$-$E_4)$] ($E_4 = P_4$ (**46**), As_4 (**47**), AsP_3 (**48**))

contain terminal *cyclo*-E_4 decks, that are located above the Cr–Cr bond, a coordination mode that has not been observed to date. They are best described as *cyclo*-E_4^{2-} ligands that derive from a formal two electron reduction of the E_4 tetrahedron. The oxidation takes place at the Cr–Cr quintuple bond which bond order is consequently reduced to four. In case of the AsP_3 compound **48**, the arsenic atom occupies exclusively the bridging positions. Furthermore, the P_4 derivative **46** reacts with $[W(CO)_5(thf)]$ to yield the mono adduct $[\{L_2Cr_2\}(\mu_3,\eta^{1:1:1:2:2}\text{-}P_4)\{W(CO)_5\}]$ (**49**). While X-ray structure analysis clearly shows the coordination of one of the terminal phosphorus atoms of the *cyclo*-P_4 ring to the $[W(CO)_5]$ fragment, VT-NMR investigations in solution indicate the coordination of a bridging P atom. Theoretical calculations point to a small energy difference between these isomers and a rapid equilibrium in solution.

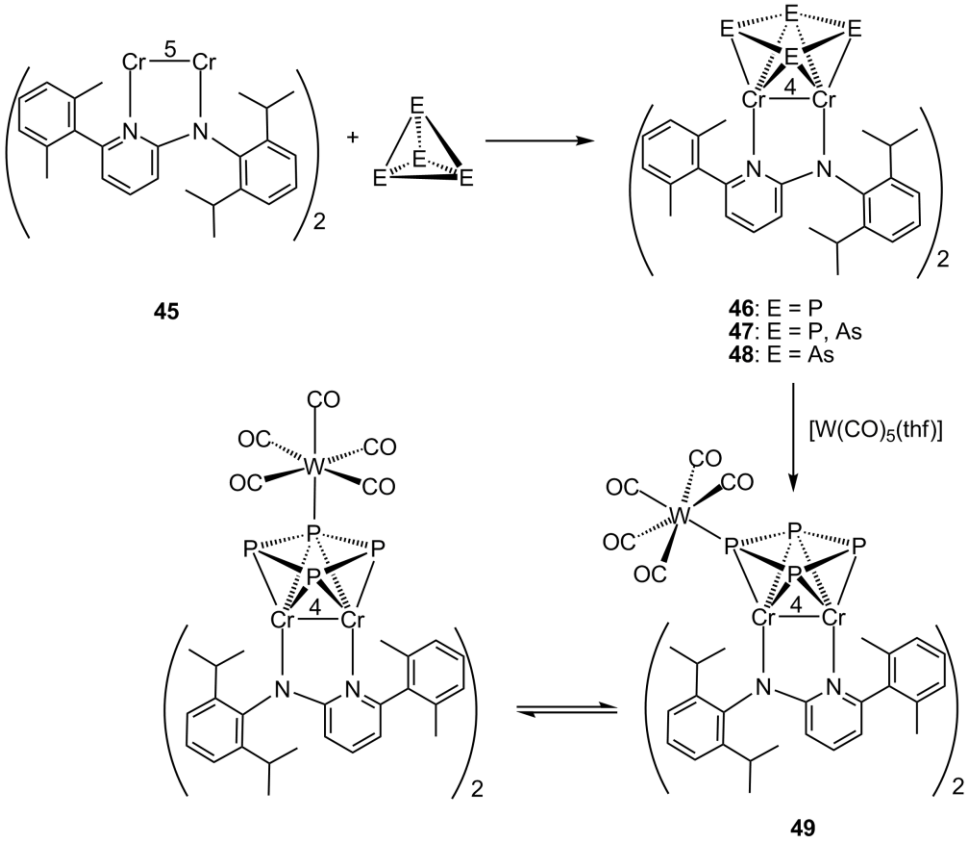

Scheme 12. Synthesis and coordination behavior of complexes with an end-on *cyclo*-E_4 unit (E_4 = P_4, As_4, AsP_3).

In the course of the studies an optimized strategy for the synthesis of the dimeric iron complex $[\{Cp'''Fe(CO)_2\}_2]$ (**10b**) was developed. Compound **10b** was successfully used for the mild and selective cleavage of one bond of the E_4 tetrahedron, which afforded the tetrapnictido-*bicyclo*[1.1.0]butane complexes $[\{Cp'''Fe(CO)_2\}_2(\mu,\eta^{1:1}\text{-}E_4)]$ (E_4 = P_4 (**9b**), AsP_3 (**51**), As_4 (**52**)) in quantitative yields (Scheme 13). Furthermore, the dimeric chromium complex $[\{Cp^*Cr(CO)_3\}_2]$ (**53**) was also employed for the activation of E_4 leading to the bridging butterfly

complexes [{Cp*Cr(CO)$_3$}$_2$(μ,η$^{1:1}$-E$_4$)] (E$_4$ = P$_4$ (**54**), AsP$_3$ (**55**), As$_4$ (**56**)) (Scheme 13). In both cases, the reaction takes place immediately at room temperature and is most likely to proceed via a radical bond cleavage mechanism induced by metal centered radicals. This leads to a fast and selective formation of the desired compounds. The bridging butterfly motif of AsP$_3$ as well as As$_4$ is unprecedented so far.

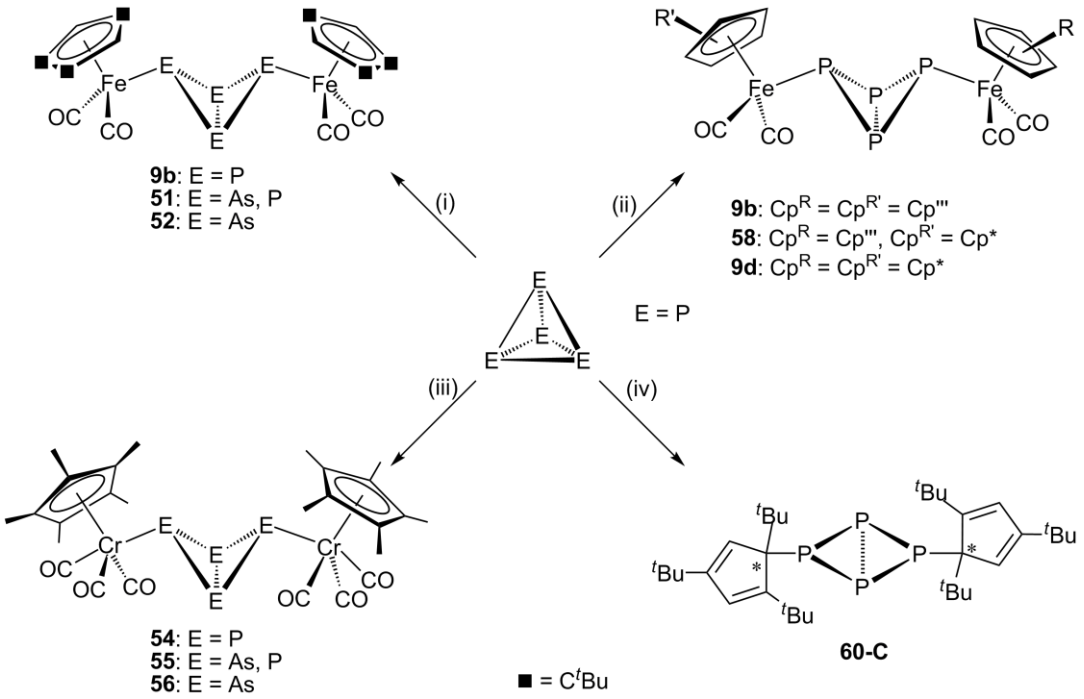

Scheme 13. Synthesis of several E$_4$ butterfly complexes (E$_4$ = P$_4$, As$_4$, AsP$_3$) derived from the reaction of the E$_4$ tetrahedron with (i) [{Cp'''Fe(CO)$_2$}$_2$] (**10b**), (ii) [{Cp'''Fe(CO)$_2$}{Cp*Fe(CO)$_2$}] (**57**), (iii) [{Cp*Cr(CO)$_3$}$_2$] (**53**) and (iv) [{Cp'''Fe(μ-Br)}$_2$] (**59**).

The obtained E$_4$ butterfly complexes exhibit similar structural features. The bond lengths between the bridgehead atoms is slightly shortened compared to the starting material while the bonds between the bridgehead atoms and the "wing-tip" atoms are slightly elongated. The bond distance between the "wing-tip" atoms E is larger for the iron derivatives than for the chromium complexes pointing to a slightly weaker interaction between the "wing-tip" P atoms. This may be an effect of the different steric demand of the metal fragments. However, the electron donating character of the [Cp^{R}M(CO)$_n$] fragments may also play an important role.

Furthermore, the novel dimeric iron complex [{Cp'''Fe(CO)$_2$}{Cp*Fe(CO)$_2$}] (**57**) was synthesized and reacted with white phosphorus to yield a statistical mixture of the butterfly complexes **9b**, [{Cp'''Fe(CO)$_2$}(μ,η$^{1:1}$-P$_4$){Cp*Fe(CO)$_2$}] (**58**) and the highly desirable [{Cp*Fe(CO)$_2$}$_2$(μ,η$^{1:1}$-P$_4$)] (**9d**), which could be separated by low temperature coloumn chromatography. This elegant methode provides an easy, large scale access to analytically pure

9d which was not possible so far and may open the way to tri and tetraphosphaferrocenes with the small Cp* ligand.

In addition to the transition-metal-mediated formation of P_4 butterfly complexes, a novel route for the synthesis of a tetraphospha-*bicyclo*[1.1.0]-butane framework with organic substituents is presented. The reaction of the 16 VE dimeric iron complex [{Cp'''Fe(μ-Br)}$_2$] (**59**) with white phosphorus leads to a direct C–P bond formation (Scheme 13). The resulting P_4 butterfly compound [Cp'''$_2$P$_4$] (**60**) is isolated as a mixture of four different isomers that could be clearly identified by ^{31}P{^{1}H}-^{31}P{^{1}H}-COSY NMR spectroscopy. In all cases, the Cp''' substituent is only bound to the P_4 butterfly framework via its tertiary carbon atoms. The formation of **60** is most likely to proceed via a radical mechanism which is corroborated by the product distribution. This unprecedented transition metal mediated C–P bond formation reaction bears large potential for developing a catalyst supported incorporation of phosphorus into organic molecules.

6.2 Reactivity and Coordination Behavior of E_4 Butterfly Complexes

While the fragmentation and reaggregation of P_4 in the coordination sphere of transition metals has been intensively studied throughout the last decades, only few results regarding the reactivity of As_n ligand complexes are known to date. This is mainly due to the lability of yellow arsenic and its challenging synthesis.

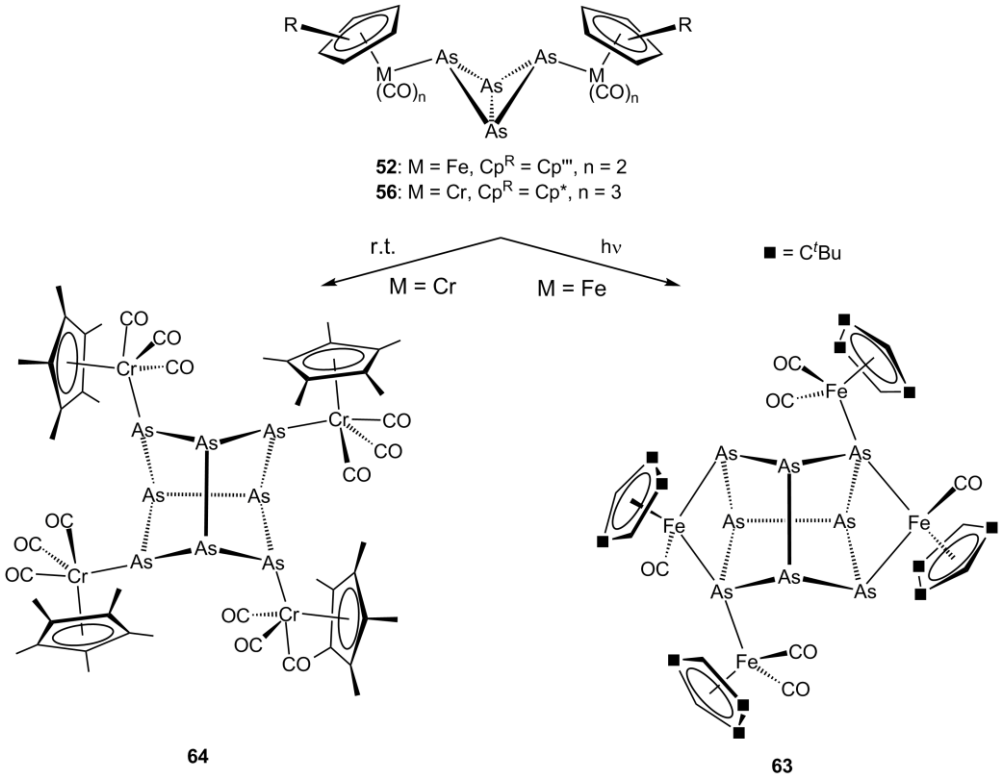

Scheme 14. Formation of the As_8 cuneane complexes **63** and **64** by the dimerization of As_4 butterfly precursor complexes.

The novel As_4 butterfly complexes [{Cp'''Fe(CO)$_2$}$_2$(μ,$\eta^{1:1}$-As_4)] (**52**) and [{Cp*Cr(CO)$_3$}$_2$(μ,$\eta^{1:1}$-As_4)] (**56**), though being isostructural with their P_4 derivatives, show a different reactivity under thermolytic and photolytic conditions. The P_4 butterfly complex **9b** looses two carbonyl ligands upon irradiation with UV light and affords the *cyclo*-P_4 complex [{Cp'''Fe}(μ,$\eta^{1:4}$-P_4){Cp'''Fe(CO)$_2$}].[89] In contrast, the As_4 butterfly complex **52** is only decarbonylated once to afford [{Cp'''Fe(CO)$_2$}(μ,$\eta^{1:2}$-As_4){Cp'''Fe(CO)}] (**62**) which readily dimerizes to give the unique As_8 complex [{Cp'''Fe(CO)$_2$}$_2$(μ_4,$\eta^{1:1:2:2}$-As_8){Cp'''Fe(CO)}$_2$] (**63**) (Scheme 14). Complex **63** exhibits an As_8 cuneane framework that is stabilized by two terminal and two bridging iron moieties. The central As_8 building unit in **63** may best be described as As_8^{4-} ligand that is isostructural as well as valence isoelectronic to the well known realgar As_4S_4. The reason for the different reactivity of the As_4 butterfly complex compared to its P_4 derivative might be the reduced relative bulk of the [Cp'''Fe(CO)$_2$] moieties with regard to the E_4 butterflyframework. In case of **56** the dimerization already takes place without irradiation and affords [{Cp*Cr(CO)$_3$}$_4$(μ_4,$\eta^{1:1:1:1}$-As_8)] (**64**), which also comprises an As_8 cuneane framework (Scheme 14). However, complex **64** contains only terminal [Cp*Cr(CO)$_3$] units and is formed without an initial carbonyl loss. The reason might be the small steric bulk of the [Cp*Cr(CO)$_3$] units, which cannot stabilize the As_4 butterfly framework and lead to an enhanced reactivity at room temperature.

In addition, DFT calculations on the model complex [{CpFe(CO)$_2$}$_2$(μ,$\eta^{1:1}$-P_4)] were performed. The frontier orbitals of the molecule are mainly localized at the phosphorus atoms and their orientation indicates that they might be accessible for coordination. Hence, the coordination properties of the complexes [{Cp'''Fe(CO)$_2$}$_2$(μ,$\eta^{1:1}$-E_4)] (E_4 = P_4 (**9b**), AsP_3 (**51**), As_4 (**52**)) and [{Cp*Cr(CO)$_3$}$_2$(μ,$\eta^{1:1}$-E_4)] (E_4 = P_4 (**54**), AsP_3 (**55**), As_4 (**56**)) towards several transition metal Lewis acids was investigated (Scheme 15). The *bicyclic* butterfly complexes serve as chelating ligands with small bite angles. Hence, they may be regarded as inorganic dppm derivatives with large steric bulk which could open new ways in "inorganometallic" coordination chemistry.

Generally, the carbonyl bands of the chelate complexes in the IR spectrum are blue-shifted compared to the corresponding starting material due to an electron withdrawing effect of the Lewis acid. In case of the P_4 butterfly complexes **9b** and **54**, the largest shift for the carbonyl resonances in the IR spectra is observed for the soft Lewis acids $[(PPh_3)Au]^+$ and $FeBr_2$ indicating a significant orbital interaction upon coordination rather than just an electrostatic interaction. Furthermore, the Fe–P or Cr–P bond lengths of the butterfly complexes are shortened in the chelate compounds with respect to the starting materials. That points to a participation of the

HOMO-1 orbital (see Figure 28) for the coordination of the Lewis acid, which has a slight antibonding character with respect to the Fe–P and Cr–P bonds.

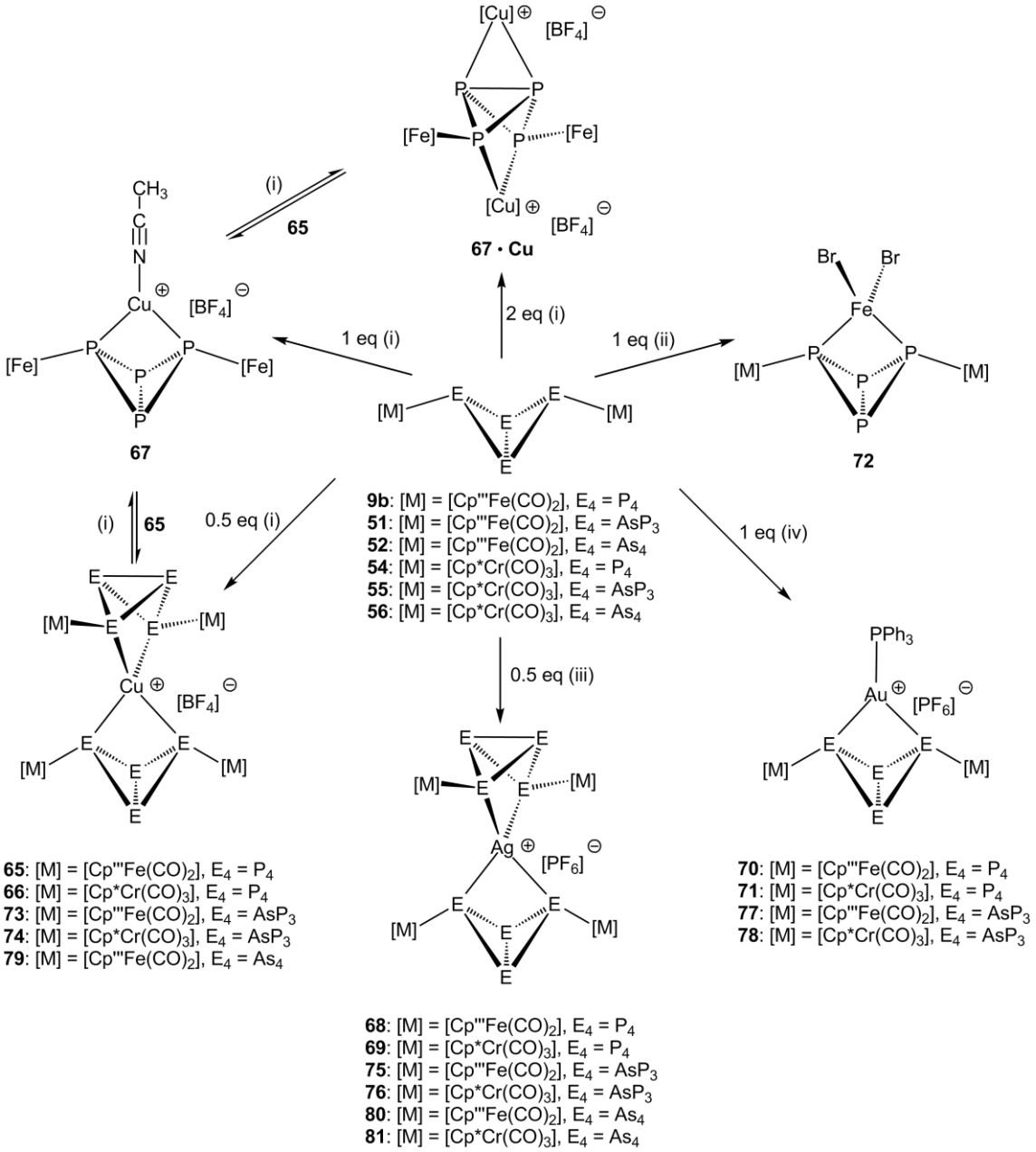

Scheme 15. Summary on the *mono* and *bis* chelate complexes from the reaction of E_4 butterfly complexes with (i) $[Cu(MeCN)_4]^+[BF_4]^-$, (ii) $[FeBr_2(dme)]$, (iii) $AgPF_6$ and (iv) $[(PPh_3)Au(tht)]^+[PF_6]^-$.

The $^{31}P\{^1H\}$ NMR spectra of the reaction mixtures show a quantitative and fast formation of the respective chelate complex. In case of the silver derivatives even Ag–P coupling is observed in the $^{31}P\{^1H\}$ NMR spectrum, pointing to a strong orbital overlap between the atoms. A dynamic behavior in solution is usually not observed on the NMR time scale. The only exception is complex $[\{Cp'''Fe(CO)_2\}_2(\mu_3,\eta^{1:1:1:1}\text{-}P_4)\{Cu(MeCN)\}]^+[BF_4]^-$ (**67**) which isomerizes in solution to afford the *bis* chelate complex **65** as well as

$[\{Cp'''Fe(CO)_2\}_2(\mu_4,\eta^{1:1:1:1:2}\text{-}P_4)\{Cu(MeCN)\}\{Cu(MeCN)_2\}]^{2+}[BF_4]^-_2$ (**67·Cu**). This labile character of the acetonitrile ligand could qualify complex **67** as unique building block for the formation of self assembled supramolecular structures as well as for catalytic applications.

In case of the AsP_3 butterfly complexs, the obtained chelates with copper and silver cations show high-order $^{31}P\{^1H\}$ NMR spectra. The reason is the low symmetry of the complexes induced by the introduction of arsenic at two out of the four coordinating atom sites. This not only influences the direct coordination environment of the Lewis acid, but also leads to magnetically inequivalent bridgehead P atoms of the AsP_3 butterfly scaffolds.The molecular structures of the *bis* chelate complexes **74**, **75** and **76** exhibit an allocation disorder of phosphorus and arsenic at the "wing-tip" positions of the butterfly framework resulting in four different occupancy combinations. This consequently leads to four possible positions of the coordinated Lewis acid. However, taking the positional disorder of the Lewis acid into account, the resulting M–P (M = Cu, Ag) bond lengths are shorter than in the corresponding P_4 chelate complexes **65**, **66**, **68** and **69**. Hence, the introduction of arsenic at the coordinating positions leads to a stronger M–P interaction. This fact is well reflected in the $^1J_{AgP}$ coupling constants observed for the complexes **75** and **76** which are about 140 Hz larger than in the P_4 derivatives. This strengthening of the M–P bonds is maximized in $[\{Cp^*Cr(CO)_3\}_2(\mu_3,\eta^{1:1:1:1}\text{-}P_4)\{Au(PPh_3)\}]^+[PF_6]^-$ (**78**) in which the gold(I) cation is linearly coordinated by the PPh_3 ligand and the "wing-tip" P atom of the AsP_3 butterfly scaffold and shows only minor interaction with the "wing-tip" arsenic atom.

6.3 Stabilization of yellow arsenic in the coordination sphere of transition metals – The intact As_4 tetrahedron as ligand

In contrast to white phosphorus, which ligand properties have been extensively studied, the coordination chemistry of yellow arsenic is still unexplored. The reason is the instability of As_4 at ambient conditions. Especially the exposure to light accelerates the decomposition of yellow arsenic to its metallic modification grey arsenic. Hence, As_4 is not storable and has to be freshly prepared in a time consuming synthesis procedure prior to use. Furthermore, stochiometric reactions are not possible. It was therefore of great interest to investigate its reactivity towards suitable Lewis acids to not only gain insight into its coordination abilities, but also to explore possible As_4 storage materials.

In order to investigate the coordination behavior of yellow arsenic, it was reacted with $[Ag(CH_2Cl_2)]^+[pftb]^-$ to afford the unique homoleptic arsenic complex $[Ag(\eta^2\text{-}As_4)_2]^+[pftb]^-$ (**82**) in excellent yields (Scheme 16). Compound **82** exhibits the unprecedented side-on coordination of

two intact As_4 tetrahedra to the Lewis acidic silver(I) cation. Raman spectroscopic investigations together with detailed DFT and CCSD(T) calculations clearly show an intact bond between the coordinating arsenic atoms as well as mainly electrostatic interactions between the silver cation and the As_4 tetrahedra. Hence, complex **82** is the first coordination compound of yellow arsenic. Surprisingly, compound **82** is light stable and can be stored under argon atmosphere without detectable decomposition. Furthermore, it is well soluble in polar solvents. Hence, it can be utilized for further reactions as "easy to handle" As_4 synthon (Scheme 16) as well as As_4 storage medium.

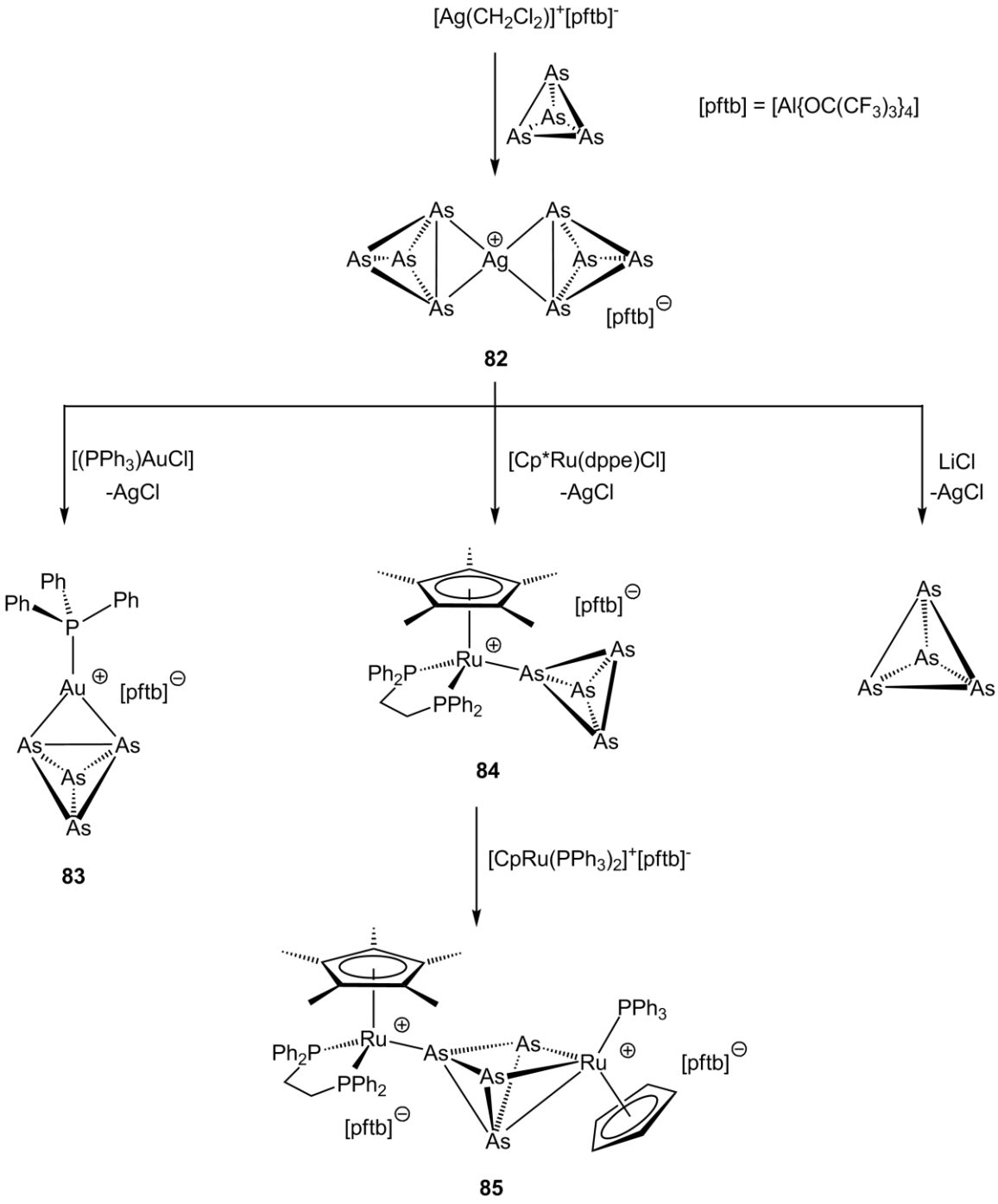

Scheme 16. Synthesis and reactivity of complexes containing yellow arsenic as ligands.

The reaction of **82** with [(PPh_3)AuCl] leads to the formation insoluble AgCl as well as [(PPh_3)Au(η^2-As_4)]$^+$[pftb]$^-$ (**83**) which is isolated in good yields. X-ray structure analysis together with DFT and CCSD(T) calculations show the coordination of an intact As_4 tetrahedron to the [(PPh_3)Au]$^+$ cation. The reaction nicely demonstrates the use of [Ag(η^2-As_4)$_2$]$^+$[pftb]$^-$ (**82**) as an As_4 transfer reagent which allows stochiometric reactions with the unstable As_4 for the first time.

As the side-on coordination of yellow arsenic could be realized successfully, the end-on coordination mode of As_4 moved into the focus of interest. While for phopshorus the coordination via its lone pairs seems to be preferred, the σ-coordination is unfavorable for arsenic. In order to evaluate the most promising Lewis acidic transition metal complex for that purpose, detailed DFT calculations were carried out that pointed on [Cp*Ru(dppe)]$^+$ as the most appropriate candidate for the vertex coordination of As_4.

The reaction of [Cp*Ru(dppe)Cl] with [Ag(η^2-As_4)$_2$]$^+$[pftb]$^-$ (**82**) as As_4 transfer reagent leads to the formation of [Cp*Ru(dppe)(η^1-As_4)]$^+$[pftb]$^-$ (**84**) (Scheme 16). Compound **84** exhibits a unique end-on coordinating, intact As_4 tetrahedron. Theoretical studies show the As_4 ligand being a σ-donor as well as π-donor/acceptor ligand leading to a short Ru–As bond. The reaction of complex **84** with [CpRu(PPh_3)]$^+$ does not lead to the expected η^1:η^1coordination of an intact As_4 tetrahedron which is in contrast to its P_4 derivative. Instead, [{Cp*Ru(dppe)}(μ,$\eta^{1:3}$-As_4){CpRu(PPh_3)}]$^{2+}$[pftb]$^-_2$ (**85**) is formed in which a [CpRu(PPh_3)] moiety coordinates to the basal As_3 unit of the η^1-As_4 ligand with an additional cleavage of one As–As bond (Scheme 16). The reason for the different reactivity of η^1-P_4 and η^1-As_4 complexes is most likely the weaker As–As single bond (36 kcal·mol^{-1}) compared to a P–P single bond (47 kcal·mol^{-1}) in the E_4 tetrahedron (E = P, As).

Furthermore, it is demonstrated that complex **82** can also be utilized as As_4 storage material from which the stabilized yellow arsenic can be realeased again. The reaction of **82** with LiCl affords the formation of the insoluble AgCl, sparingly soluble Li[pftb] as well as yellow arsenic which remains in solution. To follow this targeted As_4 release, challenging ^{75}As NMR investigations were carried out that clearly proof the liberation of As_4 from complex **82**. The so gained solutions of As_4 are two to five times higher in concentration than conventionally generated As_4 solutions[1] and show a remarkable light stability (> 4h). Moreover, only small amounts of solvent are needed and also low boiling solvents can be used. The release procedure can be done within 15 minutes which makes As_4 a readily available molecule for synthetic chemistry.

[1] conventional As_4 solutions in toluene: $c(As_4) \approx 3.7 \cdot 10^{-3}$ mol L^{-1}; As_4 solutions made from **82**: $c(As_4) \approx 1.5 \cdot 10^{-2}$ mol L^{-1}.

6.4 Yellow arsenic as a template for the formation of supramolecular aggregates

Finally, the stable As_4 solutions obtained from complex **82** were used for the template controlled self assembly of [Cp*Fe(η^5-P_5)] (**35a**) and copper(I)iodide. The reaction of **35a** with two equivalents of CuI in the presence of yellow arsenic affords the supramolecule As_4@[{Cp*Fe(η^5-P_5)}$_{10}$$Cu_{30}I_{30}$(MeCN)$_6$] (**86**) in which the As_4 tetrahedron is embedded in a cuboid-shaped inorganic host molecule (Figure 60). Compound **86** is the first macromolecule that contains an intact As_4 tetrahedron, but the tetrahedral symmetry of yellow arsenic is not adopted by the host complex. The inorganic scaffold of **86** consists of 100 non-carbon atoms. The inner cavity is of elongated shape with a length of about 10.8 Å.[130] It may be described by two half shells that are connected by a CuI belt. This belt divides the inner cavity into two parts which are occupied by one As_4 tetrahedron with a probability of 50 %.

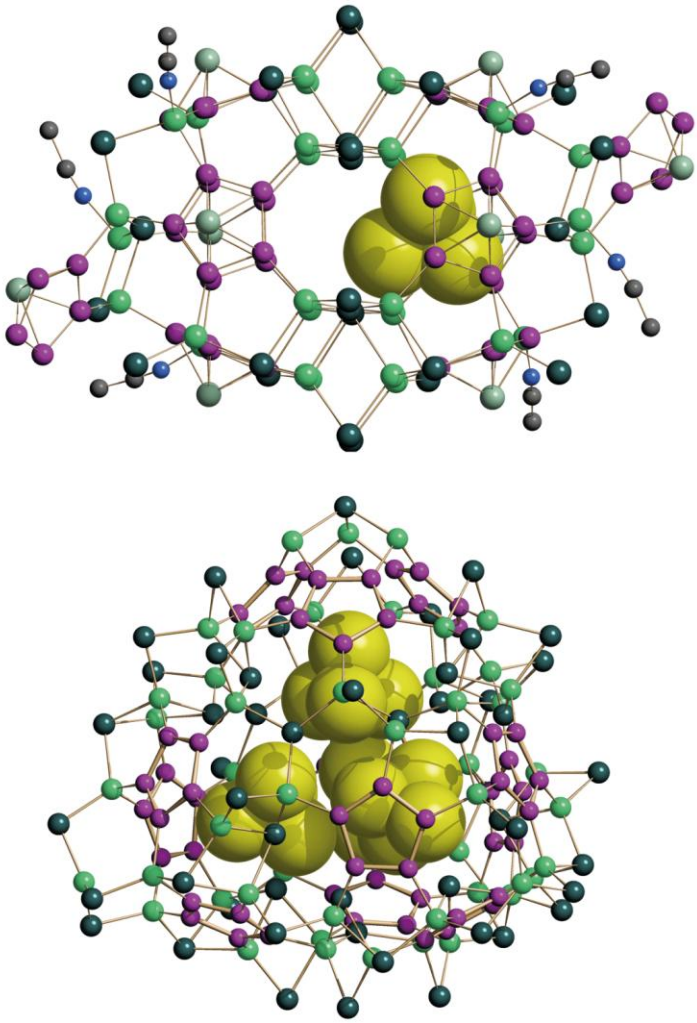

Figure 60. Molecular structures of the macromolecules **86** (above) and **87** (below) in the crystal.

An excess of lithium in solution affords the formation of $\{Z_4As_4\}@[\{Cp^*Fe(\eta^5\text{-}P_5\}_{12}Cu_{51}I_{56}(MeCN)_3]^-Z^+$ (**87**) as a second giant spherical molecule (Figure 60). X-ray structure analysis reveals an inorganic framework consisting of 12 pentaphosphaferrocene as well as 51 copper and 56 iodine atoms. Overall, it consists of 161 non-carbon atoms that together form a nearly tetrahedral shaped macromolecule with outer edge lengths of 21.3 Å and 22.5 Å.[130] The inner cavity shows an almost perfect tetrahedral shape with an edge length of about 12.9 Å[130] and is occupied by one As_4 tetrahedron which is statistically disordered over four positions. Hence, **87** is the first example of the $[Cp^*Fe(\eta^5\text{-}P_5)]$/CuI system in which the threefold symmetry of the template is adopted by the host molecule. One of the vertices of the As_4 tetrahedron points to one of the vertices of the "inner tetrahedron". In addition, six positions can be localized that are statistically occupied by four light atoms Z that interact with the As_4 tetrahedron. The nature of Z is still not fully understood. However, ^{7}Li NMR investigations indicate lithium as the light atom. This is surprising, since Li–As interactions cannot be observed in solution and nicely exemplify the potential of these supramelocular aggregates for the isolation of unknown coordination compounds.

7. Appendices

7.1 Supplementary Figures

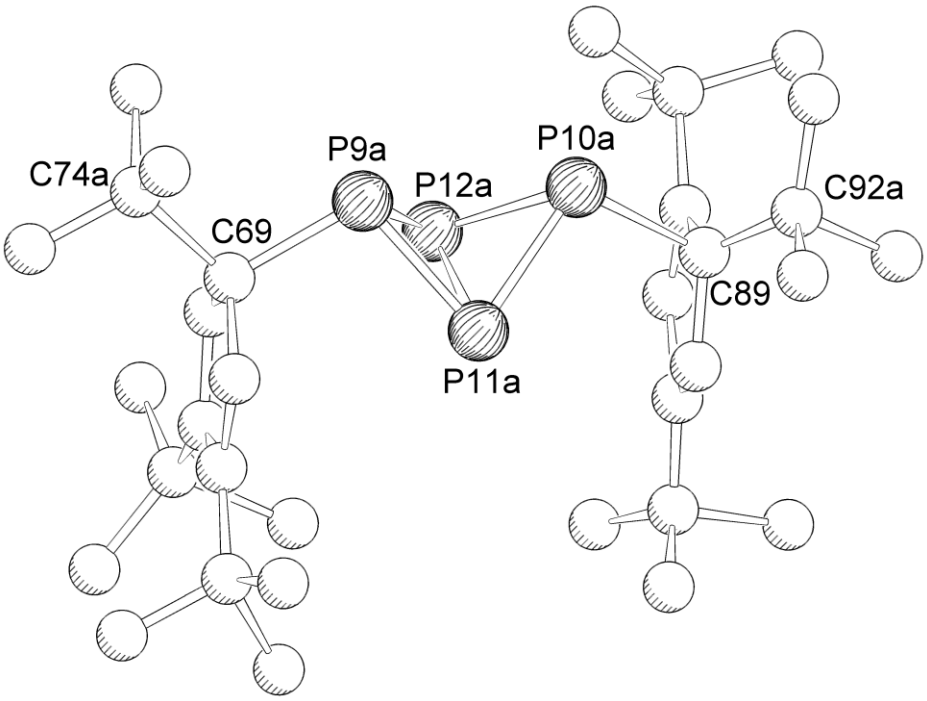

Figure 61. Molecular structure of **60-D** in the crystal. For clarity reasons only one of the two possible positions is depicted and hydrogen atoms are omitted. Selected bond lengths [Å] and angles [°]: P9a–C69 1.915(7), P10a–C89 2.099(8), P9a–P11a 2.182(4), P9a–P12a 2.219(4), P10a–P11a 2.215(4), P10a–P12a 2.207(5), P11a–P12a 2.167(5), P9a···P10a 2.787(4), P11a–P9a–P12a 59.0(1), P11a–P10a–P12a 58.7(1), P9a–P11a–P10a 78.7(2), P9a–P12a–P10a 78.0(2), P11a–P9a–C69 100.9 (3), P12a–P9a–C69 99.8(3), P11a–P10a–C89 103.2(2), P12a–P10a–C89 103.8(2), P9a–C69–C74a 103.3(5), P10a–C89 –C92a 98.0(5).

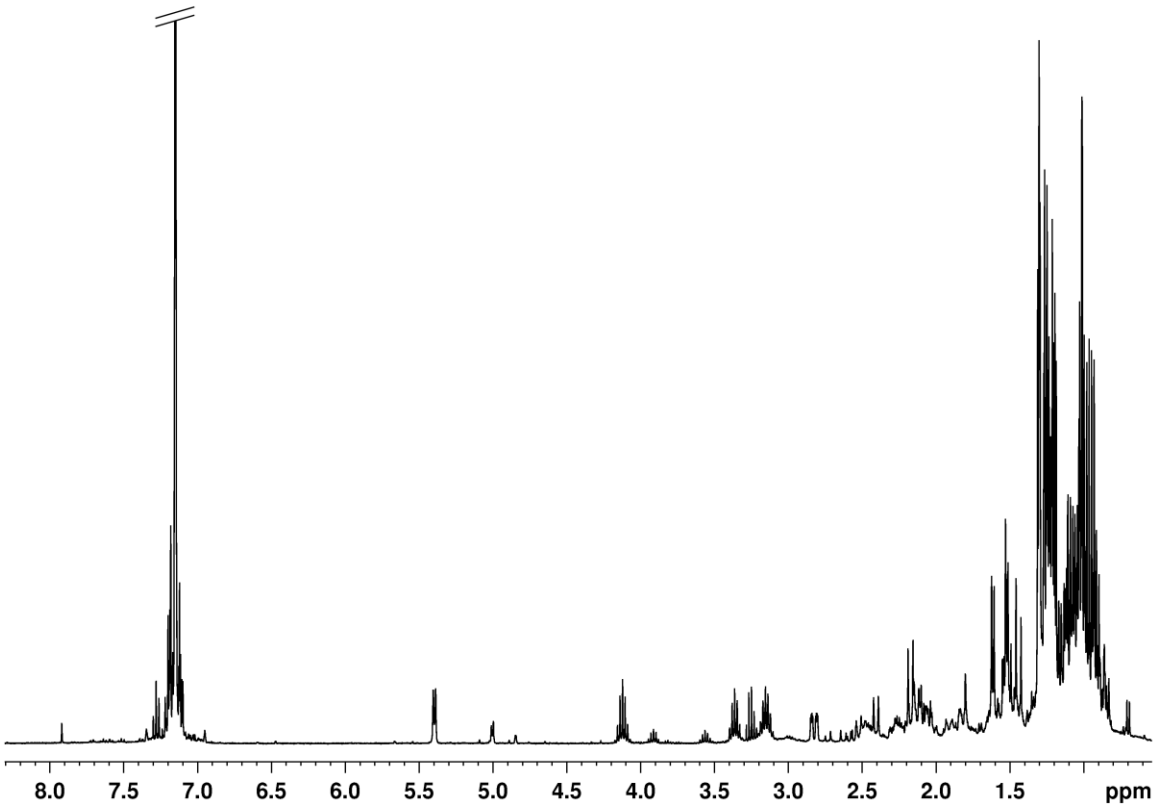

Figure 62. ^{1}H NMR spectrum (C_6D_6) of **43**.

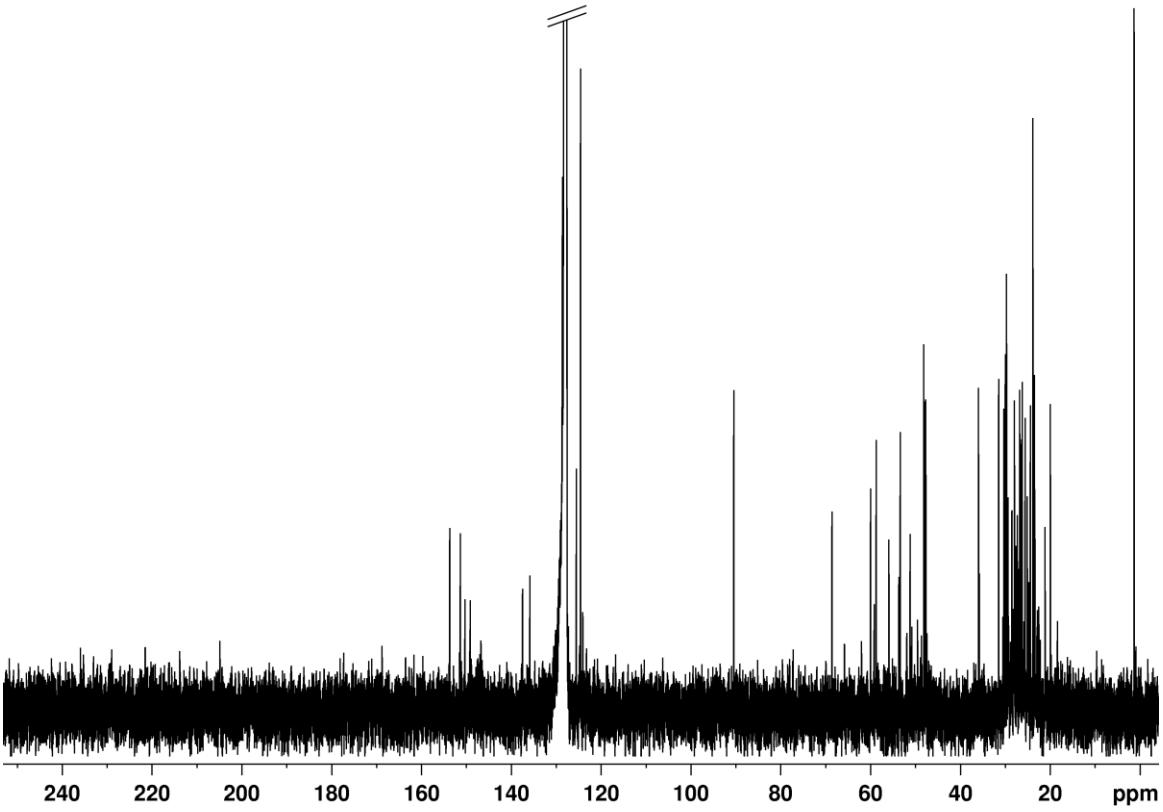

Figure 63. $^{13}C\{^{1}H\}$ NMR spectrum (C_6D_6) of **43**.

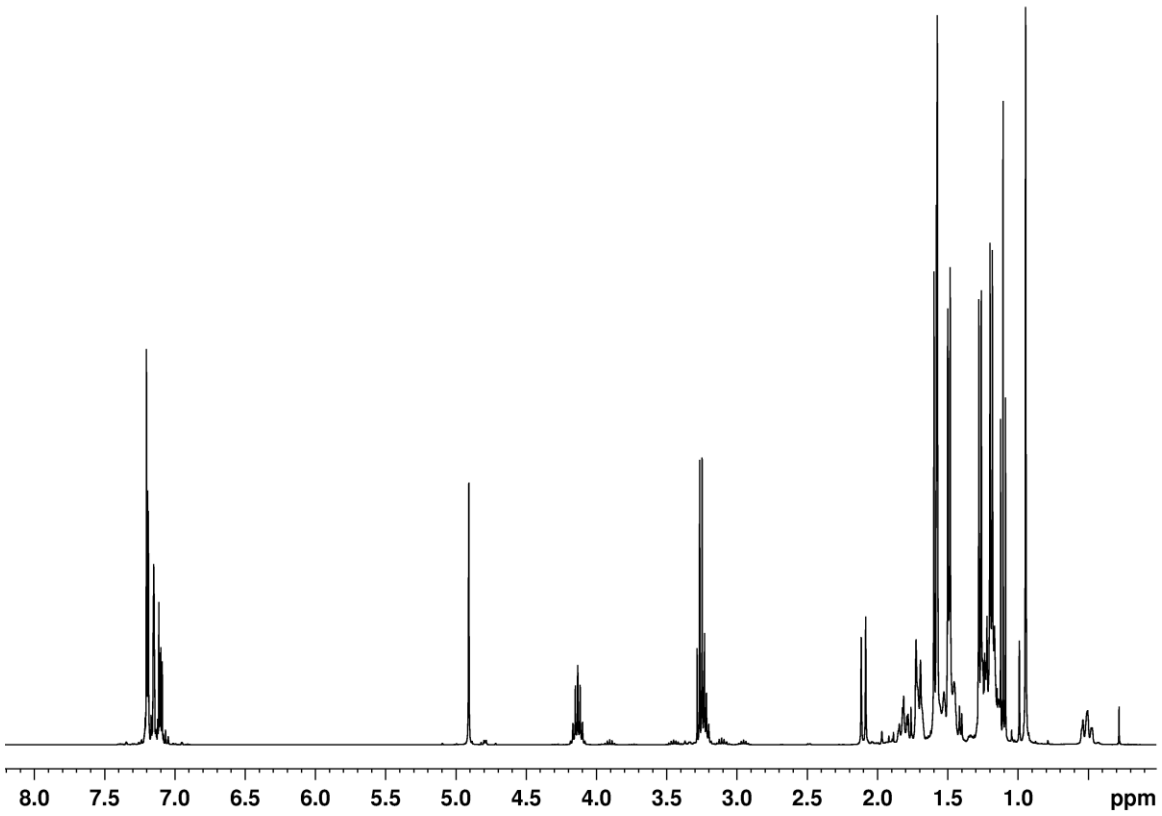

Figure 64. ^{1}H NMR spectrum (C_6D_6) of **44**.

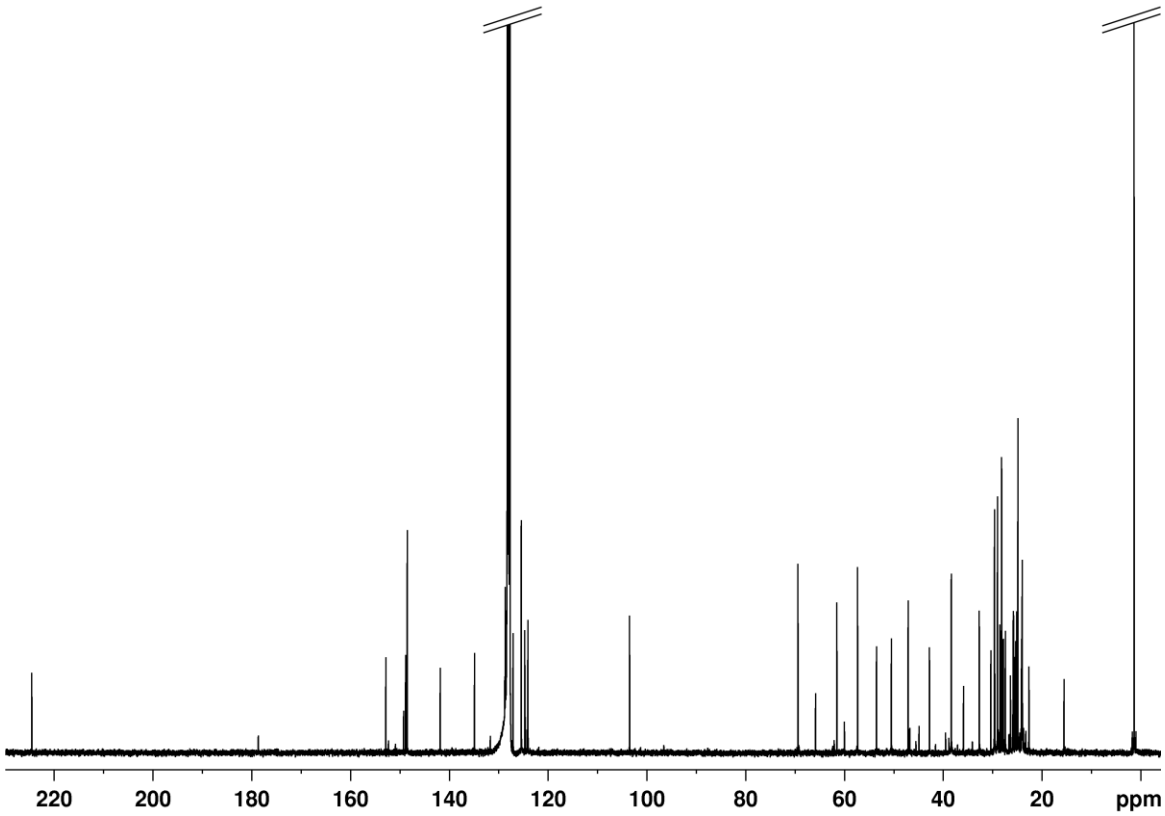

Figure 65. $^{13}C\{^{1}H\}$ NMR spectrum (C_6D_6) of **44**.

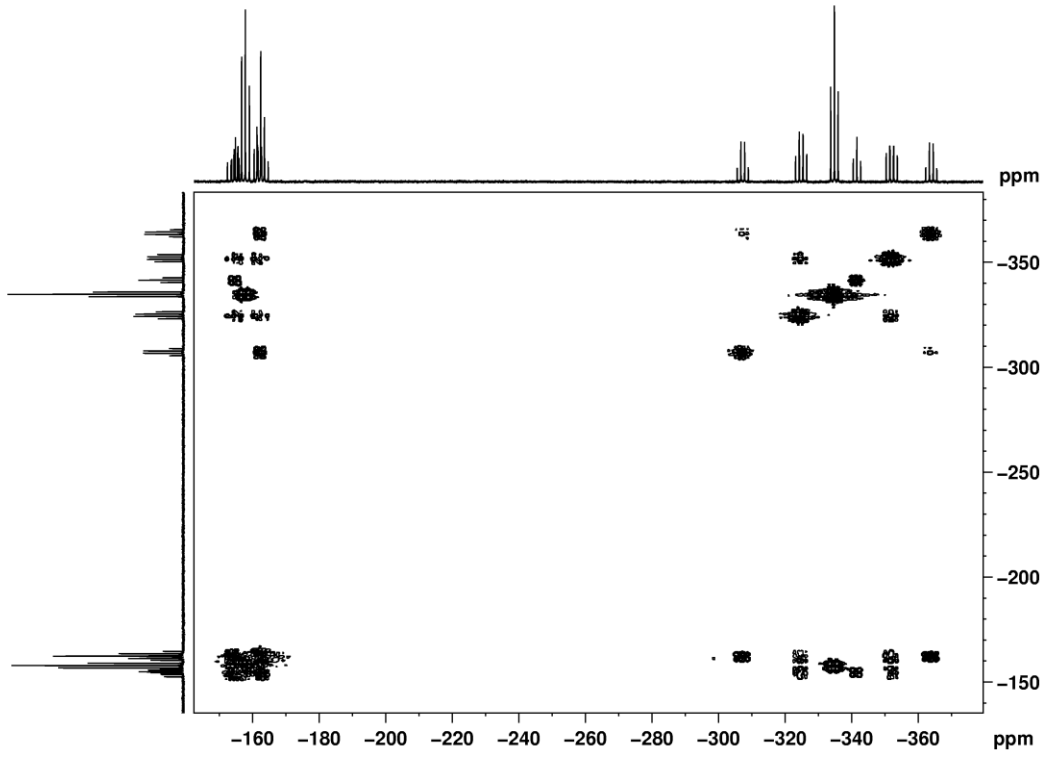

Figure 66. $^{31}P\{^{1}H\}$-$^{31}P\{^{1}H\}$ COSY NMR spectrum (C_6D_6) of a mixture of **60**-**A**, **60**-**B**, **60**-**C** and **60**-**D**.

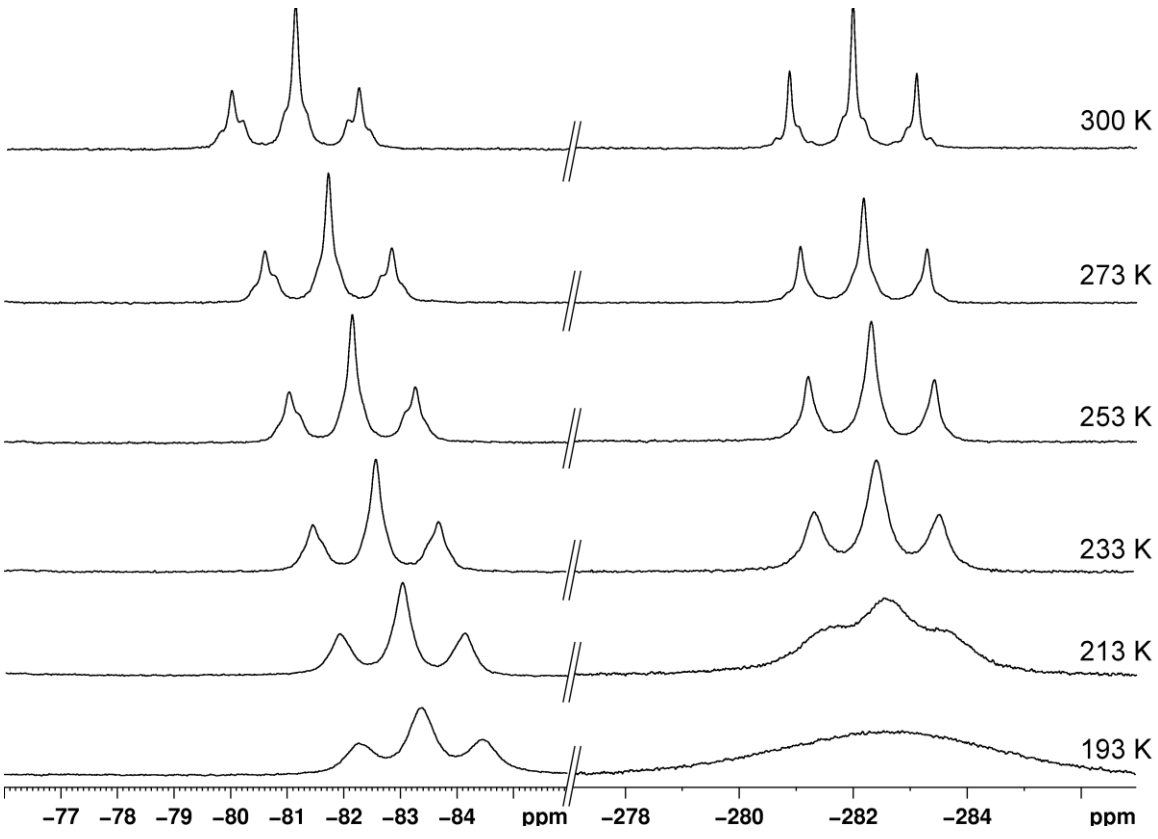

Figure 67. $^{31}P\{^{1}H\}$ VT NMR spectrum (CD_2Cl_2) of **65**.

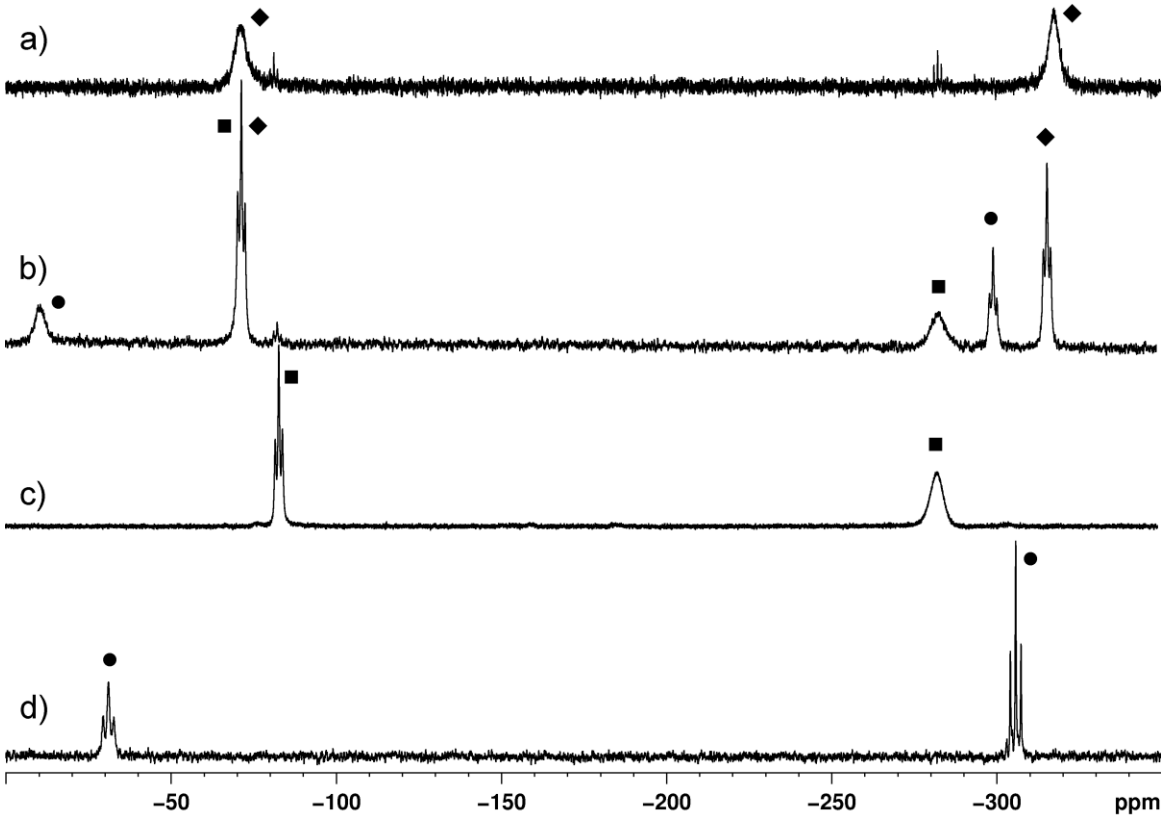

Figure 68. $^{31}P\{^{1}H\}$ NMR spectrum (CD_2Cl_2) of a) **67** at 300 K, b) **67** at 193 K c) **65** at 193 K and d) **67·Cu** at 193 K with signals for (■) $[\{\{Cp'''Fe(CO)_2\}_2(\mu_3,\eta^{1:1:1:1}\text{-}P_4)\}_2Cu]^+[BF_4]^-$ (**65**), (◆) $[\{Cp'''Fe(CO)_2\}_2(\mu_3,\eta^{1:1:1:1}\text{-}P_4)\{Cu(MeCN)\}]^+[BF_4]^-$ (**67**), and (●) $[\{Cp'''Fe(CO)_2\}_2(\mu_4,\eta^{1:1:1:1:2}\text{-}P_4)\{Cu(MeCN)\}\{Cu(MeCN)_2\}]^+[BF_4]^-_2$ (**67·Cu**).

7.2 List of Abbreviations

Å	Angstroem, 1 Å = $1 \cdot 10^{-10}$ m
°C	degree Celsius
1D	one dimensional
2D	two dimensional
AiM	atoms in molecules
Ar^{Dipp}	$-C_6H_3$-2,6-$(C_6H_3$-2,6-$^{i}Pr_2)_2$
BCP	bond critical point
br(NMR)	broad
CAAC	*cyclic* (alkyl)-(amino)carbene
CCSD(T)	coupled cluster single/double/triple excitation
COSY	correlation spectroscopy
Cp	cyclopentadienyl
Cp''	1,3-di-*tert*-butylcyclopentadienyl
Cp'''	1,2,4-tris-*tert*-butylcyclopentadienyl
Cp*	pentametyhlcyclopentadienyl
Cp^{iPr}	penta-isopropylcyclopentadienyl
Cp^{4iPr}	tetra-isopropylcyclopentadienyl
Cp^{Me}	Methylcyclopentadienyl
Cy	cyclohexyl
d	distance
d(NMR)	doublet
$\Delta E°_0$	reaction energy
$\Delta H°_{298}$	standard reaction enthalpy
$\Delta S°_{298}$	standard reaction entropy
$\Delta G°_{298}$	standard gibbs reaction energy
δ	chemical shift
$\Delta\rho_b$	Laplacian of the electron density
DFT	density functional theory
diphars	$Ph_2AsC_2H_4P(Ph)C_2H_4P(Ph)C_2H_4AsPh_2$
Dipp	2,6-diisopropylphenyl
dme	1,2-dimethoxyethane
dppe	1,2-bis(diphenylphosphino)ethane
dppm	1,2-bis(diphenylphosphino)methane
DTA	differential thermo analysis

E	heavier element of the 15th group, E = P, As, Sb
e^-	electron
EI MS	electron impact mass spectrometry
ε_b	bond elipticity
ESI MS	electron spray ionization
Et	ethyl, -C_2H_5
Et_2O	diethylether
FD MS	field desorption ionization mass spectrometry
h	hour
H_b	electronic energy density
HOMO	highest occupied molecular orbital
Hz	Hertz
^{i}Pr	*iso*-propyl
IR	infrared spectroscopy
J(NMR)	coupling constant
J	Joule
kcal	kilo Calorie
kJ	kilo Joule
K_T	equilibrium constant at given temperature T
L	ligand (specified in text)
LUMO	lowest unoccupied molecular orbital
M	metal
m/*z*	mass to charge ratio
MAS	magic angle spinning
Me	methyl
Mes	mesityl, 2,4,6-trimethylphenyl
MO	molecular orbital
m-tol	3-methylphenyl
mV	milli Volt
NHC	N-heterocyclic carbene
NMR	nuclear magnetic resonance
np_3	Tris(2-diphenylphosphinoethyl)amine)
ν	frequency/wavenumber
$\omega_{1/2}$	full width at half maximum
OTf^-	triflate, $CF_3SO_3^-$
PCM	polarized continuum

P_2N_2	$PhP(CH_2SiMe_2NSiMe_2CH_2)_2PPh$
pftb	$[Al\{OC(CF_3)_3\}_4]$
Ph	phenyl
POP	bis-[2-(diphenylphosphino)phenyl]ether
ppm	parts per million
p-tol	4-methylphenyl
q(NMR)	quartett
R	organic substituent
r.t.	room temperature
ρ_b	electron density
s(IR)	strong
s(NMR)	singlet
sec	second
sept(NMR)	septet
sh(IR)	shoulder
sMes	2,4,6-tri-tertbutylphenyl
SQUID	Superconducting Quantum Interference Device
t(NMR)	triplet
^{t}Bu	*tert*-butyl, $-C(CH_3)_3$
THF	tetrahydrofurane, C_4H_8O
tht	tetrahydrothiophene, C_4H_8S
TMS	tetramethylsilane, $Si(CH_3)_4$
triphos	1,1,1-tris-(diphenylphopshinomethyl)ethane)
vdW	van der Waals
VE	valence electron
vs(IR)	very strong
VT	Various Temperature
w(IR)	weak
WBI	Wiberg Bond Index
X	any halide, X = Cl, Br, I
Z	any light atom

7.3 List of Reported Compounds

1 $[(np3)Ni(h^1\text{-}P_4)]$

2 $[W(CO)_3(PCy_3)_2(\eta^1\text{-}P_4)]$

3 $[Re(triphos)(CO)_2(\eta^1\text{-}P_4)]^+(OTf)^-$

4a $[Cp^*Fe(dppe)(\eta^1\text{-}P_4)]^+A^-$

4b $[Cp^*Ru(dppe)(\eta^1\text{-}P_4)]^+A^-$

4c $[Cp^*Ru(PEt_3)_2(\eta^1\text{-}P_4)]^+A^-$

4d $[CpRu(PPh_3)_2(\eta^1\text{-}P_4)]^+A^-$

4e $[CpOs(PPh_3)_2(\eta^1\text{-}P_4)]^+A^-$

5a $[Ag(\eta^2\text{-}P_4)_2]^+[pftb]^-$

5b $[Cu(\eta^2\text{-}P_4)_2]^+[pftb]^-$

5c $[Au(\eta^2\text{-}P_4)_2]^+[GaCl_4]^-$

6a $[(PPh_3)_2RhCl(\eta^{1:1}\text{-}P_4)]$

6b $[(P(m\text{-}tol)_3)_2RhCl(\eta^{1:1}\text{-}P_4)]$

6c $[(P(p\text{-}tol)_3)_2RhCl(\eta^{1:1}\text{-}P_4)]$

6d $[(AsPh_3)_2RhCl(\eta^{1:1}\text{-}P_4)]$

7 $[Cp^*Co(CO)(\eta^{1:1}\text{-}P_4)]$

8 $[Mes_2P_4]$

9a $[\{Cp''Fe(CO)_2\}_2(\mu,\eta^{1:1}\text{-}P_4)]$

9b $[\{Cp'''Fe(CO)_2\}_2(\mu,\eta^{1:1}\text{-}P_4)]$

9c $[\{Cp^{iPr}Fe(CO)_2\}_2(\mu,\eta^{1:1}\text{-}P_4)]$

9d $[\{Cp^*Fe(CO)_2\}_2(\mu,\eta^{1:1}\text{-}P_4)]$

10a $[\{Cp''Fe(CO)_2\}_2]$

10b $[\{Cp'''Fe(CO)_2\}_2]$

10c $[\{Cp^{iPr}Fe(CO)_2\}_2]$

10d $[\{Cp^*Fe(CO)_2\}_2]$

11 $P_4[P\{N(SiMe_3)_2\}\{N^iPr_2\}]_2$

12 $[(Ar^{Dipp})_2P_4]$

13 $Tl_2[(Ar^{Dipp})_2P_4]$

14a $[Cp^*Nb(CO)_2(\eta^4\text{-}P_4)]$

14b $[Cp^*Nb(CO)_2(\eta^4\text{-}As_4)]$

15 $[\{Zr(P_2N_2)\}_2(\mu,\eta^{4:4}\text{-}P_4)]$

16a $[\{Cp''Fe\}_2(\mu,\eta^{4:4}\text{-}P_4)]$

16b $[\{Cp'''Fe\}_2(\mu,\eta^{4:4}\text{-}P_4)]$

17 ^{Menthyl}CAAC

18 [(^{Menthyl}CAAC)$_2$P$_4$]

19 $^{c Hex}$CAAC

20 [($^{c Hex}$CAAC)$_3$P$_4$]

21 [($^{c Hex}$CAAC)$_2$P$_4$]

22a [{CpMo(CO)$_2$}$_2$(μ,$\eta^{2:2}$-PAs)]

22b [{CpMo(CO)$_2$}$_2$(μ,$\eta^{2:2}$-PSb)]

23a [{CpCr(CO)$_2$}(η^3-P$_2$As)]

23b [{CpCr(CO)$_2$}(η^3-P$_2$Sb)]

24 [{Cp'''Fe}$_2$(μ,$\eta^{4:4}$P$_n$As$_{4-n}$)]

25 [Cp'''Fe(η^5-P$_n$As$_{5-n}$)]

26 [Cp*Fe(dppe)(η^1-AsP$_3$)]$^+$[BPh$_4$]$^-$

27 [(P^{i}Pr$_3$)$_2$(CO)$_3$Mo(η^1-AsP$_3$)]

28 AsP$_3$[P{N(SiMe$_3$)$_2$}{N^{i}Pr$_2$}]$_2$

29 [{CpMo(CO)$_2$}$_2$(μ,$\eta^{2:2}$-P$_2$)]

30 [Ag$_2$\{(CpMo(CO)$_2$)$_2$(μ_4,$\eta^{1:1:2:2}$-P$_2$)\}$_2$\{(CpMo(CO)$_2$)$_2$(μ_3,$\eta^{2:2:2}$-P$_2$)\}$_2$](OTf)$_2$

31 [Ag\{(CpMo(CO)$_2$)$_2$(μ_4,$\eta^{1:1:2:2}$-P$_2$)\}$_3$\{μ,$\eta^{1:1}$-NO$_3$\}]$_n$[NO$_3$]$_n$

32 [Cu$_2$\{(CpMo(CO)$_2$)$_2$(μ_4,$\eta^{1:1:2:2}$-P$_2$)\}$_2$Br$_2$]$_n$

33 [{Cp'''Fe(CO)$_2$}$_2$(μ,$\eta^{1:1:2:2}$-P$_4$){Co(CO)$_3$}$_2$]

34 [{Cp'''Fe(CO)$_2$}{Cp'''Fe(CO)}(μ,$\eta^{1:2:2:1}$){CuI}]$_2$

35a [Cp*Fe(η^5-P$_5$)]

35b [Cp*Fe(η^5-As$_5$)]

36 [Cu$_2$\{Cp*Fe(μ_3,$\eta^{1:1:5}$-P$_5$)\}$_2$Cl$_2$]$_n$

37a [CuBr\{Cp*Fe(μ_4,$\eta^{1:1:1:5}$-P$_5$)\}]$_n$

37b [CuI\{Cp*Fe(μ_4,$\eta^{1:1:1:5}$-P$_5$)\}]$_n$

38a [Cp*FeP$_5$]@[(CuCl)$_{10}$(Cu$_2$Cl$_3$)$_5$\{Cu(CH$_3$CN)$_2$\}$_5$\{Cp*Fe(μ_6,$\eta^{1:1:1:1:1:5}$-P$_5$)\}$_{12}$]

38b [Cp*FeP$_5$]@[(CuBr)$_{10}$(Cu$_2$Br$_3$)$_5$\{Cu(CH$_3$CN)$_2$\}$_5$\{Cp*Fe(μ_6,$\eta^{1:1:1:1:1:5}$-P$_5$)\}$_{12}$]

39 C$_{60}$@[Cu$_{26}$Cl$_{26}$(Cp*FeP$_5$)$_{13}$(H$_2$O)$_2$(CH$_3$CN)$_9$]

40 C$_2$B$_{10}$H$_{12}$@[(CuCl)$_{20}$\{Cp*Fe(μ_6,$\eta^{1:1:1:1:1:5}$-P$_5$)\}$_{12}$]

41 P$_4$S$_3$@[(CuCl)$_{20}$\{Cp*Fe(μ_6,$\eta^{1:1:1:1:1:5}$-P$_5$)\}$_{12}$]

42 P$_4$@[(Cp*FeP$_5$)$_{10}$(CuI)$_{30.1}$(CH$_3$CN)$_6$]

43 [(^{Menthyl}CAAC)$_2$As$_2$]

44 [($^{c Hex}$CAAC)$_3$As$_4$]

45 [L$_2$Cr$_2$]

46 [L$_2$Cr$_2$(μ,$\eta^{1:1:2:2}$-P$_4$)]

47 $[L_2Cr_2(\mu,\eta^{1:1:2:2}\text{-}As_4)]$

48 $[L_2Cr_2(\mu,\eta^{1:1:2:2}\text{-}AsP_3)]$

49 $[L_2Cr_2(\mu_3,\eta^{1:1:1:2:2}\text{-}P_4)\{W(CO)_5\}]$

50 $K[Cp'''Fe(CO)_2]$

51 $[\{Cp'''Fe(CO)_2\}_2(\mu,\eta^{1:1}\text{-}AsP_3)]$

52 $[\{Cp'''Fe(CO)_2\}_2(\mu,\eta^{1:1}\text{-}As_4)]$

53 $[\{Cp^*Cr(CO)_3\}_2]$

54 $[\{Cp^*Cr(CO)_3\}_2(\mu,\eta^{1:1}\text{-}P_4)]$

55 $[\{Cp^*Cr(CO)_3\}_2(\mu,\eta^{1:1}\text{-}AsP_3)]$

56 $[\{Cp^*Cr(CO)_3\}_2(\mu,\eta^{1:1}\text{-}As_4)]$

57 $[\{Cp'''Fe(CO)_2\}\{Cp^*Fe(CO)_2\}]$

58 $[\{Cp'''Fe(CO)_2\}(\mu,\eta^{1:1}\text{-}P_4)\{Cp^*Fe(CO)_2\}]$

59 $[\{Cp'''Fe(\mu\text{-}Br)\}_2]$

60 $[Cp'''_2P_4]$

61 $[\{Cp^{Me}Fe(CO)_2\}_2(\mu_4,\eta^{1:1:2:2}\text{-}P_8)\{Cp^{Me}Fe(CO)\}_2]$

62 $[\{Cp'''Fe(CO)_2\}(\mu,\eta^{1:2}\text{-}As_4)\{Cp'''Fe(CO)\}]$

63 $[\{Cp'''Fe(CO)_2\}_2(\mu_4,\eta^{1:1:2:2}\text{-}As_8)\{Cp'''Fe(CO)\}_2]$

64 $[\{Cp^*Cr(CO)_3\}_4(\mu_4,\eta^{1:1:1:1}\text{-}As_8)]$

65 $[\{\{Cp'''Fe(CO)_2\}_2(\mu_3,\eta^{1:1:1:1}\text{-}P_4)\}_2Cu]^+[BF_4]^-$

66 $[\{\{Cp^*Cr(CO)_3\}_2(\mu_3,\eta^{1:1:1:1}\text{-}P_4)\}_2Cu]^+[BF_4]^-$

67 $[\{Cp'''Fe(CO)_2\}_2(\mu_3,\eta^{1:1:2}\text{-}P_4)\{Cu(MeCN)\}]^+[BF_4]^-$

67·Cu $[\{Cp'''Fe(CO)_2\}_2(\mu_4,\eta^{1:1:1:1:2}\text{-}P_4)\{Cu(MeCN)\}\{Cu(MeCN)_2\}]^{2+}[BF_4]^-_2$

68 $[\{\{Cp'''Fe(CO)_2\}_2(\mu_3,\eta^{1:1:1:1}\text{-}P_4)\}_2Ag]^+[PF_6]^-$

69 $[\{\{Cp^*Cr(CO)_3\}_2(\mu_3,\eta^{1:1:1:1}\text{-}P_4)\}_2Ag]^+[PF_6]^-$

70 $[\{Cp'''Fe(CO)_2\}_2(\mu_3,\eta^{1:1:1:1}\text{-}P_4)\{Au(PPh_3)\}]^+[PF_6]^-$

71 $[\{Cp^*Cr(CO)_3\}_2(\mu_3,\eta^{1:1:1:1}\text{-}P_4)\{Au(PPh_3)\}]^+[PF_6]^-$

72 $[\{Cp'''Fe(CO)_2\}_2(\mu_3,\eta^{1:1:1:1}\text{-}P_4)FeBr_2]$

73 $[\{\{Cp'''Fe(CO)_2\}_2(\mu_3,\eta^{1:1:1:1}\text{-}AsP_3)\}_2Cu]^+[BF_4]^-$

74 $[\{\{Cp^*Cr(CO)_3\}_2(\mu_3,\eta^{1:1:1:1}\text{-}AsP_3)\}_2Cu]^+[BF_4]^-$

75 $[\{\{Cp'''Fe(CO)_2\}_2(\mu_3,\eta^{1:1:1:1}\text{-}P_4)\}_2Ag]^+[PF_6]^-$

76 $[\{\{Cp^*Cr(CO)_3\}_2(\mu_3,\eta^{1:1:1:1}\text{-}AsP_4)\}_2Ag]^+[PF_6]^-$

77 $[\{Cp'''Fe(CO)_2\}_2(\mu_3,\eta^{1:1:1:1}\text{-}AsP_3)\{Au(PPh_3)\}]^+[PF_6]^-$

78 $[\{Cp^*Cr(CO)_3\}_2(\mu_3,\eta^{1:1:1:1}\text{-}AsP_3)\{Au(PPh_3)\}]^+[PF_6]^-$

79 $[\{\{Cp'''Fe(CO)_2\}_2(\mu_3,\eta^{1:1:1:1}\text{-}As_4)\}_2Cu]^+[BF_4]^-$

80 $[\{\{Cp'''Fe(CO)_2\}_2(\mu_3,\eta^{1:1:1:1}\text{-}As_4)\}_2Ag]^+[PF_6]^-$

81 $[\{\{Cp^*Cr(CO)_3\}_2(\mu_3,\eta^{1:1:1:1}\text{-}As_4)\}_2Ag]^+[PF_6]^-$

82 $[Ag(\eta^2\text{-}As_4)_2]^+[pftb]^-$

83 $[(PPh_3)Au(\eta^2\text{-}As_4)]^+[pftb]^-$

84 $[Cp^*Ru(dppe)(\eta^1\text{-}As_4)]^+[pftb]^-$

85 $[\{Cp^*Ru(dppe)\}(\mu,\eta^{1:3}\text{-}As_4)\{CpRu(PPh_3)\}]^{2+}[pftb]^-_2$

86 $As_4@[\{Cp^*Fe(\eta^5\text{-}P_5)\}_{10}Cu_{30}I_{30}(MeCN)_6]$

87 $\{Z_4As_4\}@[\{Cp^*Fe(\eta^5\text{-}P_5\}_{12}Cu_{51}I_{56}(MeCN)_3]^-Z^+$

7.4 Acknowledgments

Finally, I would like to express my gratitude to:

- Prof. Dr. Manfred Scheer for ensuring remarkably good working conditions in his group, many fruitful and encouraging discussions, a large degree of freedom during my research as well as his constant interest in my personal and professional progress.
- Dr. Gábor Balázs and Dr. Michael Bodensteiner for their helpful advices on almost every chemical and crystallographic problem.
- The Fonds der chemischen Industrie for a Ph.D. fellowship.
- Prof. Dr. Rhett Kempe and Dr. Awal Noor for the fruitful collaboration on the quintuply bonded dichromium complex.
- Prof. Dr. Christopher C. Cummins and Alexandra Velian for the samples of AsP_3 and Prof. Dr. Guy Bertrand for the collaboration on the CAACs.
- Dr. Gábor Balázs, Dr. Alexey Y. Timoshkin and Prof. Dr. Marek Sierka for the DFT calculations.
- Dr. Michael Bodensteiner, Dr. Alexander V. Virovets, Dr. Eugenia Peresypkina and Dr. Manfred Zabel for their help with X-ray structure analysis.
- Dr. Maria Neumeier and Prof. Dr. Ruth Gschwind for the ^{75}As NMR measurements.
- Dr. Ilya Shenderovich, Anette Schramm, Georgine Stühler and Fritz Kastner for the measurement of my NMR spectra.
- Josef Kirmeier, Carola Prockl and Wolfgang Söllner for the mass spectrometric analyses.
- The co-workers of the micro analytical laboratory for the elemental analyses of many (unfortunately fluorine rich) samples.
- The staff of the glass blowing, electronics and mechanics facilities of the University of Regensburg.
- Dr. Gábor Balázs and Dr. Richard Layfield for proof reading this thesis.
- All former an present members of the JCF Regensburg for an exciting and unforgettable time during many successful projects.
- The Tuesday running group for kindly inviting me and for not blaming me too much throughout the writing time.
- All members of the “Männerstammtisch”: Bodi, Gabor, Stubi, Kathl and Alexey for having a “Männerstammtisch”.
- My former and present lab colleagues Dr. Fabian Dielmann, Christian Graßl and Sebastian Heinl for a perfect working atmosphere, the discussions on any acute problem and the choice of music including the “Klassik Mittwoch”.

- All present and former members of the research group: Joachim Wachter, Gábor, Mikhail, Eric, Hias, Bianca, Moatl, Stubi, Michi, Mia, Eva, Wurzel, Thomsi, Claudi, Sabine, Wascht, Moni, Kathl, Kü…..Christian, Susanne, Schotti, Musch, Nazhia (Muschine), Barbara, Walter, Petra, Lizzy, Matthias, Shining, Laurence, Ari, Christian, Welschi, Oime, Hut, Patrick, Michl, Biegi, Miriam, Ulf, Hannes, Bodi, Fabi and Conny for an unforgettable time I would never like to miss.
- My family and friends for their never-ending support….

….and Kathrin for completing me.

8. Notes and References

[1] T. L. Roberts, W. M. Stewart, *Better Crops* **2002**, *86*, 6 - 7.

[2] J. Emsley, *The 13th Element: The Sordid Tale of Murder, Fire and Phosphorus*, Wiley & Sons, New York, **2000**.

[3] W. E. Brooks, Mineral Commodity Summaries (U. S. G. survey), **2010**.

[4] F. Krafft, *Angew. Chem. Int. Ed. Engl.* **1969**, *8*, 660-671.

[5] a) R. Hultgren, N. S. Gingrich, B. E. Warren, *J. Chem. Phys.* **1935**, *3*, 351-355; b) S. Lange, P. Schmidt, T. Nilges, *Inorg. Chem.* **2007**, *46*, 4028-4035.

[6] W. L. Roth, T. W. DeWitt, A. J. Smith, *J. Am. Chem. Soc.* **1947**, *69*, 2881-2885.

[7] N. Wiberg, *Lehrbuch der Anorganischen Chemie, Vol. 101*, Berlin, New York, **1995**.

[8] R. A. L. Winchester, M. Whitby, M. S. P. Shaffer, *Angew. Chem. Int. Ed.* **2009**, *48*, 3616-3621.

[9] M. Ruck, D. Hoppe, B. Wahl, P. Simon, Y. Wang, G. Seifert, *Angew. Chem. Int. Ed.* **2005**, *44*, 7616-7619.

[10] H. Thurn, H. Kerbs, *Angew. Chem. Int. Ed. Engl.* **1966**, *5*, 1047-1048.

[11] A. Pfitzner, M. F. Bräu, J. Zweck, G. Brunklaus, H. Eckert, *Angew. Chem. Int. Ed.* **2004**, *43*, 4228-4231.

[12] A. Simon, H. Borrmann, H. Craubner, *Phosphorus, Sulfur Silicon Relat. Elem.* **1987**, *30*, 507-510.

[13] H. Okudera, R. E. Dinnebier, A. Simon, *Z. Kristallogr.* **2005**, *220*, 259-264.

[14] a) A. J. Bradley, *Phil. Mag. 6* **1924**, *47*, 657-671; b) H. Stöhr, *Z. Anorg. Allg. Chem.* **1939**, *242*, 138-144.

[15] H. Krebs, W. Holz, K. H. Worms, *Chem. Ber.* **1957**, *90*, 1031-1037.

[16] a) O. Osters, T. Nilges, F. Bachhuber, F. Pielnhofer, R. Weihrich, M. Schöneich, P. Schmidt, *Angew. Chem.* **2012**, 3049–3052; b) O. Osters, T. Nilges, F. Bachhuber, F. Pielnhofer, R. Weihrich, M. Schöneich, P. Schmidt, *Angew. Chem. Int. Ed.* **2012**, *51*, 2994-2997.

[17] A. Bettendorff, *Liebigs Ann. Chem.* **1867**, *144*, 110-114.

[18] J. Eiduss, R. Kalendarev, A. Rodionov, A. Sazonov, G. Chikvaidze, *Phys. Status Solidi B* **1996**, *193*, 3-23.

[19] H. Erdmann, M. V. Unruh, *Z. Anorg. Chem.* **1902**, *32*, 437-452.

[20] a) A. S. Foust, M. S. Foster, L. F. Dahl, *J. Am. Chem. Soc.* **1969**, *91*, 5631-5633; b) A. S. Foust, M. S. Foster, L. F. Dahl, *J. Am. Chem. Soc.* **1969**, *91*, 5633-5635.

[21] a) O. J. Scherer, *Angew. Chem. Int. Ed. Engl.* **1990**, *29*, 1104-1122; b) O. J. Scherer, *Acc. Chem. Res.* **1999**, *32*, 751-762.

[22] P. P. Power, *Nature* **2010**, *463*, 171-177.

[23] a) B. M. Cossairt, N. A. Piro, C. C. Cummins, *Chem. Rev.* **2010**, *110*, 4164-4177; b) M. Caporali, L. Gonsalvi, A. Rossin, M. Peruzzini, *Chem. Rev.* **2010**, *110*, 4178-4235; c) M. Scheer, G. Balázs, A. Seitz, *Chem. Rev.* **2010**, *110*, 4236-4256.

[24] P. Dapporto, S. Midollini, L. Sacconi, *Angew. Chem.* **1979**, *91*, 510-510.

[25] T. Gröer, G. Baum, M. Scheer, *Organometallics* **1998**, *17*, 5916-5919.

[26] M. Peruzzini, L. Marvelli, A. Romerosa, R. Rossi, F. Vizza, F. Zanobini, *Eur. J. Inorg. Chem.* **1999**, *1999*, 931-933.

[27] I. de los Rios, J.-R. Hamon, P. Hamon, C. Lapinte, L. Toupet, A. Romerosa, M. Peruzzini, *Angew. Chem. Int. Ed.* **2001**, *40*, 3910-3912.

[28] P. Barbaro, M. Di Vaira, M. Peruzzini, S. Seniori Costantini, P. Stoppioni, *Chem. Eur. J.* **2007**, *13*, 6682-6690.

[29] M. Caporali, M. Di Vaira, M. Peruzzini, S. Seniori Costantini, P. Stoppioni, F. Zanobini, *Eur. J. Inorg. Chem.* **2010**, *2010*, 152-158.

[30] I. Krossing, L. van Wüllen, *Chem. Eur. J.* **2002**, *8*, 700-711.

[31] G. Santiso-Quinones, A. Reisinger, J. Slattery, I. Krossing, *Chem. Commun.* **2007**.

[32] L. C. Forfar, T. J. Clark, M. Green, S. M. Mansell, C. A. Russell, R. A. Sanguramath, J. M. Slattery, *Chem. Commun.* **2012**, *48*.

[33] A. P. Ginsberg, W. E. Lindsell, *J. Am. Chem. Soc.* **1971**, *93*, 2082-2084.

[34] O. J. Scherer, K. Pfeiffer, G. Wolmershäuser, *Chem. Ber.* **1992**, *125*, 2367-2372.

[35] R. Riedel, H.-D. Hausen, E. Fluck, *Angew. Chem.* **1985**, *97*, 1050-1050.

[36] O. J. Scherer, G. Schwarz, G. Wolmershäuser, *Z. Anorg. Allg. Chem.* **1996**, *622*, 951-957.

[37] O. J. Scherer, T. Hilt, G. Wolmershäuser, *Organometallics* **1998**, *17*, 4110-4112.

[38] H. Sitzmann, T. Dezember, W. Kaim, F. Baumann, D. Stalke, J. Kärcher, E. Dormann, H. Winter, C. Wachter, M. Kelemen, *Angew. Chem.* **1996**, *108*, 3013-3016.

[39] J.-P. Bezombes, P. B. Hitchcock, M. F. Lappert, J. E. Nycz, *Dalton Trans.* **2004**.

[40] A. R. Fox, R. J. Wright, E. Rivard, P. P. Power, *Angew. Chem. Int. Ed.* **2005**, *44*, 7729-7733.

[41] O. J. Scherer, J. Vondung, G. Wolmershäuser, *Angew. Chem. Int. Ed. Engl.* **1989**, *28*, 1355-1357.

[42] O. J. Scherer, J. Vondung, G. Wolmershäuser, *J. Organomet. Chem.* **1989**, *376*, C35-C38.

[43] W. W. Seidel, O. T. Summerscales, B. O. Patrick, M. D. Fryzuk, *Angew. Chem.* **2009**, *121*, 121-123.

[44] J. D. Masuda, W. W. Schoeller, B. Donnadieu, G. Bertrand, *Angew. Chem. Int. Ed.* **2007**, *46*, 7052-7055.

[45] G. D. Frey, V. Lavallo, B. Donnadieu, W. W. Schoeller, G. Bertrand, *Science* **2007**, *316*, 439-441.

[46] J. D. Masuda, W. W. Schoeller, B. Donnadieu, G. Bertrand, *J. Am. Chem. Soc.* **2007**, *129*, 14180-14181.

[47] O. Back, G. Kuchenbeiser, B. Donnadieu, G. Bertrand, *Angew. Chem. Int. Ed.* **2009**, *48*, 5530-5533.

[48] Y. Wang, Y. Xie, P. Wei, R. B. King, H. F. Schaefer, P. v. R. Schleyer, G. H. Robinson, *J. Am. Chem. Soc.* **2008**, *130*, 14970-14971.

[49] J. E. Davies, L. C. Kerr, M. J. Mays, P. R. Raithby, P. K. Tompkin, A. D. Woods, *Angew. Chem. Int. Ed.* **1998**, *37*, 1428-1429.

[50] S. Umbarkar, P. Sekar, M. Scheer, *Dalton Trans.* **2000**.

[51] C. Schwarzmaier, Diploma thesis, University of Regensburg (Regensburg), **2008**.

[52] B. M. Cossairt, M.-C. Diawara, C. C. Cummins, *Science* **2009**, *323*, 602.

[53] B. M. Cossairt, C. C. Cummins, *J. Am. Chem. Soc.* **2009**, *131*, 15501-15511.

[54] O. J. Scherer, H. Sitzmann, G. Wolmershäuser, *Angew. Chem. Int. Ed. Engl.* **1984**, *23*, 968-969.

[55] M. Scheer, *Dalton Trans.* **2008**.

[56] M. Eberl, Ph.D. thesis, University of Regensburg (Regensburg), **2011**.

[57] O. J. Scherer, T. Brück, *Angew. Chem.* **1987**, *99*, 59-59.

[58] O. J. Scherer, C. Blath, G. Wolmershäuser, *J. Organomet. Chem.* **1990**, *387*, C21-C24.

[59] J. Bai, A. V. Virovets, M. Scheer, *Angew. Chem.* **2002**, *114*, 1808-1811.

[60] H. Krauss, G. Balazs, M. Bodensteiner, M. Scheer, *Chem. Science* **2010**, *1*.

[61] a) J. Bai, A. V. Virovets, M. Scheer, *Science* **2003**, *300*, 781-783; b) M. Scheer, J. Bai, B. P. Johnson, R. Merkle, A. V. Virovets, C. E. Anson, *Eur. J. Inorg. Chem.* **2005**, *2005*, 4023-4026; c) M. Scheer, A. Schindler, J. Bai, B. P. Johnson, R. Merkle, R. Winter, A. V. Virovets, E. V. Peresypkina, V. A. Blatov, M. Sierka, H. Eckert, *Chem. Eur. J.* **2010**, *16*, 2092-2107.

[62] M. Scheer, A. Schindler, R. Merkle, B. P. Johnson, M. Linseis, R. Winter, C. E. Anson, A. V. Virovets, *J. Am. Chem. Soc.* **2007**, *129*, 13386-13387.

[63] M. Scheer, A. Schindler, C. Gröger, A. V. Virovets, E. V. Peresypkina, *Angew. Chem. Int. Ed.* **2009**, *48*, 5046-5049.

[64] A. Biegerl, Ph.D. thesis, University of Regensburg (Regensburg), **2010**.

[65] A. Schindler, Ph.D. thesis, University of Regensburg (Regensburg), **2010**.

[66] O. Back, B. Donnadieu, P. Parameswaran, G. Frenking, G. Bertrand, *Nat Chem* **2010**, *2*, 369-373.

[67] Y. U. Morino, Takeshi; Ito, Tetsuzo, *Bull. Chem. Soc. Jpn.* **1966**, *39*, 64-71.

[68] a) P. Pyykkö, M. Atsumi, *Chem. Eur. J.* **2009**, *15*, 186-197; b) P. Pyykkö, M. Atsumi, *Chem. Eur. J.* **2009**, *15*, 12770-12779.

[69] C. Schwarzmaier, A. Noor, G. Glatz, M. Zabel, A. Y. Timoshkin, B. M. Cossairt, C. C. Cummins, R. Kempe, M. Scheer, *Angew. Chem. Int. Ed.* **2011**, *50*, 7283-7286.

[70] A. Noor, G. Glatz, R. Müller, M. Kaupp, S. Demeshko, R. Kempe, *Nat Chem* **2009**, *1*, 322-325.

[71] WIN-DAISY module in TopSpin 2.1, (Bruker BioSpin), **2007**.

[72] L. R. Maxwell, S. B. Hendricks, V. M. Mosley, *J. Chem. Phys.* **1935**, *3*, 699-709.

[73] B. M. Cossairt, C. C. Cummins, A. R. Head, D. L. Lichtenberger, R. J. F. Berger, S. A. Hayes, N. W. Mitzel, G. Wu, *J. Am. Chem. Soc.* **2010**, *132*, 8459-8465.

[74] H. A. Spinney, N. A. Piro, C. C. Cummins, *J. Am. Chem. Soc.* **2009**, *131*, 16233-16243.

[75] O. J. Scherer, M. Swarowsky, G. Wolmershaeuser, *Organometallics* **1989**, *8*, 841-842.

[76] S. Deng, Diploma thesis, University of Karlsruhe (Karlsruhe), **2002**.

[77] M. Ehses, A. Romerosa, M. Peruzzini, *Topics in Current Chemistry* **2002**, *220*, 107-140.

[78] L. Yoong Goh, T. W. Hambley, D. J. Darensbourg, J. Reibenspies, *J. Organomet. Chem.* **1990**, *381*, 349-356.

[79] T. J. Jaeger, M. C. Baird, *Organometallics* **1988**, *7*, 2074-2076.

[80] T. Hilt, Ph.D. thesis, University of Kaiserslautern (Kaiserslautern), **1999**.

[81] M. Vitale, K. K. Lee, C. F. Hemann, R. Hille, T. L. Gustafson, B. E. Bursten, *J. Am. Chem. Soc.* **1995**, *117*, 2286-2296.

[82] P. Jutzi, S. Opiela, *J. Organomet. Chem.* **1992**, *431*, C29-C32.

[83] R. G. Teller, J. M. Williams, *Inorg. Chem.* **1980**, *19*, 2770-2773.

[84] M. M. Rauhut, A. M. Semsel, *J. Org. Chem.* **1963**, *28*, 471-473.

[85] B. M. Cossairt, C. C. Cummins, *New J. Chem.* **2010**, *34*, 1533-1536.

[86] H. Sitzmann, R. Boese, *Angew. Chem. Int. Ed. Engl.* **1991**, *30*, 971-973.

[87] M. Wallasch, G. Wolmershäuser, H. Sitzmann, *Angew. Chem. Int. Ed.* **2005**, *44*, 2597-2599.

[88] M. D. Walter, P. S. White, *New J. Chem.* **2011**, *35*, 1842-1854.

[89] M. Eberl, Diploma thesis, University of Regensburg (Regensburg), **2006**.

[90] M. E. Barr, B. R. Adams, R. R. Weller, L. F. Dahl, *J. Am. Chem. Soc.* **1991**, *113*, 3052-3060.

[91] a) O. J. Scherer, R. Winter, G. Heckmann, G. Wolmershäuser, *Angew. Chem.* **1991**, *103*, 860-861; b) K. Mast, J. Meiers, O. J. Scherer, G. Wolmershäuser, *Z. Anorg. Allg. Chem.* **1999**, *625*, 70-74.

[92] a) S. Deng, Ph.D. thesis, University of Regensburg (Regensburg), **2007**; b) O. J. Scherer, T. Hilt, G. Wolmershäuser, *Angew. Chem.* **2000**, *112*, 1483-1485; c) O. J. Scherer, T. Hilt, G. Wolmershäuser, *Angew. Chem. Int. Ed.* **2000**, *39*, 1425-1427.

[93] P. Comba, C. Katsichtis, B. Nuber, H. Pritzkow, *Eur. J. Inorg. Chem.* **1999**, *1999*, 777-783.

[94] O. Moudam, A. Kaeser, B. Delavaux-Nicot, C. Duhayon, M. Holler, G. Accorsi, N. Armaroli, I. Seguy, J. Navarro, P. Destruel, J.-F. Nierengarten, *Chem. Commun.* **2007**, 3077-3079.

[95] Y. K. Gun'ko, H. Hayden, Opto-Ireland, **2005**.

[96] S. J. B. Price, C. Brevard, A. Pagelot, P. J. Sadler, *Inorg. Chem.* **1985**, *24*, 4278-4281.

[97] C. S. W. Harker, E. R. T. Tiekink, *J. Coord. Chem.* **1990**, *21*, 287-293.

[98] O. Crespo, M. C. Gimeno, A. Laguna, P. G. Jones, *Dalton Trans.* **1992**, 1601-1605.

[99] R. K. O'Reilly, M. P. Shaver, V. C. Gibson, A. J. P. White, *Macromolecules* **2007**, *40*, 7441-7452.

[100] J. D. Gilbertson, N. K. Szymczak, D. R. Tyler, *J. Am. Chem. Soc.* **2005**, *127*, 10184-10185.

[101] W.-J. van Zeist, F. M. Bickelhaupt, *Dalton Trans.* **2011**, *40*, 3028-3038.

[102] G. A. Bain, J. F. Berry, *J. Chem. Educ.* **2008**, *85*, 532.

[103] J. E. Huheey, E. A. Keiter, R. L. Keiter, *Anorganische Chemie - Prinzipien von Struktur und Reaktivität, Vol. 3*, Walter de Gruyter & Co. KG, Berlin, **2003**.

[104] R. Ares, M. López-Torres, A. Fernández, M. T. Pereira, A. Suárez, R. Mosteiro, J. J. Fernández, J. M. Vila, *J. Organomet. Chem.* **2003**, *665*, 87-94.

[105] P. D. Enlow, C. Woods, *Organometallics* **1983**, *2*, 64-68.

[106] a) V. C. Cook, A. C. Willis, J. Zank, S. B. Wild, *Inorg. Chem.* **2002**, *41*, 1897-1906; b) O. M. Ni Dhubhghaill, P. J. Sadler, R. Kuroda, *Dalton Trans.* **1990**, 2913-2921.

[107] H. Brunner, *Angew. Chem. Int. Ed.* **1999**, *38*, 1194-1208.

[108] http://www.webelements.com.

[109] S. Ahrland, J. Chatt, N. R. Davies, *Q. Rev. Chem. Soc.* **1958**, *12*, 265-276.

[110] S. J. Lippard, J. J. Mayerle, *Inorg. Chem.* **1972**, *11*, 753-759.

[111] G. Salem, A. Schier, S. B. Wild, *Inorg. Chem.* **1988**, *27*, 3029-3032.

[112] O. M. A. Salah, M. I. Bruce, P. J. Lohmeyer, C. L. Raston, B. W. Skelton, A. H. White, *Dalton Trans.* **1981**, 962-967.

[113] M. F. Davis, M. Jura, W. Levason, G. Reid, M. Webster, *J. Organomet. Chem.* **2007**, *692*, 5589-5597.

[114] O. J. Scherer, H. Sitzmann, G. Wolmershäuser, *J. Organomet. Chem.* **1986**, *309*, 77-86.

[115] I. Krossing, *Chem. Eur. J.* **2001**, *7*, 490-502.

[116] L. J. Gregoriades, H. Krauss, J. Wachter, A. V. Virovets, M. Sierka, M. Scheer, *Angew. Chem. Int. Ed.* **2006**, *45*, 4189-4192.

[117] M. Di Vaira, M. Peruzzini, P. Stoppioni, *C.R. Chim.* **2010**, *13*, 935-942.

[118] M. Di Vaira, P. Frediani, S. S. Costantini, M. Peruzzini, P. Stoppioni, *Dalton Trans.* **2005**, 2234-2236.

[119] M. I. Bruce, B. G. Ellis, P. J. Low, B. W. Skelton, A. H. White, *Organometallics* **2003**, *22*, 3184-3198.

[120] M. Cao, L. V. Do, N. W. Hoffman, M.-L. Kwan, J. K. Little, J. M. McGilvray, C. B. Morris, B. C. Söderberg, A. Wierzbicki, T. R. Cundari, C. H. Lake, E. J. Valente, *Organometallics* **2001**, *20*, 2270-2279.

[121] D. C. Smith, C. M. Haar, L. Luo, C. Li, M. E. Cucullu, C. H. Mahler, S. P. Nolan, W. J. Marshall, N. L. Jones, P. J. Fagan, *Organometallics* **1999**, *18*, 2357-2361.

[122] E. Becker, C. Slugovc, E. Rüba, C. Standfest-Hauser, K. Mereiter, R. Schmid, K. Kirchner, *J. Organomet. Chem.* **2002**, *649*, 55-63.

[123] B. M. Trost, M. U. Frederiksen, M. T. Rudd, *Angew. Chem. Int. Ed.* **2005**, *44*, 6630-6666.

[124] a) T. Hausler, W. S. Sheldrick, *Z. Naturforsch. B, Chem. Sc.* **1997**, *52*, 679; b) I. M. Müller, S. Oczko, *Z. Anorg. Allg. Chem.* **2005**, *631*, 110-114; c) O. J. Scherer, C. Blath, G. Heckmann, G. Wolmershäuser, *J. Organomet. Chem.* **1991**, *409*, C15-C18; d) R. H. B. Mais, H. M. Powell, *J. Chem. Soc.* **1965**, 7471-7481.

[125] M. Neumeier, Ph.D. thesis, University of Regensburg (Regensburg), **2012**.

[126] A. Abragam, *The Principles of Nuclear Magnetism*, Clarendon Press, Oxford, England, **1961**.

[127] G. Balimann, P. S. Pregosin, *J. Magn. Reson.* **1977**, *26*, 283-289.

[128] a) S. Welsch, C. Gröger, M. Sierka, M. Scheer, *Angew. Chem. Int. Ed.* **2011**, *50*, 1435-1438; b) A. Schindler, C. Heindl, G. Balázs, C. Gröger, A. V. Virovets, E. V. Peresypkina, M. Scheer, *Chem. Eur. J.* **2012**, *18*, 829-835.

[129] P. Mal, B. Breiner, K. Rissanen, J. R. Nitschke, *Science* **2009**, *324*, 1697-1699.

[130] Given distances are corrected by the van der Waals radius of the respective atoms (P: 0.180 nm, Cu: 0.140 nm, I: 0.198 nm). Distances between *cyclo*-P_5 rings refer to the distance beween the midpoints of the rings.

[131] V. Lavallo, Y. Canac, C. Präsang, B. Donnadieu, G. Bertrand, *Angew. Chem.* **2005**, *117*, 5851-5855.

[132] W. Strohmeier, F.-J. Müller, *Chem. Ber.* **1969**, *102*, 3608-3612.

[133] E. Dehmlov, C. Z. Bollmann, *Z. Naturforsch. B, Chem. Sc.* **1993**, *48*, 4.

[134] M. W. Stoddart, J. H. Brownie, M. C. Baird, H. L. Schmider, *J. Organomet. Chem.* **2005**, *690*, 3440-3450.

[135] P. Leoni, A. Landi, M. Pasquali, *J. Organomet. Chem.* **1987**, *321*, 365-369.

[136] J.-P. Barras, S. G. Davies, M. R. Metzler, A. J. Edwards, V. M. Humphreys, K. Prout, *J. Organomet. Chem.* **1993**, *461*, 157-165.

[137] P. Braunstein, H. Lehner, D. Matt, K. Burgess, M. J. Ohlmeyer, **2007**, 218-221.

[138] V. Riera, J. Ruiz, X. Solans, E. Tauler, *Dalton Trans.* **1990**, 1607-1611.

[139] M. Gonsior, I. Krossing, N. Mitzel, *Z. Anorg. Allg. Chem.* **2002**, *628*, 1821-1830.

[140] A. Noor, F. R. Wagner, R. Kempe, *Angew. Chem. Int. Ed.* **2008**, *47*, 7246-7249.

[141] B. M. Cossairt, C. C. Cummins, *Inorg. Synth.*

[142] M. I. Bruce, C. Hameister, A. G. Swincer, R. C. Wallis, S. D. Ittel, **2007**, 270-272.

[143] a) A. D. Becke, *J. Chem. Phys.* **1993**, *98*, 5648-5652; b) C. Lee, W. Yang, R. G. Parr, *Phys. Rev. B* **1988**, *37*, 785-789.

[144] a) F. Weigend, R. Ahlrichs, *Phys. Chem. Chem. Phys.* **2005**, *7*, 3297-3305; b) F. Weigend, F. Furche, R. Ahlrichs, *J. Chem. Phys.* **2003**, *119*, 12753-12762.

[145] Gaussian 03 Revision E.01, (Gaussian Inc.), **2004**.

[146] a) P. A. M. Dirac, *Proc. R. Soc. Lon. Ser-A* **1929**, *123*, 714-733; b) J. C. Slater, *Phys. Rev.* **1951**, *81*, 385-390; c) S. H. Vosko, L. Wilk, M. Nusair, *Can. J. Phys.* **1980**, *58*, 1200-1211; d) J. P. Perdew, *Phys. Rev. B* **1986**, *33*, 8822-8824.

[147] A. Schafer, H. Horn, R. Ahlrichs, *J. Chem. Phys.* **1992**, *97*, 2571-2577.

[148] a) TURBOMOLE V6.3, (University of Karlsruhe and Forschungszentrum Karlsruhe GmbH (1998 - 2007); TURBOMOLE GmbH (since 2007)), **2011**; b) R. Ahlrichs, M. Bär, M. Häser, H. Horn, C. Kölmel, *Chem. Phys. Lett.* **1989**, *162*, 165-169; c) O. Treutler, R. Ahlrichs, *J. Chem. Phys.* **1995**, *102*, 346-354.

[149] A. Hellweg, C. Hättig, S. Höfener, W. Klopper, *Theor. Chem. Acc.* **2007**, *117*, 587-597.

[150] D. Andrae, U. Häußermann, M. Dolg, H. Stoll, H. Preuß, *Theor. Chem. Acc.* **1990**, *77*, 123-141.

[151] R. F. W. Bader, *Chem. Rev.* **1991**, *91*, 893-928.

[152] DGrid V4.5, (Radebeul), **2009**.

[153] a) P. Deglmann, F. Furche, R. Ahlrichs, *Chem. Phys. Lett.* **2002**, *362*, 511-518; b) P. Deglmann, F. Furche, *J. Chem. Phys.* **2002**, *117*, 9535-9538.

[154] Diamond 3.0, (Crystal Impact GbR), **1997 - 2010**.

[155] E. Keller, *Chem. unserer Zeit* **1980**, *14*, 56-60.

[156] CrysAlisPro 1.171.35.11 or earlier versions (Agilent Technologies), **2006 - 2011**.

[157] G. Sheldrick, *Acta Cryst. A* **2008**, *64*, 112-122.

[158] A. Altomare, G. Cascarano, C. Giacovazzo, A. Guagliardi, *J. Appl. Cryst.* **1993**, *26*, 343-350.

[159] L. Palatinus, G. Chapuis, *J. Appl. Cryst.* **2007**, *40*, 786-790.

[160] L. Farrugia, *J. Appl. Cryst.* **1999**, *32*, 837-838.